NASA CR-66432

HORIZON DEFINITION STUDY SUMMARY

Horizon Definition Study

Distribution of this report is provided in the interest of information exchange. Responsibility for the contents resides in the author or organization that prepared it.

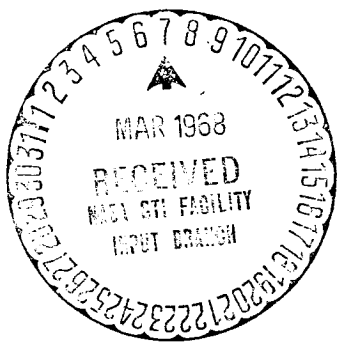

May 1967

Prepared under Contract No. NAS 1-6010 by

HONEYWELL INC.
Systems & Research Division
Minneapolis, Minn.

for

NATIONAL AERONAUTICS AND SPACE ADMINISTRATION

NASA CR-66432

HORIZON DEFINITION STUDY SUMMARY

By Jerry C. Bates
and
Clarence A. Jensen

HORIZON DEFINITION STUDY

May 1967

Prepared under Contract No. NAS 1-6010 by
Honeywell Inc.
Systems and Research Division
Minneapolis, Minnesota

for

NATIONAL AERONAUTICS AND SPACE ADMINISTRATION

FOREWORD

This report summarizes the results of An Analytical and Conceptual Design Study for an Earth Coverage Infrared Horizon Definition Study performed under National Aeronautics and Space Administration Contract NAS 1-6010 for Langley Research Center.

The basic goal of the study was to define, and conceptually configure, all of the necessary experiment elements for a complete description of the earth' s infrared horizon on a global basis for all temporal conditions. From this basic goal, the experiment and the data required to fulfill the experiment was determined. This fully established the feasibility from an experimental data requirements view.

After definition of the experiment requirements, the complete conceptual design of all elements to meet these requirements was effected. The flight techniques to be used, the spacecraft with its required subsystems, and all supporting elements were defined.

Honeywell Inc., Systems and Research Division, performed this study program under the technical direction of Mr. L. G. Larson. The program was conducted from 28 March 1966 to 10 October 1966 (Part I) and from 10 October 1966 to 29 May 1967 (Part II). GCA Corporation participated in the areas of meteorology and atmospheric physics; and RCA, Astro-Electronics Division; Control Data Corporation; and Gulton/Spectrolab participated in the data handling and communications, attitude determination, and the power subsystem areas, respectively.

Gratitude is extended to NASA Langley Research Center for their technical guidance, under the program technical direction of Messrs. L. S. Keafer and J. A. Dodgen, with direct assistance from Messrs. W. C. Dixon, Jr., E. C. Foudriat, H. J. Curfman, Jr., and R. E. Davis, as well as the many people within their organization.

CONTENTS

ILLUSTRATIONS

TABLES

HORIZON DEFINITION STUDY SUMMARY

By Jerry C. Bates
and
Clarence A. Jensen

SUMMARY

The feasibility and merit of a comprehensive horizon definition program are investigated in this study. The potential of the earth's infrared horizon to provide information sufficient for high-accuracy reference systems was determined and evaluated, and data requirements for the program were established. A complete orbital experiment and mission were configured, after analysis of possible flight techniques, to allow for an evaluation of the feasibility of collecting the required data. A program plan was developed providing for the experimental data within a five-year period.

The data produced during the study indicated that the carbon dioxide absorption band is an extremely stable radiation source and offers the potential of providing a reference for future space guidance, navigation, control, and pointing systems accurate to approximately 0.01 degree at an altitude of 250 nautical miles. The data also revealed this reference would contain systematic variations with season and latitude but is not affected by local meteorological and geomorphological phenomena. The study indicated that systematic variations in the horizon could be measured in an experiment which collected data globally over 13 consecutive 28-day time cells and 588 spatial cells.

Operation of a satellite in a 250 nautical mile and near-polar orbit was shown to be the most cost effective manner in which to collect the required experimental data. Two or possibly three vehicles should be planned to assure that the data is collected continuously for the one-year operation.

A 750 pound "rolling wheel" satellite was determined to be feasible and within the current state of the art. The rolling-wheel concept allowed for a completely passive spacecraft and experiment package.

INTRODUCTION

Since flight first began, there has been a need to know the orientation of the flight vehicle with respect to the earth. Traditionally, this orientation has been determined on atmospheric flight vehicles by means of gyroscopic devices utilizing the earth's gravity vector. The advent of space flight, wherein a zero-gravity field exists, has negated the use of these gravity-vector stabailized systems. However, the earth-oriented attitude requirement remains. Two basic categories of systems have been developed to meet this requirement. These are systems utilizing fixes on the known positions of celestial bodies and those systems that utilize characteristics of the earth's horizon to determine local vertical.

Systems which employ celestial references require a priori knowledge of the positions of the celestial bodies and a complex mathematical transformation of this information to a local vertical orientation - which leads to systems which cannot be employed in a spacecraft for real-time usage. In contrast with the complexity of this system, however, is a system that measures some characteristic of the earth's horizon at two or more points around the horizon circle and determines local vertical directly from these measurements.

As a result of its simplicity and real-time operation, horizon sensor systems have been employed in a variety of spacecraft (e. g., Nimbus, Tiros, ATS, Mercury, Gemini, Apollo, Ranger, Mariner, and Agena flights). In these missions, horizon sensor systems have been used for determining local vertical during boost, orbit injection, operational phases, and for re-entry alignment.

Early attempts at using sensor systems utilized the visual spectrum to define the actual hard horizon of the earth. This spectrum, and later uses of the near-infrared spectrum, proved unreliable for use since large cloud masses obscured or otherwise affected the expected measurement. Recent studies have defined the 15μ carbon dioxide spectral region as the infrared spectrum most applicable for horizon sensor systems.

In March 1966, a study contract was awarded by the Langley Research Center to Honeywell, Systems and Research Division, to investigate the characteristics of the carbon dioxide horizon. This study was conducted to provide for definition of the infrared horizon, to select an optimum spectral region for high-accuracy horizon sensor systems, and to analyze theoretically the variability of the horizon as a function of altitude over a wide range of spatial and temporal conditions. The study also included a requirement to define an appropriate experiment to make horizon measurements in the spectral region of interest. This effort included the conceptual design of experiment subsystems to permit evaluation of the feasibility of conducting a comprehensive horizon definition program.

BACKGROUND

Although horizon sensors for vehicle guidance and control have been in existence since 1958 and are used on the majority of orbital spacecraft, the state of the art in their design has been limited because many infrared characteristics of the earth's radiance profile are not well known. These characteristics must be accurately determined in order to realize the ultimate design and maximum accuracy of horizon sensors. Given a comprehensive knowledge of the horizon profile, an optimum sensor mechanization can be designed by incorporating signal processing logic with optical and electronic filtering, electronic compensation, and computer modeling techniques.

Since the first horizon sensors were flown a great deal has been learned, through theoretical and experimental programs, about the infrared horizon as viewed from space. Although these analyses and tests have served to define important constraints on systems design, sufficient information has not been available to provide data which would allow the design of sensors capable of providing an adequate attitude reference in the 0.01-degree class.

A short synopsis of the historical development of the problem will assist in developing a thorough understanding of the study approach and conclusions. Since the initiation of the United States' space program, the earth's infrared horizon has been used to determine attitude of many satellites. In some cases horizon sensors have been used as the primary or back-up sensors for attitude control and stabilization; in other cases the sensors have been used merely to determine attitude for purposes of controlling scientific packages or analyzing the scientific data.

Satellites, such as Nimbus and OGO, use horizon sensors as primary attitude sensing elements for stabilization of the spacecraft to local vertical. The Discoverer series, Mercury, and Gemini used horizon sensors as back-up to inertial attitude systems and to establish local vertical references. Tiros spin-stabilized weather satellites were provided with horizon sensors to determine when the line of sight was crossing the earth for operating the cameras.

Various configurations of horizon sensors have been designed: for example, fixed-point sensors which view the horizon at several fixed points relative to the spacecraft; conical scanners which sweep out a conical segment intercepting both the earth and space; and the dithering sensor which oscillates between space and earth as it scans in azimuth. These examples are illustrated in Figure 1.

The first horizon sensors, developed as early as 1957, operated on radiation within the atmospheric window, nominally 2 to 18μ wavelengths or wider.

This broad band was selected for its high energy level to maximize signal-to-noise ratio based on considerations of detectors, optics, and electronics state of the art. A further consideration by the early horizon sensor designers was a desire to sense the actual "hard" earth horizon which is made possible by the transparency of the atmosphere to radiation in this spectral band.

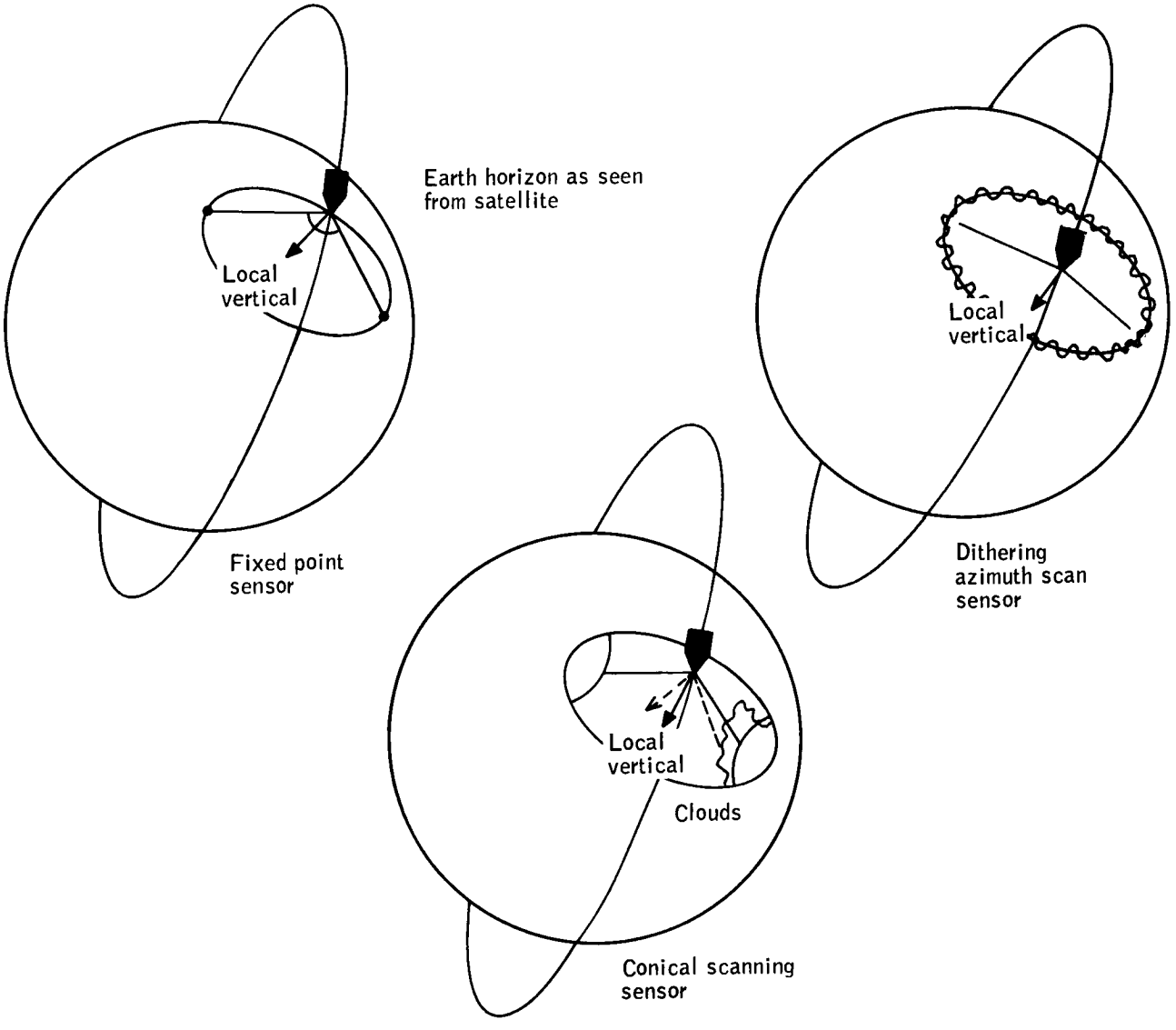

Figure 1. Examples of Horizon Sensor Operation

Erratic behavior on the early flights resulted in erroneous vertical reference with steady-state error reaching five degrees and transients considerably greater. These flight results provided the impetus for further detailed examinations of the horizon phenomena. It appeared from theoretical work that the earth's horizon was not a well-defined discontinuity between the cold of space and the warm planet; furthermore, the effects of clouds became increasingly apparent. Experiments conducted by the U.S. Air Force on U-2 flights confirmed the existence of "cold clouds" effects on horizon sensors. It was concluded that these clouds absorb infrared radiation within this spectral region and re-emit at their nominal temperature, thereby appearing as a colder body than the earth. As can be seen in Figure 2, the cloud condition within the atmosphere has a significant effect on the energy emitted by the earth. Another important aspect of this problem is also shown in this figure; little, if any, cloud effect is apparent in the spectral interval of approximately 14 to 16μ. Interest in this spectral range developed rapidly. In 1962 the IRATE experiment was conducted, and the inherent stability of the CO_2 absorption band was demonstrated. Corroboration of the experimental results was developed by the Tiros satellite data. By comparison of radiometers operating in various spectral regions, cloud effects were shown to be prevalent in some spectral regions but of little apparent significance in the 14 to 16μ region. However, none of these programs provided radiance profiles of high resolution and, in many cases, no reference of the profiles to the earth's crust was made.

Another step was made in the theoretical activity when several radiance curves were calculated for specific model atmospheres to establish the effects of seasonal and geomorphological conditions. Figure 3 shows results of this work by Hanel, Bandeen, and Conrath. As may be noted from these curves, profile variations in both shape and amplitude do exist for various conditions. At this point, however, a sufficient data sample was not available, therefore precluding statistical analysis of these variations. Numerous investigators have sought to ascertain an optimum spectral interval for horizon sensor operation. Their activity also was greatly hampered by the lack of accurate horizon radiance data.

The National Aeronautics and Space Administration Langley Research Center (NASA LRC) and the United States Air Force Space Systems Division (AF SSD) have sponsored experimental programs to examine the effects of narrow bandwidth for horizon definition. NASA LRC originated the D-61 program in 1961 to make comparative measurements of the ultraviolet, visible, and infrared earth horizons. The IRATE and the Kodak experiments were conducted to examine narrow bands in the infrared region. The IRATE program made comparative measurements on five infrared spectral bands, one of the bands being the 14 to 16 micron CO_2 absorption region.

Significant improvement for horizon sensing resulted from operating in this region over the other four bands. The Kodak program, on the other hand, made comparative measurements on 3, 2, and 1 micron bandwidths centered at 15 microns; fewer anomalies were identified in narrower bandwidths. NASA LRC has had a continuing program of horizon definition in existence since these early experimental attempts. Included in this continual program are

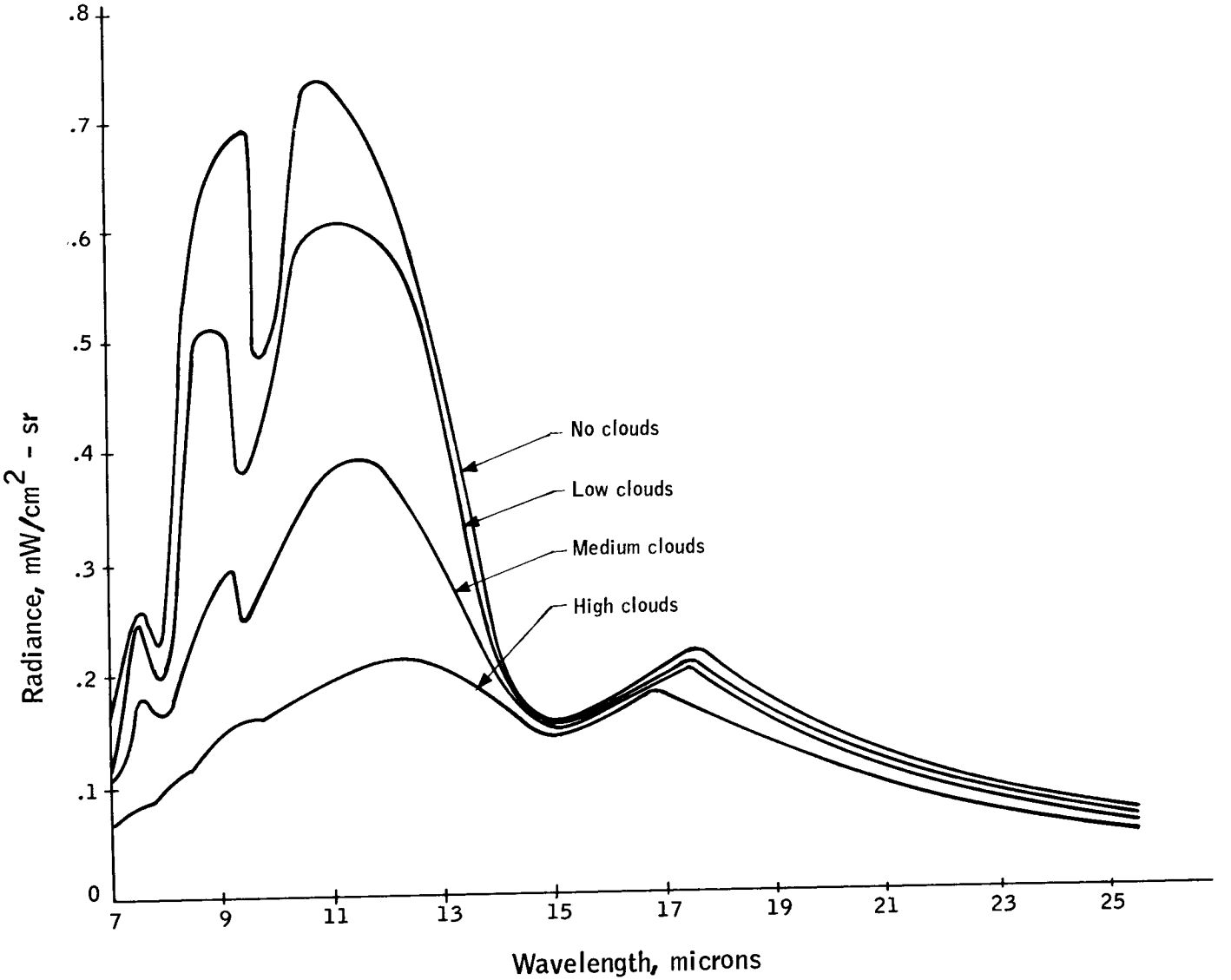

Figure 2. Calculations of Radiance as a Function of Wavelength

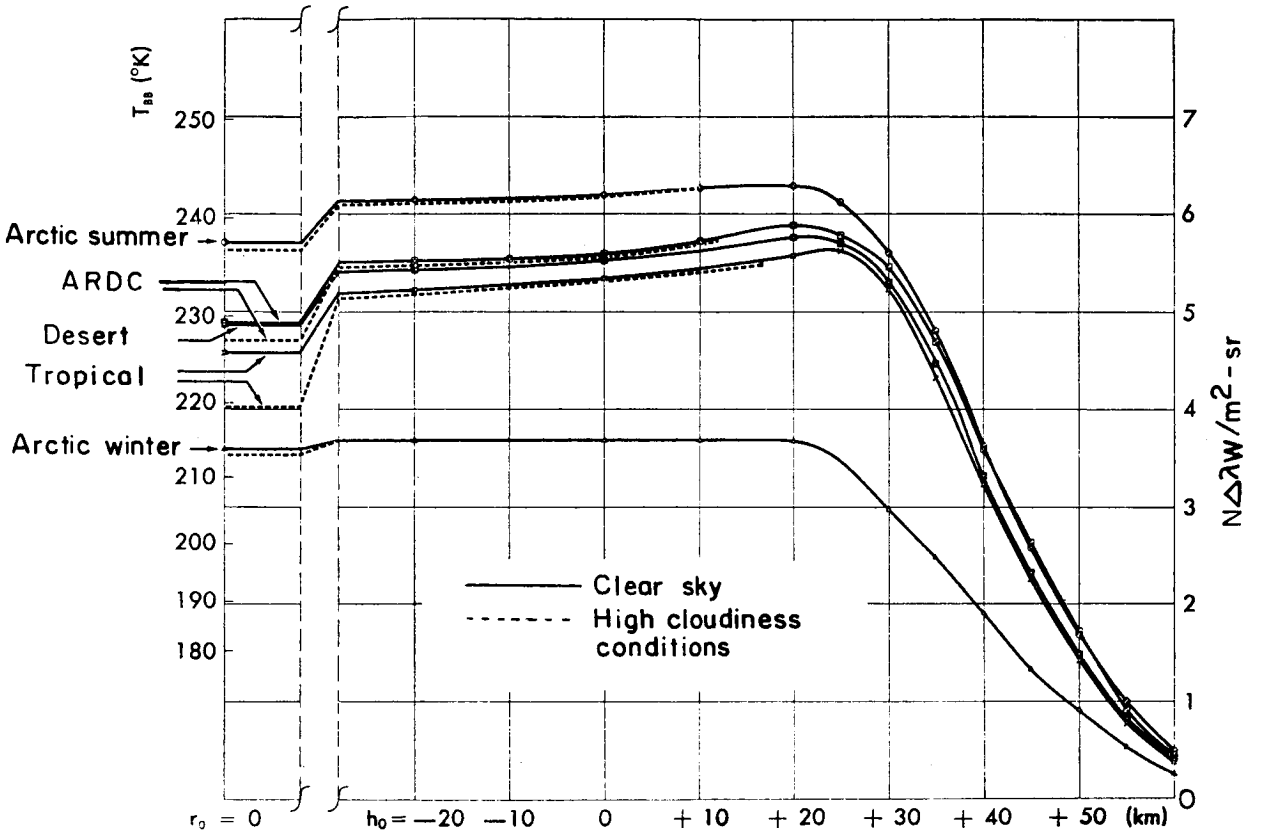

Figure 3. Curves of Radiance in the 15 Micron CO_2 Band versus Altitude for Five Model Atmosphere (ref. 1)

the X-15 radiometer program which is obtaining some high-resolution, high-spatial accuracy horizon definition data and the Scanner program.

As a first step in obtaining high-resolution, earth-coverage radiance profiles referenced to the earth's hard horizon, NASA Langley Research Center initiated Project Scanner in 1963. This program, consisting of a series of ballistic probes, culminated in the first successful attempt to gather a relatively large body of accurate radiance profiles. The first launch was accomplished in August 1966; more than 400 high-resolution profiles were accumulated (ref. 2).

The Langley experiment is the most significant in the area of horizon definition conducted to date. Although its fundamental goal was to collect high resolution horizon profiles in both the CO_2 absorption band (14 to 16μ) and the far infrared (20 to 40μ water vapor), the experiment also verified the accuracy of computational techniques for calculating radiance as a function of tangent height from vertical temperature and pressure data in the atmosphere. Figure 4 illustrates the comparison of experimental and theoretical profiles. Project Scanner also provided visibility of the effects of a "cold cloud" on the limb of the profile in the far infrared (see Figure 5). This program also verified the stability of the 14 to 16μ region and provided for some resolution of latitudinal variations. Although highly successful, this program does not provide the desired earth coverage and latitudinal variations over a long period of time. These summary presentations indicate the total data base that exists and their attendant shortcomings in time and space coverage. A complete tabulation of horizon definition experiments is included in Table 1.

As discussed, experiments in space have been designed to find the best spectral range for horizon sensing and to collect more information on the infrared characteristics of the atmosphere. Because of these experiments, it is generally agreed now that horizon sensing should be carried out at those wavelengths at which the atmospheric carbon dioxide molecule exhibits spectral resonance, particularly at the 14 to 16 micron wavelength band. The task of determining the shape and magnitude of the earth's radiance profile in this wavelength band and the variations exhibited in them remains to be completed.

STUDY OBJECTIVE AND APPROACH

Variations in the shape and magnitude of the earth's radiance profiles are expected to be of two types - systematic and nonsystematic. Elimination of the effects of systematic variations can be designed into a horizon sensor. However, compensation for the effects of nonsystematic errors can be achieved only if it is determined that, for certain sensor mechanizations, the effects of these variations are minimized. Thus, the definition and development of an optimal horizon sensor for accurate vehicle attitude determination depends ultimately on the ability to define adequately the horizon radiance profiles and their variations on the earth.

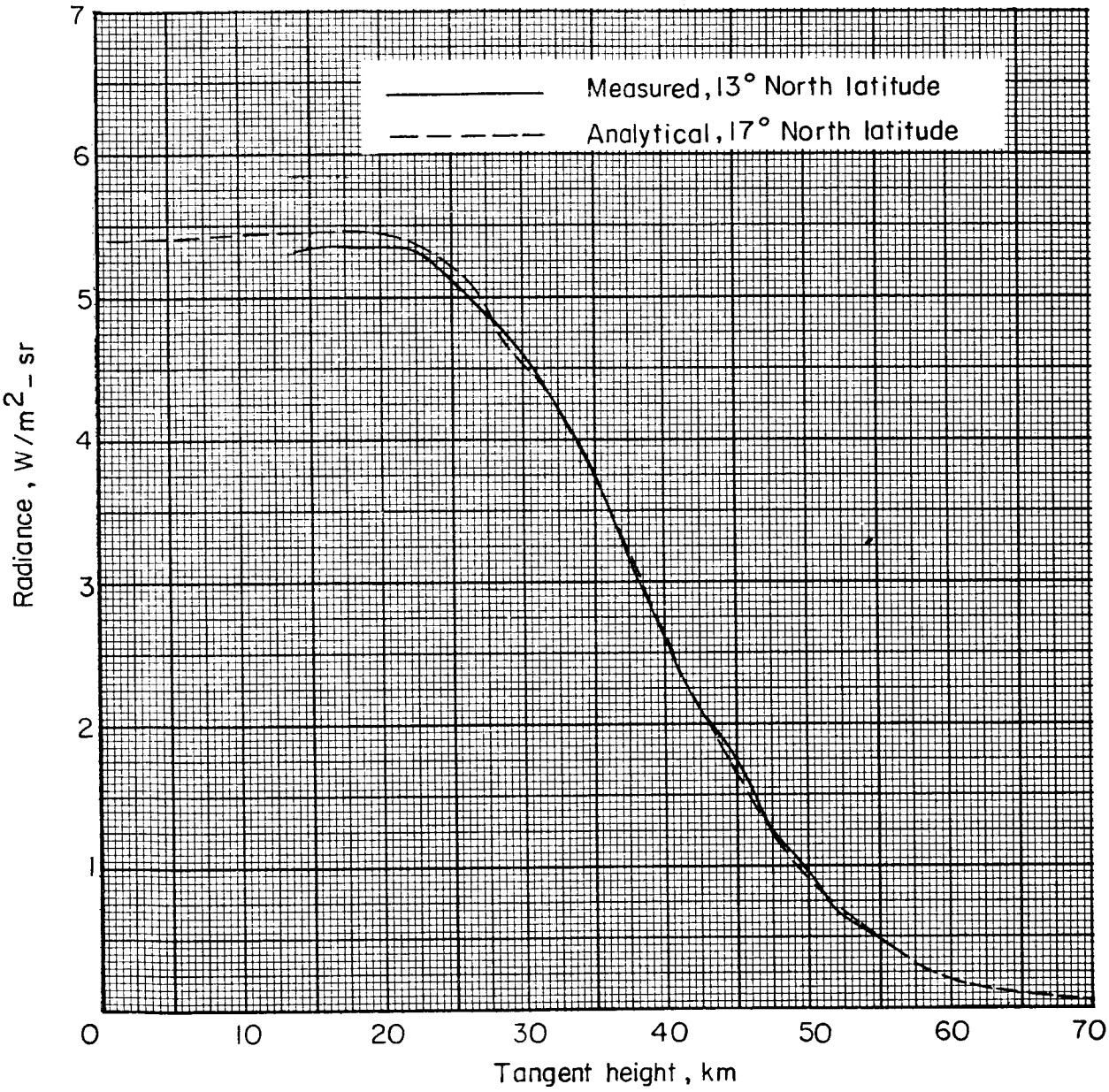

Figure 4. Comparison of Measured and Analytical Radiance Profiles in 615 cm^{-1} to 715 cm^{-1} Band (ref. 2)

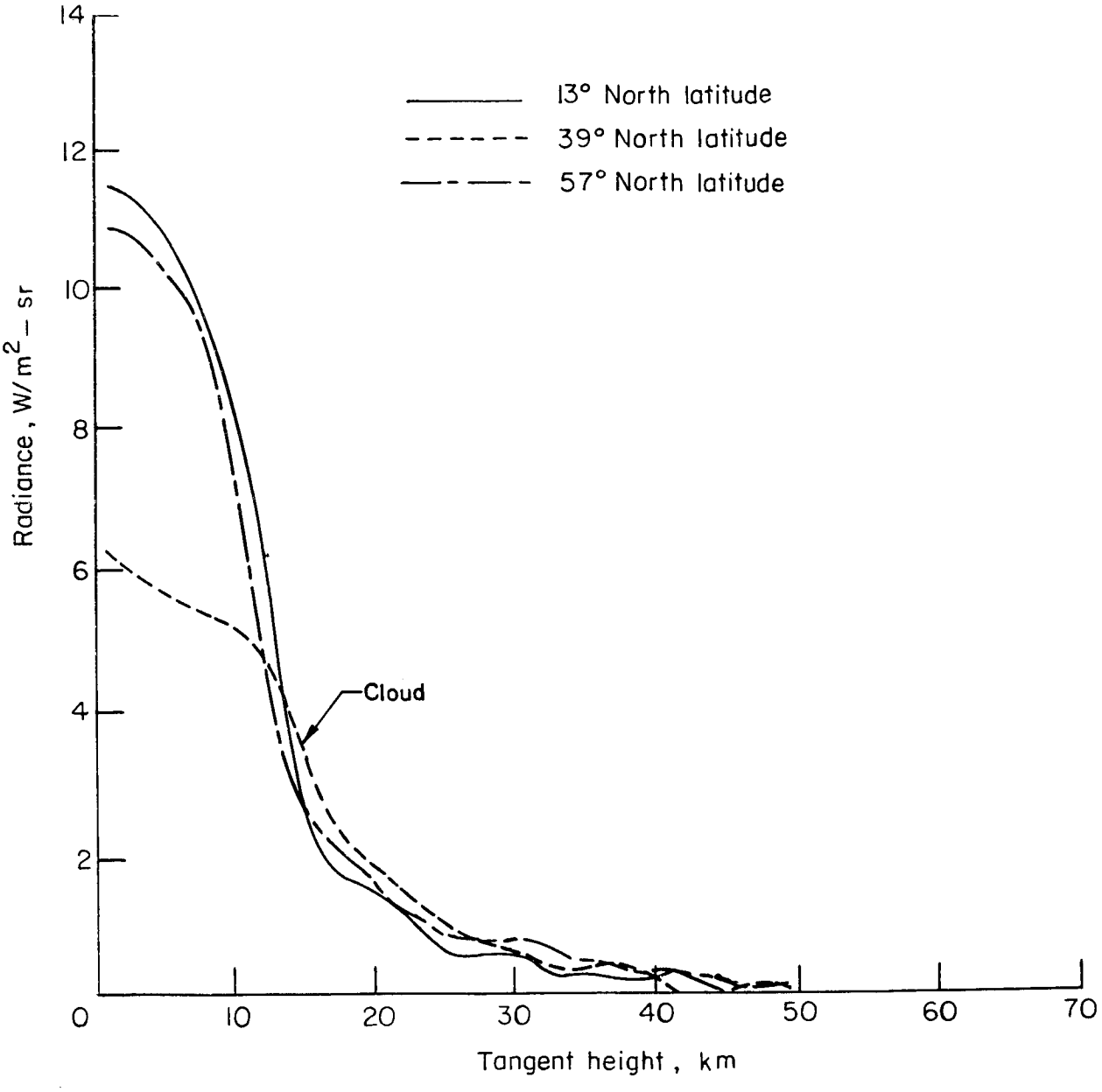

Figure 5. Measured Radiance Profiles in 315 cm^{-1} to 475 cm^{-1} Band (ref. 2)

TABLE 1. - EXPERIMENTAL HORIZON DEFINITION PROGRAMS - PARTIAL LISTING

Agency	Vehicle	Spectral regions, μ	Definition, km	Spatial positioning, km
NASA LRC	D-61-1	.23 to .29	12	None
NASA LRC	Rocket probe	.29 to 1.0	12	
		.75 to 3.0	12	
		1.8 to 25.0	36	
USAF (Eastman Kodak)	Discoverer satellite	14.0 to 15.2	5	None
		13.7 to 15.6		
		13.6 to 16.5	9	None
		14.0 to 15.2		
NASA LRC	X-15	0.8 to 2.8	2	5
		10 to 14	2	5
		14 to 20	2	5
USAF (Lockheed)	U-2	5.0 to 18.0	9	None
USAF (Lockheed) IRATE	Discoverer satellite	5 to 18.0	32	
		12.5 to 18.0	32	
		14 to 16	32	None
		15 to 18	32	
		15 to 35	4	
USAF	Discoverer satellite	12 to 18		
		8 to 17	?	None
		14 to 35		
DOD (AFCRL)	Aerobee	10.2 to 11.8	6	
		14.0 to 15.6	9	6
		19.5 to 31.8	6	
NASA LRC	Project Scanner	14 to 16	2	2
		20 to 40	2	2

The measurement program for determining the radiative properties of the earth's horizon as viewed from space must not only provide sufficient empirical information on all the variations likely to occur in the radiance profile but must also isolate the systematic variations from the nonsystematic ones for separate assessment. The influence of different sensor mechanizations and signal processing on the detected nonsystematic variations must be made explicit. Measurements must be obtained as they relate to geographical location, seasonal and diurnal variations, meteorological conditions, geomorphological features, and solar phenomena. Furthermore, the measurements must be made in sufficient quantity to establish statistical confidence.

Such a program must include both detailed considerations of the earth's radiance profiles and their variations and extrapolation of these results to horizon sensor and data reduction applications. Also included must be consideration of flight techniques most suitable for a horizon definition measurement study. Each of these flight techniques must be evaluated on a mission-success, cost-effectiveness basis. With the successful culmination of a complete program, the most comprehensive data base and analytical and design techniques related to the earth's radiation profile and the design of horizon sensors will be available.

This horizon definition program suggests an approach that will evaluate the characteristics of the horizon based on available atmospheric data and determine the amount of data necessary to define the entire earth's infrared horizon. From such information various flight techniques which could potentially collect this data can be analyzed to establish which of the selected techniques has the highest degree of probable mission success as a function of program costs. The following are then established as the major objectives of this study:

- Estimate the data requirements for a comprehensive horizon definition program and provide for a preliminary evaluation of flight techniques for gathering the specified data.

- Provide for full definition of an experiment to collect the required data and conceptually design the experiment systems to evaluate the feasibility of the program.

With these objectives, three major areas of study are necessary: data requirements definition to specify how much and what kind of data is required for a meaningful experiment; flight techniques evaluation to determine a cost-effective experiment mechanization; and conceptual experiment systems design to demonstrate feasibility of the selected flight technique.

The data requirements study encompasses a determination of the quantity, quality, type, and location of radiance measurements which must be gathered to define adequately the horizon radiance over the entire earth's surface. The data time cycle must also be determined and radiance accuracies established which will enable the program goals to be achieved. Figure 6 represents an expansion of the data requirements study task which is basically the

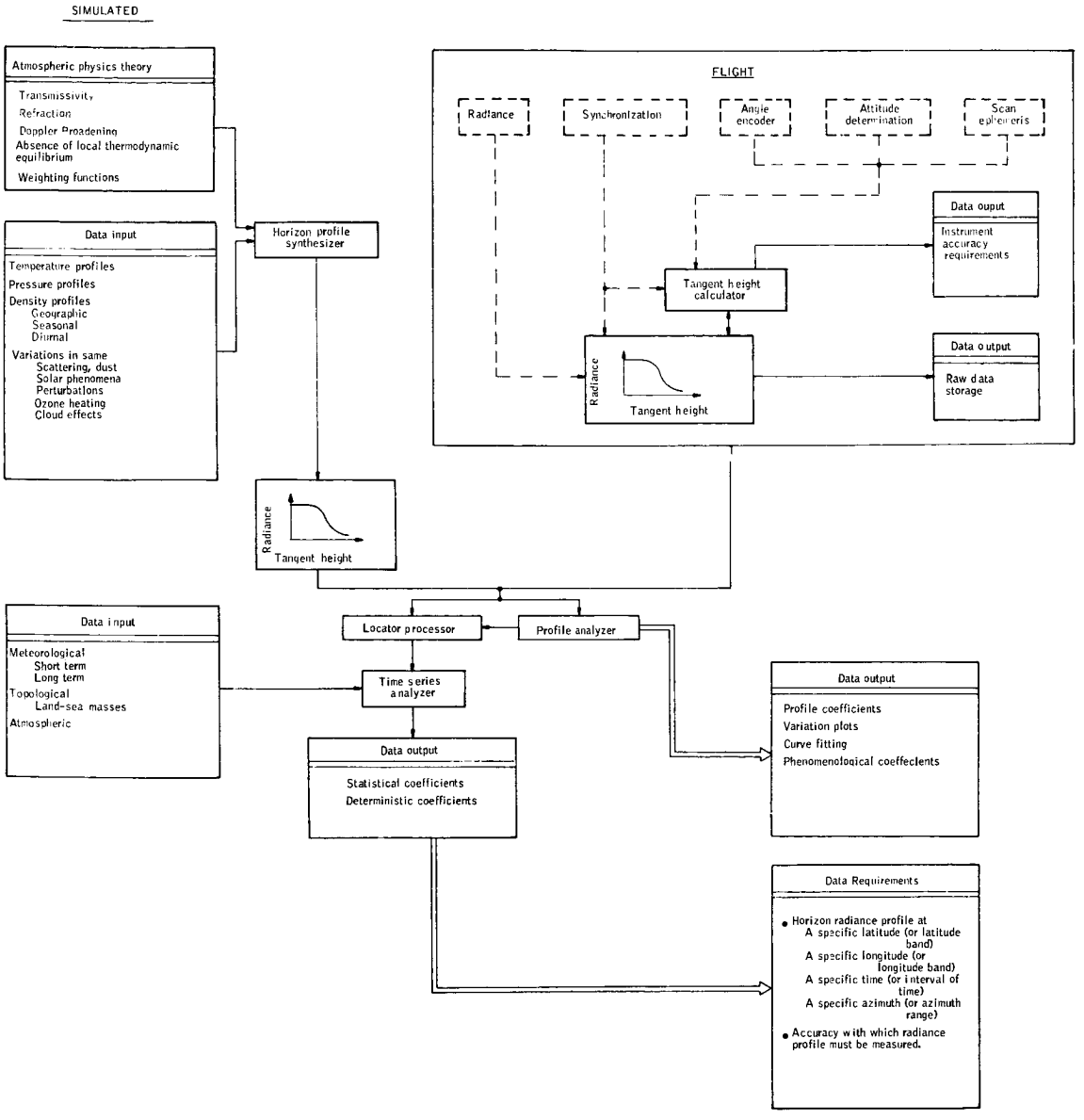

Figure 6. Approach for Determining Data Requirements

formulation of a mathematical model to assess various horizon sensing techniques and determine experimental data requirements. The dual branches identified as "simulated" and "flight" denote the objective of patterning the formulating approach so that the mathematical model, after a minimum of modification, can also serve as the ground data-reduction technique for the flight program.

The horizon profile synthesizer generates profiles from empirically available temperature and pressure data, utilizing a computer program which analytically reflects all the physical processes causing significant changes in the magnitude and shape of the earth's 14 to 16 μ horizon radiance profile.

The resulting synthetic profiles are operated on by the locator processor and the profile analyzer. The locator processor reduces each profile to a single number representing indicated altitude, which enables efficient computer analysis. The locators used are simulations of operations carried out by an existing or conceptual horizon sensor. These single "horizon" numbers are then correlated with a body of empirical data, using the time series analyzer. Each indicated altitude ℓ is a function of all implicit variables

$$\ell = (t_1, t_2, \theta, \phi, \text{others})$$

where

t_1 = short-term variation

t_2 = long-term variation

θ = latitude

ϕ = longitude

and "others" denotes such variables as azimuth and meteorological or topological conditions. The time series analysis isolates the systematic spatial and temporal variations from the nonsystematic or random variations. The relative importance and, therefore, the order this analysis will take is established by the profile analyzer which determines the variables causing the greatest systematic effect.

The output of the data requirements task describes the quality, quantity, and distribution of the horizon profiles. These outputs are prerequisites to the flight techniques analysis which will yield the selected technique and the required mission. This analysis considers various techniques and configurations, evaluates the cost and reliability of each, and defines configurations and techniques which produce the necessary data within projected funding limitations, with an acceptable relationship of quantity and reliability, i.e., effectiveness. Figure 7 established this study element's approach relationship.

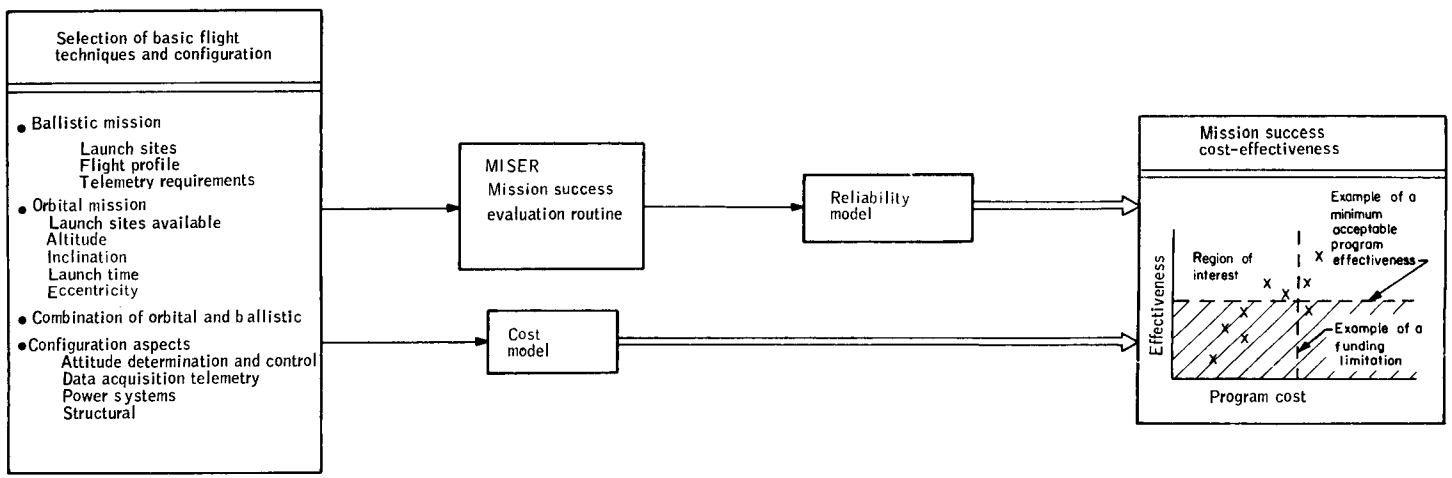

Figure 7. Approach for Flight Technique Analysis

Given a recommended flight technique, a conceptual design of the experiment and its systems was initiated to evaluate feasibility. The study approach utilized involved identification of all functions required to conduct the experiment, followed by a systematic investigation of the techniques which could be employed to provide for each function. Each function and its associates were traded off with one another to ensure that an efficient system was configured. Sensitivity studies were conducted, where appropriate, and state-of-the-art constraints were identified.

The complete system concept included appropriate coverage of each function. The functions were separated into three basic phases:

- Prelaunch operations
- Orbital operations
- Ground operations

Figure 8 identifies the major functions for the above phases and, in addition, continues with a subfunctional breakdown and a numerical identification. Each of these subfunctions is described to establish clearly the scope of the subfunction. This analysis and the numerical identification served to facilitate communication of tradeoff study information and other functionally related data during the course of the study.

Each of the three main analysis areas comprising the total horizon definition program are summarized more fully in the following sections of this report.

DATA REQUIREMENTS

Factors which affect horizon radiance profiles can be defined as either explicit or implicit. Explicit factors are those which relate directly to the input quantities in the radiative transfer equation. Temperature and pressure, for example, are explicit factors which exert an influence upon the magnitude and shape of the horizon radiance profile by means of their functional relationship with the Planck source function and the atmospheric transmissivity. Implicit factors, on the other hand, specify the conditions which are associated with an individual profile or group of profiles, including such factors as latitude, longitude, time of year, time of day, various atmospheric (or meteorological) conditions, and underlying topography.

The radiance I(h), which effectively emanates from each tangent height h of the radiance profile, is the result of a double integration over the atmospheric optical path and the wavelength, plus a boundary condition integrated over the wavelength only. The form of the equation is

$$I(h) = \int_{\Delta\lambda} B(\lambda, T_1)\, \tau(\lambda, u_1)\, d\lambda + \int_{\Delta\lambda} \int_{u_1}^{0} B(\lambda, T) \frac{\partial \tau}{\partial u}\, d\lambda\, du \qquad (1)$$

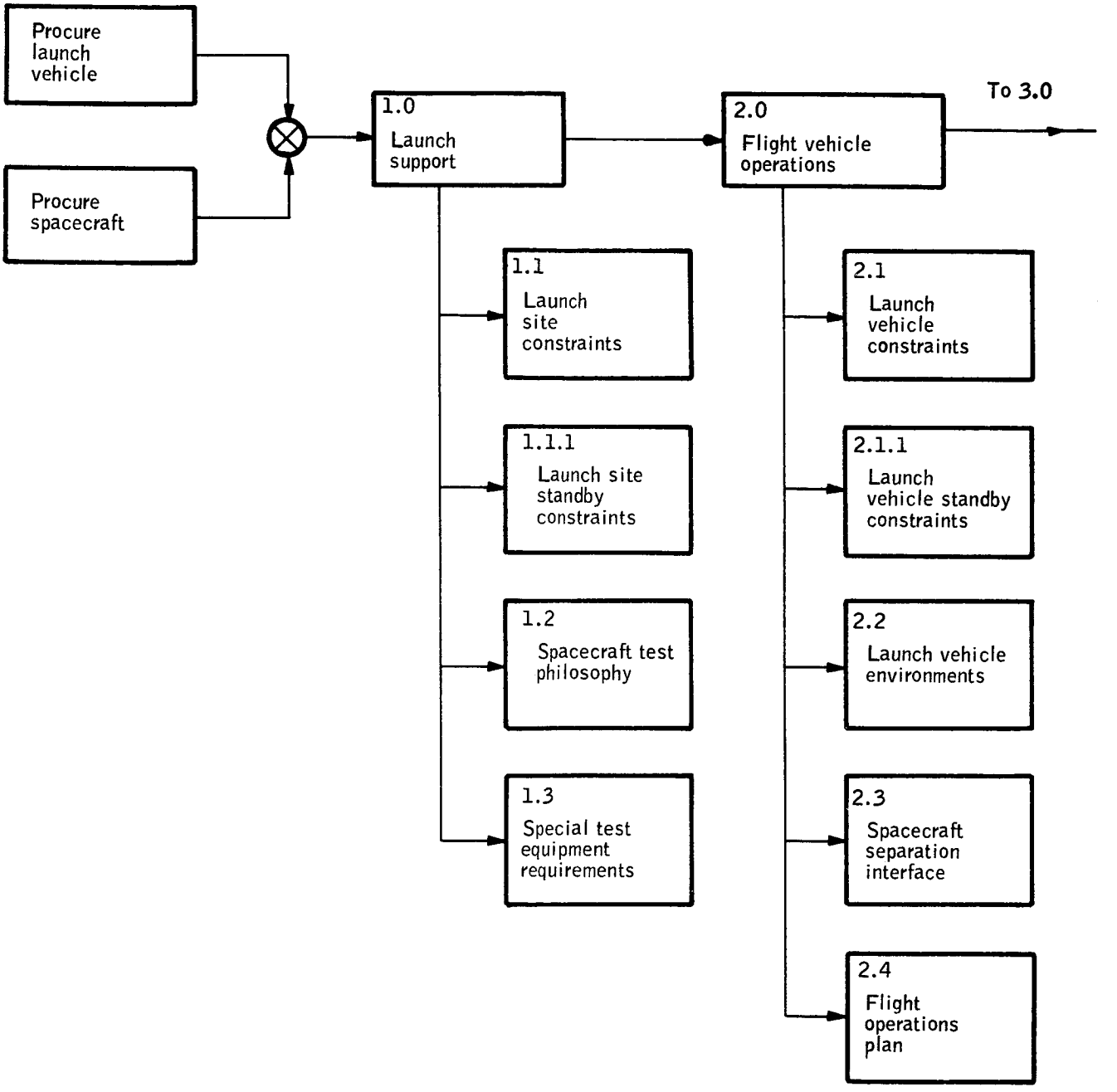

Figure 8. HDS System Functional Diagram

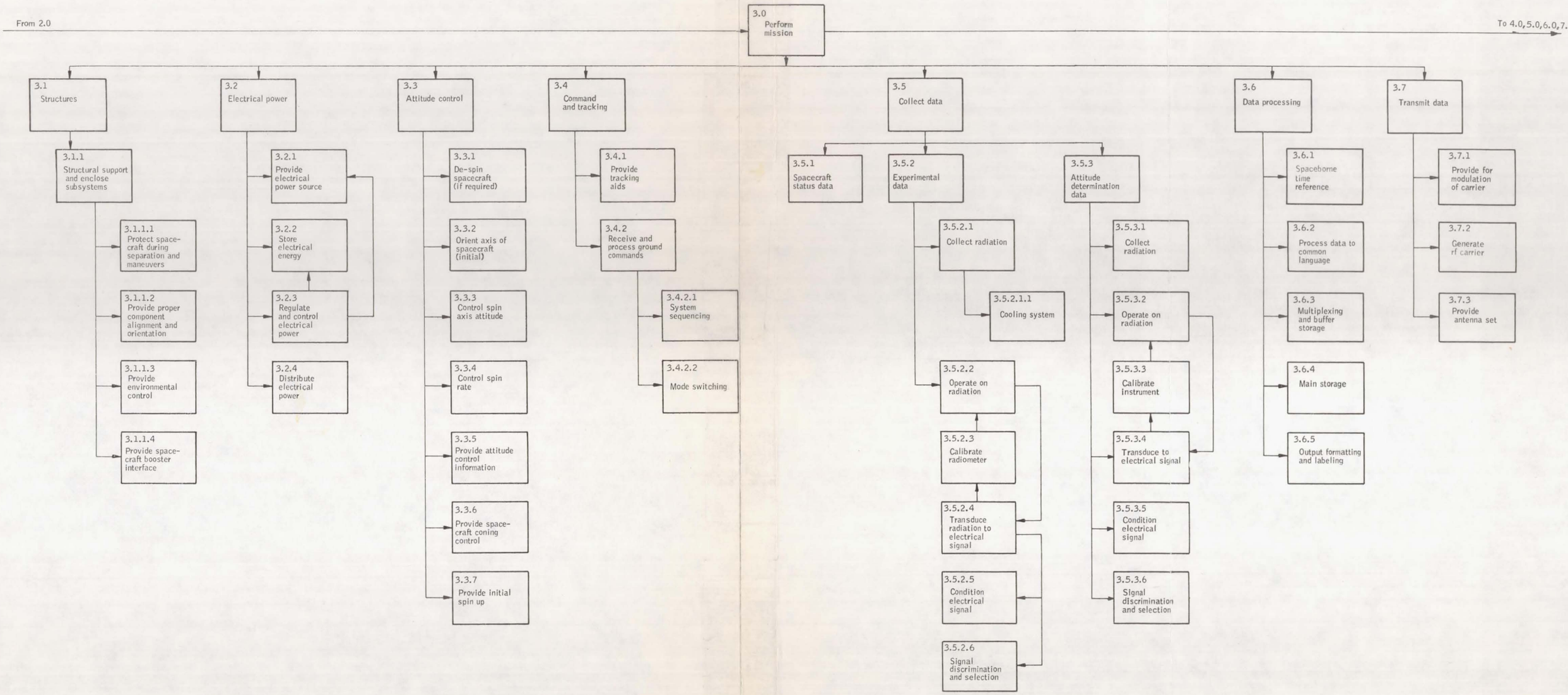

Figure 8. HDS System Functional Diagram - Continued

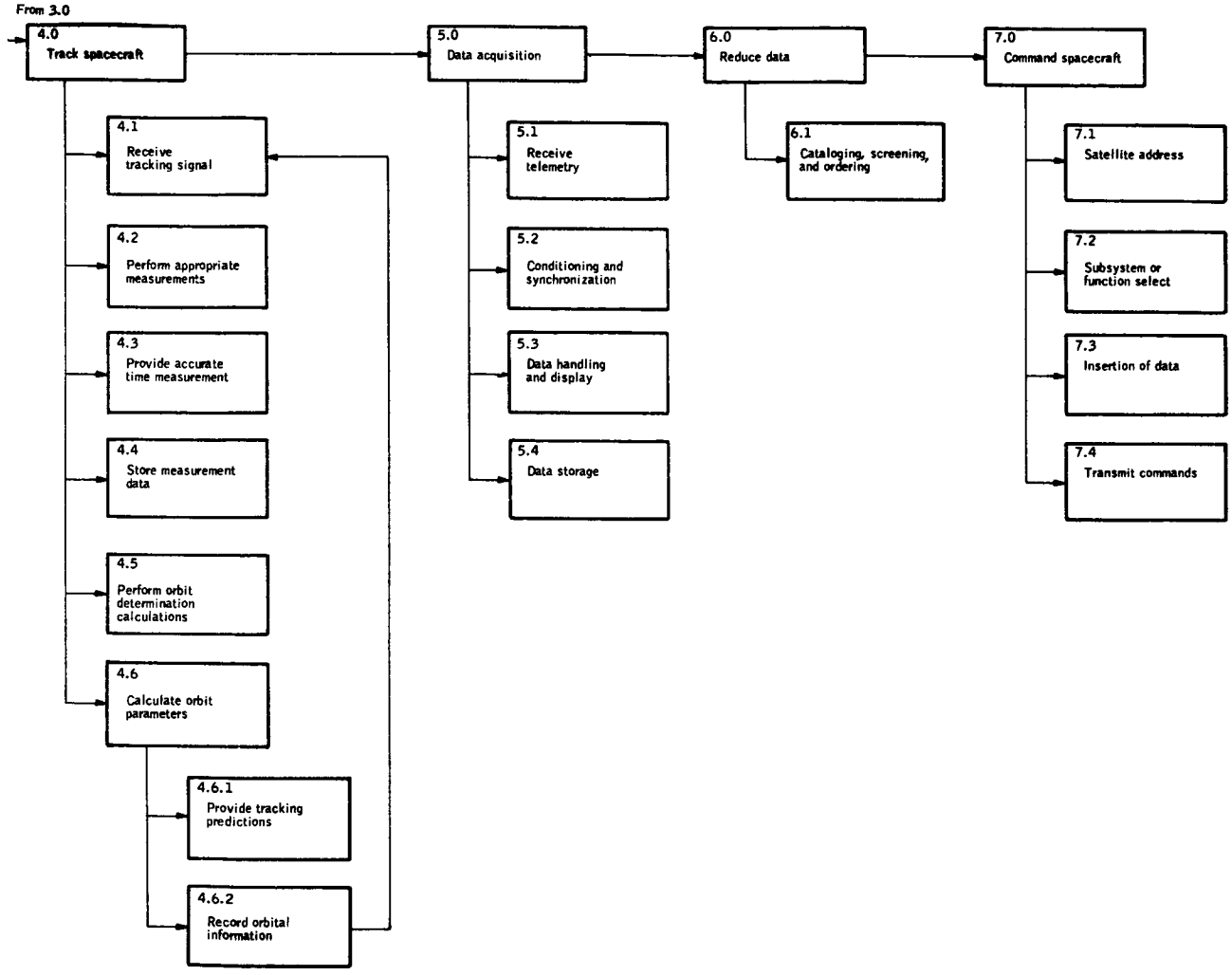

Figure 8. HDS System Functional Diagram - Concluded

Page intentionally left blank

To make best use of available tabulated data, this equation is integrated by parts to yield

$$I(h) = \int_{\Delta\lambda} B[\lambda, T(u = 0)]\, d\lambda + \int_{\Delta\lambda}\int_{u_1}^{0} \tau(u) \frac{\partial B(\lambda, T)}{\partial u}\, d\lambda\, du \qquad (1a)$$

where

$B(\lambda, T)$ = source function (including pseudo-source such as solar scattering from stratospheric dust, clouds, and scattered earth-shine in addition to the primary Planck source function),

$\tau(u, \lambda)$ = spectral transmissivity of CO_2 (reflects choice of absorption model and effects due to pressure and Doppler broadening),

u = optical path,

λ = wavelength in the spectral interval $\Delta\lambda$ (including consideration of the filter spectral response when integrating over $\Delta\lambda$), and

T = temperature at the point specified by u.

At each wavelength λ the spectral transmissivity τ is a function of temperature and pressure as well as optical path u. Temperature and pressure are specified by calculating an effective temperature T_e and an effective pressure p_e for each atmospheric optical path. All of the preceding parameters explicitly affect the radiance $I(h)$ and, for convenience, are hereinafter referred to as explicit factors.

The two most prominent explicit factors in the foregoing equations are temperature and pressure. These factors exert influence on the magnitude and shape of the horizon radiance profile through the functions (such as atmospheric transmissivity or the derivative of the Planck function) which appear in the integrand of the radiation equation. However, by the barometric equation

$$p = p_o \left(\exp - \int_o^h \frac{g(h)}{RT(h)}\, dh \right) \qquad (2)$$

where g is gravitational acceleration and R is universal gas constant, pressure is related to the temperature as a function of the altitude h. Hence, temperature as a function of altitude is the explicit factor to which the magnitude and shape of the radiance profile are most sensitive. This conclusion has two important ramifications. First, the most important inputs to the mathematical model for synthesizing radiance profiles are the empirically

derived temperature profiles. Second, variations in both the magnitude and shape of the radiance profile are most likely due to changes in the factors which affect the temperature.

Implicit factors provide a description of the specific conditions which apply to a given horizon radiance profile. Such factors as latitude, longitude, season, local time, and associated meteorological and topological conditions provide the basis for statistically evaluating a large body of radiance profiles to determine the variational components attributable to each factor.

The knowledge of the implicit factors to be gained in the experiment will ultimately be applied to the systematic correction of horizon sensing instruments on the basis of latitude, longitude, and observation time as well as supplementary corrections based upon significant variations in meteorological and other environmental conditions.

Development of the horizon radiance measurement program necessarily depended upon a detailed examination of both explicit and implicit factors. No comprehensive body of measured horizon radiance profiles exists which covers the 14 to 16 micron CO_2 absorption band. Therefore, by means of computer simulation, the necessary body of synthesized profiles was generated based upon numerical integration of the radiative transfer equation and using the best available estimates of explicit factors obtainable from theoretical and empirical radiance studies and meteorological data observations (i.e., temperature and pressure). Each synthesized profile is identifiable with a specific set of spatial and temporal conditions and can be further associated with the atmospheric and topological conditions which apply at a particular place and time.

These data indicate two specific areas of study:

1. The data input required in terms of the explicit and implicit factors, and
2. Atmospheric physics studies to determine the exact characteristics of the source function, atmospheric transmittance, and spectral interval.

After development of the radiance profiles, methods for analyzing the data content of the profile group for determination of systematic and nonsystematic variations were defined. Two basic methods were defined - a locator processor concept which operates on each horizon profile, as would a horizon sensor, to reduce the profile to a single indicated horizon and a profile analyzer concept which enabled analysis of total profiles and profile subgroups to determine dominant features of the profiles or groups and to assist in defining locator concepts.

The entire body of synthesized profiles thus provides the basis for analyzing the statistical variability of the factors to define the data sampling requirements for a comprehensive program of horizon radiance measurement.

INPUT DATA

Before a definite commitment could be made to the selection of a particular body of basic data and specific methods of generating required inputs, preliminary studies were performed to obtain an indication of which factors were more significant and, therefore, more deserving of concentrated attention. These preliminary studies showed that spatial and temporal variability in the temperature (and pressure) profile produced the most important effects upon the behavior of the horizon radiance profile. Major attention was focused, therefore, upon procuring data and developing analytical techniques for generating a representative body of temperature profiles covering the altitude range of 0 to 90 km. Nevertheless, the problems of CO_2 variability and high-cloud occurrence also received considerable attention since it was necessary to determine on a quantitative basis the upper limits of their effects upon the radiance profiles.

TEMPERATURE/PRESSURE PROFILES

The ideal approach to the generation of a representative body of temperature/pressure profiles would be to sample selectively from a source of complete and accurate basic data available on a global basis over a period of several years. Ideally, these basic data would have been taken at sufficiently close intervals in time and space that all scales of temperature variability could have been rigorously examined in terms of the associated variance in horizon profiles. Unfortunately, this ideal data base does not exist at this time.

Radiosonde data from 0 to 30 km are regularly available at 12-hour intervals over relatively dense observational networks in North America and Eurasia, but truly global coverage does not exist. Rocketsonde data from 30 to 60 km are available at two- to three-day intervals from 18 stations over North America, and many of these stations do not report regularly. Evidently, then, rocketsonde data coverage is even less global in extent than radiosonde data. From 60 to 90 km, extrapolation techniques must be used based on sporadic soundings of actual data. Figure 9 shows two representative temperature profiles and illustrates the altitude regions and relative density of coverage from each measurement system.

In view of the above limitations in basic data coverage, the choice of representative study cases for the determination of sounding profiles was necessarily constrained. Nevertheless, by careful selection of cases, sampling of a large number of temperature profiles representative of different time and space scales was possible.

The study cases which were selected include the following basic categories:

1. Large-scale synoptic variability over North American and surrounding oceans - sampled at eight representative times within a one-year period.
2. Small-scale spatial variability along a cross section from the British West Indies to the Southwestern United States - sampled at two representative times.

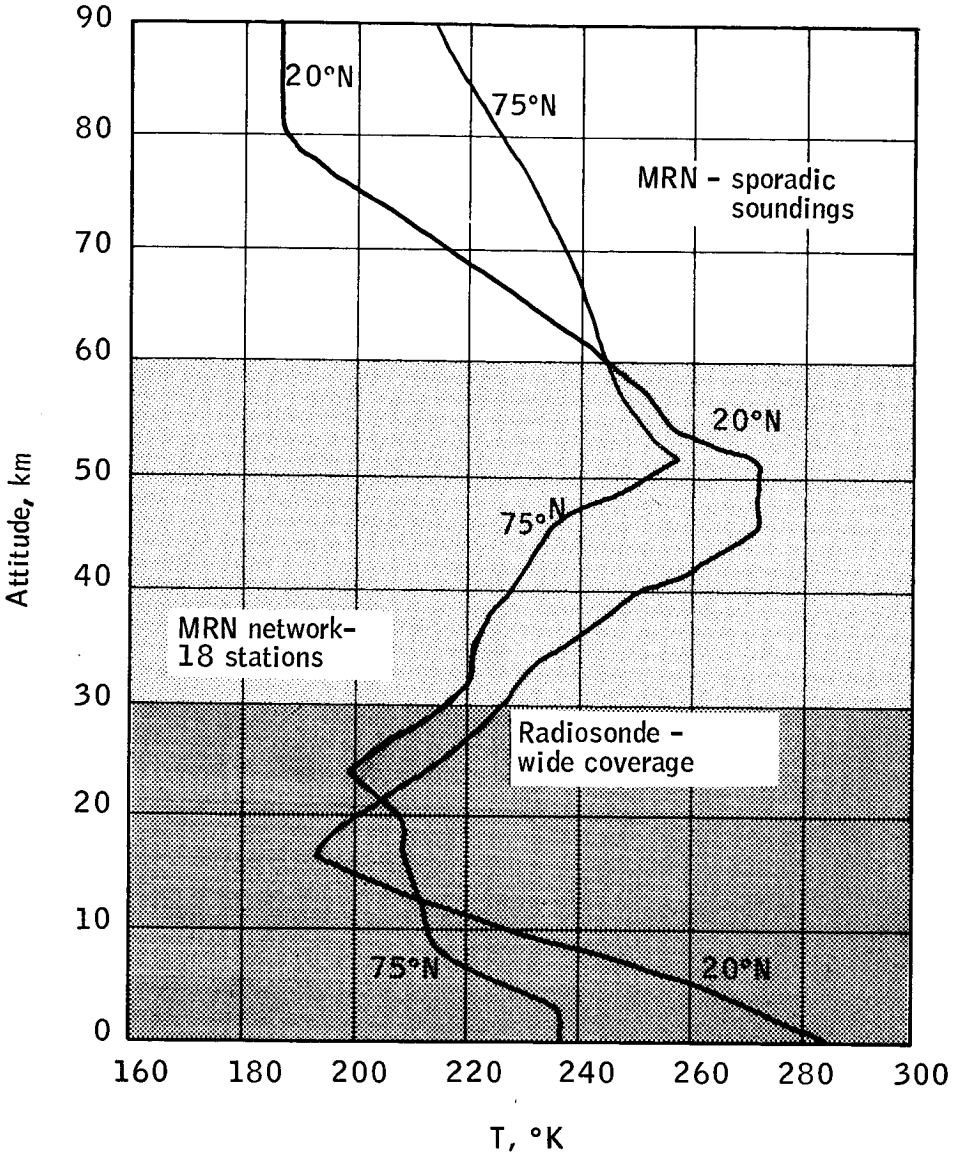

Figure 9. Density of Regularly Reported Meteorological Information

3. Small-scale temporal variability at three locations in the Southern United States and Northern Canada - sampled at select periods when 3-day, 12-hour, and 4-hour time resolution could be obtained.

4. Temporal variability at a northern-latitude station during a case of true stratospheric warming - sampled throughout a 27-day period.

5. Large-scale climatological variability over North America and surrounding oceans - determined from seasonal statistics.

6. Individual temperature profiles from all over the world for comparison with the basic body of data - total of 46 profiles acquired from the Southern Pacific Ocean areas and Antarctica.

Figure 10 shows the location for each of the selected sets of temperature/pressure profiles. The total set of 1039 temperature profiles from these study cases represents the largest collection of profiles ever assembled systematically for horizon radiance studies.

Studies were conducted to estimate the accuracy of the temperature profiles chosen for the study. Component errors which were analyzed included those in the reported data, errors of grid-point interpolation from analyzed charts, errors of subjective interpretation of data, extrapolation errors, and tabulation errors.

PROFILE IDENTIFIERS

To account accurately for the implicit factors affecting the horizon radiance profiles, a profile identification scheme based on select identifiers was developed. Each profile embodies within it a large variety of information relating to

1. Significant features of the vertical temperature distribution (for example, temperature and height of the tropopause),

2. Associated meteorological conditions (for example, the large-scale atmospheric circulation regime within which the specific profile location occurs), and

3. Various circumstantial factors such as location, date/time, and topography (which help to explain why certain profile characteristics happen to occur).

The profile classification scheme developed provides a simple, quantified basis for describing each profile in terms of the many implicit factors related to profile variability.

Two classifications of identifiers were selected for the study - primary identifiers and reserve identifiers. Tables 2 and 3 list each respective

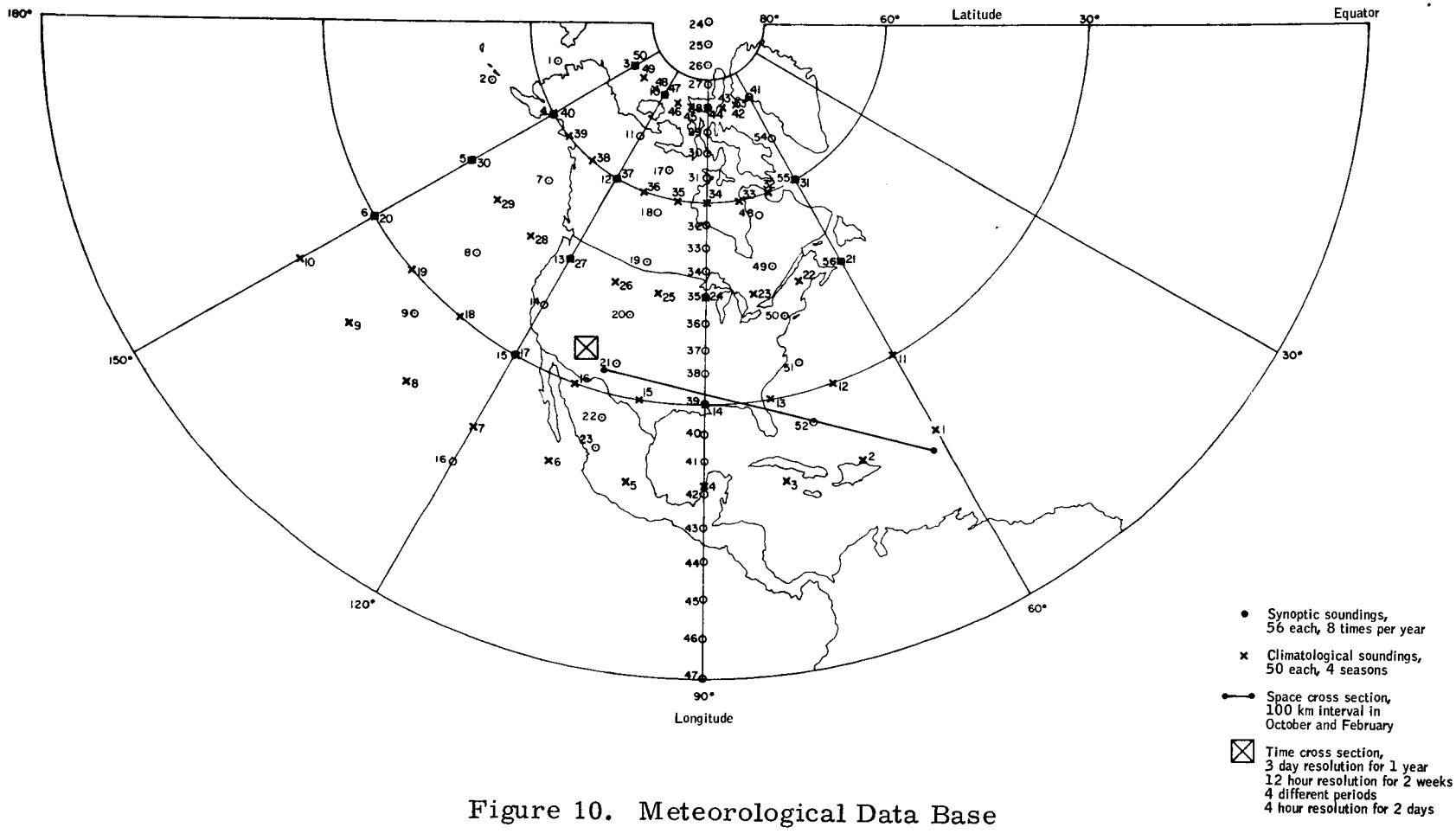

Figure 10. Meteorological Data Base

TABLE 2. - PRIMARY IDENTIFIERS

1. Latitude
2. Longitude
3. Date
4. Local time (day, night, polar day, polar night)
5. Topographic regime
   - 0) Sea
   - 1) Land < 0.5 km
   - 2) Land 0.5 - 1.5 km
   - 3) Land 1.5 - 2.5 km (Note: no profiles were determined at locations whose elevations exceed 2.5 km)
6. Temperature at 10 mb
7. Temperature at tropopause
8. Temperature at stratopause
9. Lapse rate from 500 mb to tropopause
10. Lapse rate from tropopause to 10 mb
11. Lapse rate from 10 mb to stratopause base
12. Circulation regime - location relative to profile

TABLE 3. - RESERVE IDENTIFIERS

1. Number of atmospheric profile
2. Season (Spring, Summer, Fall, Winter, Arctic Summer, Arctic Winter)
3. Atmospheric anomaly index
   a. Aleutian anticyclone
   b. Hurricane
   c. Stratospheric warming
4. Mesopause temperature when real data is available
5. 10-mb height
6. Tropopause height
7. Stratopause height
8. Confidence factor
   a. Real data
   b. Interpolated
   c. Extrapolated

identifier used. The primary identifiers are those that were considered in this study for statistical analysis in the data requirements study. These identifiers are the ones which proved to be most closely related to the temperature and pressure profiles and, therefore, were most highly correlated with the various locators used. Reserve identifiers were those which are proposed for future analyses, or for sorting purposes. These identifiers were not used in the statistical analysis of the total body of data.

CO_2 VARIATIONS

The concentration of atmospheric carbon dioxide is of considerable importance to the horizon definition problem. When scanning the horizon with a satellite-mounted detector sensitive to radiation in the 14 to 16 μ CO_2 band, the measured radiance emitted by the atmosphere is intimately related to the concentration of carbon dioxide. Thus, the observed horizon radiance profile would be affected by large variations in the concentration of carbon dioxide. Present knowledge was reviewed regarding the concentration of atmospheric carbon dioxide and its variation with time and space.

From analyses of CO_2 concentration observations on a diurnal, monthly, and annual basis, as well as variations occurring in altitude and latitude, a standard vertical profile of CO_2 concentration from earth's surface to 90-km altitude was obtained. Briefly, these observations indicate that the average concentration of carbon dioxide is about 0.0314-percent volume, i.e., 314 parts per million (ppm), above a height of one kilometer; the average deviations about the mean concentration is at all levels less than ±3 percent, and the concentration generally decreases slightly with height in the atmosphere. Estimates of the average deviation of CO_2 concentration about the mean values are indicated in Figure 11a. These results provide the basis for calculating the effects of CO_2 concentration and variability upon the horizon radiance profiles.

In order to investigate the effects of CO_2 variation upon horizon radiance profiles, a series of studies were performed in which radiance profiles were computed for various profiles of CO_2 concentration. First, a comparison was made between radiance profiles computed on the basis of (a) the mean CO_2 concentration profile, and (b) an assumed, average concentration of 314 ppm throughout the 0 to 90 km layer. No detectable differences between the two radiance profiles could be observed. Next, a series of CO_2 concentration profiles, based upon ± 2 percent, ±10 percent (see Figure 11b), and ±20 percent variations from the mean profile, were used to compute the corresponding horizon radiance profiles.

Sensitivity analyses of radiance profiles based upon ±2 percent and ±10 percent variations in the CO_2 concentration show an insignificant effect. Since a ±3 percent variation is shown by this study to be a representative value between 0 and 90 km, CO_2 variability may be safely neglected. A standard

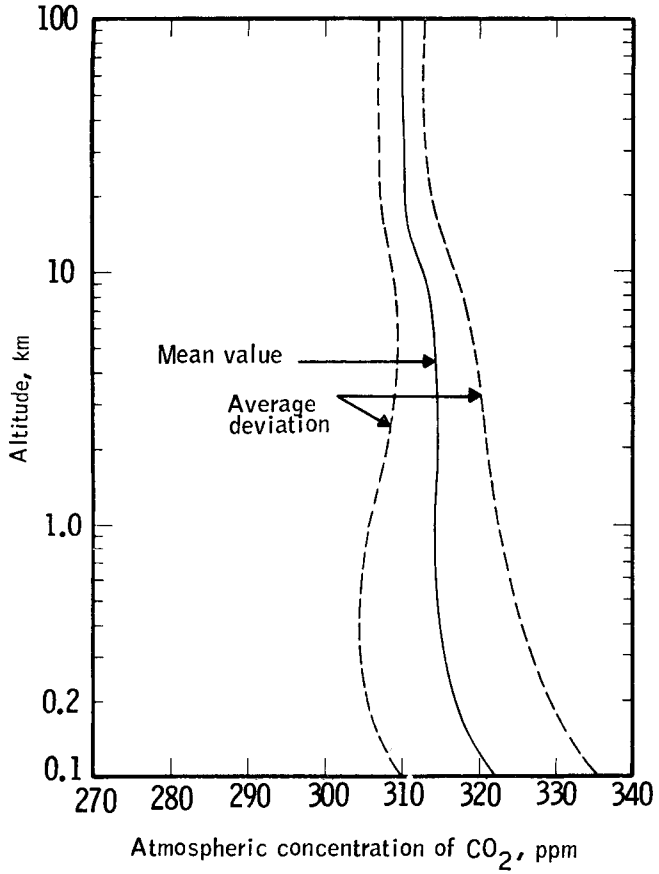

a. CO_2 variation 0 to 100 km ± 3%

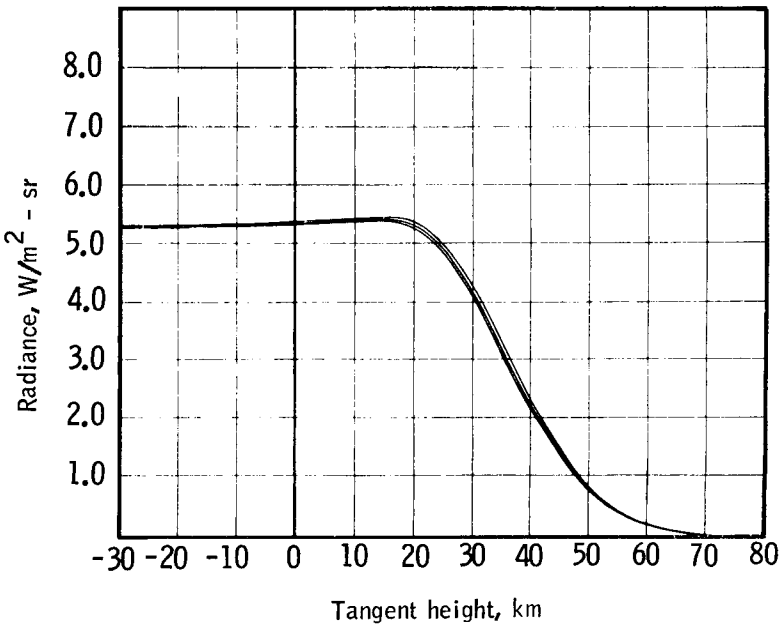

b. Radiance profile variation -30 to +80 km ± 10%

Figure 11. CO_2 Studies

CO_2 concentration of 314 ppm throughout the entire 0 to 90 km layer was, therefore, used as an explicit factor in the mathematical model, and no further attention was directed toward CO_2 variability as an implicit factor.

CLOUD EFFECTS

Cloud effects were studied to provide a body of background information relating to cloud characteristics and frequencies of occurrence and to evaluate the effect of cloudiness upon the determination of horizon radiance profiles.

The highest clouds, as observed by radar, occur in severe thunderstorm situations in mid-latitudes, in the intertropical convergence zone in the tropics, and in the heavy monsoon cloud build-ups over Southeast Asia. Although these high cloud conditions are somewhat exceptional, they provide a means for assessing the effects of severe conditions on the temperature profiles and, hence, the radiance profiles. Similar observations have been made using radiometric devices on satellites. For example, Tiros III window measurements have been used to deduce high cloud cover from the observation of very low temperatures over certain areas. The Nimbus I and II satellites also provided powerful tools for studies of cloud-top heights from blackbody temperature measurements in the atmospheric window.

Clouds may affect 15-micron horizon sensors in two ways: (1) by acting as cold radiation sources, and (2) by cutting out the CO_2 radiation emitted from below cloud-top level. Both these factors serve to reduce the radiance measured from a satellite. Higher and, hence, colder clouds (i.e., colder up to the tropopause temperature minimum) are expected to have the greatest effect in terms of radiance reduction. To determine the effects of clouds on radiance profiles as a function of nadir angles, a parametric study was carried out for six sample cases, based upon climatological profiles for January and July at 20, 45, and 70° N, consistent with the results of cloud-cover analyses.

The effects of clouds upon radiance profiles strongly depend upon the nadir angle. For nadir angles above 71.8 degrees (corresponding to tangent heights greater than -30 km), the percentage deviations in radiance do not exceed five percent for a typical case. Radiance due to cloud effect is shown to decrease from five to zero percent over the -30 to +20 km tangent-height range; at higher tangent heights there is no cloud effect at all. The results also indicate that the 16-km cloud-top altitude is the most significant level, below and above which lesser percentage deviations in radiance levels occur due to cloud effects.

ATMOSPHERIC PHYSICS AND PROFILE SYNTHESIS

Conversion of the temperature-pressure profiles, accumulated from meteorological soundings as discussed previously, represents the next task in the sequence of defining data requirements for a horizon definition program. It

was pointed out that prior work in calculating radiance profiles was restricted to a few average temperature profiles due to this lack of a sufficient body of data.

The meteorological data forms the basis for synthesizing horizon radiance profiles. Temperature profiles may be transformed into radiance profiles; however, analysis of the physics of the upper atmosphere must be conducted prior to application of the radiative transfer equation. In addition, certain numerical techniques must be examined before developing the comprehensive computer model for synthesizing profiles. Applying the meteorological data to the computational model, as modified by basic atmospheric physics, results in the formation of a vast set of horizon radiance profiles from which requirements for measuring the earth's infrared horizon may be determined.

Atmospheric Physics

An accurate mathematical representation of the earth's horizon radiance profile requires very detailed analyses of the physics of the upper atmosphere and an examination of the basic radiation equation for transfer of energy through the earth's atmosphere.

Radiation equation. -- The radiant energy emitted by the earth and atmosphere in the carbon dioxide band is expressed by equation (1a).

The integrand of this equation consists of two primary quantities, the source function and the transmittance function, each of which are functions of key atmospheric variables.

Source function: In thermodynamic equilibrium, the source function in the radiative transfer equation depends upon the atmospheric temperature and the frequency of the radiation. Thermodynamic equilibrium prevails in the atmosphere when the vibrational (and rotational) energy levels of the gas molecule remain populated according to a Boltzmann distribution determined by the local kinetic temperature. This is possible only if collisions are frequent enough to maintain such a distribution in spite of the radiative processes. The time required to establish a Boltzmann distribution by collisions is called the relaxation time and is inversely proportional to atmospheric pressure. If the relaxation time is short compared with the average lifetime of the excited levels, as in the lower atmosphere, a Boltzmann distribution can be maintained and thermodynamic equilibrium prevails. If the relaxation time is long, as in the upper atmosphere where collisions are less frequent because of low pressures, a Boltzmann distribution cannot be maintained. Under these conditions when a photon is absorbed by a molecule, it will be re-emitted (scattered) without passing into the kinetic energy of translation, and a state of absence of local thermodynamic equilibrium prevails. At these levels the source function must be calculated from considerations of molecular collisions and radiative transitions.

At low altitudes the molecular collision rate maintains a Boltzmann distribution of molecules in vibrational states in local thermodynamic equilibrium

with the rotational and translational energy. Here the source function must be the Planck function $B_\nu(T)$, by application of Kirchoff's Law.

Curtis and Goody (ref. 3) showed that the appropriate source function for the combined effect of collisional and radiative excitation has the form

$$J_\nu = \frac{\theta}{\theta + \lambda} B_\nu + \frac{\lambda}{\theta + \lambda} F_\nu \tag{3}$$

where

$$F_\nu = \frac{\int d\epsilon \int d\nu \, nk_\nu I_\nu}{4\pi \int d\nu \, nk_\nu} \tag{4}$$

where F_ν is the source function for incoherent scattering, n is the CO_2 number density at the considered altitude, k_ν is the absorption coefficient per molecule, and $d\epsilon$ is a small incremental solid angle. That is, the energy absorbed at the scattering point is related to the integral of the incident intensity I_ν over the fine structure of the band and the whole sphere of incident directions.

The current state of knowledge concerning experimental and theoretical values of λ, the vibrational relaxation time, and the consequent nonequilibrium source functions does not permit a conclusive result regarding the magnitude of the effects of absence of local thermodynamic equilibrium (LTE). The value adopted for the vibrational relaxation time λ is one which leads to an equilibrium source function of the form

$$J_\nu = \frac{\theta}{\theta + \lambda} B_\nu \tag{5}$$

The value of $\lambda(STP)$ at standard conditions of temperature and pressure is thus taken as

$$\lambda(STP) = 1.0 \times 10^{-6} \text{ sec}$$

even though the experimental values of $\lambda(STP)$ for CO_2 - N_2 collisions are as large as 1.0×10^{-5} second. The value of λ then becomes

$$\lambda(T_i p_i) = \lambda(STP) \frac{2 p_o}{(p_i + p_{i+1})} \frac{(T_i + T_{i+1})}{2 T_o}^{1/2} \tag{6}$$

with

$$p_o = 1 \text{ atm and } T_o = 273°K$$

The consequences of this choice on the horizon profile calculated from the 1962 Standard Atmosphere is depicted in Figure 12.

Transmittance function: Atmospheric transmittance is a complicated function of three integrated variables over the path of the radiation beam, i.e., optical depth, pressure, and temperature. The pertinent results of several CO_2 transmittance studies, as described immediately following, were assembled and fitted with an analytic function suitable for use in calculation of horizon radiance profiles.

Within the 15μ CO_2 band, transmittance varies with wavelength as a function of CO_2 concentration and atmospheric temperature and pressure. Pressure and temperature dependence is caused by the effects of pressure and temperature on the widths of the CO_2 absorption lines. Calculation of the shape of the absorption lines employs two theories of line broadening - Lorentz or collision broadening and Doppler broadening. At lower tangent heights the Lorentz line shape alone is applicable; in the upper atmosphere Doppler broadening must also be considered.

In the absence of broadening processes of any kind, the absorption and emission spectra of molecular species would consist of discrete lines of wave numbers in the electromagnetic spectrum. This would be the case since absorption and emission in an isolated molecule is the quantized energy difference between various vibrational and rotational states of the molecule or between excited states of the electrons. Only photons which add or subtract the right amount of energy to move the molecule from one discrete energy level to another are absorbed and emitted. However, a number of physical processes operate to perturb these energy levels, thus giving the lines a definable shape and permitting reaction with a range of photons whose wave numbers are close to the unperturbed discrete line.

The Doppler width depends on the velocity of the emitter or absorber and thus, by kinetic theory, on the temperature, and the effect is independent of pressure.

The method selected for computing the Doppler correction to the Lorentz transmittance of carbon dioxide applies a multiplicative correction factor calculated from theoretical results. The numerical values of the carbon dioxide properties required for this calculation are taken from the data of Stull, Wyatt, and Plass (ref. 4).

The form of the corrected Doppler transmittance is

$$\tau_{\nu\,cor} = \tau_{\nu}(1 - \text{"SUM Y"}) \qquad (7)$$

In this expression τ_{ν} is the spectral transmittance based on the Lorentz line shape only. The correction factor (1 - "SUM Y") is a function of the spectral interval, the optical path, and the temperature.

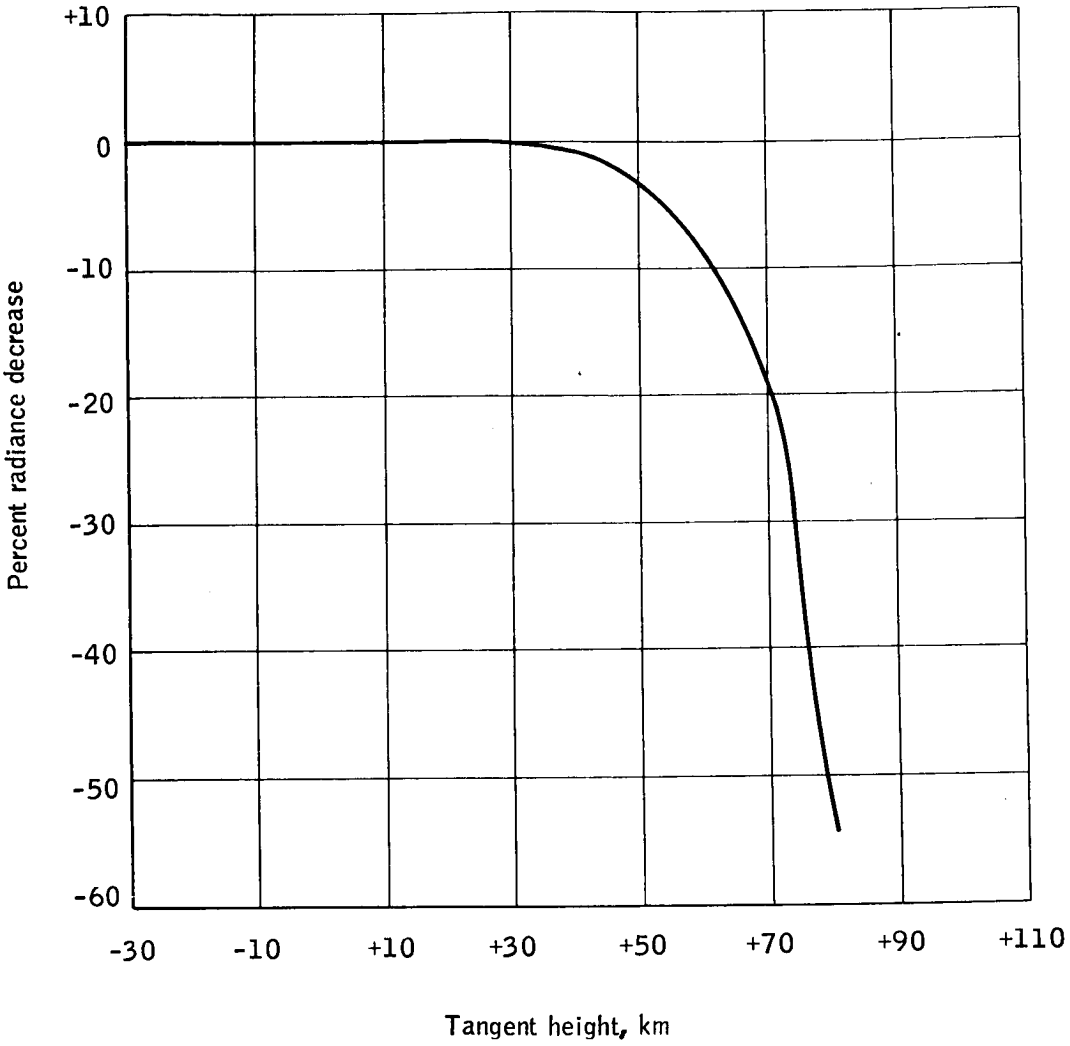

Figure 12. Percentage Effect of the Absence of LTE on the 1962 Standard Atmospheric Horizon Profile

During the period of development of the computer capability for synthesizing horizon profiles corrected for the effect of Doppler broadening, experiments conducted included comparison of horizon profiles with and without the Doppler correction. Typical of these results is the comparison between two such curves for the 1962 Standard Atmosphere shown in Figure 13.

In this study, transmittance tables resulting from previous studies were consulted to obtain transmittance values. The combined data, tabulated for homogeneous paths and for nonhomogeneous atmospheric paths, provided a range of variables suitable for use in this study, although either source alone was insufficient.

The 15 micron CO_2 band was divided into 10 spectral intervals to permit accurate evaluation of the relative value of the regions of different absorption properties within the total range selected. Interval sizes were based on the shape of CO_2 transmittance versus wave-number curves and the spectral resolution available in the tabulated data. Figure 14 shows the 15μ CO_2 band and the absorptivity as a function of wave number for different amounts of CO_2. The band is centered around the strongly absorbing region of the Q branch at about 667.5 cm^{-1}. Adjacent to the band center at lower and higher wave numbers are the P and R branches, respectively. The total spectral range considered for horizon profile studies extends from 600 to 725 cm^{-1}. The total spectral range is subdivided into 10 smaller spectral intervals by requiring that the absorption properties within each interval be similar. These 10 spectral intervals are listed in Table 4.

TABLE 4. - SPECTRAL DIVISION OF THE CO_2 BAND

Subinterval no.	Spectral interval, cm^{-1}
1	600 - 615
2	615 - 625
3	625 - 635
4	635 - 645
5	645 - 665
6	665 - 670
7	670 - 690
8	690 - 705
9	705 - 715
10	715 - 725

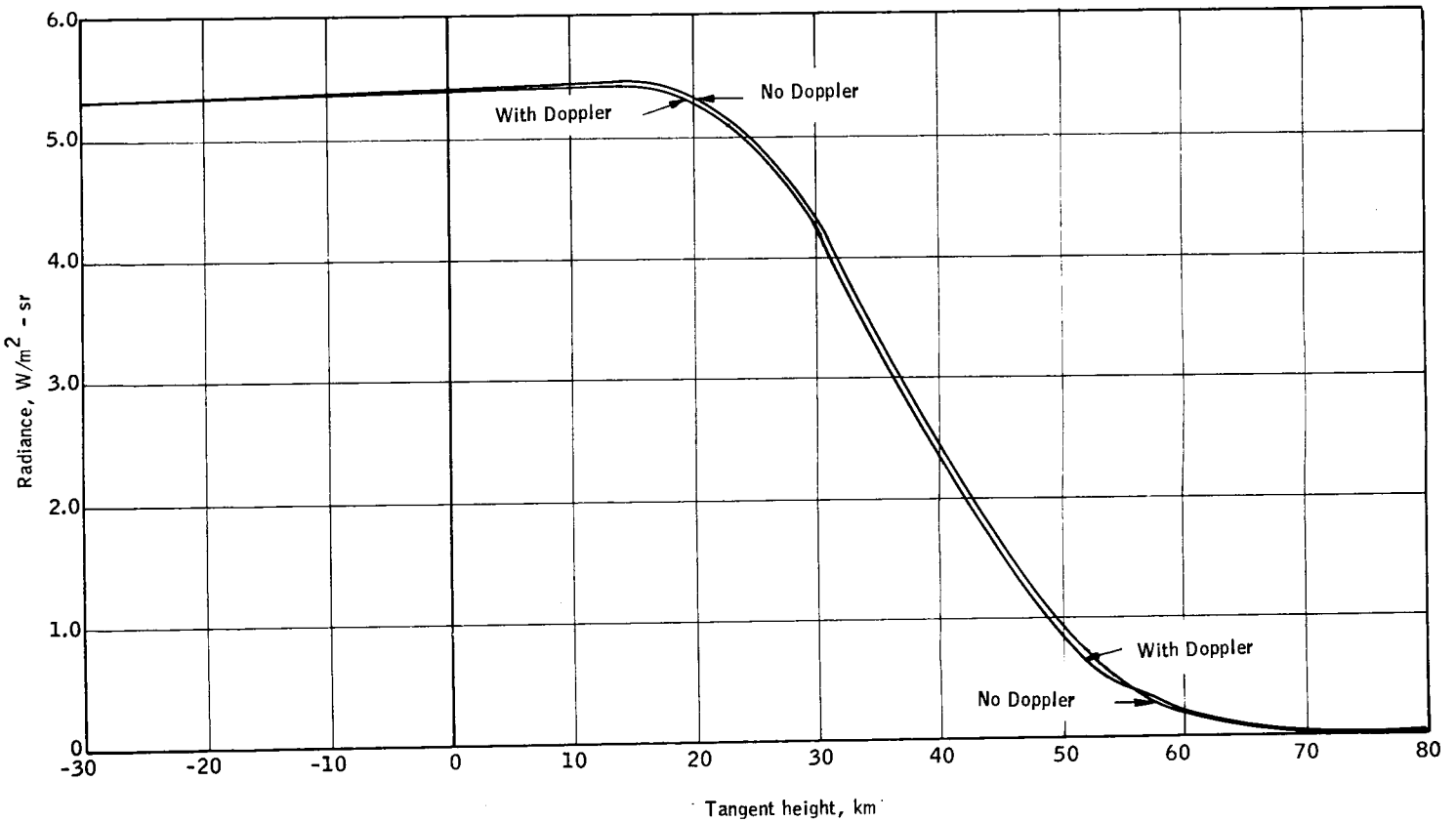

Figure 13. Qualitative Effect of Doppler Broadening

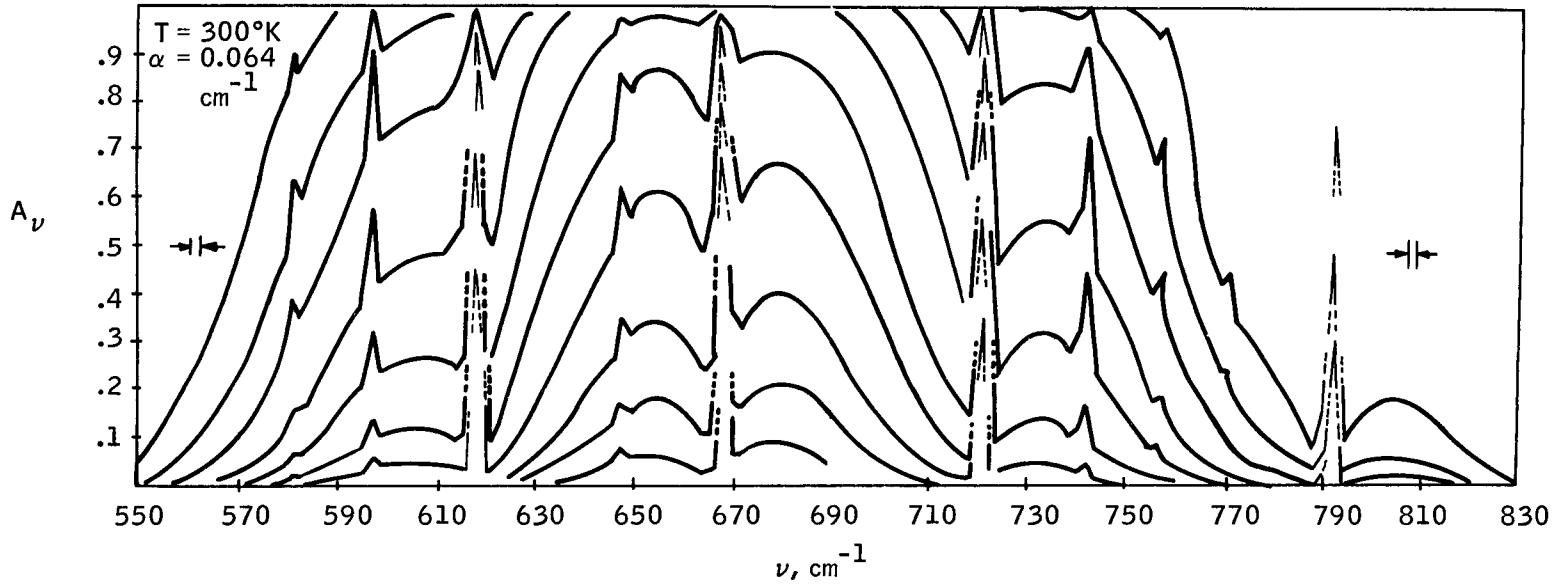

Figure 14. Calculated Absorption Spectogram of the 15μ CO_2 Band

Before making a final decision as to the spectral division of the CO_2 band, possible sources of transmittance data that are suitable for horizon radiance calculations must be considered. One pecularity of the problem is that rather large optical path lengths of CO_2 occur at rather low pressures. This is due to the slant angle at which the atmosphere is viewed. Any transmittance tables must include this combination of large path lengths and low pressures to be suitable.

The data available from Stull, Wyatt, and Plass are preferred for horizon profile applications. The spectral resolution available here was suitable for evaluation of the optimum spectral range in the vicinity of 15 microns for horizon sensing purposes; no other source offers comparable resolution. The ranges of pressure, temperature, and optical path for which transmittance data are provided are sufficient to eliminate the necessity for extrapolation in optical path and pressure which would be required with the use of other sources when calculating horizon radiance.

The latter of these benefits is realized because two types of data are used in the curve-fitting procedure. Data is tabulated giving the transmittance of path lengths homogeneous with respect to temperature and pressure and of slant paths through the 1962 Standard Atmosphere. The slant-path data was applied to advantage by computing the effective temperature, pressure, and optical path to which the tabulated slant-path transmittance applied. These values filled a void existing in the homogeneous path data and all other sources of data by specifying the transmittance for low pressures and small optical paths. The necessary range of temperature, however, is found only in the homogeneous path data.

Refraction. -- In computing the radiance for a given tangent height h, the effect of atmospheric refraction is considered. Inclusion of this effect causes the path of a beam of radiant energy to deflect from a straight line s, the path for a refractionless atmosphere (see Figure 15), to the path s', thereby changing the transmittance of the path from $\tau(s)$ to $\tau(s')$.

To compute the exact path for a refracted beam of radiant energy, the index of refraction of air η, which is a function of temperature and pressure, would have to be given in analytic form. However, knowledge of the pressure and temperature in the atmosphere is restricted to a finite array of points (p_i, T_i) at the altitudes z_i as shown in Figure 15, and thus an approximate method for computation of s' is used.

The atmosphere is divided into a set of n concentric spheres at the altitudes z_i whose pressures and temperatures are p_i and T_i, respectively; the pressure and temperature at the surface are p_{n+1} and T_{n+1}, respectively. Within the shell bounded by two adjacent spheres (e.g., the ith shell), the index of refraction of air η changes from $\eta(p_i, T_i)$ to $\eta(p_{i+1}, T_{i+1})$, where

$$\eta(p_i, T_i) = 1 + \frac{cp_i}{T_i}$$

and

$$c = 77.526 \times 10^{-6} \text{ °K-mb}^{-1}$$

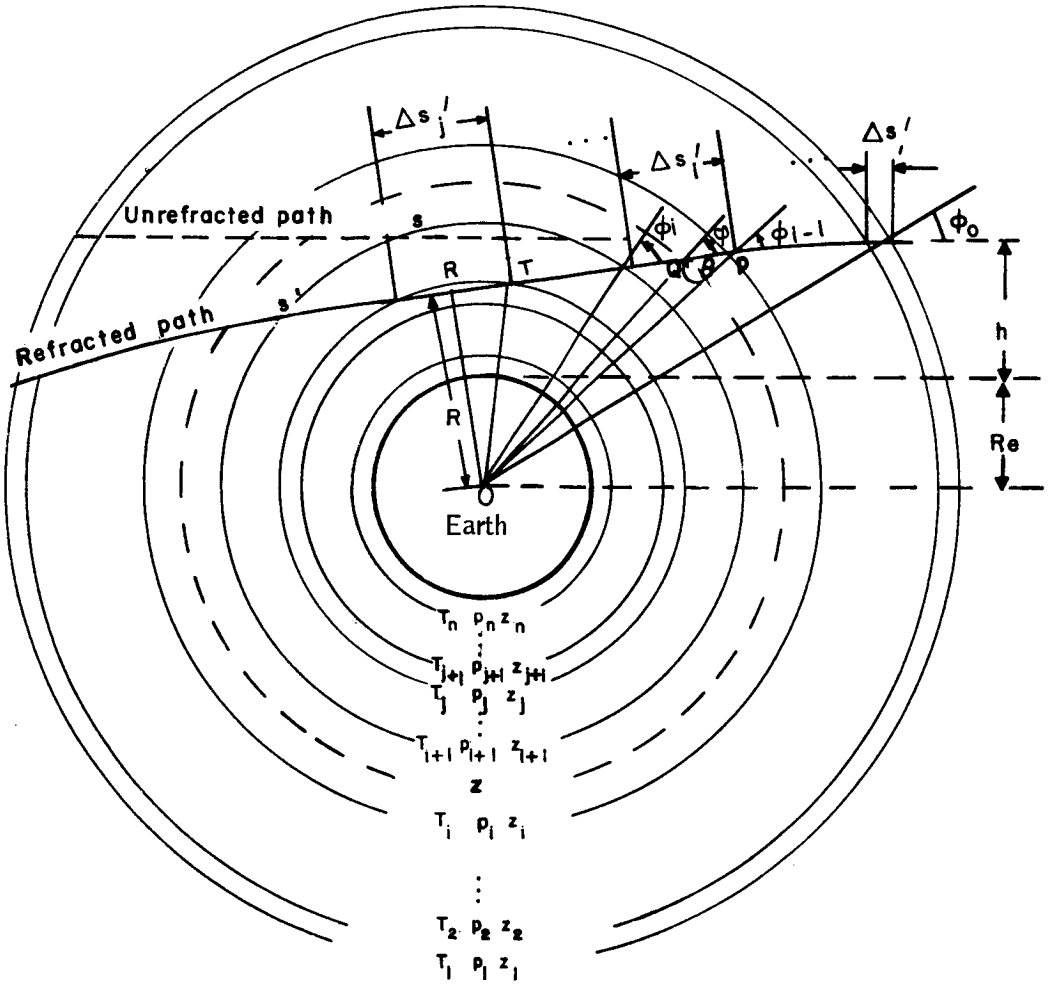

Figure 15. Atmospheric Model for Computation of the Path of a Refracted Beam of Radiant Energy for the Tangent Height h

This change is negligible compared to the overall change in η from 90 km, z_i, to the surface of the earth. Thus, for the ith shell (i = 1, 2, ..., n) the index of refraction is assumed to be constant and equal to

$$\bar{\eta}_i = 1 + \frac{c}{2}\left(\frac{p_i}{T_i} + \frac{p_{i+1}}{T_{i+1}}\right) \tag{8}$$

The path s' thus consists of the set of elemental segments $\Delta s'_i$ (i = 1, 2, ..., j) as shown in Figure 15. The path s' can either completely traverse a shell as the elemental segment $\Delta s'_i$ (i = 1, 2, ..., j-1) or partially traverse a shell as the elemental segment $\Delta s'_j$.

Profile Synthesis

Reduction of the complex mathematical descriptions of the atmosphere to a numerical model for the synthesis of radiance profiles required conduction of many auxiliary analyses. The closed-form integral description of the radiative transfer equation had to be rewritten in a form suitable for numerical computation. Attendant studies to define an atmospheric model compatible with numerical techniques and studies to determine the accuracy of these techniques were performed.

A secondary consideration was the numerical computation time required to convert a temperature-altitude profile into an equivalent horizon radiance-altitude profile. Analysis was performed to determine an accurate representation of the physics involved consistent with computational efficiency. In all cases, accuracy of the physical representation took precedence over any consideration of computational efficiency.

The studies consisted of determining the numerical integration form of the radiative transfer equation, numerical evaluation of the weighting function, atmospheric temperature-altitude model, tangent-height resolution, and numerical integration stop criterion.

Numerical evaluation of the radiation equation. -- To compute the radiance at each tangent height, a numerical analog to the mathematical model must be selected. The geometrical path length s is measured along a scan line. Three functions of s, the CO_2 optical depth u(s), the effective pressure $\bar{p}(s)$, and the effective temperature T(s), are computed using the following:

$$u(s) = \int_o^s c(s)\frac{p(s)}{p_o}\frac{T_o}{T(s)}ds \tag{9}$$

$$\bar{p}(s) = \frac{1}{p_o} \frac{\int_o^{u(s)} p(u)\, du}{\int_o^{u(s)} du} \tag{10}$$

$$T(s) = \frac{1}{p_o} \frac{\int_o^{u(s)} T(u)\, du}{\int_o^{u(s)} du} \tag{11}$$

where $c(s)$ is the mixing ratio of CO_2, p_o and T_o are the pressure and temperature at STP, and $p(s)$ and $T(s)$ are the pressure and temperature of each value of s.

Numerical evaluation of weighting functions. -- Given a tangent height, the value of the weighting function for the ith shell and kth spectral subinterval is

$$W_{ik} = \frac{\left(\Delta\tau_{\nu_k}\right)_i}{z_i - z_{i+1}} \tag{12}$$

where $(\Delta\tau_{\nu_k})_i$ is the change in τ_{ν_k} across the ith shell. The average weighting function for the ith shell for the complete spectral interval is

$$W_i = \frac{\sum_{k=1}^{\ell} W_{ik} \Delta\nu_k}{\sum_{k=1}^{\ell} \Delta\nu_k} \tag{13}$$

Shell structure studies. -- The number of shells used in radiance profile calculations was minimized without sacrificing computational accuracy while providing efficient computer utilization. Based on the results of the shell structure studies, approximately 65 atmospheric shells were used in the radiance profile calculations, the exact number being dependent on the altitude of the 10-mb level. The result is based on radiance profile calculations using atmospheric models of 29, 58, 116, and 203 shells. As the temperature data was supplied to the horizon profile synthesis task, it consisted of temperatures at the altitude of the 850, 700, 500, 300, 200, 100, 50, 30, and 10 mb-levels and, thereafter, at 3-km intervals beginning at the first integral multiple of three above the altitude of the 10-mb level.

Tangent-height resolution. -- As with the atmospheric shell model, the number of tangent heights at which radiance is calculated must be selected to prevent suppression of any perturbation in the profile caused by atmospheric phenomena or anomalies. Care was taken in selecting the atmospheric shell model to be certain that the calculation was capable of providing adequate resolution to the input data; this is the parallel step to be certain that the same resolution is given to the output data. A secondary criterion in the selection of tangent-height resolution was to minimize the number of tangent heights while maintaining the required resolution. This criterion was imposed to allow efficient use of the computer in the calculation of the 1085 radiance profiles.

The study was conducted by constructing temperature profiles containing anomalies of larger magnitude than expected in the actual input data and then determining the smallest tangent-height resolution required to demonstrate the effects of those anomalies on the radiance profile. Results showed that anomalies in the input produced significant perturbations in the radiance profile over a tangent-height range of from about 10 km to below 40 km and that a resolution of one km is required to produce and display the perturbations.

Consequently, to bracket this region of tangent heights, a resolution of one km over a range of tangent heights from 0 km to 50 km was selected. Outside this range,input anomalies caused less severe perturbations; thus, a larger resolution could be used as shown in the table below.

Tangent-height range, km	Resolution, km
-30 to -10	5
-10 to 0	2
0 to 50	1
50 to 60	2
60 to 80	5

Integration stop criterion. -- The final experiment in numerical analysis was the selection of a suitable criterion for terminating the integration of the radiative transfer equation as the contributions to the total radiance become negligible. Since the contribution of any shell, or integration step, is proportional to the change in transmittance over the interval on the path of integration, a criterion was developed based on the value of the transmittance. The transmittance can only decrease along the path of integration, and its minimum value is zero. Consequently, when the value of the transmittance becomes sufficiently close to zero, the integration may be terminated without changing the results.

SPECTRAL ANALYSIS STUDIES

The objective of the 15μ CO_2 band spectral interval study was to determine those spectral intervals within the 600 to 725 cm^{-1} band that enhance horizon definition and those that cause a deterioration in horizon definition. An analysis of selected climatological horizon radiance profiles, combined with instrument signal-to-noise considerations, leads to the selection of an optimum integrated band for horizon definition.

Following the specification of the total carbon dioxide spectral region to be considered and the recommendation for division of this region, extensive analyses were conducted to determine the variations in each of the spectral interval radiance profiles caused by the space and time variations over the surface of the earth. Analysis of these variations lead to a complete understanding of the profile variations for the total spectral interval and to the final selection of a spectral band on which to base requirements.

The basic data used in these studies consisted of twenty climatological profiles reflecting seasonal and latitudinal changes of atmospheric characteristics and the 1962 Standard Atmosphere in the case of the weighting functions.

These twenty profiles selected for the spectral analysis studies represent the typical space and time variations within the total body of data. The profiles are representative of January, April, July, and October at north latitudes of 20°, 30°, 45°, 60°, and 75°.

The studies completed to determine the horizon variability within any given spectral interval and the total spectral region included the calculation of horizon radiance profiles, weighting functions, and analysis of the effects of water vapor and ozone for each of the ten basic spectral intervals.

Based on these results, the radiance profiles for individual spectral intervals were summed in the combinations suggested to develop a final recommendation for the total range of spectral integration of the 15-micron horizon radiance profile. The effects of clouds were compared for the recommended spectral range and the total range considered.

The aforementioned studies led to the recommendation to utilize the 615 to 715 cm^{-1} band as optimum in increasing the energy available while decreasing the variations in the profiles. The wave number intervals studied and deleted are illustrated in Figure 16 where absorption in these wave bands is plotted as a function of wave number for two different partial pressures.

SUMMARY

The output of the horizon profile synthesis computer program consists of the radiance in each of the 10 spectral intervals from 600 to 725 cm^{-1} for the

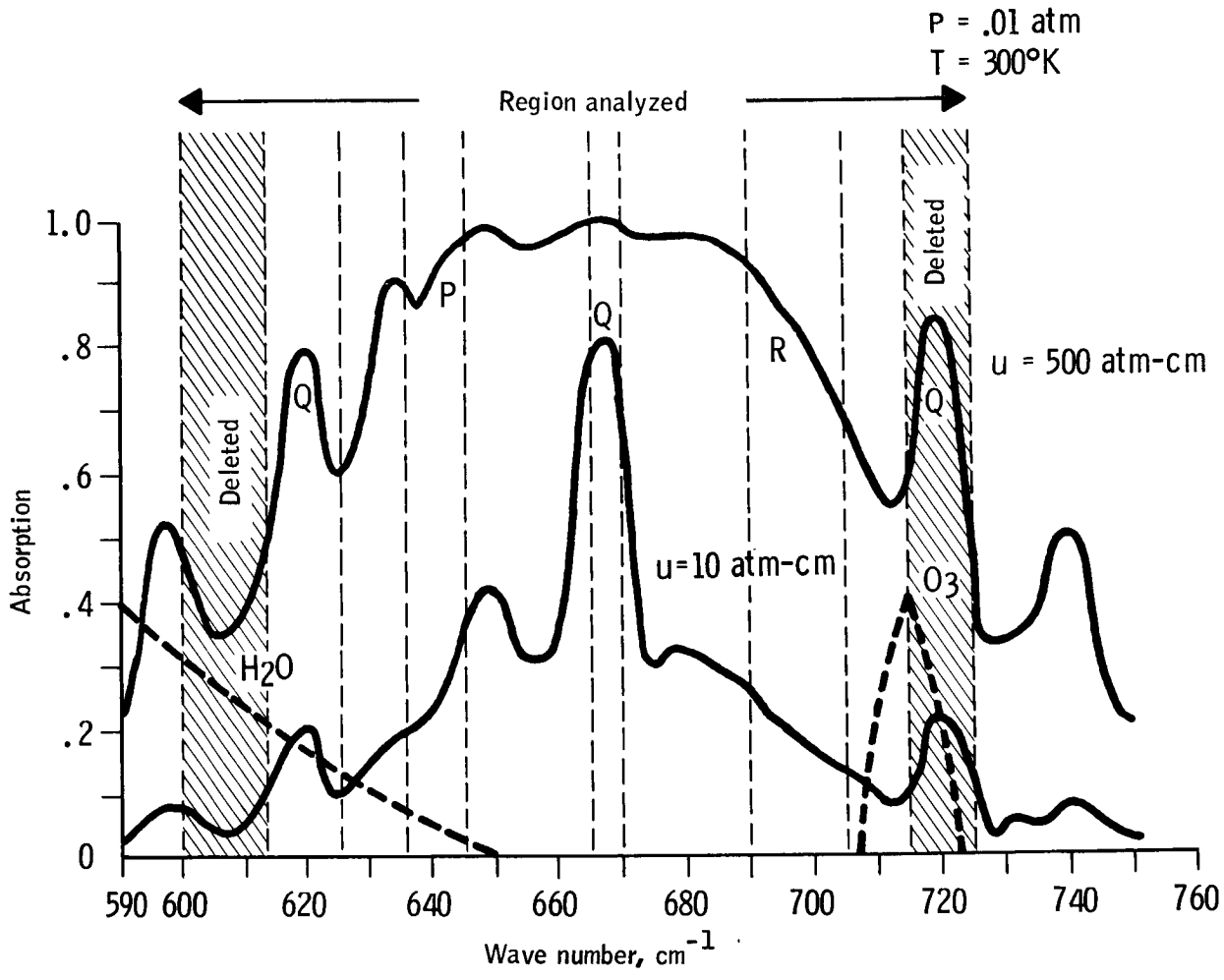

Figure 16. CO_2 Spectral Absorption

entire body of data analyzed. This includes all profiles of the synoptic, time cross section, space cross section, climatological, and auxiliary data; each case is numerically coded and stored on magnetic tape.

The eight center spectral intervals were summed to find the horizon radiance profile from 615 to 715 cm^{-1}. The result of this summation is also recorded on tape in a format suitable for analysis in subsequent study tasks. A line printer was used for visual display of this data; a digital listing and a printer plot of the 615 to 715 cm^{-1} profile is provided for each case. Input temperature and pressure data and the resulting output radiance profiles have been prepared for a total of 1085 cases.

During the studies related to the accumulation of the data base, the development of a computational model, and the profile synthesizer studies, a number of significant contributions to the state of the art were developed. These contributions include the development of a large body of empirical temperature and pressure data over the altitude range of 0 to 90 km and over a wide range of climatological, synoptic, spatial, and temporal conditions over the North American continent. Table 5 summarizes the synthesizer studies conducted and identifies their significance while Table 6 summarizes the characteristics of the resulting computational program.

The flexibility of the computational program is illustrated in Table 7.

TABLE 5. - SUMMARY OF PROFILE SYNTHESIZER STUDIES

Refraction	Include effects of atmospheric refraction. Integral is along refracted path.
Doppler broadening	Inclusion of molecular line absorption model for low pressures.
Thermal nonequilibrium	Compensate blackbody function for effect of insufficient molecular collisions at low pressure.
Weighting function study	Determination of radiance distribution as a function of altitude for a given tangent height.
Spectral interval study Cloud effects Reference profiles Water vapor Ozone Climatological profiles Synoptic profile statistics Weighting functions	Determine spectral interval giving maximum ratio of radiance/instability.
Shell number study	Minimize computer time by reducing number of shells.
Tangent-height resolution Lapse rate Spectral plots Cloud studies	Minimize computer time by reducing numbers of tangent heights.
Integration stop	Minimize computer time by preventing computation of negligible radiance.
Azimuth	Determine effects of viewing azimuth (determines validity of assuming constant atmosphere around data point).
CO_2 variations	Determine effect on profile of extreme variations in upper atmospheric CO_2.
Cloud studies	Determine effect of clouds on the radiance profile.

TABLE 6. - SUMMARY OF COMPUTATIONAL MODEL RESULTS

Parameter	Initial	Present
Tangent-height limit	60 km	80 km
Tangent-height resolution	5 km	5, 2, 1 km
Wave band	625 to 725 cm^{-1} (13.8 to 16.0 μ)	615 to 715 cm^{-1} (14.0 to 16.3 μ)
Wave-no. resolution	25 cm^{-1} (0.55 μ)	5 to 20 cm^{-1} (0.1 to 0.5 μ)
Shell number	200	65
Transmissivity model	Wark	Plass/House
Molecular absorption model	Lorentz	Doppler/Lorentz
Thermodynamic nonequilibrium	No	Yes
Atmospheric refraction	Yes	Yes
Clouds	No	Yes

TABLE 7. - AVAILABLE COMBINATIONS OF COMPUTATIONAL OPTIONS

x - available
o - not available

	Clouds	Transmissivity gate	Refraction	Azimuth	Thermal equilibrium	Doppler broadening	CO_2 - Plass	CO_2 - Elsasser	H_2O - Elsasser	O_3 - Elsasser	Weighting functions	Filters
Clouds												
Transmissivity gate	X											
Refraction	X	X										
Azimuth	O	X	X									
Thermal equilibrium	X	X	X	X								
Doppler broadening	X	X	X	X	X							
CO_2 - Plass	X	X	X	X	X	X						
CO_2 - Elsasser	X	X	X	X	X	O	O					
H_2O - Elsasser	X	X	X	X	X	O	X	X				
O_3 - Elsasser	X	X	X	X	X	O	X	X	X			
Weighting functions	O	X	X	O	X	X	X	X	X	X		
Filters	X	X	X	X	X	X	X	X	X	X	X	

RADIANCE PROFILE ANALYSIS

Once the horizon radiance profiles are synthesized, two procedures are available for analysis of the profiles in preparation of establishing data requirements. The first technique uses a procedure called locator processing wherein the profile functions are reduced to a series of numbers, rather than a series of functions. The second technique, profile analysis, considers the entire profile for analysis. This involves a statistical analysis of the profile means and standard deviations for various input conditions.

Although profile analysis represents a valuable tool in understanding profile variations and potentially deriving radiance profiles, it is considered to be less useful than the locator concept for defining data requirements for horizon definition. Three major reasons account for this conclusion: computer numerical analysis of entire profiles is a complex and inefficient process; such analysis tends to suppress actual profile variations; and there is little relationship between this technique and methods for actual horizon profile measurement.

The locator concept was therefore adopted as the more useful analytical tool for analyzing profile variations leading to data requirements definition. Since locator processing is a simplified analysis technique, profile analysis is considered necessary to assure that proper locator operations are considered.

LOCATOR CONCEPT

In the locator processing technique, a "locator" was an operation performed on the horizon profile function to yield a number defined as the "indicated altitude". The primary purpose of these studies was to provide a means of statistically analyzing the body of radiance profiles which were synthesized during the program. Each locator was an analytical function which simulated the operation which may be carried out by some conceivable horizon sensor; however, the locator does not necessarily consider the actual mechanization of the sensor. Examples of locators are the altitudes at which 50 percent of the peak radiance occurs and the radiance at the inflection point in the profile. A large number of potential locators were identified, and the total set of synthesized profiles operated on these locators. The result gives a technique which allows analysis of the means and standard deviations of each locator to show the relative accuracy of each locator technique. Those locator techniques were selected which show the most promise of providing reasonable values for time series analysis.

There was an additional significant fallout from adopting the locator concept, i. e., conversion of the profile into numbers; various horizon sensor detection techniques operate in this manner to determine or define the radiance profile in terms of its different characteristics by operating on the profile with various rules to determine an indicated altitude. Also, the

uncertainity in the horizon for various horizon sensor techniques was determined. An extrapolation of this procedure would provide for a complete definition of horizon-sensor accuracy, including horizon-sensor uncertainity.

Numerous locators were identified and mathematically defined for use as a technique in statistical analysis of horizon-profile variations.

Three techniques were utilized in identifying locators: (1) a search of the literature was made to determine locators already identified at the beginning of the study; (2) new locators were identified by studying radiance profile characteristics; and (3) Barnes Engineering Company, a major horizon sensor supplier, was subcontracted to conduct an independent study to determine existing locators and to identify new locators.

The only constraint on identifying locators is that the particular characteristic used be determined from knowledge of only the radiance profile shape and amplitude and not of its position with respect to the mean sea level horizon. Where applicable, these characteristics also apply to normalized radiance, that is, to each radiance profile normalized to its peak value of radiance. Table 8 is a total list of locators defined for this study. Figure 17 is an example of a locator concept which uses a fixed radiance threshold to define the located horizon h_ℓ.

To determine the behavior of the located horizon with various input threshold constants in those locators which operate with input constants and to obtain estimates of the located horizon stability for those locators not requiring input constants, all locators on the master locator list which were not previously rejected were exercised in the locator processor on a subset of horizon profiles selected to give coverage over one year for latitudes from the equator to the North Pole. Twenty-three locators were used. Within those locators requiring threshold constants, 53 extra constants (or sets) were used, so that for each radiance profile processed 76 located horizons or the equivalent were calculated. In addition, means, variances, and maximum and minimum were calculated for each of the 76 different locators (or threshold constants).

Results of the locator experiments show that:

- Locators requiring input constants obtain the most stable horizon when input constants associated with higher tangent heights are used.
- Locators dependent on the altitude at which peak radiance occurs are not useful since the radiance profiles exhibit both limb brightening and limb darkening which causes a large variation in altitude of peak radiance; these locators are L9 to L12, L14, and L15.
- Locators based on derivatives of radiance are less stable than locators based on radiance or integrated radiance (including normalized radiance).

TABLE 8. - MASTER LOCATOR LIST

Locator		Inputs	Function defining h_ℓ (h_ℓ = located horizon)
L1	Fixed radiance	N(h), C_1	$C_1 = N(h_\ell)$
L2	Normalized radiance	N(h), C_2	$C_2 = \frac{N(h_\ell)}{N_m}$
L3	Integrated radiance	N(h), C_3	$C_3 = \int_{h_\ell}^{\infty} N(h)\, dh$
L4	Integrated normalized radiance	N(h), C_4	$C_4 = \frac{1}{N_m} \int_{h_\ell}^{\infty} N(h)\, dh$
L5	Slope	N(h), C_5	h_ℓ = largest $h<h$ ($N = 0$) at which $C_5 = \frac{dN}{dh}$
L6	Slope of normalized radiance	N(h), C_6	h_ℓ = largest $h<h$ ($N = 0$) at which $\frac{1}{N_m} \frac{dN}{dh} = C_6$
L7	Slope extrapolation	N(h), C_7, C_{7a}	$h_\ell = \frac{C_{7a}\, h(C_7) - C_7\, h(C_{7a})}{C_{7a} - C_7}$
L8	Slope extrapolation, normalized radiance	N(h), C_8, C_{8a}	$h_\ell = \frac{C_{8a}\, h(C_8) - (C_8)\, h(C_{8a})}{C_{8a} - C_8}$

TABLE 8. - MASTER LOCATOR LIST - Continued

Locator		Inputs	Function defining h_ℓ (h_ℓ = located horizon)
L9	Average radiance	N(h)	$h_\ell = h(\bar{N})$; $\bar{N} = \frac{1}{h(0) - h(N_m)} \int_{h(N_m)}^{\infty} N(h)\, dh$;
L10	Average normalized radiance	N(h)	$h_\ell = h\left(\frac{\bar{N}}{N_m}\right)$ $\frac{\bar{N}}{N_m} = \frac{1}{h(0) - h(1.0)} \int_{h(1.0)}^{h(0)} \frac{N}{N_m}\, dh$
L11	Radiance centroid	N(h)	Radiance centroid = N_{cg} $h_\ell = h(N_{cg})$ $N_{cg} = \frac{\int_0^{N_m} N\, h\,(N)\, dN}{\int_0^{N_m} h(N)\, dN}$
L12	Centroid of normalized radiance	N(h)	$h_\ell = h\left(\frac{N}{N_{m_{cg}}}\right)$ $\frac{N}{N_{m_{cg}}} = \frac{\int_0^1 \frac{N}{N_m}\, h\left(\frac{N}{N_m}\right) d\frac{N}{N_m}}{\int_0^1 h\left(\frac{N}{N_m}\right) d\frac{N}{N_m}}$

TABLE 8. - MASTER LOCATOR LIST - Continued

Locator		Inputs	Function defining h_ℓ (h_ℓ = located horizon)
L13	Mean between two slopes	N(h), C_{13}	$h_\ell = \frac{1}{2}(h_1 + h_2)$ h_1 = largest $h<h(0)$ at which $\frac{dN}{dh} = C_{13}$ h_2 = largest $h< h_1$ at which $\frac{dN}{dn} = C_{13}$
L14	Mean between slopes, normalized radiance	N(h)	$h_\ell = \frac{1}{2}(h_1 + h_2)$ h_1 = largest $h<h(0)$ at which $\frac{d}{dn}\left(\frac{N}{N_m}\right) = C_{14}$ h_2 = largest $h<h_1$ at which $\frac{d}{dn}\left(\frac{N}{N_m}\right) = C_{14}$
L15	Average altitude	N(h)	$h_\ell = h(N_m) + \frac{1}{N_m}\int_{h(N_m)}^{h(0)} N(h)\, dh$
L16	Altitude centroid	N(h)	$h_\ell = \frac{\int_{h(N_m)}^{h(0)} h\, N(h)\, dh}{\int_{h(N_m)}^{h(0)} N(h)\, dh}$
L17	Inflection point	N(h)	h_ℓ = largest $h<h(0)$ at which $\frac{d^2N}{dn^2} = 0$
L18	Two-color difference	$N(h, \Delta\lambda_1)$, $N(h, \Delta\lambda_2)$	h_ℓ = h at which $N_1 - N_2$ is maximum

TABLE 8. - MASTER LOCATOR LIST - Continued

Locator		Inputs	Function defining h_ℓ (h_ℓ = located horizon)
L19	Normalized integral	N(h), C_{19}	$C_{19} = \dfrac{\int_{h_\ell}^{\infty} N(h)\,dh}{\int_{h(N_m)}^{\infty} N(h)\,dh}$
L20	Radiance compensated integral	N(h), C_{20_a}, C_{20_b}	$h_\ell = h_1 - h_2$ h_2: $C_{20_a} = \frac{1}{N_m}\int_{h_2}^{\infty} N(h)\,dh$ h_1: $C_{20_b} = N(h_1)$
B1	Signal harmonics		Defined in reference 5
B2	Three-point slope extrapolation	N(h), N_1, N_2, N_3	$h_\ell = h(N_1) + \dfrac{[h(N_3) - h(N_2)]}{N_2 - N_3} N_1$
B3	Corrected slope extrapolation	N(h), N_1, N_2, N_3	$h_\ell = h(N_1) + \dfrac{h(N_3) - h(N_2)}{N_2 - N_3} \left[N_1 + f(N_p)\right]$

TABLE 8. - MASTER LOCATOR LIST - Concluded

Locator		Inputs	Function defining h_ℓ (h_ℓ = located horizon)
B4	Modified normalized radiance	N(h), $\frac{N}{N_{m_1}}$, $\frac{N}{N_{m_2}}$	$h_\ell = \frac{1}{2}(h_1 + h_2)$ $\quad h_1 = h\left(\frac{N}{N_{m_1}}\right)$ $\quad h_2 = h\left(\frac{N}{N_{m_2}}\right)$
B5	Modified inflection point	N(h)	$h_\ell = \frac{1}{2}(h_1 + h_2)$ h_1: $\frac{N'(h_1)}{N'_m} = -0.5$ and $\frac{dN'}{dh} < 0$ h_2: $\frac{N'(h_2)}{\lvert N'_m \rvert} = -0.5$ and $\frac{dN'}{dh} > 0$ where $N' = \frac{dN}{dh}$ and $\lvert N'_m \rvert$ = maximum magnitude of $\frac{dN}{dh}$
B6	Minimum curvature	N(h)	h_ℓ = largest h at which $\frac{d^3N}{dh^3} = 0$ and $\frac{d^2N}{dh^2} < 0$
B7	Maximum curvature	N(h)	h_ℓ = largest h at which $\frac{d^3N}{dh^3} = 0$ and $\frac{d^2N}{dh^2} > 0$
B8	Midpoint between maximum and minimum curvature	N(h)	$h_\ell = \frac{1}{2}(h_1 + h_2)$; $h_1 = h_\ell$ from B6 $\quad h_2 = h_\ell$ from B7
B9	Two-color normalized difference	N(h, $\Delta\lambda_1$) N(h, $\Delta\lambda_2$)	h_ℓ = altitude at which $\frac{d\Delta N}{dh} = 0$ $\Delta N(h) = N(h, \Delta\lambda_1) - N(h, \Delta\lambda_2)\left\lvert\frac{N_m(h, \Delta\lambda_1)}{N_m(h, \Delta\lambda_2)}\right\rvert$
B10	Modified two-color normalized difference	N(h, $\Delta\lambda_1$) N(h, $\Delta\lambda_2$)	$h_\ell = \frac{h_1 + h_2}{2}$ h_1 = h at which $\Delta N = 0.5\,\Delta N_m$ and $\frac{d\Delta N}{dh} > 0$ h_2 = h at which $\Delta N = 0.5\,\Delta N_m$ and $\frac{d\Delta N}{dh} < 0$ where ΔN_m = peak value of ΔN $\Delta N(h)$ = defined under B9

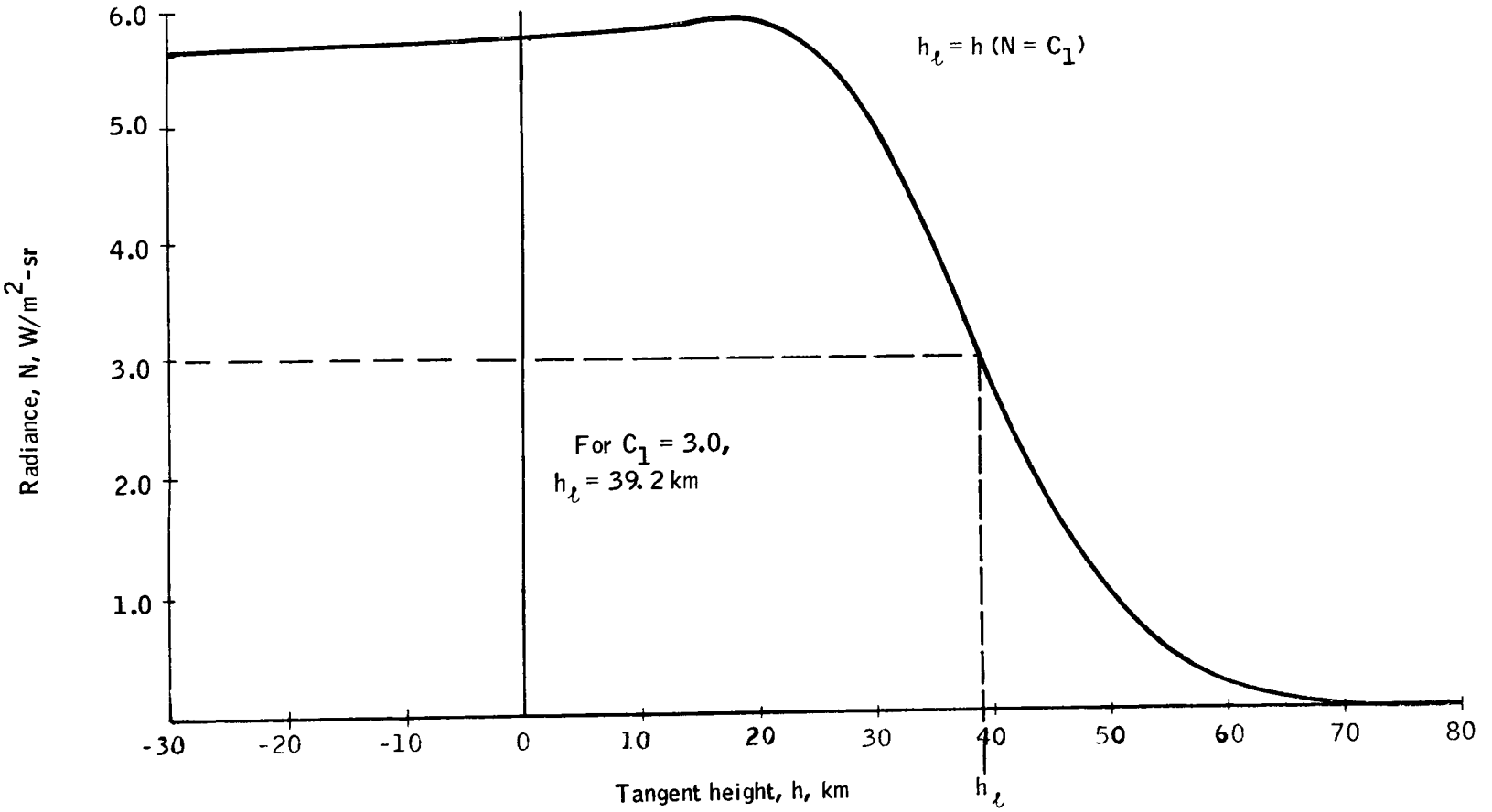

Figure 17. Locator L1 Fixed Radiance

- The smallest located horizon standard deviation, based on current state-of-the-art thresholds, is 1.20 km (0.025° from 300 n.mi., 560 km orbit) and is obtained using a fixed value of integrated normalized radiance of 2.5. Best stability obtainable with a factor of five improvement in state of the art is a standard deviation of 0.9 km, for several locators.

Based on experimental results and the previously discussed locator selection criteria, locators and input constants to be operated on by the statistical analyzers were selected to ensure that the horizon definition experiment collected data which could be used to determine capabilities of currently operational horizon sensors; locators reflecting mechanizations of these sensors were selected for time series analysis. Those locators which fit into this category are L1, L2, L3, L4, L5, and L7.

PROFILE ANALYSIS

This portion of the study was designed to establish the effects of all factors which cause significant changes in the magnitude and shape of the profile and thereby assure that the proper locators are used to represent profile variations.

The mathematical model used for such profile analysis was developed to display variations in the radiance profile over the entire tangent-height range. Two approaches were used: (1) statistical analysis, and (2) curve fitting employing both empirical and phenomenological methods.

The statistical analysis approach was enlarged to include the calculation and display of statistics not only of radiance as a function of tangent height but also of several radiance profile characteristics common to two or more locators as defined in the previous section. Input data available was analyzed to determine the effects of the various temporal, spatial, and atmospheric identifiers. A total of 839 different radiance profiles were arranged into 99 different sets and subsets, the resultant output being the tabulation and printer plots of statistics of six radiance profile characteristics for each.

The curve-fitting approach was used to determine a closed-form function which adequately fits the radiance profiles calculated by the profile synthesizer; coefficients and exponents of the closed-form function could then be analyzed to determine their spatial and temporal variations. Two methods were used in this effort.

In the first, the objective was to determine empirically a closed-form function of only one independent variable, tangent height. Functions were selected based on standard curve-fitting techniques, e.g., various polynomial forms, on experience from knowledge of different functional forms which result in curves resembling a radiance profile, and on a suggested technique of plotting particular characteristics of radiance versus

tangent height by transformation of variables until a recognizable form was obtained. Two functions representing the best compromise between simplicity and accuracy of fit were fitted to 20 climatological radiance profiles representing five latitudes and four seasons, and the coefficients were examined to determine their variation.

The objective of the other approach was to determine those few key atmospheric parameters having the strongest influence on radiance and develop a closed-form function, with the key atmospheric parameters being the independent variables, for calculating radiance profiles. A selected set of conditions was then used to calculate several radiance profiles by both the closed-form phenomenological function and by the profile synthesizer to obtain estimates of the accuracy of the closed form over a variety of conditions.

Diurnal Effects

The term diurnal is applied to the daily component of variation in radiance profiles. Studies of the diurnal variation resulted in the following significant results: (1) the maximum value of diurnal temperature amplitude is approximately 7°C, occurring throughout the year near 55 km in the equatorial region; (2) mean diurnal temperature amplitude at 45° N is 0.5° to 1.5°C less than that at the equator; (3) diurnal temperature amplitude at 75° N is considerably less than at lower latitudes with large seasonal changes from relative minima at the solstices to relative maxima at the equinoxes; and (4) the smallest diurnal temperature variations occurs in the polar regions at the solstices, where the peak variation probably does not exceed 1°C. Figure 18 illustrates the variation of the diurnal temperature during a 24-hour period.

Only a small sample of profiles was available which reflected these diurnal variations. Due to the extremely small sample size available, no conclusive results could be obtained regarding the diurnal variability. The above diurnal temperature variations study suggests, however, that diurnal effects in the radiance profile data should be deterministic from a sufficiently large sample. Table 9 shows the effects of the diurnal temperature variation on a typical low-latitude, summer radiance profile.

Seasonal Effects

The high-resolution Cape Kennedy and Fort Churchill profiles were used to obtain seasonal estimates at fixed latitudes and longitudes. Synoptic profiles were grouped by latitude bands to obtain estimates of the effect of latitude on seasonal variations. The following groupings were used:

Seasonal, low latitude effects, longitude fixed.

Seasonal, high latitude effects, longitude fixed.

Seasonal, high and low latitudes combined.

Seasonal, low latitudes, latitude and longitude varying.

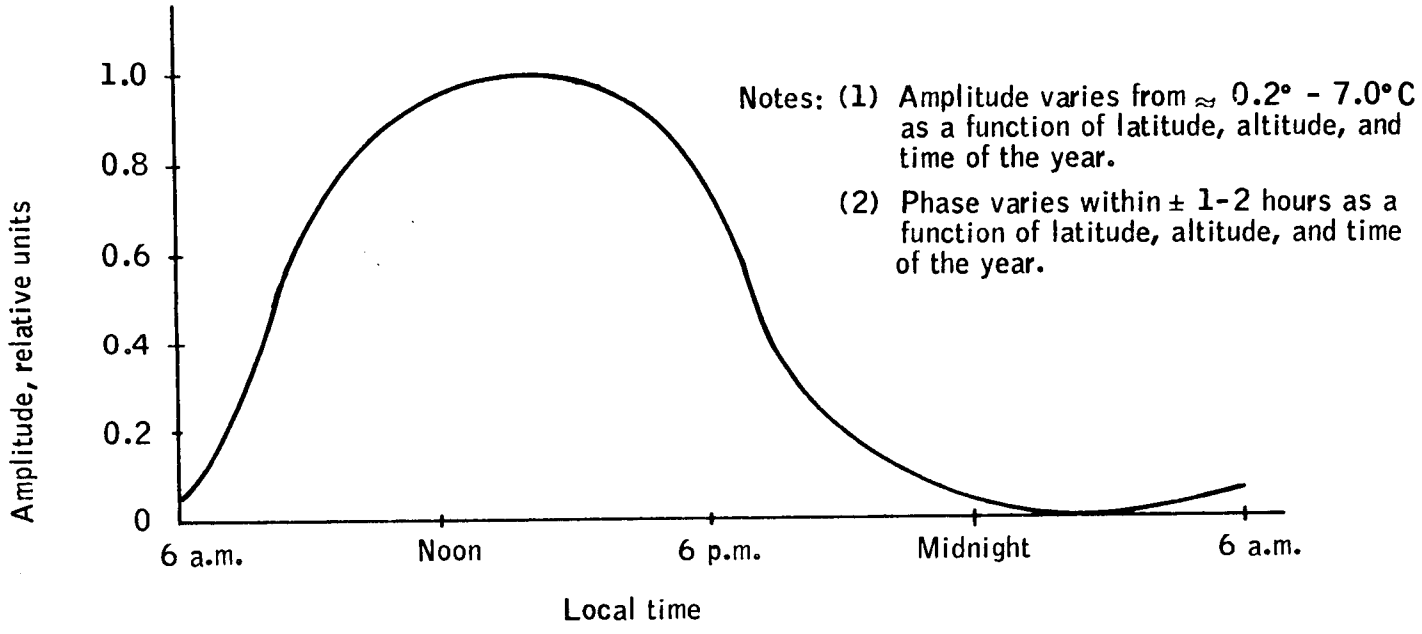

Figure 18. Typical Curve of Diurnal Temperature Variation

TABLE 9. - PERCENT RADIANCE DEVIATION PER 1°C TEMPERATURE ERROR VERSUS TANGENT HEIGHT

Temperature error identifier	Tangent height, km											
	-30	-20	-10	0	10	20	30	40	50	60	70	80
Profile 943:												
2°, 0-30 km	1.1	1.0	1.0	1.0	1.0	0.9	0.04	-	-	-	-	-
6°, 0-30 km	1.2	1.2	1.2	1.2	1.1	1.1	0.07	-	-	-	-	-
-6°, 0-30 km	-1.0	-1.0	-1.0	-1.0	-1.0	-0.9	-0.03	-	-	-	-	-
4°, 30-60 km	0.7	0.7	0.8	0.8	0.9	1.0	1.8	1.7	1.6	0.5	-	-
12°, 30-60 km	0.8	0.8	0.8	0.9	0.9	1.0	1.9	1.8	1.7	0.5	-	-
-12°, 30-60 km	-0.7	-0.8	-0.8	-0.8	-9.9	-1.0	-1.9	-1.5	-1.4	-0.4	-	-
7°, 60-90 km	0.01	0.01	0.01	0.01	0.01	0.01	0.02	0.03	0.1	1.5	3.0	5.1
21°, 60-90 km	0.02	0.02	0.02	0.02	0.02	0.02	0.02	0.04	0.2	1.6	3.2	6.7
-21°, 60-90 km	-0.01	-0.01	-0.01	-0.01	-0.01	-0.01	-0.01	-0.02	-0.09	-1.2	-2.0	-3.1
Profile 883:												
10°, 60-90 km	0.02	0.02	0.02	0.02	0.02	0.03	0.04	0.09	0.2	1.5	2.8	3.1
30°, 60-90 km	0.02	0.02	0.02	0.03	0.03	0.03	0.04	0.1	0.3	1.7	2.3	3.1
-30°, 60-90 km	-0.01	-0.01	-0.01	-0.01	-0.01	-0.02	-0.02	-0.05	-0.1	-1.3	-1.9	-2.0

When all latitudes and longitudes were averaged by season it is noted that radiance is highest in summer and lowest in winter, as expected, but that in spring radiance is higher than in autumn, as shown in Figure 19. The difference between the spring and summer means is greater than the difference between the fall and winter means. The standard deviation is significantly greater in winter than in other seasons, which do not exhibit consistent differences. At low tangent heights the standard deviation is lowest in autumn and increases in this order: summer, spring, and winter. At higher tangent heights, the standard deviation progressively increases from a low in spring to a high in winter.

Seasonal Effects With Latitude

Synoptic data were grouped into seasonal and latitudinal sets, averaged over longitude. From a listing of profiles by latitude, histograms for various latitude bands were determined. Latitude bands of 30 degrees were necessary to obtain a significant sample size. Seasonal differences are greater at higher latitudes. Lower latitudes do not exhibit the normal tendency for radiance to be higher in summer than in spring; radiance decreases in this order: spring, summer, fall, and winter. Radiance at lower latitudes is, in every season, greater than the overall average. Lower latitudes also do not exhibit the same variation in standard deviation as the total population; summer, rather than winter, exhibits the largest standard deviation. Middle and upper latitudes behave similarly to the total population.

Latitudinal Effects

Certain of the latitudinal effects were obtained with the aforementioned subsets. To estimate an overall latitudinal effect, synoptic profiles were grouped by latitude in 15-degree bands.

For all tangent heights, radiance decreases with higher latitudes. Above about 30 km the profiles in each latitude band are uniformly separated; below 30 km radiance in the polar region is significantly below radiance in any of the other latitude bands, where the difference is small. There is a definite trend for the standard deviation to increase with increasing latitude.

Longitudinal Effects

The synoptic radiance profiles were divided into longitude groupings by season in a manner similar to that by which latitude groupings were derived.

Although the differences are relatively small, there is a trend for radiance to decrease with eastward longitudinal displacement over the North American grid area. This longitudinal variation is more difficult to explain, in terms of a definite physical basis, than the latitudinal variation, which reflects a fundamental relationship in terms of the pole-equator distribution of incident solar radiant energy. Near the earth's surface and in the lower troposphere, significant longitudinal variations in temperature and other atmospheric parameters are a common occurrence, especially over large continents and

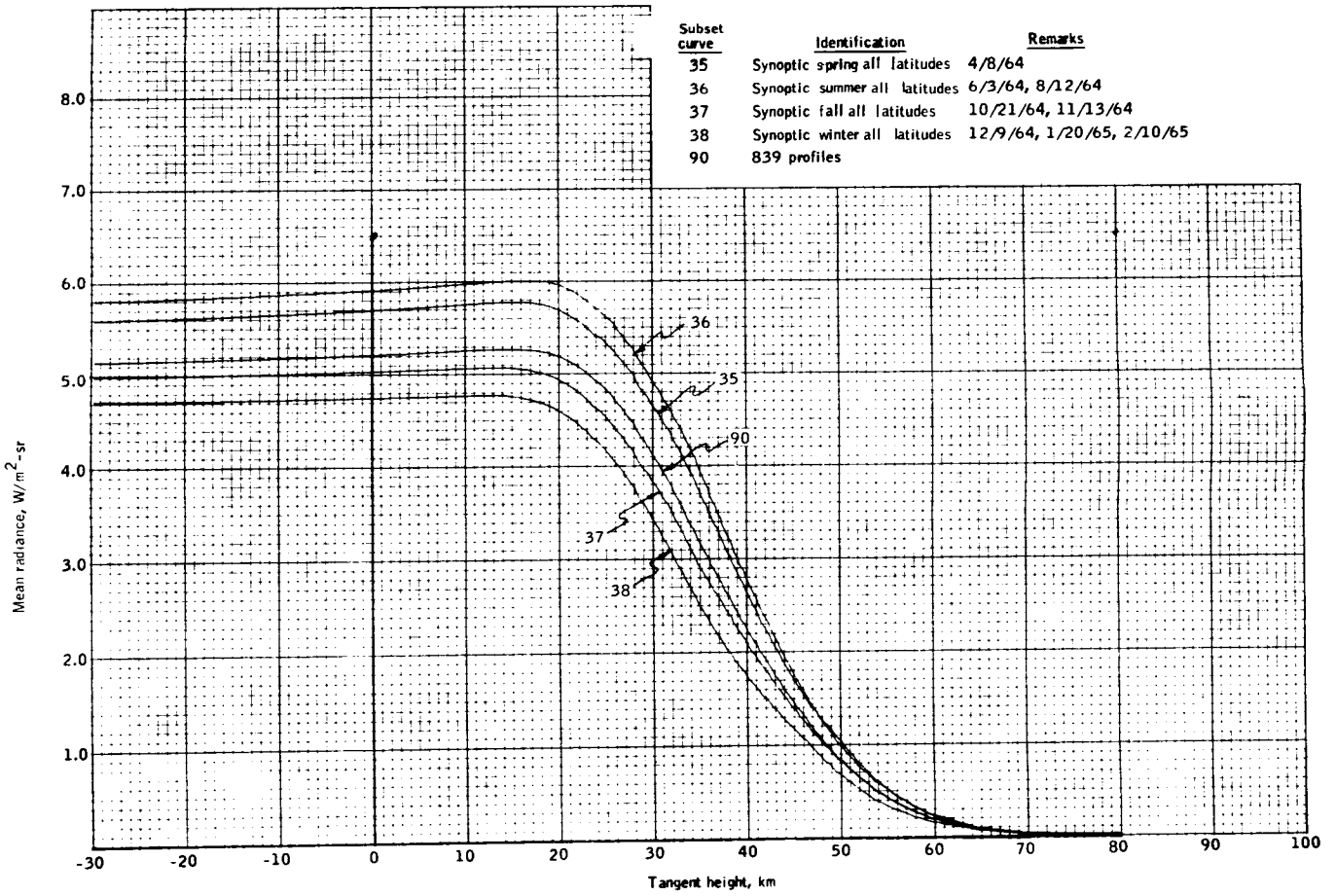

Figure 19. Mean Radiance versus Tangent Height, Seasonal Subsets

adjacent ocean areas. Vestigial indications of systematic longitudinal variations at stratospheric levels are entirely feasible and have been, in fact, noted in various meterological studies. Although the general sparseness of upper air data above 20 to 30 km makes close delineation of the longitudinal variation difficult, it is reasonable to conclude that it is a real effect, but relatively weak with respect to the latitudinal variation.

Atmospheric Identifier Effects

Atmospheric identifier effects were studied in terms of the following identifiers: 10 mb, tropopause,and stratopause temperatures; and temperature lapse rates from 500 mb to the tropopause, from the tropopause to 10 mb, from 10 mb to the stratopause.

Results indicate that radiance does not exhibit systematic behavior with tropopause temperature, but standard deviation does show a definite trend to increase with increasing tropopause temperature. There appears to be a pronounced systematic effect with respect to the 10-mb temperature. Near peak radiance, radiance is almost linearly related tc temperature at this level. A similar relationship exists at other tangent heights. The 10-mb temperature is closely associated with limb brightening. At 210°K neither brightening nor darkening exists. Below that temperature limb darkening occurs; above that temperature limb brightening becomes more pronounced with increasing temperatures. Standard deviation behaves erratically with 10-mb temperature.

There is a suggestion, although not conclusive, of a possible trend of increasing radiance with increasing stratopause temperature. Standard deviation does not exhibit systematic behavior with stratopause temperature.

Radiance may be nonlinearly related to the 500 mb/tropopause lapse rate and the 10 mb/stratopause lapse rate. Radiance changes from one lapse rate to the next in successively larger increments. No systematic variation of radiance with tropopause/10 mb lapse rate was found. Only tropopause/10 mb lapse rate was found to affect radiance standard deviation, the standard deviation decreasing in decreasing increments as lapse rate increases.

Land/Sea Effects (Topographical)

All input data were identified as belonging to one of three land/sea categories or subsets-one being sea, the other two being land of varying surface height.

The results show that profile shape and magnitude is not significantly affected by either sea mass or land mass. Obviously, then, land masses of varying heights are not significant in either profile shape or magnitude.

CLOSED-FORM FUNCTIONAL REPRESENTATION OF RADIANCE PROFILES

The objective of this study was to identify and evaluate closed-form mathematical functions which could be used for generalized representation of 14 to 16 micron radiance profiles. A large number of different functions were considered in the study; a complete description of the study and its results is contained in the Part I study report (ref. 6). Of the techniques considered the most basic was a phenomenological function which served to relate the horizon radiance profiles to a limited number of input data for key atmospheric variables, e.g., temperature at select levels. Coefficients and exponents of this function could then, hopefully, be analyzed to determine their spatial and temporal variations and thereby provide another valuable tool for the study of radiance variation factors. Once such a relationship was established, it could be used to estimate horizon radiance profiles for various atmospheric conditions based upon input values of select atmospheric variables. Advantages of such a technique are: (1) the equation of radiative transfer would not have to be integrated to calculate each radiance profile from the complete vertical profile; (2) insight is gained on the physical relationships between radiance and atmospheric variables; and (3) the inverse of such a technique would allow inferences about atmospheric structure to be made from observations of the horizon profile.

The general approach used was to derive an approximate form of the basic radiative transfer equation that applies to horizon radiance calculations. With the approximate equation and with the standard atmosphere structure and radiance profile as a reference, simple computations may be used to estimate the horizon radiance profile for any atmospheric structure.

The equation that forms the basis for estimating the horizon radiance profile for any atmospheric structure can be expressed as

$$N(h) = N_s(h) \times \frac{B\left[\tau(h')\right]}{B\left[\tau_s(h')\right]} \times \left[\frac{1 - \tau(h)}{1 - \tau_s(h)}\right] \qquad (14)$$

where B is the Planck function integrated over the 15μ CO_2 band, τ is the transmissivity of the band, T is temperature, $\tau_s(h)$ is the transmissivity of the entire path that is tangent to the earth's atmosphere at height h, subscript s refers to standard atmosphere values, and h' is a function of tangent height h. This equation can be further simplified for very approximate calculations of horizon radiance by assuming that h does not vary from atmosphere to atmosphere (an assumption that is fairly valid for a uniformly mixed gas like carbon dioxide) and that the ratio of the Planck functions for the 15μ band is equal to the ratio of the temperatures raised to the fourth power. The effective emitting heights $h'(h)$ can be determined once and for all from centroids of the weighting functions

computed for the standard atmosphere at various tangent heights. The standard atmosphere temperature at the effective emitting height h' is known, and the horizon radiance of the standard atmosphere $N_S(h)$ can also be established. Thus, the only variable input necessary to estimate the horizon radiance at the tangent height h for any atmosphere is the temperature at effective emitting height h'. The number of input temperatures required to specify a complete horizon radiance profile depends upon the tangent-height resolution desired and the variation of h' with tangent height. For example, $h'(h)$ is essentially constant for low tangent heights (< 20 km), thus allowing the specification of the part of the profile below 20 km tangent height with the use of a single input temperature. This technique was tested against a horizon radiance profile calculated by the profile synthesizer program, and agreement between the two profiles is remarkably good.

For more accurate estimates of horizon radiance the basic equation becomes

$$N(h) = N_s(h) \frac{B[T(h')]}{B[T_s(h')]} \frac{[1 - T_s(h - \Delta h)]}{[1 - T_s(h)]} \tag{15}$$

The above technique was tested on an extreme temperature profile, and based on the results the radiance profile for an atmosphere can be reliably estimated at ±5 percent of peak radiance. The test used as input data nine values of temperature between 20 km and 60 km and the value of the departure of the 10-mb height from that of the standard atmosphere. A good approximation to a radiance profile may be obtained with less input data. In particular, only four values of temperature (at 25, 30, 40, and 50 km) plus the 10-mb height departure should yield a reasonably accurate estimate of the complete horizon radiance profile.

The use of closed-form functions with phenomenological coefficients provides a promising means for conveniently representing horizon radiance profiles. However, for determing experiment data requirements, this method was adjudged to be inadequate, at least without further study and development.

STATISTICAL ANALYSIS

Analysis of the variations in horizon radiance profiles as a function of several variables is simplified by analyzing the variations of a set of numbers which represents some characteristic of the set of profiles (locators). Discussed here are the analytical techniques used to analyze the altitude variations at which the defined locators exists; also presented are the results of these analyses. These analysis techniques comprise the Time Series Analyzer (TSA) module. The TSA module is a functional block within the mathematical model of the HDS (refer to Figure 6).

The analysis objectives of the TSA module are to establish the significant and statistical variations of indicated altitudes for a variety of locators so that data requirements can be specified for a data measurement program.

The analysis approach used to isolate the systematic spatial and temporal variations from the nonsystematic or random variations is illustrated in Figure 20. Analysis philosophy leading to this particular approach was based on the need to establish qualitatively the relative significance of the effects of factors (latitude, longitude, time, etc.) on indicated altitudes and subsequently to determine quantitatively the significant systematic and random variations in space and time. The overall analysis approach and procedure used on the body of data (sets of indicated altitude and identifiers) can best be described in terms of a preliminary analysis, temporal variations analysis, and a spatial variations analysis.

Preliminary Analysis

The preliminary analysis consists of those techniques required to establish qualitative relationships between indicated altitudes and identifiers. The techniques include statistical parameter computations, correlation analysis, and analysis of variance. The temporal analysis consisted of curve fitting to variations in time and of statistical analysis of the residuals. Residual analysis was oriented toward determining significant spectral components not harmonically related to a fundamental one-year period. The analysis was accomplished by autocorrelation and power spectrum analysis techniques. Spatial analysis consisted of analysis techniques similar to those used in the temporal analysis.

The sample means and sample standard deviations of the synoptic sets of data are presented in Table 10. The locators and identifiers for which the analysis was performed are listed as 30 variables in the first column. In general, the results indicate that the mean values vary in season as would be expected and that the standard deviations are largest in the winter months. The simple correlation coefficient between pairs of variables was computed for the complete set of data (profiles 1 to 839), and the variables identified in Table 10. This analysis identified significant correlation between each pair of locators and several identifiers. The results are tabulated in matrix form in Table 11.

A preliminary examination of the data for significant factors was performed. Analysis of variance was used to determine the relative effects of factors on indicated altitudes and selected identifiers. Interactions between factors were also determined. A review of the list of identifiers indicated that a preliminary analysis of variance would be a three-way cross classification, the classes (factors) being those of latitude, longitude, and synoptic dates. Results indicate that longitudinal variations are less significant than latitudinal and synoptic temporal variations by an order of magnitude. Also indicated is the fact that latitudinal and synoptic temporal variations have relatively strong interactions, which is also true for longitudinal and synoptic temporal variations. These results imply that it is reasonable to seek

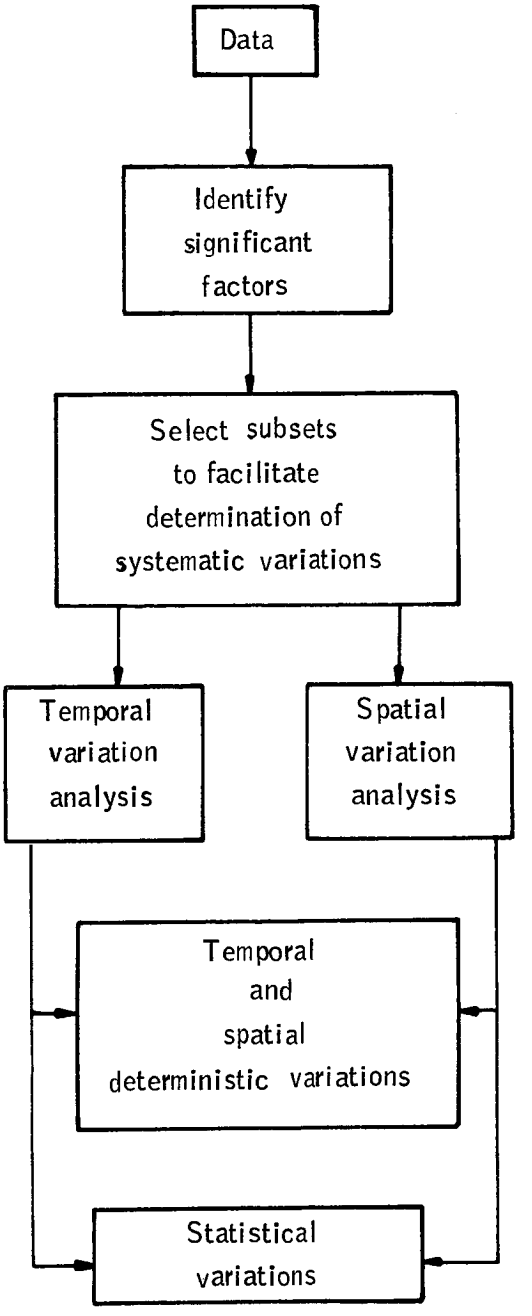

Figure 20. Analysis Approach Flow Chart

TABLE 10. - SUBSET STATISTICS

Statistic		Sample mean							Sample standard deviation							
Subset (a)	101	102	103	104	105	106	107	108	101	102	103	104	105	106	107	108
1.0 T10 mb	232.62	235.68	234.88	223.86	223.48	219.50	220.38	227.00	3.48	1.99	2.67	7.04	5.89	11.95	10.01	8.37
2.0 T tropo	211.66	214.66	213.74	209.71	210.20	212.14	209.30	209.55	10.82	10.11	11.05	9.27	9.88	9.52	8.93	10.04
3.0 T strato	283.49	277.32	271.89	276.59	277.93	266.89	266.32	274.59	3.71	3.32	6.98	5.43	6.24	5.15	10.88	6.07
4.0 LR_1	-5.44	-6.50	-6.13	-5.05	-5.44	-5.34	-5.04	-5.40	1.74	1.11	0.90	1.71	1.58	2.07	1.95	1.54
5.0 LR_2	1.03	1.20	1.29	0.97	0.92	0.58	0.80	1.13	0.99	0.74	0.72	1.03	1.00	1.18	0.98	0.99
6.0 LR_3	2.68	3.48	2.48	2.76	2.53	2.36	2.46	2.65	0.54	0.58	0.34	0.46	0.28	0.42	0.42	0.32
7.0 L1 (0.2)	61.35	61.86	60.95	59.95	60.24	58.40	58.45	59.28	0.37	0.27	0.73	1.15	0.59	1.36	1.71	1.57
8.0 L1 (1.0)	50.72	50.60	50.03	48.22	48.71	45.22	46.00	47.82	0.35	0.51	0.97	1.79	1.05	3.10	2.97	2.09
9.0 L1 (2.0)	43.67	44.75	43.20	40.71	40.91	36.77	37.84	39.96	0.83	0.53	1.54	2.66	1.67	3.70	3.80	3.18
10.0 L1 (3.0)	38.6	40.51	38.47	34.91	35.09	30.86	31.32	34.15	1.23	0.58	1.44	2.93	1.85	4.83	4.79	3.31
11.0 L2 (0.06)	57.96	58.04	57.61	57.44	57.69	56.19	56.24	56.71	0.22	0.18	0.46	0.93	0.57	0.75	1.18	1.17
12.0 L2 (0.3)	45.13	45.40	44.79	43.97	44.34	41.40	42.31	43.66	0.81	0.32	0.50	1.62	1.16	2.24	2.35	1.91
13.0 L2 (0.5)	39.10	40.11	38.69	37.38	37.58	34.86	35.53	36.90	1.16	0.60	0.57	2.16	1.61	2.37	2.34	2.02
14.0 L2 (0.7)	33.48	34.68	33.80	31.75	31.80	29.64	30.14	31.52	1.82	0.85	0.53	2.22	1.60	2.96	2.38	1.69
15.0 L2 (0.95)	23.71	24.34	24.09	22.32	22.29	20.76	21.10	22.34	2.47	1.24	0.81	2.57	2.27	3.56	2.98	2.45
16.0 L3 (1.5)	59.38	59.54	58.94	58.12	58.76	57.61	57.64	58.08	0.20	0.18	0.50	0.88	0.34	1.06	1.09	1.09
17.0 L3 (7.5)	49.79	49.94	49.26	48.09	48.52	46.16	46.43	47.54	0.33	0.40	0.78	1.28	0.65	1.83	2.04	1.67
18.0 L4 (0.50)	55.68	55.59	55.27	55.14	55.62	54.73	54.75	54.75	0.14	0.13	0.34	0.73	0.38	0.52	0.66	0.77
19.0 L4 (2.5)	44.85	44.65	44.34	43.98	44.40	42.48	42.85	43.62	0.32	0.22	0.43	1.01	0.68	1.25	1.50	1.25
20.0 L5 (-0.01)	69.05	69.37	68.94	68.10	68.25	66.19	66.16	67.21	0.19	0.15	0.44	0.95	0.46	1.69	2.09	1.71
21.0 L5 (-0.05)	56.68	58.75	58.28	57.20	57.48	53.53	54.58	55.99	0.33	0.63	0.92	1.51	0.89	3.61	2.69	2.12
22.0 L6 (-0.003)	66.24	66.51	65.88	65.60	65.80	63.67	63.64	64.46	0.25	0.28	0.54	1.13	0.70	1.15	1.85	1.67
23.0 L6 (-0.015)	54.66	52.95	53.46	58.83	52.99	49.13	51.04	52.79	0.32	0.89	0.61	1.52	1.83	3.51	2.58	1.56
24.0 L7 (0.75, 1.5)	59.23	58.64	58.25	57.78	58.16	55.74	56.11	57.13	0.64	0.70	0.76	1.02	0.58	1.87	1.86	1.15
25.0 L8 (0.06, 0.50)	60.53	60.49	60.19	60.17	60.43	59.10	59.07	59.41	0.26	0.20	0.48	0.85	0.61	0.55	1.04	1.08
26.0 L8 (0.3, 0.6)	53.95	53.40	53.32	53.24	53.92	50.66	51.78	53.18	0.59	0.61	0.86	1.44	1.35	2.06	2.60	2.05
27.0 L17	36.57	39.38	36.38	34.98	34.30	31.25	32.38	32.75	3.33	2.48	1.79	2.96	1.46	3.02	1.80	2.09
28.0 SL1	5.81	6.21	5.86	5.10	5.09	4.69	4.71	5.02	0.22	0.30	0.47	0.34	0.18	0.54	0.54	0.51
29.0 SL2	0.0037	0.0045	0.0033	0.0020	0.0020	0.0007	0.0010	0.0024	0.001	0.0005	0.0008	0.0015	0.0009	0.0021	0.0016	0.0011
30.0 B2	59.05	57.97	57.85	57.10	57.62	55.23	55.64	56.72	0.91	0.62	0.80	1.07	0.58	2.17	1.99	1.15

[a] CODE
101 - April synoptic case
102 - June synoptic case
103 - August synoptic case
104 - October synoptic case
105 - November synoptic case
106 - December synoptic case
107 - January synoptic case
108 - February synoptic case

TABLE 11. - CORRELATION MATRIX, ρ x 100

	Variables	1	2	3	4	5	6	7	8	9	10	11	12	13	14	15	16	17	18	19	20	21	22	23	24	25	26	27	28	29	30	Sample mean	SD
1 0	$T_{10\ mb}$		-24	26	-38	67	-5	72	79	82	85	48	65	69	75	83	72	77	34	58	76	73	53	59	58	35	47	31	84	28	59	227.9738	8.3378
2 0	T_{tropo}			-6	11	-86	-16	-11	-22	-30	-24	-21	-45	-46	-47	-64	-9	-16	-21	-37	-17	-16	-21	-38	4	-10	-36	-10	6	-12	3	208.1367	9.4775
3 0	T_{strato}				-6	18	46	60	62	54	50	64	59	51	41	27	51	63	55	68	57	58	63	58	67	62	63	30	42	16	66	273.2229	7.5934
4 0	LR_1					26	-2	-27	-31	-32	-34	-19	-29	-29	-32	-38	-25	-30	-12	-25	-30	-31	-23	-25	-22	-16	-24	-6	-31	-47	-21	-5.3816	1.6920
5 0	LR_2						8	44	56	63	61	40	67	70	73	90	42	50	34	58	50	48	43	60	25	26	52	24	36	24	26	1.3241	0.9654
6 0	LR_3							30	29	33	28	38	43	43	33	13	23	29	35	42	24	25	36	31	20	32	40	39	15	10	17	2.6300	0.5568
7 0	L1 (0.2)								93	91	91	91	82	82	79	66	95	98	81	88	96	91	93	69	86	85	69	50	84	25	83	60.1471	1.3415
8 0	L1 (1.0)									97	95	82	91	89	87	77	87	97	68	92	95	94	85	85	84	71	78	51	84	28	85	48.5626	2.2276
9 0	L1 (2.0)										97	78	93	94	92	83	86	95	65	89	93	90	82	80	73	65	77	52	85	30	72	41.3993	3.0978
10 0	L1 (3.0)											74	87	91	92	82	86	94	59	84	93	90	78	77	75	61	66	55	89	30	74	35.9114	3.7219
11 0	L2 (0.06)												82	78	71	56	85	88	94	92	88	83	98	68	80	97	75	47	58	19	76	57.3184	0.9179
12 0	L2 (0.3)													96	91	80	76	88	72	96	85	85	83	88	66	69	90	50	64	26	65	44.1544	1.7855
13 0	L2 (0.5)														95	84	76	86	67	91	84	82	80	82	62	62	77	58	68	28	61	37.9308	2.1490
14 0	L2 (0.7)															88	75	84	60	85	82	80	74	79	60	55	66	57	70	29	60	32.4929	2.1997
15 0	L2 (0.95)																64	72	46	72	72	70	59	70	47	40	60	36	61	26	47	23.2653	2.5535
16 0	L3 (1.5)																	93	83	82	91	86	86	82	80	80	64	46	81	24	77	58.5755	0.8726
17 0	L3 (7.5)																		76	91	97	95	90	78	88	80	75	51	86	27	86	48.3069	1.5343
18 0	L4 (0.5)																			84	74	69	90	56	69	94	68	40	41	14	64	55.2685	0.5936
19 0	L4 (2.5)																				88	88	92	86	78	83	88	50	62	24	77	44.0113	1.0905
20 0	L5 (-0.01)																					93	92	75	85	80	71	49	83	26	83	68.0813	1.3463
21 0	L5 (-0.05)																						85	78	88	75	74	48	79	26	86	56.9505	2.2435
22 0	L6 (-0.003)																							71	82	95	75	48	62	24	78	65.3731	1.3065
23 0	L6 (-0.015)																								70	56	81	44	55	26	73	52.6438	2.1750
24 0	L7 (.75, 1.5)																									79	58	42	72	21	97	57.5098	1.4171
25 0	L8 (0.06, 0.50)																										68	36	48	18	74	59.9607	0.8324
26 0	L8 (0.3, 0.6)																											28	45	20	58	53.1006	1.7249
27 0	L17																												44	17	40	34.8248	3.4883
28 0	SL1																													28	71	5.3027	0.5570
29 0	SL2																														20	0.0025	0.0047
30 0	B2																															56.9889	1.4878

the deterministic variations of season first, latitude second, and longitude third if it can be determined that there is a deterministic trend in longitude. Because of the interactions, seasonal corrections must be determined separately for each latitude.

Temporal Analysis

A temporal analysis was then conducted on the Cape Kennedy one-year sequence and the White Sands Missile Range (WSMR) high-resolution time sequence. Trigonometric functions (sine and cosine) were selected based on the a priori knowledge of seasonal and diurnal periodicities. A fundamental period of one year was selected. Due to the equally spaced data values, the curve-fit technique was considerably simplified. Terms of the series are independent of each other, and thus, the series can be truncated after calculation of as many coefficients as desired without affecting the values of the coefficients. Therefore, those coefficients were calculated out to the 122nd term (every data point was fit) for the Cape Kennedy sequence, and then a test of significance was applied to the first 21 terms. The test of significance produces an F value which can be compared to a value obtained from a cumulative F distribution table. If the F value calculated is greater than the table value, then the coefficient is regarded as significant. On this basis, the trigonometric series was terminated at the point where the last significant term appears.

In cases where a large number of insignificant terms appear between significant terms, the last term is seldom included unless it very significantly reduces the mean-square error about the curve fit. The test of significance (99-percent confidence level) on the coefficients indicated that, as a general rule, coefficients of terms beyond the 13th term were of little significance. A further consideration used to select the number of terms to retain in the trigonometric series was to consider the mean-square residual after fitting to each term. The numerical value of the mean-square residual is an estimate of the inherent statistical variance σ^2 of the data about the fitted curve. For terms beyond the 13th, σ^2 decreased very little, which indicated that higher-order terms do not significantly contribute to determination of time variations.

The conclusion is that little can be gained in terms of reducing the mean-square error term by including more than the first 13 terms of the trigonometric series; that is, all the significant variation is contained in these first 13 terms. To confirm this observation, a power spectrum analysis was performed on the residuals of the sixth-harmonic curve fits to establish the strength of higher harmonics and frequency components not harmonically related to the basic one-year period. Results of this analysis confirmed that the residual contained low levels of frequency components above the 13th term of the curve fit. Correlation time associated with the residuals was noted to be approximately one week and thus corresponds closely to short-term random weather patterns.

Spatial Analysis

The spatial analysis consisted of curve fitting to determine significant variations in latitude and longitude of the synoptic time data and the WSMR-to-Antigua space series. The mathematical techniques are essentially the same as those used in the temporal analysis. Two curve fits were made to latitude variation. The first was a trigonometric series fit to the indicated altitudes as a function of latitude on the 90th meridian for each synoptic case. The second was a trigonometric series fit to the coefficients of the synoptic temporal variations of each grid point as a function of latitude along the 90th meridian. A trigonometric series was selected for the fit based on physical intuition and as a result of reviewing latitudinal plots along with the 90th meridian. Both of these curve fits used the nonuniform sampling, least-squares curve-fitting technique. The significant result of this analysis was that good fits could be made to the latitudinal variations of the time-fit coefficients with small uncertainty. This situation indicates that in a surface fit (time and latitude) the majority of the uncertainty can be allotted to the time-fit uncertainty. This allows the time statistics obtained at Cape Kennedy to be extrapolated in space since the space-fit uncertainty is small in comparison. This is the technique used to obtain better estimates of uncertainties at locations other than Cape Kennedy when determining sampling requirements.

The longitudinal variations are not as significant as those of time or latitude, as was seen in the preliminary analysis. However, reviewing the isopleths of indicated altitude lines indicates that there are longitudinal variations in the upper latitudes which appear relatively strong in the winter months. The precise form of these deterministic longitudinal variations cannot be determined; however, the relaxation of isopleths of indicated altitude lines in the upper latitudes during the summer months indicates a deterministic trend in time. On this basis, the data sampling requirements analysis takes this factor into consideration.

The trend of the indicated altitudes between WSMR and Antigua is primarily due to the change in latitude. The magnitude of change in indicated altitude for this space series is comparable to the latitudinal variation along the 90th meridian for the same latitude change and month. Since the change in latitude is small, a second-order polynomial curve fit was used to remove the trend.

After removing the mean and trend terms from the data, the residual was subjected to an autocorrelation and power spectrum analysis. The significant results are that the residuals are small, and, therefore, detection of any deterministic variations in this series, other than the latitudinal trend, would not significantly reduce uncertainty in the observed data. This further indicates that small-scale land-sea effects are negligible.

DATA SAMPLING REQUIREMENTS

Based on analysis of the synthesized data, an estimate was made of the spatial and temporal variations for a set of locators. These variations, and the uncertainty in the corrected indicated altitudes, are then the criteria on which data sampling requirements are based. The approach to obtaining data requirements from the results of the data analysis for a given locator is outlined in Figure 21. Space and time cells are obtained as a direct result from the estimate of the deterministic variations, and the estimate of the uncertainty associated with a space-time cell was used to determine how many samples are required in the cell. The uncertainty value assigned to a space-time cell was obtained by extrapolation of a best estimate of uncertainty calculated from a large body of data. The best estimate is that obtained at Cape Kennedy for the one-year time series. Extrapolation of the statistics of Cape Kennedy data to other locations was based on the trends of the less accurate estimates associated with the synoptic temporal variations.

The criteria used to establish how many samples are required in a space-time cell was to establish a 95-percent confidence interval for the uncertainty σ due to nature. The estimate of this uncertainty $\hat{\sigma}$ is obtained from the residual analysis, as noted earlier, and is used in establishing the confidence interval. It is σ which is extrapolated from Cape Kennedy to other latitudes and thus provides the means of extrapolating statistical sampling requirements to other latitudes.

Consideration was then given to the sets of data sampling requirements which correspond to the sets of locators used in the analysis. A final data sampling requirement was selected which will provide the most information without imposing impractical constraints on the mission.

After the spatial, temporal, and statistical sampling requirements had been established for the area covered by the data source map, considerations were given to the effects of azimuth and widening of the basic spectral interval on these requirements. The space-time cells identified were then extrapolated to the rest of the world. Stratospheric charts, Tiros data, and isopleths of indicated altitude were used as aids in the extrapolation.

Temporal and Spatial Cells

The time series analysis of the Cape Kennedy one-year sequence provided an estimate of the seasonal variations. Seasonal variations exceeding the sixth harmonic of the fundamental one-year period were found to be insignificant. Based on this determination and to satisfy frequency sampling requirements, the time cells were broken into 13 time intervals divided equally throughout the year. Further noted was that the correlation time associated with the Cape Kennedy sequence, after the deterministic adjustment, was on the order of one week. This result indicates that data sampling within time cells of 28 days should be spread throughout the interval to preclude excessive redundant samples being accumulated within a period of a few days. The diurnal data analysis did not provide sufficient conclusive results for determination

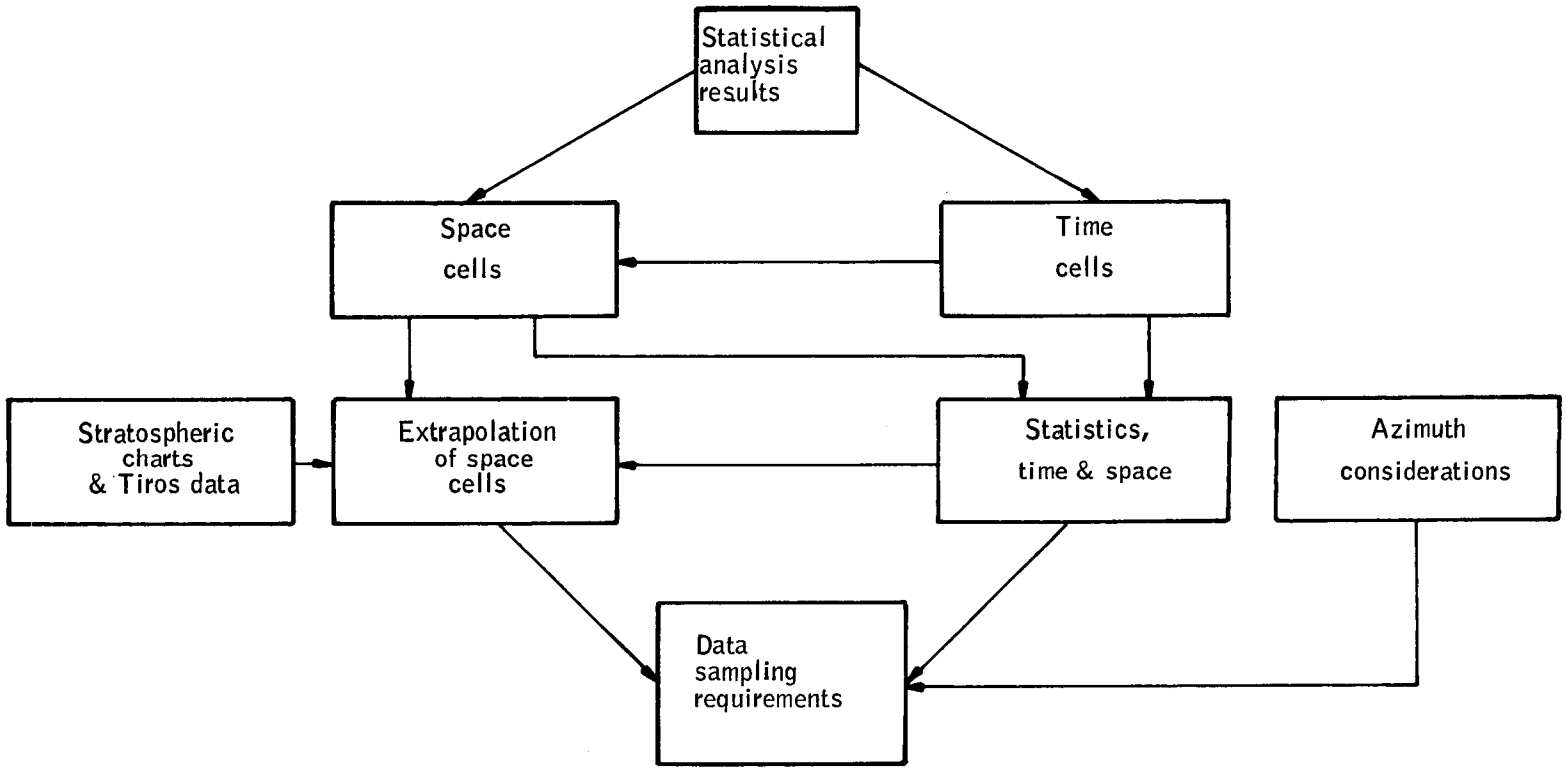

Figure 21. Data Sampling Requirements Analysis Procedure

of sample requirements. However, to assure that diurnal variations are included in the data and yet preclude excessive redundancy, two samples per cell per day, on the average, was utilized in configuring the total data requirements. This will provide some control over the diurnal effect, and better estimates of diurnal effects will be obtained.

Determination of spatial cells is based on the spatial analysis results. Latitude has a significant deterministic trend; however, longitudinal variations are for the most part nondeterministic. There are indications of longitudinal trends; however, the form of the fit could not be determined.

The criteria used to establish latitudinal cell resolution was interrelated with two factors:

- Number of coefficients required to fit to latitude
- Observation of seasonal variations as a function of latitude

A lower bound on the number of latitude intervals was selected on the basis of the number of coefficients required to determine a good fit to latitude. This assumed a priori that the data to be gathered will vary in latitude such that trigonometric functions can be fit with small error. If, in fact, the flight data cannot be fit as assumed, then there is the chance that it wasn't sampled with sufficient resolution in latitude to determine a new form of fit. Therefore, it was decided to determine the seasonal variations as a function of latitude and select latitude intervals based on amplitude quantization levels of indicated altitude. The level of amplitude quantization was selected to be smaller than the statistical temporal uncertainty. A basic latitudinal resolution of 10° was used for the study.

Statistical Sampling Requirements

The value of $\hat{\sigma}$ obtained from the Cape Kennedy one-year sequence analysis is a good estimate of the uncertainty associated with temporal variations. This estimate was extrapolated to other latitudes, using the residual statistics of the synoptic time curve fits as a guide. This extrapolation is illustrated in Figure 22. Locator L4 (2.5) was selected since it represented upper bounds of interest in the areas of state-of-the-art locators. Assuming that $\hat{\sigma}$ could be extrapolated uniformly in longitude (this assumption implied that a curve fit in latitude could be made equally good for all longitudes), then all space-time cells have an uncertainty $\hat{\sigma}$ upon which a confidence interval could be set. From Figure 22, it is shown that $\hat{\sigma}$ values of 0.5 and 1.0 km cover the range of uncertainties.

The 95-percent confidence interval on $\hat{\sigma}$, I_c, based on Chebyshev's inequality was found to be the following approximate expression:

$$I_c \cong \frac{3\hat{\sigma}}{\sqrt{N-1}} \tag{16}$$

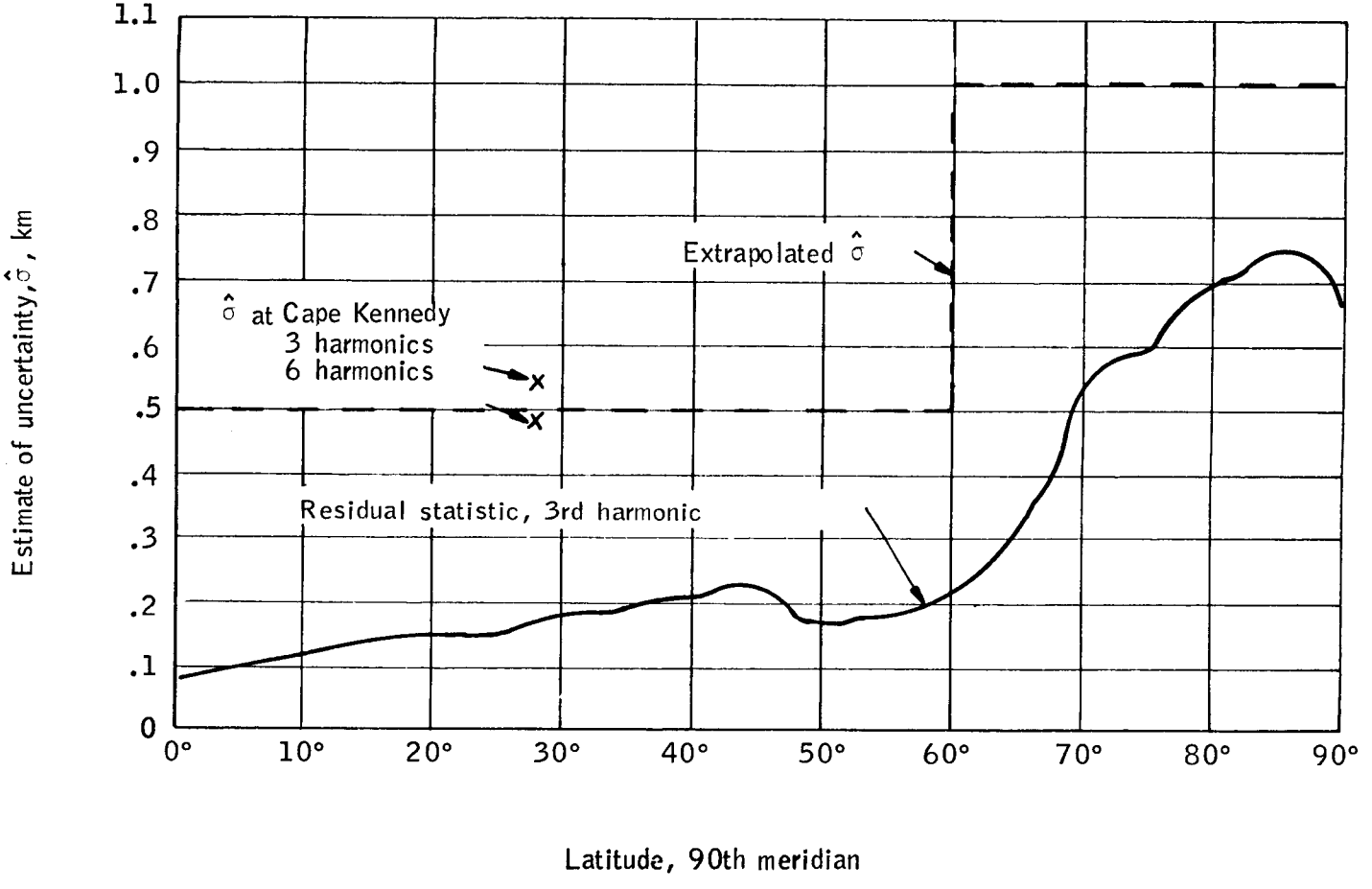

Figure 22. Extrapolation of Cape Kennedy Statistics for Locator L4 (2, 5)

where N is the number of samples required per space/time cell (28-day time cell is assumed). A value of 0.5 km was determined as a reasonable upper bound of I_c.

A total of 12 locators was used to analyze, in detail, the sampling requirements for each space/time cell. Table 12 shows the number of samples N required as a function of latitude for each of the locators.

The results in Table 12 show

1. Cell sample size requirements for locators L4(0.5) and L2(0.95) are completely subsumed by those for locator L4(2.5),
2. Sample sizes required for the other locators are, in varying degrees, considerably larger than for L4(2.5), and
3. Data requirement for locator L17 stands out by itself as extremely large.

From a horizon sensing mechanization standpoint, use of the locator L17 has proven from past experience to be extremely unstable which results in the anamolous data requirements. In view of this, locator L17 was eliminated from any further consideration. Interpolation of space-cell requirements was based upon the numbers determined for locators L4(2.5) and L1(3.0). These numbers represent the opposite extremes for the 11 locators being considered.

The next step in the analysis was to determine, for the various locators, the increases in cell sample size ΔN needed to compensate for the effects of random radiometer errors in order to maintain a given level of confidence in the time series analysis of HDS data. This provides a series of graphs for the various locators relating a given size radiance error to an equivalent tangent-height error which, in turn, can be used to compute ΔN. In this analysis, a value of 0.003 W/m^2-sr was used for the error standard deviation in radiance σN. This value reflects a $3\sigma N$ value of 0.01 W/m^2-sr required to resolve radiance profile variations and differences to the altitude resolution of 0.5 km ascertained above.

The computation of ΔN's was based primarily upon the σN versus σ_e (equivalent error standard deviation in tangent height) graph for the mean profile case. However, a detailed analysis was also made for the minimum profile (worst) case to determine the additional cell samples which would be required for special error compensation at high latitudes (i.e., 50 to 90°) in the winter season (i.e., the four 28-day time cells spanning the months December through February). It was shown that relatively small additional samples were required, in the case of all locators, to compensate for random radiometer error effects in low radiance profiles at higher latitudes in winter.

A further step in the analysis was to consider the additional samples required to compensate for data losses resulting from telemetry gaps, garbled transmissions, and other forms of operational degradation. The best available estimate is that such losses will be approximately five percent of the total data sample. Table 13 lists the data sampling requirements for the various locators which result when errors and losses are both taken into account.

TABLE 12. - CELL SAMPLE SIZE (N) FOR VARIOUS LOCATORS

Latitude, deg	Locator											
	L1 (0.2)	L1 (1.0)	L1 (2.0)	L1 (3.0)	L2 (0.06)	L2 (0.3)	L2 (0.5)	L2 (0.95)	L4 (0.5)	L4 (2.5)	L7	L17
0-10	16	20	16	17	16	16	16	16	16	16	32	156
10-20	17	20	16	18	16	16	19	16	16	16	32	163
20-25	17	18	20	25	16	16	29	16	16	16	21	346
25-30	17	19	28	31	16	18	37	16	16	16	20	270
30-35	17	19	28	31	16	19	37	16	16	16	25	252
35-40	16	19	25	21	16	20	34	16	16	16	25	166
40-45	17	32	27	34	16	20	32	16	16	16	29	240
45-50	17	32	27	37	16	20	27	16	16	16	33	261
50-55	20	34	31	54	16	17	21	16	16	16	33	377
55-60	26	52	45	77	16	18	20	16	16	16	28	440
60-70	49	121	96	131	27	41	31	24	17	27	67	431
70-80	60	131	121	137	44	57	51	33	27	38	90	485
80-90	60	118	116	93	48	59	52	33	31	42	129	453

TABLE 13. - DATA SAMPLING REQUIREMENTS FOR RECOMMENDED LOCATORS, COMPENSATED FOR ERRORS AND LOSSES[a]

Latitude interval, deg	L4 (0.5)	L2 (0.95)	L4 (2.5)	L2 (0.06)	L2 (0.3)	L1 (0.2)	L2 (0.5)	L7	L1 (1.0)	L1 (2.0)	L1 (3.0)
0-10	287	327	286	397	298	291	291	574	357	286	304
10-20	287	327	286	397	298	309	345	574	357	286	321
20-30	303	346	302	514	446	436	917	649	544	857	1 235
30-40	607	692	605	888	811	670	1 442	1 002	758	1 113	1 147
40-50	607	692	605	888	919	763	1 388	1 570	1 546	1 418	2 237
50-60	607	692	605	888	804	1 033	964	1 545	2 078	1 995	4 127
60-70	322	519	510	907	1 346	1 519	1 061	2 757	4 449	4 537	8 255
70-80	512	713	718	1 478	1 871	1 860	1 745	3 703	4 817	5 718	8 633
80-82.6	216	317	353	701	904	834	834	2 450	1 859	2 680	2 539
Totals: Northern Hemisphere - 1 time cell	3 793	4 625	4 270	7 058	7 697	7 715	8 987	14 824	16 765	18 890	28 798
Globe - 1 time cell	7 586	9 250	8 540	14 116	15 394	15 430	17 974	29 648	33 530	37 780	57 596
Globe - 13 time cells	98 618	120 250	111 020	183 508	200 122	200 590	233 662	385 424	435 890	491 140	748 748

[a]Based upon a 95-percent confidence level

A further analysis had as its objective the development of a recommended data sampling methodology which would be operationally simple and readily implementable.

The starting point for this study was an examination of the profile acquisition rates (profiles/min) needed to satisfy the error- and loss-compensated set of data sampling requirements. Table 14 lists these rates for the 11 locators in terms of 10° latitude intervals. These rates cover a range from 0.127 to 3.473 profiles/min. A single, passive radiometer operating only in the down-scanning mode cannot completely satisfy the L1(3.0) data sampling requirement between 60 to 90° latitude at the desired 95-percent level of confidence unless provisions for horizon scanning at this rate are provided.

The implications of very low data acquisition rates must also be carefully examined to avoid too large a space interval between successive samples. At a rate of 0.127 profile/min, the satellite, with its ground speed of slightly more than 4° latitude/min, would traverse a distance of 32° latitude between profile acquisitions. The separation distance should probably not exceed 10° latitude; otherwise, there would not be a satisfactory basis for studying small-scale time/space correlations between successive radiance profiles and for making detailed error analyses along individual orbits. For this reason, a minimum profile acquisition rate of 0.375 profile/min was adopted, even though this rate does provide 28-day data samples in low-latitude cells which are considerably in excess of the stipulated requirements for Fourier time series analysis at the 95-percent confidence level.

Further analysis of the sampling methodology problem was based upon an examination of the sensitivity of the 95-percent confidence level to changes in the number of profiles acquired for the various space-cell distributions. It can be shown (ref. 7) that the confidence interval on σ (the measure of uncertainty in the statistical analysis of a cell sample) is given by

$$I_c = \left\{ \sqrt{1 + \left[\frac{2}{m\,(N-1)\,(1-P/100)} \right]^{1/2}} - \sqrt{1 - \left[\frac{2}{m\,(N-1)\,(1-P/100)} \right]^{1/2}} \right\} \hat{\sigma} \quad (17)$$

where I_c is the confidence interval, $\hat{\sigma}$ the sample estimate of σ (the true standard deviation), m the number of time cells, N the number of samples per cell, and P the percent level of confidence. Obviously, for a given value of I_c, P decreases as (N-1) decreases. If, for example, the value of (N-1) associated with P = 95 percent decreases to $\frac{(N-1)}{2}$, then P decreases to 90 percent (for a constant I_c). The following table lists some representative multiples of (N-1) versus percent confidence levels:

TABLE 14. PROFILE ACQUISITION RATES, PROFILES/MIN, NEEDED TO SATISFY COMPENSATED DATA SAMPLING REQUIREMENTS[a]

Latitude interval, deg	Locator										
	L4 (0.5)	L2 (0.95)	L4 (2.5)	L2 (0.06)	L2 (0.3)	L1 (0.2)	L2 (0.5)	L7	L1 (1.0)	L1 (2.0)	L1 (3.0)
0-10	0.128	0.145	0.127	0.177	0.133	0.129	0.129	0.255	0.159	0.127	0.135
10-20	0.127	0.145	0.127	0.176	0.132	0.137	0.153	0.254	0.158	0.127	0.142
20-30	0.133	0.152	0.133	0.226	0.196	0.192	0.403	0.285	0.239	0.377	0.543
30-40	0.265	0.302	0.264	0.388	0.354	0.292	0.629	0.437	0.331	0.486	0.501
40-50	0.263	0.300	0.262	0.385	0.398	0.331	0.601	0.680	0.670	0.614	0.969
50-60	0.263	0.296	0.259	0.380	0.344	0.422	0.413	0.662	0.890	0.855	1.786
60-70	0.135	0.218	0.215	0.382	0.566	0.639	0.446	1.160	1.872	1.909	3.473
70-80	0.197	0.274	0.276	0.568	0.720	0.715	0.671	1.424	1.853	2.199	3.320
80-90	0.177	0.215	0.239	0.475	0.612	0.565	0.565	1.660	1.259	1.816	1.720

[a] Based upon a 95-percert confidence level.

(N-1) multiple	Percent level of confidence
5	99
2	97.5
1	95
0.67	92.5
0.5	90
0.33	85
0.25	80

Apparently, from these values, the cell sample can be considerably reduced and a useful level of confidence will still be obtained. A 95-percent level of confidence is generally regarded as very good (and is the level adopted in the statistical design of many experiments), a 90-percent level can be regarded as good, 85 percent as fair, and 80 percent (or even lower) as still useful. At the 95-percent level of confidence, the odds of being correct regarding the statistical properties of an individual time/space cell are 19 to 1; at 90 percent, 9 to 1; at 80 percent, 4 to 1; at 50 percent, 1 to 1, or even odds. At this point, the problem changes from one of statistical definition to one of decision making regarding the acceptance of given levels of calculated risk for the many hundreds of time/space cells which constitute the basic experiment. (In a subsequent section of this report, radiometer error considerations are described which lead to choosing a confidence level of 90 percent.

The sampling problem was re-examined, therefore, in terms of providing a reasonable compromise which would attain a 95-percent level of confidence for most locators but which could be releaxed in a relatively few instances to values of 90- and 85-percent confidence. Results of this analysis, which was necessarily conducted on a qualitative basis, led to the formulation of the recommended sampling methodology outlined in Table 15. Three data acquisition rates were selected: 0.429 profile/min from 0 to 30° latitude, 0.750 profile/min from 30 to 60°, and 1.00 profile/min from 60 to 90°. The total one-year data sample collectable at these rates amounts to 378 508 profiles, a value which includes an overall loss allowance factor of five percent. The useful sample then would constitute 360 484 profiles.

The levels of confidence attainable in analyzing the cell samples with the recommended methodology are shown in Table 16 as a function of 10° latitude intervals. These results indicate that a confidence level of at least 98 percent can be achieved for three locators, at least 95 percent for seven locators, at least 89 percent for 10 locators, and at least 82 percent for all 11 locators. Over the latitude range 0 to 50°, the confidence levels for all locators exceed 93 percent. These results are regarded as quite satisfactory, overall, since the L1(3.0) locator has a very demanding set of data sampling requirements when considered exclusively at the 95-percent confidence level. The average number of profile samples acquired per orbit with the recommended sampling methodology is 67.88.

The results of the various studies described above represent a preliminary attempt to size the experiment in such terms as to provide a reasonable basis for potential application to a large number of horizon locators. For convenience, attention has been limited to 11 locators; however, the data sample will, of course, be generally applicable to the study of various other

TABLE 15. - NUMBER OF DATA SAMPLES OBTAINABLE WITH RECOMMENDED VARIABLE RATE SAMPLING METHODOLOGY

Latitude interval, deg	Data acquisition rate, profile/min	Number of data samples
0-10	0.429	963
10-20	0.429	967
20-30	0.429	975
30-40	0.750	1718
40-50	0.750	1731
50-60	0.750	1751
60-70	1.00	2377
70-80	1.00	2600
80-90	1.00	1476

Totals:

Northern Hemisphere - 1 time cell - 14 558

Globe - 1 time cell - 29 116

Globe - 13 time cells - 378 508

TABLE 16. - LEVEL OF CONFIDENCE, PERCENT, IN DATA SAMPLES OBTAINED WITH RECOMMENDED SAMPLING METHODOLOGY

Latitude interval, deg	Locator										
	L4 (0.5)	L2 (0.95)	L4 (2.5)	L2 (0.06)	L2 (0.3)	L1 (0.2)	L2 (0.5)	L7	L1 (1.0)	L1 (2.0)	L1 (3.0)
0-10	98.5	98.3	98.5	97.9	98.5	98.5	98.5	97.0	98.1	98.5	98.4
10-20	98.5	98.3	98.5	97.9	98.5	98.4	98.3	97.0	98.2	98.5	98.3
20-30	98.4	98.2	98.5	97.4	97.2	97.8	95.3	96.7	97.2	95.6	93.7
30-40	98.2	98.0	98.2	97.4	97.6	98.0	95.8	97.1	97.8	96.8	96.7
40-50	98.2	98.0	98.3	97.4	97.3	97.8	96.0	95.5	95.5	95.9	93.5
50-60	98.3	98.0	98.3	97.5	97.7	97.0	97.2	95.6	94.1	94.3	88.2
60-70	99.3	98.9	98.9	98.1	97.2	96.8	97.8	94.2	90.6	90.4	82.6
70-80	99.0	98.6	98.6	97.2	96.4	96.4	96.6	92.9	90.7	89.0	83.4
80-90	99.1	98.9	98.8	97.6	96.9	97.2	97.2	91.7	93.7	90.9	91.4

locators whose statistical properties are such that their sampling requirements lie within the wide range covered between the L4(2. 5) and L1(3. 0) locators. For example, the recommended sampling methodology should provide an adequate basis for Fourier time series analysis of other locators such as L3(7. 5) and of locators in the L1, L2, and L4 families with other values of the integral of normalized radiance, such as L2(0. 9), L4(7. 5), and L4(1. 0). Figure 23 shows the sampling requirements for the limiting locators, L1(3. 0) and L4(2. 5), and the recommended sampling rate for the HDS experiment.

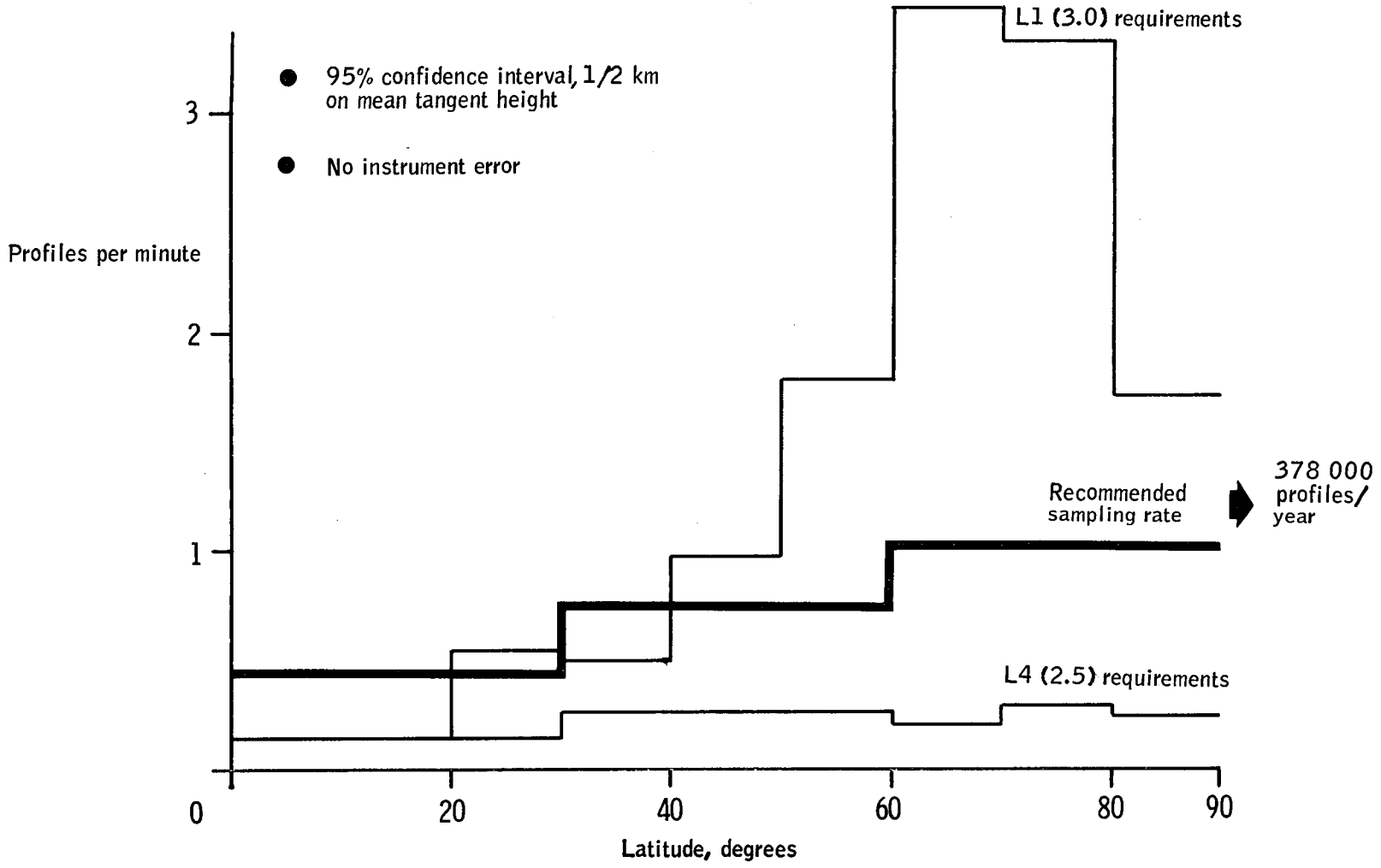

Figure 23. Sampling Requirements for Limiting Locator Cases

FLIGHT TECHNIQUE EVALUATION

Having defined the data sampling requirements for a global coverage horizon definition program, study emphasis was directed toward assessing the relative merits of various techniques for gathering the required data. For this purpose, a "flight techniques evaluation" was conducted.

A flight technique is defined as a vehicle configuration or series of configurations which has a specific horizon radiance profile data-gathering capability when placed into a particular orbit or series of flight paths. The flight technique analyses provide sufficient data for an initial selection of missions and configurations which are suitable for obtaining the data required to define adequately the earth's 15μ infrared horizon. Reliability, cost, and mission success probability are integral parts of the models used to examine the various techniques.

The nature of the data sampling requirements is such that the choice of feasible mission concepts must be directed toward measuring systems which can provide comprehensive global coverage over a one-year period. Otherwise, it will not be possible to determine with a high degree of statistical confidence the spatial and temporal variations in radiance profiles and indicated horizon altitudes. In particular, the results of the data sampling requirements study have shown the importance of latitudinal and seasonal variations in radiance profiles; these variations would be extremely difficult to evaluate adequately on the basis of fragmentary data samples where extensive interpolation and extrapolation would be necessary.

An operational system of three or more earth-equatorial-orbit satellites, although capable of providing continuous coverage of tropical and mid-latitude regions, would nevertheless fail to provide sampling data in polar regions where measurements of radiance profile variability are especially critical. An extensive series of ballistic probes, although launched from various locations at different times of the year, would still provide too coarse a statistical "sieve" for detecting important, smaller-scale variations in the earth's radiance profile. Attention was necessarily directed, therefore, towards low-level, near-polar orbiting satellites as the primary means for obtaining the required sampling data, since they can readily provide complete global coverage (all cells) with sufficient time resolution to study the significant temporal variability within each cell.

Thus, in the analysis of mission concepts and flight techniques, emphasis was placed upon near-polar orbiting satellites. Ballistic probes were also considered as a possible alternative to compare their effectiveness and cost with satellite techniques.

The ultimate objective of this study was to define and evaluate, on a quantitative cost/effectiveness basis, the various alternative flight techniques and configurations which could conceivably be used to perform the horizon definition experiment. A general outline of the study approach which was used is presented in Figure 24.

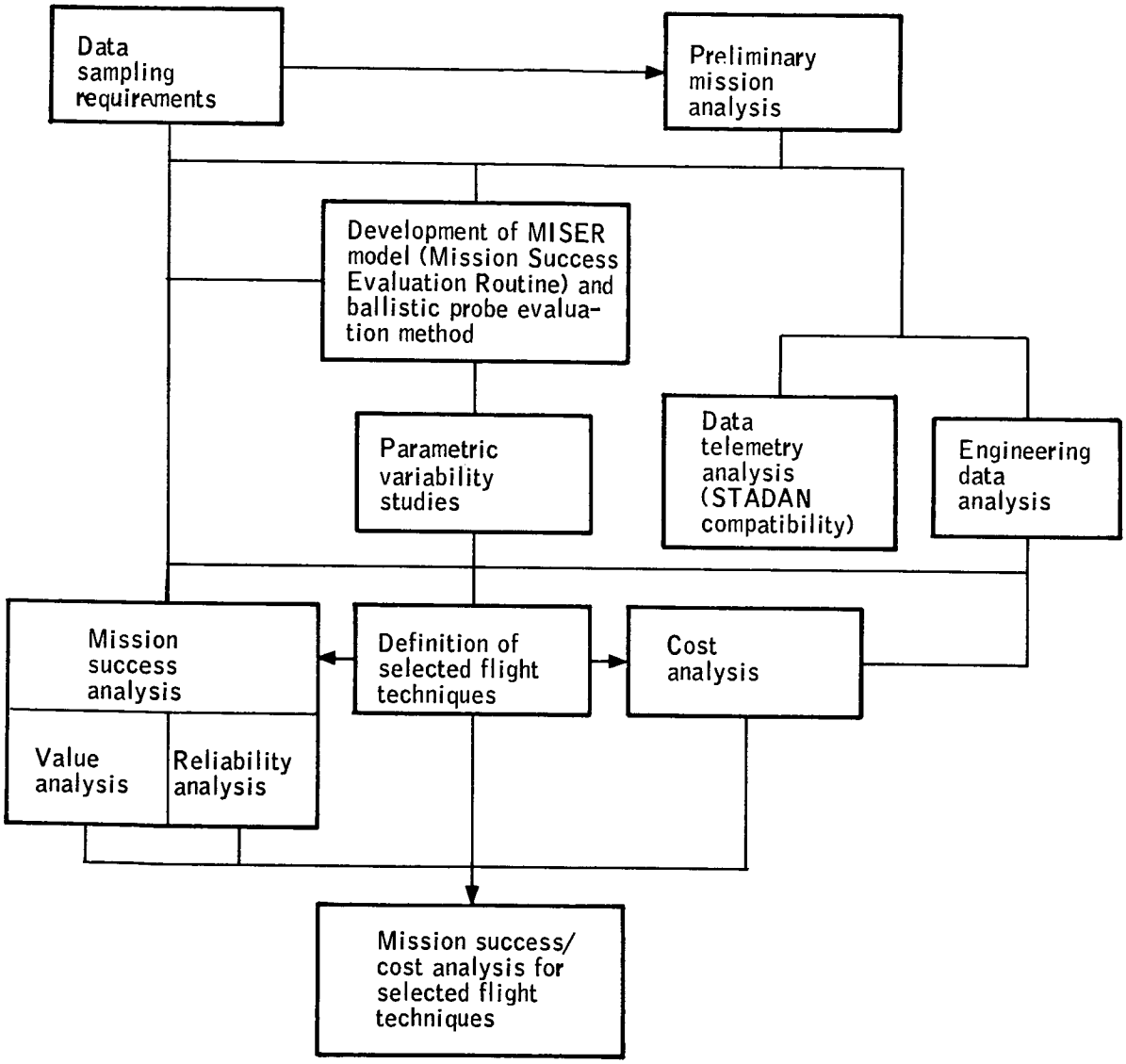

Figure 24. Study Approach Outline

A key element in the study approach was the development of the Mission Success Evaluation Routine (MISER) computer model for evaluating satellite flight techniques (the ballistic probe evaluation method was, by comparison, quite simple and straightforward; therefore, this evaluation did not involve computer analysis). The MISER model was used for two important purposes:

1. To perform a series of parametric variability studies which, together with the data telemetry analysis and engineering data analysis, served to define the satellite flight techniques deserving further consideration, and

2. To perform the mission success analysis which, together with the cost analysis, provided the overall cost/effectiveness basis for evaluating each selected satellite flight technique.

The MISER model, as supplemented by the ballistic probe evaluation method, provided the basis for performing the mission success analysis in terms of its two integral components: value analysis and reliability analysis. Value analysis was used to determine the effectiveness with which a flight technique with perfect reliability can fulfill the basic data sampling requirements as specified in the preceding section. Reliability analysis provided the means whereby the actual reliability of each flight technique can be factored into the determination of an overall value of mission success. Then, on the basis of cost estimates for each selected flight technique, a final determination can be made of the combined mission success/cost factors which apply to each technique.

MISSION AND CONFIGURATION SELECTION

On the basis of analytical studies, it was possible to select 10 candidate flight techniques for gathering the data required for the horizon definition experiment. The flight techniques defined in this section were then subjected to mission success and cost analyses to determine their relative cost effectiveness.

Three basic flight technique concepts have been identified:

1. Two or more orbital vehicles with payload limitation,

2. A single orbital vehicle to accomplish the mission regardless of payload weight, and

3. A series of ballistic probes.

The basic concepts are further defined by the parameters that are required inputs to the cost and mission success models. The principal parameters are spacecraft configuration, number of flights, standby flights, orbit parameters, scan yaw angles, scan frequency, and booster type.

The actual techniques defined within the framework of the above parameters were:

- Seven orbital techniques with standby units,
- A long-term orbital mission with on-board redundancy, and
- Two ballistic probe techniques.

The flight technique spacecraft configurations were defined by the following subsystems:

- Experiment package (containing the primary mission sensors).
- Telemetry, tracking, and command communications.
- Data management.
- Attitude control.
- Power.
- Structure.

The experiment package contains attitude determination hardware and the infrared measurement package. The attitude determination utilizes a star-mapper, star tracker, or any other sensor and associated signal shaping and functional electronics as required. The infrared package contains the radiometer(s) and associated electronics.

Telemetry, tracking, and command communications consist of the beacon, antennas, spacecraft command logic, and diagnostic data handling functions.

Data management comprises the equipment to store and manage the experiment package data. This includes the storage (core or tape recorder), transmitters, and associated electronics.

Attitude control is to be self-contained and provide the required orientation for the defined configuration. The attitude control consists of an attitude sensor, attitude control devices, and the necessary control electronics. A configuration is defined by momentum storage, gravity gradient, pneumatic, or magnetic attitude control mechanizations. The power subsystem contains solar cells, power storage, power regulation, and associated logic circuitry for power control.

The structure is the spacecraft' s main frame. It supports all subsystems and provides rigid mounting.

The flight techniques and configuration selections are listed in Tables 17 and 18 where:

TABLE 17. - FLIGHT TECHNIQUE PARAMETERS

Flight technique	Spacecraft configuration	Number of flights	Standby flights	Orbit altitude [a], n. mi. /km	Orbit inclination	Number of yaw angles	Yaw angles	Scan frequency, scan/min	Booster type
M1	1	1	2	250/460	90°	2	0° 180°	5.0 5.0	Improved Delta
M2	1	1	3	250/460	90°	2	0° 180°	5.0 5.0	Improved Delta
M3	2	1	3	250/460	90°	2	-20° +50°	5.0 5.0	Improved Delta
M4	3	1	3	250/460	90°	4	-20° -160° +50° +130°	2.5 2.5 2.5 2.5	Improved Delta
M5	4	1	3	250/460	90°	4	-20° -160° +50° +130°	2.5 2.5 2.5 2.5	TAT Improved Delta
M6	5	1	2	250/460	90°	4	-20° -160° +50° +130°	2.5 2.5 2.5 2.5	Improved Delta
M7	5	1	3	250/460	90°	4	-20° -160° +50° +130°	2.5 2.5 2.5 2.5	Improved Delta
M8	6	1	0	250/460	90°	4	-20° -160° +50° +130°	2.5 2.5 2.5 2.5	TAT Improved Delta
M9	7	10	0	500/920			All		
M10	7	100	0				All		

[a] Non-orbital apogee for flight techniques M9 and M10

TABLE 18. - SPACECRAFT CONFIGURATIONS

Subsystem / Configuration	Experiment 1) Radiometer 2) Attitude determination 3) Electronics	Telemetry, tracking, and command communications	Data management	Attitude control	Power	Structure
1	1) Single, passive 2) Starmapper 3) Electronics	Same as Tiros	Core storage	Wheel magnetic and pneumatic	Body mounted solar panels	Same as Tiros
2	1) Single, active 2) Star tracker 3) Electronics	Between Tiros and Nimbus	Core storage	Earth stabilized gravity gradient	Body mounted solar panels	Same as Nimbus
3	1) Double, passive 2) Starmapper 3) Electronics	Same as Nimbus	Tape recorder	Wheel magnetic and pneumatic	Body mounted solar panels	Same as Tiros
4	1) Double, active 2) Star tracker 3) Electronics	Same as Nimbus	Tape recorder	Earth stabilized gravity gradient	Body mounted solar panels	Same as Nimbus
5	1) Double, passive 2) Starmapper 3) Electronics	Same as Tiros	Core storage	Wheel magnetic and pneumatic	Body mounted solar panels	Same as Tiros
6	Redundant 1) Double, passive 2) Starmapper 3) Electronics	Triple redundant Same as Tiros	Redundant Core storage	Triple redundant Wheel magnetic and pneumatic	Redundant Body mounted solar panels	Same as Tiros + 30 percent
7	1) Single, active 2) Starmapper 3) Electronics	Same as Scanner	None	Same as Scanner	Batteries	Same as Scanner

Number of flights -- The number of flights refers to the number of satellites that are programmed for the mission.

Standby flights -- Standby flights are complete vehicles prepared to be launched only in the event of failure of the operating vehicle. Depending on the required mission reliability, the number of standby flights is selected to acquire a specific reliability.

Orbit parameters -- The orbit parameters are altitude and inclination. These parameters affect the mission success computation and the launch site and, consequently, must be defined for each technique.

Yaw angle -- The yaw angle is the azimuth angle of the radiometric scanner(s) line of sight measured from the spacecraft velocity vector. The angle is defined as positive to the right and negative to the left. Multiple "scanners" does not necessarily imply multiple radiometers; it can be a single radiometer scanning at more than one yaw angle.

Scan frequency -- The scan frequency refers to the total quantity of horizon profiles per minute of all the scanners on the spacecraft. All radiometric scanners on a given spacecraft are assumed to have the same frequency.

Booster type -- The booster type will be determined by the thrust required to lift the package into orbit. This requirement is dictated by the weight of the spacecraft and the orbit altitude.

COST MODEL

A cost model was developed to assess the relative cost value of the flight techniques. The model was based on a statistical analysis of historical cost and engineering data of past and concurrent unmanned space programs. This data provided sufficient information to guide the cost effectiveness analysis.

The command and support costs were neglected because the data requirements for the Horizon Definition Study will govern the extent of these costs. Since data requirements are the same for all techniques, the command and support costs will be a constant.

EVALUATION RESULTS

The results of cost, reliability, and mission success analyses were merged into a single tabulation of data for the specific techniques selected. Graphic displays of the success versus cost data are shown in Figure 25. Technique M10 (100 ballistic probes) is not shown because of the extreme cost level. The data shown does not indicate a trend of increasing success with increasing cost. This is due to the limited selection of techniques involved. If the techniques were optimized for each cost level, the resulting optimum locus would necessarily follow a monotonic trend of success with cost.

Although the specific techniques shown in Figure 25 are limited in number, certain things are evident. First, the level of mission success obtainable with ballistic probes is very low, even with liberal allowances made in their favor. Second, a fairly high mission success level may be obtained at a normalized program cost of 60 to 70. On the basis of the total flight techniques evaluation study, a passively controlled, rolling-wheel spacecraft concept was selected as the most cost-effective method of obtaining the experiment data.

This method provides the most reliable spacecraft by eliminating the necessity for an active, on-board control and stabilization subsystem and for active scanning elements in the radiometer and starmapper subsystems. Inherent in the choice of a passively controlled, rolling-wheel spacecraft are the concepts of utilization of a core storage memory and solar cell power. Elimination of the requirements for active, on-board elements increases the probability of mission success and simultaneously reduces the mission cost.

In the remaining elements of the study, these concepts were the only restrictions placed on the conceptual design since no configuration requirements directly are inferred. The design concept for the spacecraft to be utilized in the Horizon Definition Study mission fulfill these requirements.

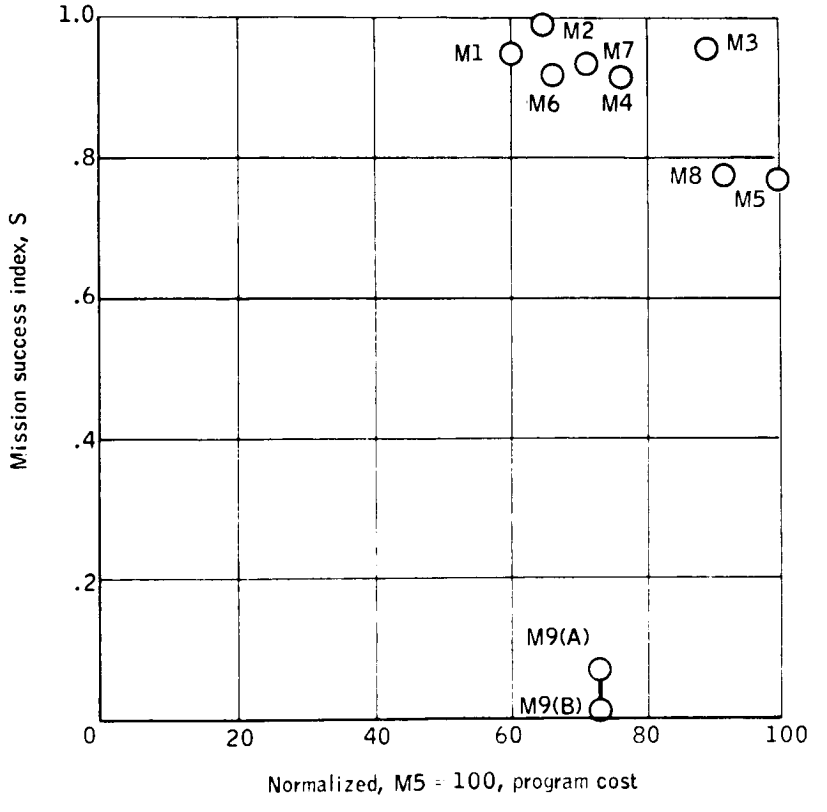

Notes: M10 is omitted because of extreme cost
M9(A): no data constraint
M9(B): data constraint

Figure 25. Mission Success Versus Program Cost

EXPERIMENT REQUIREMENTS

Analysis of the body of data, the data requirements, and the results of the flight techniques evaluation determined the experiment requirements. A conceptual design was then configured to evaluate the feasibility of meeting the experiment requirements. The salient features of the experiment requirements are as follows.

RADIOMETRIC REQUIREMENTS

The radiometric requirements define the approximate nature of the earth's phenomenon which is to be observed. The accuracy of each observation and the quantity and global distribution is established. These requirements are subdivided into the spectral interval, profile accuracy, and data requirements.

Spectral Interval

The objective here was to utilize the maximum energy possible (broadest spectral interval) which still resulted in a horizon profile which was invariant to atmospheric and geomorphological effects.

The spectral interval is selected as the 615 to 715 cm^{-1} (14.0 to 16.28 μ) carbon dioxide absorption band. This band has been established as being capable of providing the most stable horizon profiles.

Profile Accuracy

The accuracy of the radiance profile refers to the variation of the measured radiation from the absolute radiation. Measurement instruments must be designed to accommodate all these requirements expressed in terms of radiance characteristics and resolution. The basic requirements for horizon profile positional accuracy relates to both the horizontal position and the altitude at which radiometric readings are taken. The basic requirement for horizontal resolution is ≤ 25 km with the altitude or tangent-height resolution requirement being ± 0.25 km over the complete altitude interval of +80 to -30 km.

These radiance profile measurement requirements are summarized below.

- Spectral interval: 615 to 715 cm^{-1} (14.0 to 16.28μ)
- Profile accuracy
  - Tangent height range: +80 km to -30 km
  - Instantaneous value of radiance measured must be assignable to a tangent-height value to within ± 0.25 km.
  - Radiance characteristics and resolution:

Maximum peak radiance = 7.0 W/m^2 - sr.
Minimum peak radiance = 3.0 W/m^2 - sr.
Maximum slope = 0.6 W/m^2 - sr - km.
Minimum slope = 0.02 W/m^2 - sr - km.
Maximum slope change = 0.15 W/m^2 - sr - km^2.
Radiance magnitude resolution = 0.01 W/m^2 - sr.

- Horizontal resolution: 25 km

Data Requirements

Data requirements for the Horizon Definition Study (HDS) experiment, as refined during the study, are as follows:

- One-year continuous coverage
- Maximum of 10° latitude separation between successive samples
- 13 time cells (28 days/cell)
- 588 space cells

Latitude (30°S to 30°N)	128
Latitude (30°N to 60°N)	134
Latitude (60°N to 90°N)	96
Latitude (30°S to 60°S)	134
Latitude (60°S to 90°S)	96

- Average number of samples per cell

Latitude (30°S to 30°N)	45
Latitude (30°N to 60°N)	39
Latitude (60°N to 90°N)	67
Latitude (30°S to 60°S)	39
Latitude (60°S to 90°S)	67

- Total samples (one year) 378 508

SYSTEM REQUIREMENTS

The system requirements derived from the basic data and the flight techniques evaluation are as follows.

Mission Profile

Nominal circular, polar orbit of approximately 500-km altitude.

Tracking and Data Acquisition

Limited to the existing Satellite Tracking And Data Acquisition Network (STADAN) with minimum modification.

Experiment Package

- Passive radiometric and attitude measurements with redundancy (more than one unit) in the experiment package for the radiometer and attitude determination device.
- Minimum scan rate > 0.5 scans/min average.
- Maximum scan angle with respect to orbit plane $\leq 5°$.

Spacecraft

- Rolling-wheel configuration (spin axis normal to the orbit plane)
- Weight in less than 800-pound class mandatory.

State of the Art

Proven subsystems shall be employed wherever possible.

MISSION STUDIES

The mission profile study dealt with the evaluation of orbit and orbit-related parameters pertinent to the experiment effectiveness, system design, or mission operations planning. Computerized mathematical modeling was used to a great extent in performing this analysis. This automation (1) enabled a more precise analysis to be made, (2) greatly extended the number of parameters and range of parameter variations possible, and (3) made generalized models available for rapid study of new orbits and/or parameters which were needed as the system study progressed. Accurate trajectory simulations were neither required nor performed in this study; rather, the emphasis was on parametric evaluation of the variables pertinent to the mission planning and systems design. Although there was considerable overlap and reiteration, the mission profile study was essentially conducted in two phases:

1. Parametric investigations. Objective was to examine the orbits feasible from an experiment point of view in order to assess the effects on the system and mission. During this phase, no attempt was made to narrow the selection of possible profiles.
2. Orbit selection and analysis. Those orbits which appeared to best meet the mission goals and yield possible solutions to system design problems were examined in more detail. Analysis of deviations from nominal orbits and their effects were made. Then, a detailed analysis of a selected orbit was conducted which included a fairly exhaustive evaluation of sun-angle geometry, tracking/telemetry coverage, drag decay, etc.

PARAMETRIC INVESTIGATIONS

The mission profile investigation was guided by the following basic requirements:

- Orbit altitude will be above 150 km.
- Orbit will be chosen with consideration of STADAN system coverage.
- Orbit will be compatible with launch site and launch vehicle.
- Orbit will be near-polar.
- Orbit duration will be at least a year.

The first three requirements are fundamental; the last two result from the data requirements studies.

Although the minimum orbit altitude is explicit, in reality the orbit altitude is primarily determined by the one-year duration requirement, as will be seen later.

STADAN utilization is imposed on the mission profile analysis as a general requirement. Coverage with the STADAN system, assuming circular orbits, is primarily a function of orbit altitude and inclination.

The launch site and launch vehicle requirement relates to launch site and booster limitations. In conjunction with requirement for a near-polar orbit, the launch site requirement dictates a choice of Vandenberg/WTR for the launch site if heavy payload penalties are to be avoided. Compatibility of the orbit with the launch vehicle consists primarily of payload-weight/orbit-parameter constraints and orbital injection-error tolerances which are suitable.

The near-polar requirement stems from the need for global coverage. The term "near-polar" is used since the polar regions can be seen by a satellite in orbits which are "near enough" to polar.

The orbit duration requirement reflects the need for data coverage over a complete range of seasons. Primarily, this requirement affects the orbit-altitude choice, since orbital altitude determines the orbital decay rate.

In addition to these basic requirements, the need for consideration of diurnal variation data was imposed on the study. This aspect has influenced the selection of alternate orbits and was a prime factor in the selection of the orbit discussed later.

With the mission requirements as a guide, an analysis of several areas including atmospheric effects, solar illumination, telemetry/tracking coverage, and launch site and booster constraints, was undertaken.

Atmospheric Effects on Missions

In spite of the extremely low atmospheric densities encountered at orbital altitudes, the effects of the atmosphere are still measurable and possibly significant below 600 kilometers altitude. The two primary effects are reflected in orbit lifetime and orbit determination accuracy. This section will deal only with orbital lifetime effects.

The problem of determining orbit lifetime for elliptic orbits is somewhat involved and has received considerable treatment in the past. A circular orbit can be assumed at this stage of the study, since no ellipticity requirement has as yet been found. Figure 26 shows the circular orbit decay profile. This result is based on M/C_DA of 100 kg/m^2 (about 20 pounds per square foot) which is an estimated value for the spacecraft. Here, M is the spacecraft mass, C_D is the effective drag coefficient, and A is the effective frontal area. For a different M/C_DA, merely multiply all time values on the graph by 0.01 times M/C_DA in kilograms per square meter.

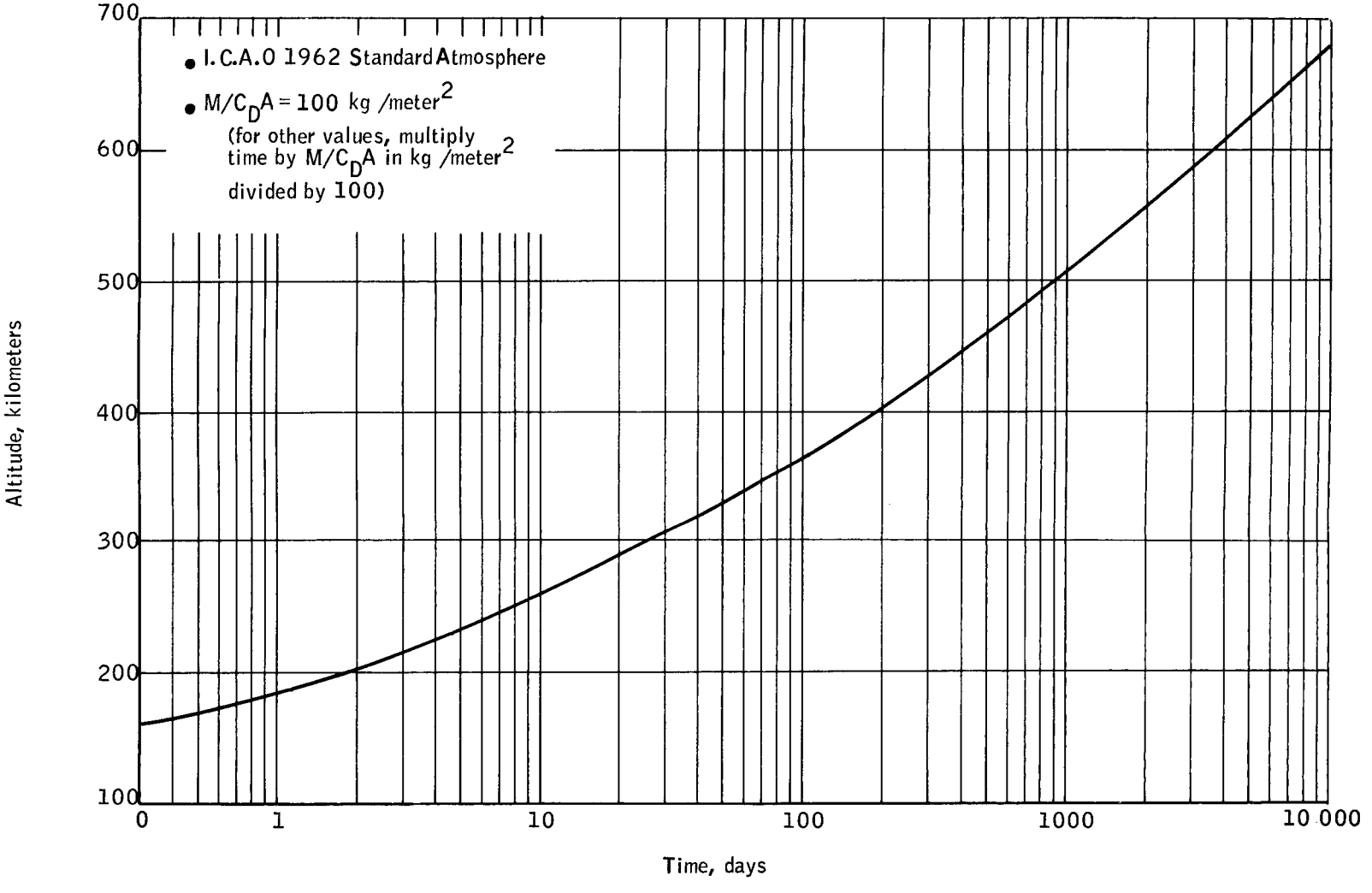

Figure 26. Circular Orbit Decay Profile

Orbit lifetime can be read from Figure 26 directly (from altitude at left to curve, down to lifetime in days). Note that for $M/C_DA = 100$ kg/m^2, a one-year life means a minimum of 440-km altitude. Because of injection errors, atmospheric variations, and orbit determination requirements, this minimum altitude would not be adequate.

For current purposes, a 500-km altitude has been selected. Allowing for an injection error of 60 km in semimajor axis (400-km altitude), this still allows a one-year life, assuming $M/C_DA = 100$ kg/m2.

Solar Illumination Profiles

Evaluation of solar-illumination and sun-angle profiles were made using a computer simulation. With inputs consisting primarily of orbit altitude, inclination, initial node location, and date of launch and assuming circular orbits, the program yields a time history of (1) fraction of orbit in earth's shadow, (2) angle from sun line to orbit perpendicular and (3) local sun time at ascending node. The analysis took into account the orbital motion of the earth, including first- and second-order eccentricity terms and the first-order nodal precession of the spacecraft orbit itself.

Figures 27 and 28 are sample plots showing the shadow fraction and sun angle for 6 p.m. launches for a sun-synchronous and a polar orbit, respectively.

Angles plotted in Figure 28 are restricted to the range 0 to 90 degrees. For polar orbits, in reality, the sun moves from one side of the orbit plane to the other. This would be obvious if the sun line and orbit normal were taken as vectors rather than merely lines, in which case the angles would be from 0 to 180 degrees.

Dozens of parameter combinations were tested, and certain generalizations became obvious as the data was evaluated. The polar orbit always exhibits a sun-shadow profile and a sun-angle profile which places severe demands on a "no-moving-parts" spacecraft regardless of launch date or initial nodal location. The sun-synchronous orbit, on the other hand, possesses clear-cut advantages from the same viewpoint.

A comparison of Figures 27 and 28 readily illuminates the advantages of a sun-synchronous orbit. If solar-cell power is to be used on the spacecraft, a relatively constant solar aspect angle with the sun-synchronous orbit is highly desirable. Also, the time position and magnitude of the shadow portion of the sun-synchronous orbit may be controlled by selection of the launch date and initial nodal location.

Telemetry/Tracking Coverage

To assure compatibility of the mission profile with the STADAN (Satellite Tracking And Data Acquisition Network), computer programs were developed to determine visibility times for selected stations as a function of orbit parameters. The primary inputs to these programs were orbit altitude, orbit inclination, ascending node location, minimum station elevation angles for acquisition, and minimum visibility time over each station.

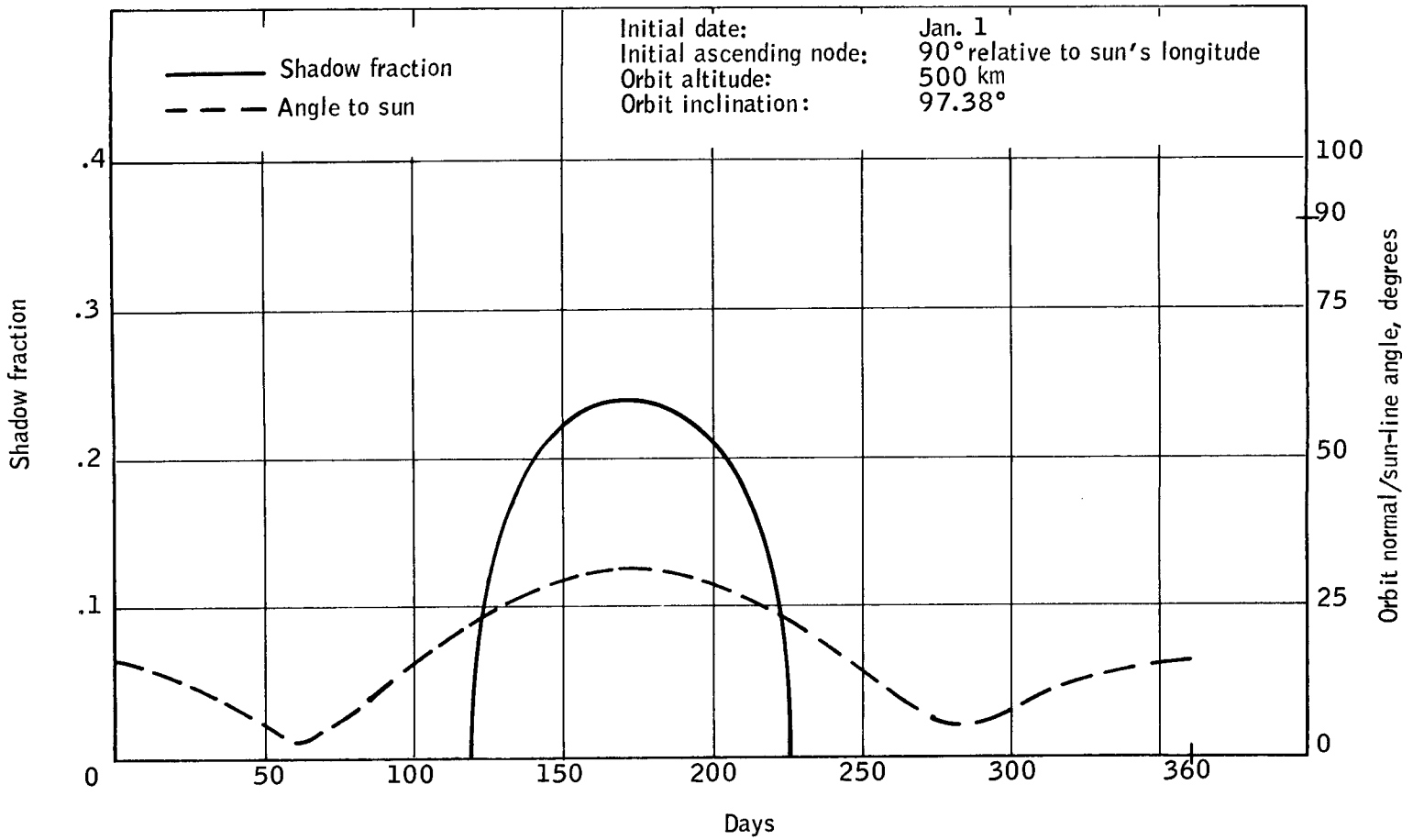

Figure 27. Shadow Fraction and Sun Angle, 500 km, Sun-Synchronous Orbit, 6 p.m. Launch

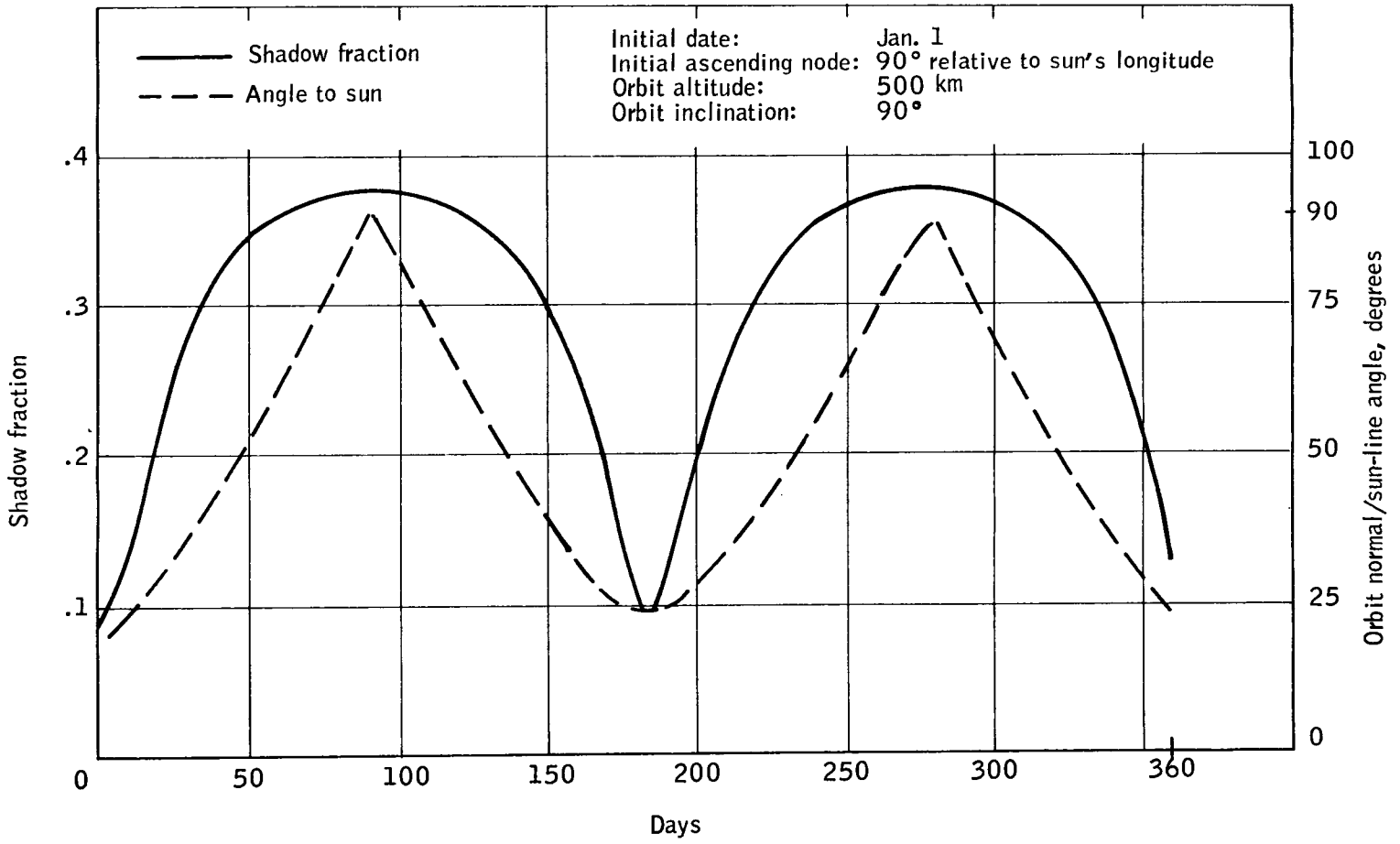

Figure 28. Shadow Fraction and Sun Angle, 500 km, Polar Orbit, 6 p.m. Launch

Studies of near-polar orbits using the STADAN system do not show drastic variations in coverage with the various orbits. Figure 29 shows coverage for a 500-km, sun-synchronous orbit. The stations used were the STADAN sites equipped for range/range-rate tracking (Alaska, Carnarvon, Rosman, Santiago, and Tananarive). Note that the total coverage (per orbit) and maximum single-station time (per orbit) are both plotted. Minimum elevation is 10 degrees. Use of the total STADAN system tends to reduce the differences in coverage caused by different orbit parameters. Since the differences between coverage on the orbits under serious consideration were not great, tracking/telemetry coverage was not a significant orbit-choice tradeoff parameter. A slight advantage in coverage was obtained using a polar orbit rather than a sun-synchronous one, but this is outweighted by sun-angle considerations.

Launch Site, Booster Constraints

For near-polar orbits, the Western Test Range (WTR) is clearly the most advantageous site for launching. Severe range-safety constraints in the form of ascent trajectory "dog-legging" or plane-changing would be imposed on an Eastern Test Range (ETR) launch. Thus, for all foreseeable HDS orbital launches, the WTR will be considered for use.

Potential booster capabilities were analyzed by assuming a nominally polar, 500-km circular orbit. The approximate payload capability of some feasible launch vehicles from WTR for this orbit are as follows:

• Scout (1966)	260 lbs
• Scout (study)	390
• DSV-3G Delta (2-stage, direct injection)	420
• DSV-3G Delta (2-stage, Hohmann transfer)	670
• DSV-3L Delta (2-stage, direct injection)	790
• DSV-3E/X-258 Delta	1050
• DSV-3L Delta (2-stage, Hohmann transfer)	1210
• DSV-3L/FW-4 Delta	1970

The use of 2-stage versions of the Delta results in a particular advantage - increased injection accuracy. While this is not extremely important for all missions, it is crucial for atainment of sun-synchronous orbits such as the selected orbit. Based on approximate vehicle weight, an initial recommendation of the DSV-3G or DSV-3L (2-stage) Delta vehicle for the HDS mission was made. Estimated injection errors for the 2-stage Delta (from Delta Payload Planner's Guide, Douglas Aircraft Co.) are approximately:

i (inclination)	0.06 deg, 1 sigma
a (semi-major axis)	10 n. mi. = 18.5 km, 1 sigma

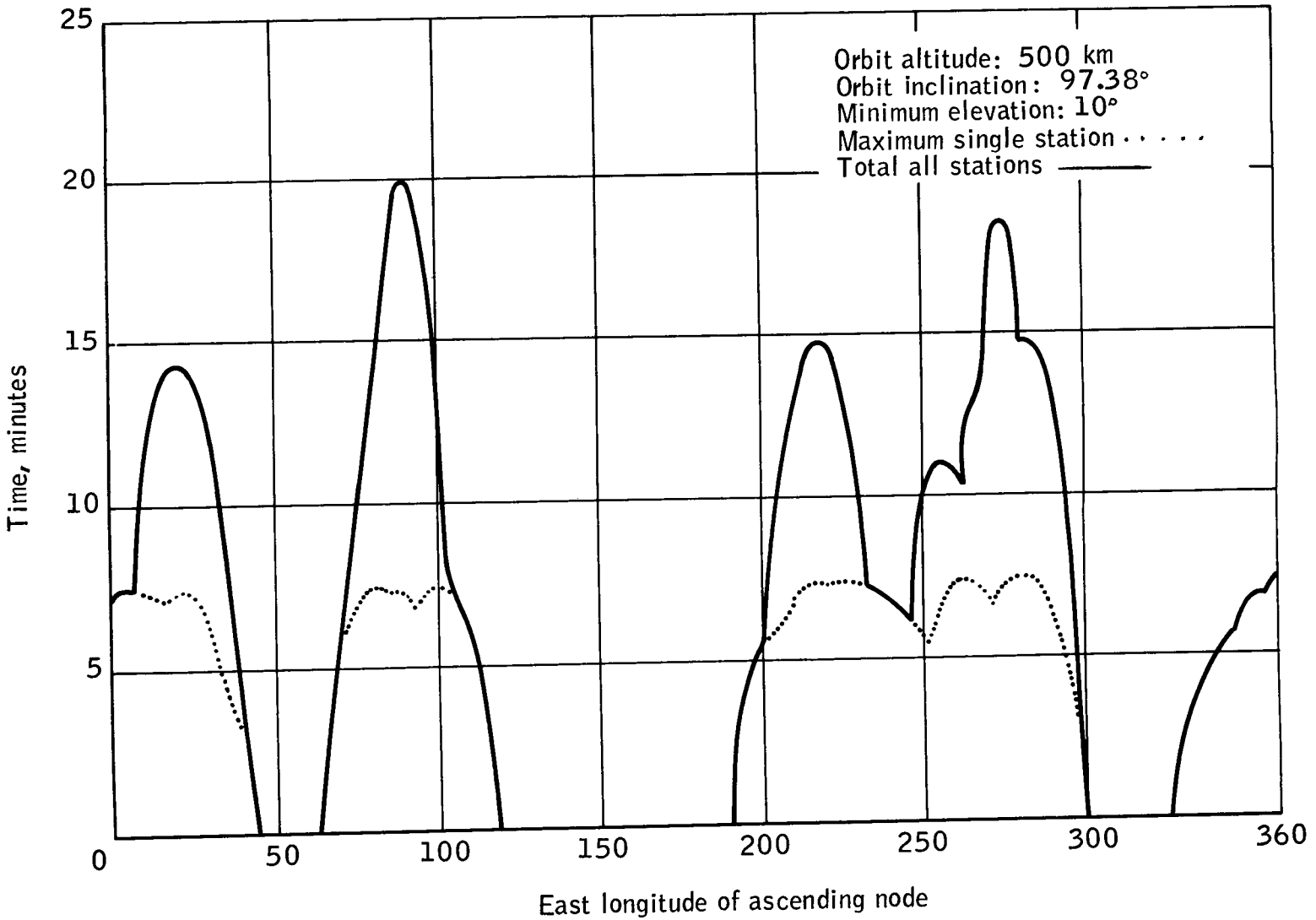

Figure 29. STADAN System Coverage: Time Above Minimum Elevation Sun-Synchronous Orbit, 500 km

Converting this data to an equivalent total 3-sigma error in inclination (in terms of effect on nodal precession rate) for a 500-km, sun-synchronous orbit gives

$$\Delta i_{3\sigma} = 0.266 \text{ deg}$$

This value was used in predicting possible drift of the "sun synchronous" orbit relative to the sun. Effects of this orbital drift error will be discussed more fully in the analysis of the selected orbit.

ORBIT SELECTION AND ANALYSIS

Potential orbital profiles were subjected to analysis and comparison. The primary areas affected were (1) solar power acquisition, (2) thermal control, (3) experiment package, and (4) polar and diurnal data coverage. For solar power production, a relatively constant solar/spacecraft aspect angle is desired which leads to consideration of sun-synchronous orbits. This concept also provides for radiative thermal control by knowledge of the relative solar position at all times. By maintaining the relatively constant solar aspect angle, the baffling requirements for all optical instruments on-board is also less stringent. These tradeoffs and considerations of the diurnal temperature variations (Figure 18) led to the selection of a "3 o' clock" sun-synchronous orbit. In fact, this orbit appears to be the best from the standpoint of polar and diurnal data coverage. Considering the power subsystem, this orbit is satisfactory, although a nodal time nearer to 6 o' clock would be preferable.

Figures 30 through 32 illustrate the sun-earth-orbit geometry as a function of time for the 3 o'clock orbit. A 28 October launch date is used although this is not a requisite; this date is representative of the effects of other launch dates. In each case, curves for 3-sigma fast and 3-sigma slow precession are included with the nominal curve. These 3-sigma curves are based on the 0.266-degree, 3-sigma inclination error corresponding to use of a two-stage Delta launch vehicle.

Figure 30 shows the orbital shadow fraction variation. As the curves indicate, a fairly constant percentage of sun time is available with this profile.

Figure 31 shows the variation in sun-line/orbit-normal angle. Allowing for 3-sigma variations, angles from 31 to 65 degrees are possible, although the nominal orbit varies only from 44 to 57 degrees. These variations have great impact on the power subsystem problems.

Figure 32 shows the local solar time at the ascending node versus time from launch. The nominal orbit holds within 30 minutes of 3 o'clock, while the 3-sigma curves give variations of up to 50 minutes from 3 o'clock.

The complement of the orbit-normal/sun-line angle is the minimum radiometer scan-line/sun-line angle if the radiometer scans in the orbit plane. Figure 33 shows the variation of the forward-scan/sun-line angle (at the time of "scan-intercept-earth") with latitude of the scan point for the "worst case" 28 October, 3-sigma slow-precession orbit.

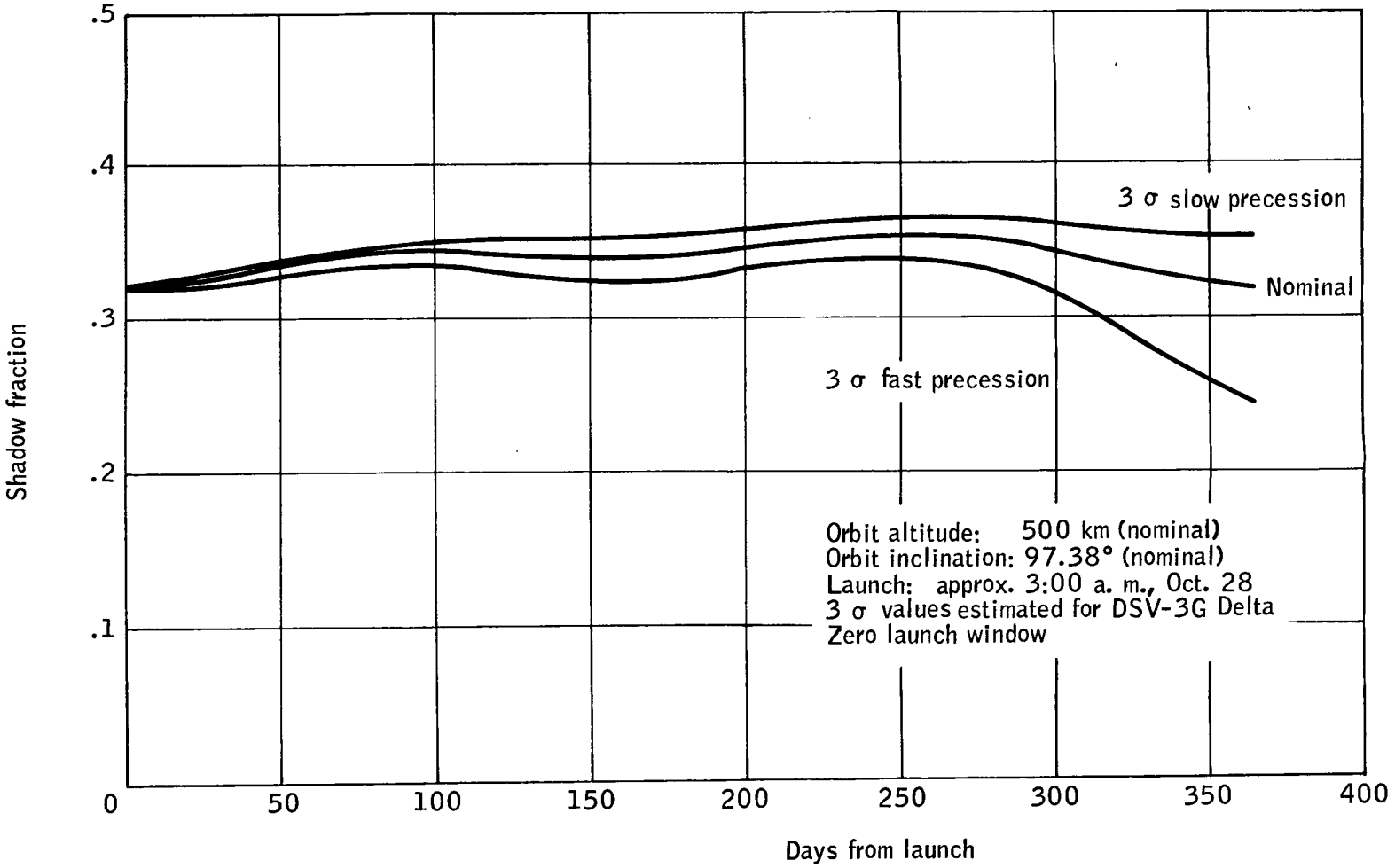

Figure 30. Shadow Fraction versus Days

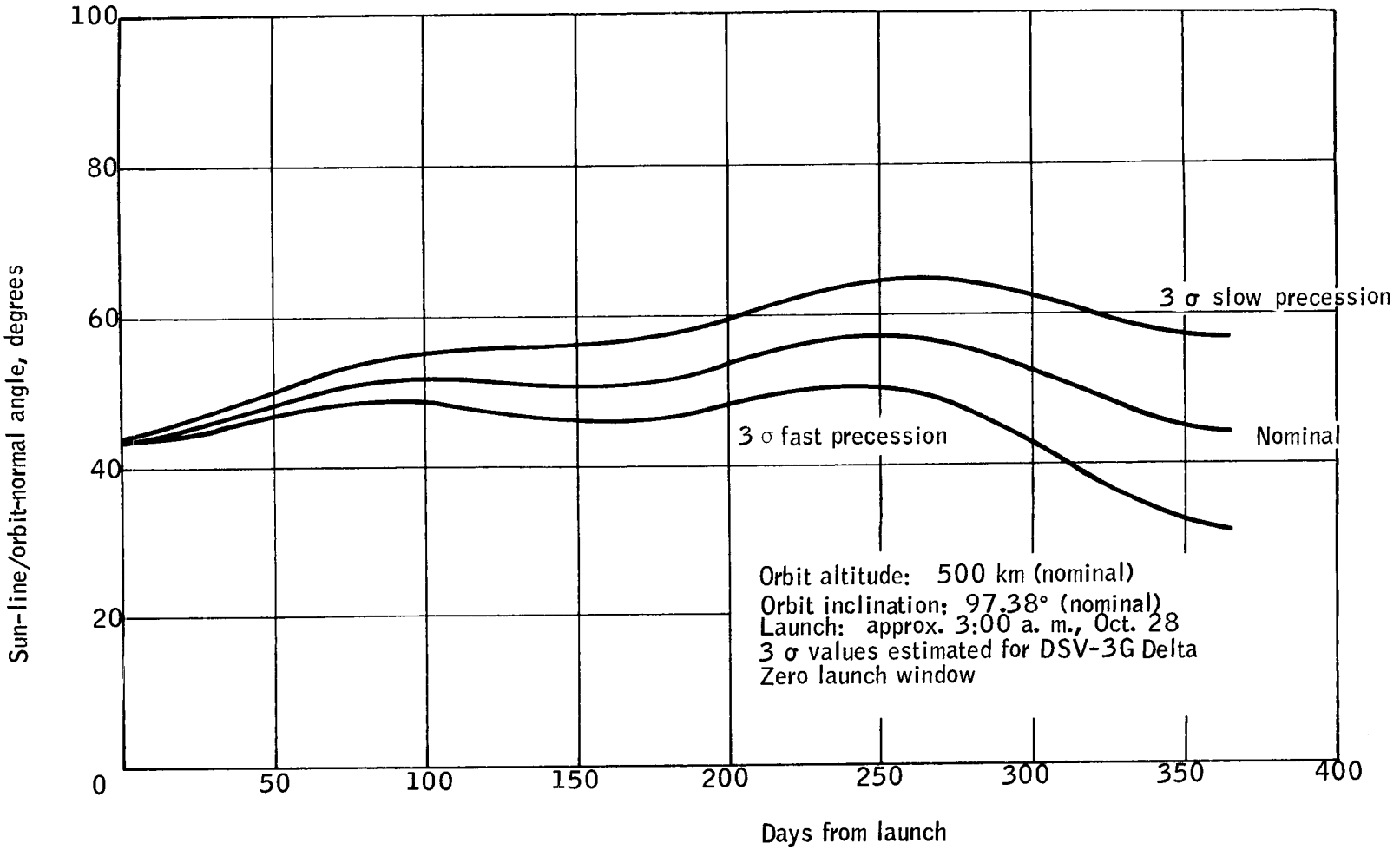

Figure 31. Sun-Line/Orbit-Normal Angle versus Days

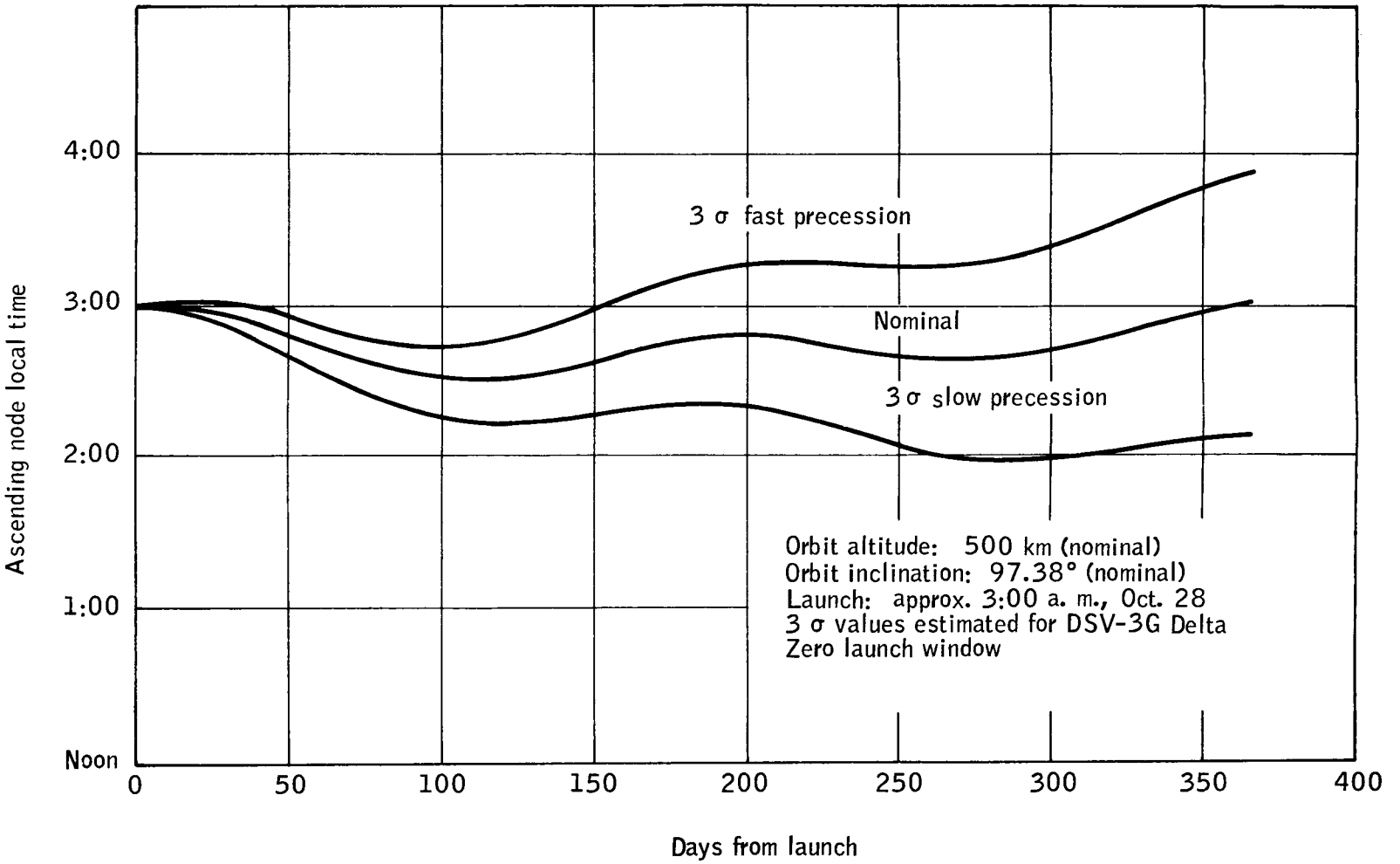

Figure 32. Ascending Node Local Time versus Days

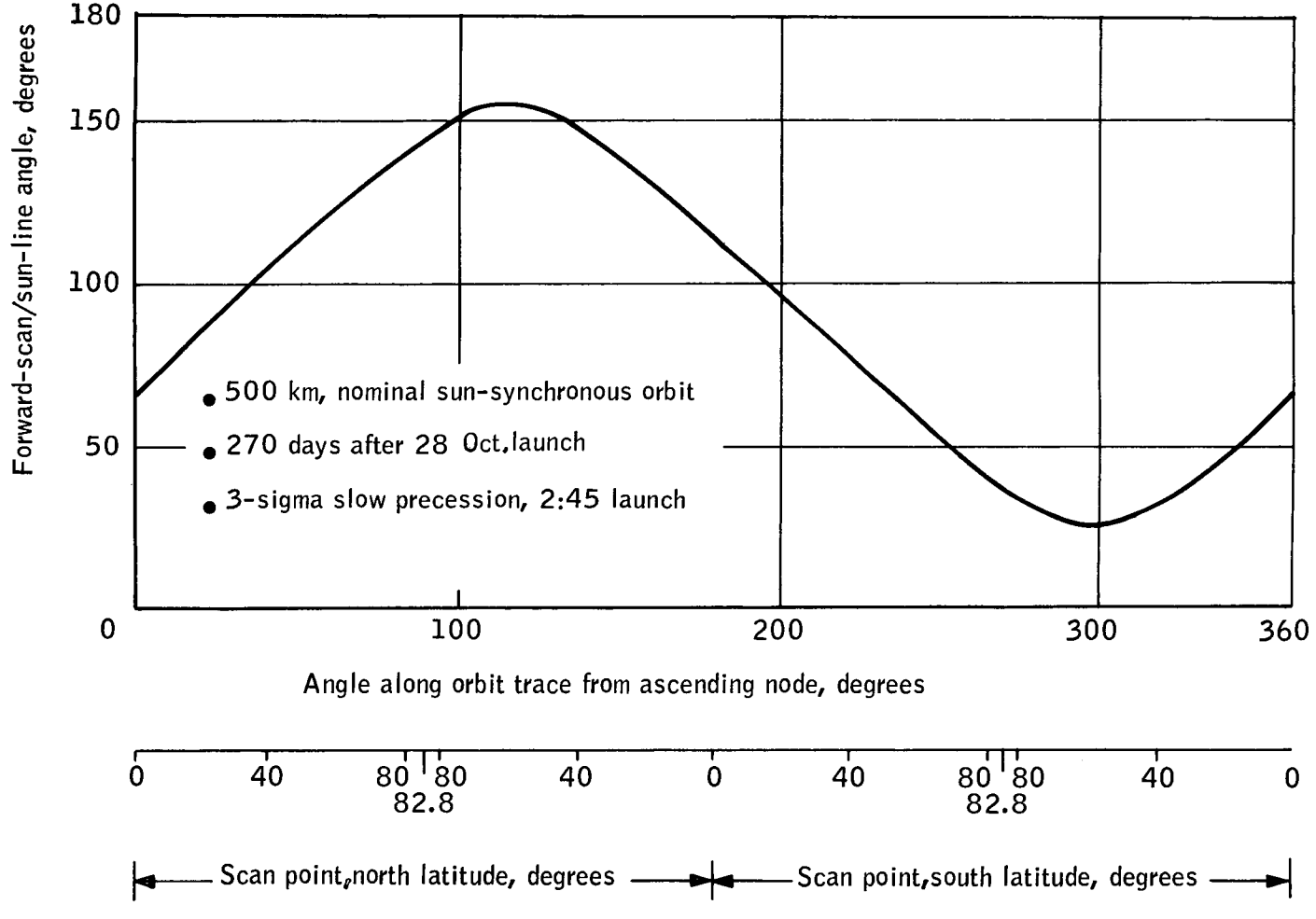

Figure 33. Scan-Line/Sun-Line Angles, "Worst" Case

CONCLUSIONS

Based on the analyses conducted in the mission profile study together with the various system experiment definition investigations, the following conclusions were reached:

1. A nominally circular, 500-km altitude, sun-synchronous orbit (97.38 degrees inclination) with initial ascending node at 3:00 p.m. local time and launch date of 28 October meets experiment and system requirements for the mission.
2. The WTR should be used for the launch site, and a 2-stage Improved Delta vehicle should be used to achieve adequate injection accuracy.
3. A 30-minute launch window, in conjunction with the latest Douglas estimates of 2-stage Delta, 3-sigma injection errors, results in possible sun-line/orbit-normal angles between 29 and 65 degrees by the end of a one-year mission. The orbital shadow fraction can vary from 0.221 to 0.364 and the nodal crossing local time can vary from 2:00 to 4:04.
4. Orbit altitude may be increased somewhat should this become necessary to increase orbit-prediction accuracy or to insure minimal orbit decay during the mission.
5. The possibility remains to change or place specific constraints on launch date, to reduce allowable launch window, to bias launch window centering, to compensate for launch delay with appropriate precession-effecting guidance corrections, or to change the nominal launch time. These actions may be desirable or necessary during the development program either (a) because of experiment requirements or (b) because of sun-angle considerations in the system design.
6. Tracking and telemetry coverage obtainable with the 500-km sun-synchronous orbit and the STADAN system is adequate. Once-per-orbit coverage is available in all but a very small range of the possible orbit nodal conditions. Use of a polar orbit could eliminate the few one-orbit "holes" but only at great expense in terms of yearly sun-angle variation and consequent system design problems.

SPACECRAFT STRUCTURAL DESIGN AND SUBSYSTEM INTEGRATION

A spacecraft structural design and subsystem integration study was conducted to determine feasibility of a totally integrated spacecraft system to fulfill the experiment requirements. The spacecraft system considered consists of two basic elements:

1. A highly sophisticated scientific experiment package, and
2. The subsystems necessary to collect the scientific data and relay it to the ground stations in support of the scientific experiment package.

The structural subsystem is the uniting point where all the subsystems and components must be married into an integrated system and, as such, serves as the focal point for this portion of the study. However, since the structural subsystem must support the experiment package, it must be compatible with and must not place restrictions on the experiment package.

The design constraints applied to the structural design and subsystem integration study efforts, as derived from the basic HDS system requirements, were as follows:

- Utilize a near-polar orbit at about 500 km-altitude
- Utilize proven state-of-the-art subsystems wherever possible
- Keep the spacecraft weight in the under 800-lb (Improved Delta) or less class
- Utilize a totally passive system if possible (with redundancy as needed)
- Provide a very stable platform from which to make scientific measurements

The spacecraft structural subsystem in its central coordinating role must serve to support and enclose the subsystems, provide subsystem alignment and body rigidity, protect the subsystems from the external environment, support the interconnecting networks, maintain a proper operating environment, and provide spacecraft/booster interface. Each of these requirements is directly connected to the requirements of the individual subsystems.

A review of the system and subsystem requirements discussed above suggested that a spin-stabilized spacecraft, spinning about an axis normal to the orbit plane, in a nominal 3 p.m./3 a.m., sun-synchronous orbit, would best meet the requirements. This was the baseline approach used in the conceptual design study effort.

The system and subsystem requirements suggested a "rolling wheel" configuration compatible with an Improved Delta launch vehicle, i.e., less than 57 inches in diameter and under 800 lbs. The baseline spacecraft system was then apportioned into six subsystems, each of which was individually examined and conceptually configured during the study. The subsystems were:

- The experiment package, consisting of the radiance measurement instrument, the attitude determination equipment, and their supporting electronics. This is the primary subsystem in the total spacecraft, and all other subsystems must support it.
- The attitude control subsystem, consisting of the equipment necessary to maintain proper spacecraft orientation and stabilization.
- The data handling subsystem, consisting of the equipment necessary to process and store data between transmission periods.
- The communications subsystem, consisting of the equipment necessary to provide up and down communication links and to provide spacecraft location information.
- The power subsystem, consisting of the equipment necessary to provide and distribute power for all spacecraft needs.
- The structural subsystem, consisting of the hardware necessary to support, enclose, and protect an integrated spacecraft system and to provide the mechanisms necessary to fulfill the system deployment and positioning requirements.

By anticipating what might be desirable properties in the spacecraft to meet the requirements of each of the subsystems, a spacecraft configuration matrix was generated.

Such properties as experiment package compatibility, structural strength, component mounting volume, flat surface availability, booster interface, etc., were assigned weighting factors for different cross-sectional cylinders ranging from triangular through round. This numerical approach, combined with a practical viewpoint inspection, suggested that a cylinder with hexagonal cross section would best meet the needs of this spacecraft and was adapted as the baseline configuration. Salient features of this configuration are:

- Experiment package compatibility
- Spacecraft symmetry
- Simple construction
- Flat surfaces for mounting solar cells
- Flat surfaces for fold-out panels
- Flat internal surfaces for component mounting
- Satisfactory booster/fairing interface

To demonstrate feasibility of a spacecraft system concept to incorporate the necessary subsystems, three areas were considered to be of major importance and were studied in detail.

1. A balance calculation method was developed, computerized, and exercised to determine the dynamic properties of the conceptual spacecraft

2. Analyses were conducted to assure that the thermal design was feasible

3. A conceptual spacecraft was configured, demonstrating compatibility of all the subsystems with the total system as well as with each other.

Other areas which do not have a direct affect on the feasibility of the concept were inherently covered in the study. These included items such as structural-electrical interfaces, launch and orbital environment considerations, and booster interfaces.

EXPERIMENT PACKAGE

The conceptual design of an instrument system which collects data for horizon definition in the carbon dioxide absorption band has been studied here for application in future horizon sensor design. To obtain data useful for instrument design, precise radiance profile data accurately referenced to a geocentric coordinate system is required. Reference to a geocentric system requires knowledge of the instantaneous attitude and position of the vehicle. Position information is obtained from ground tracking stations and is external to the experiment package. Instantaneous attitude must be derived from measurements made in the spacecraft proper and requires some form of attitude reference system tied directly to a radiometer.

In addition to measurement requirements, constraints on the design were developed from a flight techniques evaluation in the same study. Initial constraints on the design included a rolling-wheel spacecraft concept (no active radiometer scanning) and the use of a passive attitude determination subsystem. Size constraints were developed from the Thor-Delta, particularly a length constraint of approximately 48 inches. Orbital parameters derived from the basic data requirements dictated a radiometer line of sight essentially normal to the spin axis and a closest approach of the sun to the radiometer line of sight of approximately 26 degrees. A basic general requirement of full redundancy in the attitude determination and radiometer subsystems was also established.

A passive starmapper with slit reticle and photomultiplier detector was selected as the basic attitude determination system as a starting point for instrument design. However, a study of the baffling requirements for the starmapper led to the selection of a starmapper-sun sensor combination for attitude determination. Use of sun sensors during daylight operation eliminates the necessity for trying to operate a sensitive starmapper exposed to sunlight. Although feasible the design, fabrication, and testing of a baffle with 10^{12} attenuation are extremely difficult problems.

The experiment package subsystem interactions, the design of each of the elements, and the attitude determination process are discussed in the following sections.

Radiometer-Starmapper Relationship

The error in measuring tangent height can be attributed to three basic geometrical errors. Two of these, altitude and in-track errors, are related to vehicle position. The third, angular orientation error, is related to the attitude determination problem. The total error in tangent height can be expressed (to first order) as

$$\Delta h_t = \frac{\partial h_t}{\partial h} \Delta h + \frac{\partial h_t}{\partial s} \Delta s + \frac{\partial h_t}{\partial \epsilon} \Delta \epsilon \qquad (18)$$

where

Δh_t = tangent height

h = spacecraft altitude

s = horizontal coordinate along scan azimuth

ϵ = angular orientation of scan axis in a vertical plane

The altitude and in-track errors are due primarily to:

1. Tracking error (instrument error)
   a. Position measurement
   b. Timing error
2. Orbit prediction error
   a. Gravitational
   b. Geodetic/station location
   c. Drag uncertainty

while the angular orientation error is due primarily to:

1. Radiometer/starmapper/sun sensor misalignment
2. Starmapper/sun-sensor measurement error (instrument)
3. Internal timing and data-handling errors
4. Attitude determination model errors
5. Star ephemeris errors

The three error coefficients $\frac{\partial h_t}{\partial h}$, $\frac{\partial h_t}{\partial s}$, and $\frac{\partial h_t}{\partial \epsilon}$ are functions of altitude. Also, the errors Δh and Δs are functions due to practical considerations in the orbit determination process. Expansion of equation (18) into constituent errors thus results in a tangent-height parametric equation which can be used in system tradeoffs.

Manipulation of the error equation with reasonable estimates of orbit determination accuracies gives an immediate indication of measurement system error as a function of orbital altitude. For a given set of radiometer/starmapper parameters, timing error level, attitude determination model errors, and star ephemeris errors (usually negligible), a "minimum tangent-height-error" altitude will usually exist. By the same type of analysis, for given orbit determination accuracy (orbit altitude), timing error level, and star ephemeris error, tangent-height error level will approach an asymptotic level with increased radiometer/starmapper system accuracy and attitude determination model accuracy.

The measurement system error analysis was conducted on an iterative basis. From an initial estimate of the error breakdown, or "budget", the error levels were reallocated as the study progressed. For example, star ephemeris (star position) error was found to be of the order of 0.1 arc second (about 1.2 meters in tangent height) which is negligible. STADAN system timing error of about two milliseconds converts to about 6 meters in tangent height, which is also very small. It is anticipated that spacecraft internal timing error, corresponding to on-board clock stability over one (or a few) spacecraft rotation, can be held to a level which gives negligibly small tangent-height error. The same is true for the digitizing of sensor data and other data-handling functions. This leaves four major sources of error:

1. Lumped-parameter position determination error
2. Radiometer/starmapper/sun sensor alignment error
3. Starmapper/sun-sensor measurement error
4. Attitude determination model error

In practice, separation of the latter two error sources is difficult. Therefore, position determination, instrument alignment, and instrument/model errors are the principal sources of tangent-height error in the overall measurement system. Since position determination is an operational problem involving fairly fixed levels of capability, the only means left to the HDS system designer for holding (or increasing) the measurement accuracy lies in the alignment and instrument/model areas.

Radiometer System Requirements

The basic HDS program objectives have been stated in terms of the functional relationship between radiance and tangent height, the variability thereof, and the total data required. To accomplish these objectives, they must be translated into radiometric requirements. These requirements are in terms of sensitivity, resolution, accuracy, and the conditions under which such requirements apply.

Specifically, the quantities which define radiometric performance are:

- Sensitivity - expressed as Noise-Equivalent Radiance (NER) or that input signal level required to produce a signal equal to the noise level at the radiometer output.
- Resolution or transfer function - the relationship between input and output expressed as a function of the spatial frequency content of the input.
- Radiometric accuracy - expressed in terms of signal-level-dependent (scale) and signal-level-independent (bias) components and distinction between constant, slowly varying, and rapidly varying contributors.

In addition, entities that define the conditions under which these three basic performance criteria must exist are

- Dynamic range - range of input radiance levels over which the requirements apply.
- Spectral interval.
- Mission constraints - determination of the relationship between time and spatial frequencies as well as definition of thermal, volume, and weight constraints.

Quantitative derivation of the above requirements and constraints from the experimental objectives determines the performance desired of the radiometer and becomes the grounds for the first-order assessment of feasibility. The method used was to synthesize the phenomena to be measured and the characteristics of the measurement instrument and to evaluate the resultant simulated measurement with respect to the degree to which the program objectives were achieved.

Requirements and constraints. -- The basic radiometric objective is to obtain data upon the earth infrared horizon of sufficient quality for two applications: to determine the ultimate, obtainable horizon sensor performance as limited by the characteristics of the horizon itself, and to further develop understanding of the physics involved in the emission of the earth atmosphere.

For horizon sensor applications, the desire is to determine the horizon variability that is random or effectively nondeterministic as opposed to that which can be explained, predicted, and, hence, corrected. Synthesization of the infrared horizon radiance versus tangent-height profiles was performed for a wide variety of conditions and as a function of spectral interval. The latter quantity was chosen to provide the most stable horizon, and the expected deterministic and nondeterministic variabilities were estimated and may be summarized as:

- Maximum peak radiance = 7.0 W/m^2 - sr
- Minimum peak radiance = 3.0 W/m^2 - sr
- Maximum slope = 0.6 W/m^2 -sr-km
- Minimum slope = 0.02 W/m^2 -sr-km
- Maximum rate of change of slope = 0.15 W/m^2 -sr-km^2

These requirements are summarized in Table 19 together with the affected radiometer characteristics. These requirements ensure that the earth's horizon profile will be reproduced accurately under all measurable conditions. By meeting these requirements, systematic variations in the horizon radiance profile over all time and space can be determined to the 0.5 km resolution ascertained in the data requirements study. Table 19 illustrates the point that no one of the parameters (sensitivity, resolution, or accuracy) that are needed to define a radiometer is singly dependent upon a given measurement requirement, which is why simulation of the measurement process has been used to define the requirement parameters.

The constraints that the mission places upon the radiometer design chiefly derive from two factors: the spacecraft is a spin-stabilized, rolling-wheel configuration and is nominally in a 3 p.m., sun-synchronous orbit (Figure 34). The following considerations then apply:

- Passive scanning is available.
- Thermal control and choice of operational temperatures can utilize the fact that one side of the spacecraft is never illuminated by the sun.
- The angle between the sun line and radiometer line of sight can be as small as 26 degrees.
- Orbital altitude is 500 km which implies a conversion factor of 0.02°/km tangent height.
- Spin rate is three rpm which implies a scan rate of 18°/second or 800 km tangent height/second.

Profile/radiometer synthesis studies. -- Two types of studies were performed:

1. To determine the effects of all the possible types of radiometric error upon horizon-detection capability versus the magnitudes of those errors;
2. To quantify the errors attributable to system resolution or frequency response.

Radiometer accuracy: Effects of radiometer errors on the data measurement requirements were determined by analyzing a set of 120 synthesized radiance profiles with the expected types and magnitudes of radiometer errors and calculating the error in the located horizon which would be obtained by various horizon-detection techniques.

TABLE 19. - PROGRAM MEASUREMENT REQUIREMENTS

Requirement	Affected parameters
1. Spectral interval: 14.0 to 16.28 μ	Type of optics and detector operating temperatures
2. Resolve radiance signals ≤ 0.01 W/m^2 -sr at spatial frequencies up to 1.0 cycle/km	System transfer function (optics, detector, and electronics) Sensitivity (NER) Radiometric accuracy
3. Conform to (2) over the range of absolute radiance: 0.01 to 7.0 W/m^2-sr	Dynamic range Sensitivity (NER) Radiometric accuracy
4. Measured radiance assignable to tangent-height accuracy of ±0.25 km from -30 km to + 80 km	Attitude determination accuracy Transfer function Sensitivity Radiometric accuracy
5. Meet all requirements for one-year life in orbit	Applicable technology and hardware operating temperatures
6. Azimuth resolution ≤ 25 km	Sensitivity

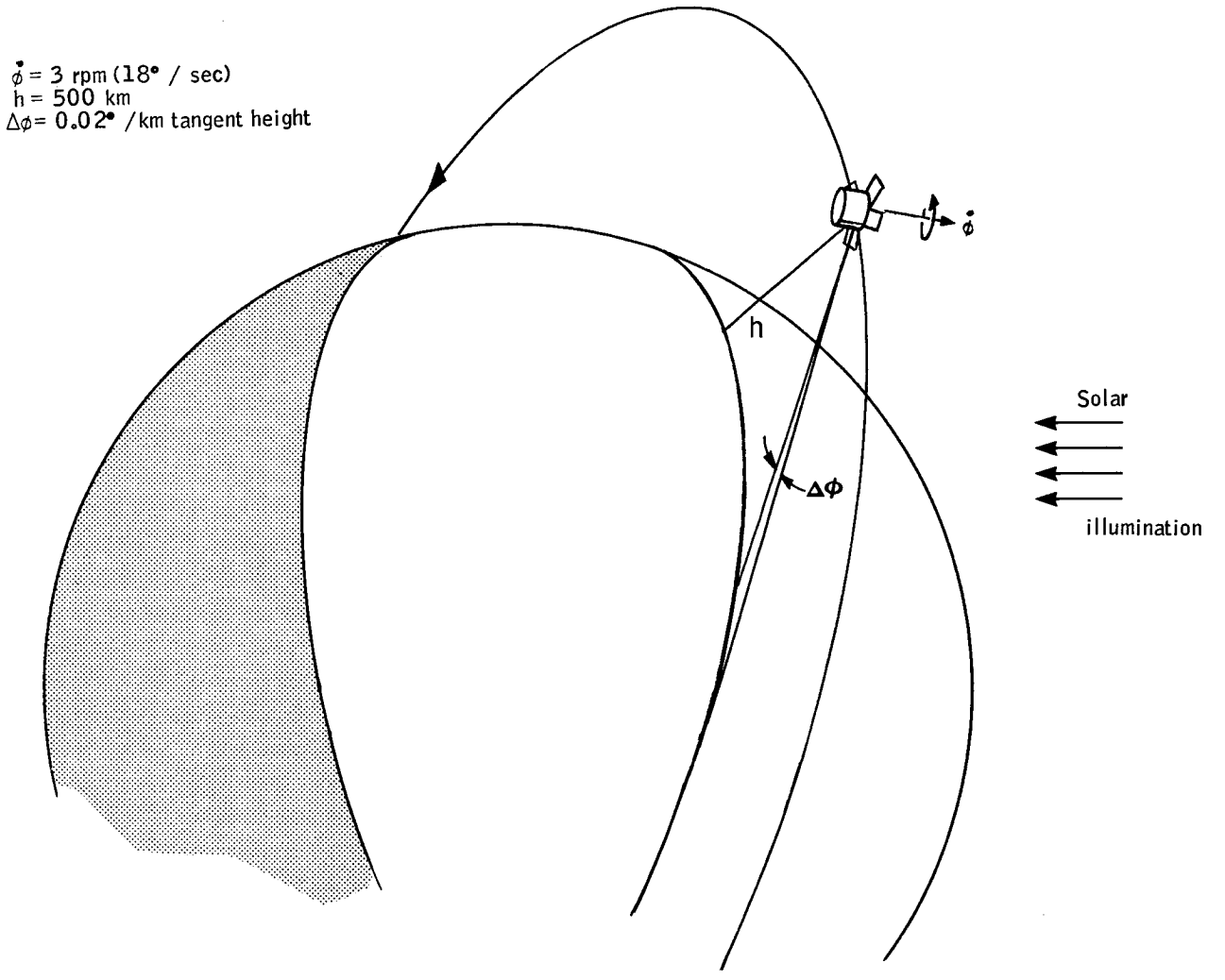

Figure 34. System Constraints

Each of these profiles was perturbed by four values of six different types of radiometer error. Radiometer errors were divided into two basic errors - scale and bias. These two kinds of errors affect radiance measurements in three different ways.

The first type of error is one that is constant in time, such as a calibration error. When a given radiometer is calibrated, all of the instrument errors (e.g., nonlinearity, offset, etc.) can be assumed to be calibrated out, but a residual calibration uncertainty remains because of the uncertainty of the radiance input itself. By analysis and test, the maximum values of the uncertainty can be bracketed, but within this tolerance range the actual value of the error is not known. However, the error that existed at the time of calibration remains fixed for a given instrument. That is, if the calibration radiance N_o is known to within ±1 percent, then for a given calibration the input radiance lies between $0.99\ N_o$ and $1.01\ N_o$. If the input radiance is assumed to be $0.995\ N_o$, then a fixed calibration error of 0.5 percent exists for the instrument for all time. These fixed errors appear to have no effect on local vertical because all profiles are affected in the same direction, and the errors subtract out when differences are taken to find local vertical. However, they do affect located horizons since they propagate into located horizon errors as a function of profile shape and magnitude. Unless horizons 180 degrees apart are identical, an error in local vertical will be obtained.

Errors that vary over the operation of the devices are generally termed precision, or repeatability, error within an instrument. In-flight calibration will be available for the radiometer, so this class of errors will be discussed further. Since repeated calibration is to be done, the stability of the calibration is critical; this stability includes that of the calibration source and of the radiometer response.

Instabilities are of two kinds - those that fluctuate rapidly, e.g., detector or electronics noise, and those that fluctuate slowly, e.g., temperature-caused drift. For the HDS radiometer application, a slowly varying error is assumed to be one which has a constant magnitude over a single profile measurement but which varies from profile to profile. A rapidly varying error is one which changes in magnitude from point to point on each profile being measured. Both of these errors were assumed to be normally distributed.

The body of data operated on by different horizon detection techniques to determine horizon error consisted of 24 different sets of 120 radiance profiles in each set. Each of these sets of profiles was operated on by four different threshold techniques with two threshold values used for each technique as summarized in Table 20.

TABLE 20. - HORIZON DETECTION TECHNIQUES

Threshold technique	Threshold values
Radiance magnitude, (L1)	2.0, 3.0 W/m^2 - sr
Normalized radiance magnitude, (L2), of peak radiance	0.15, 0.90 (15%, 90%)
Integral of radiance, (L3)	4.5, 20.0 W-km/m^2-sr
Integral of normalized radiance, (L4)	2.5, 10.0 km

Sensitivity of each locator concept to attitude error was examined and presented as in Figure 35. These data were then combined to produce criteria that would allow determination of the actual horizon error to within one-half kilometer for the 90-percent confidence level.

Radiometer specifications derived from these analyses are

- Scale calibration: 3% (1.0% design goal)
- Scale drift: 0.72%
- Scale noise: 0.27%
- Bias calibration: 0.01 W/m^2 -sr
- Bias drift: 0.01 W/m^2 -sr
- Bias noise: 0.01 W/m^2 -sr

Radiometric resolution study: Radiometer resolution is a function of the collecting aperture diameter of the optical system, the detector field of view, and the electronics bandwidth.

To evaluate the effects of the various combinations of radiometric parameters on the horizon measurement, the set of 120 profiles, discussed earlier, was operated on by simulated radiometers. The resulting errors were then computed in terms of located horizon, local vertical, and the radiance tangent-height function itself. Twenty-seven cases were evaluated employing all combinations of the following parameters:

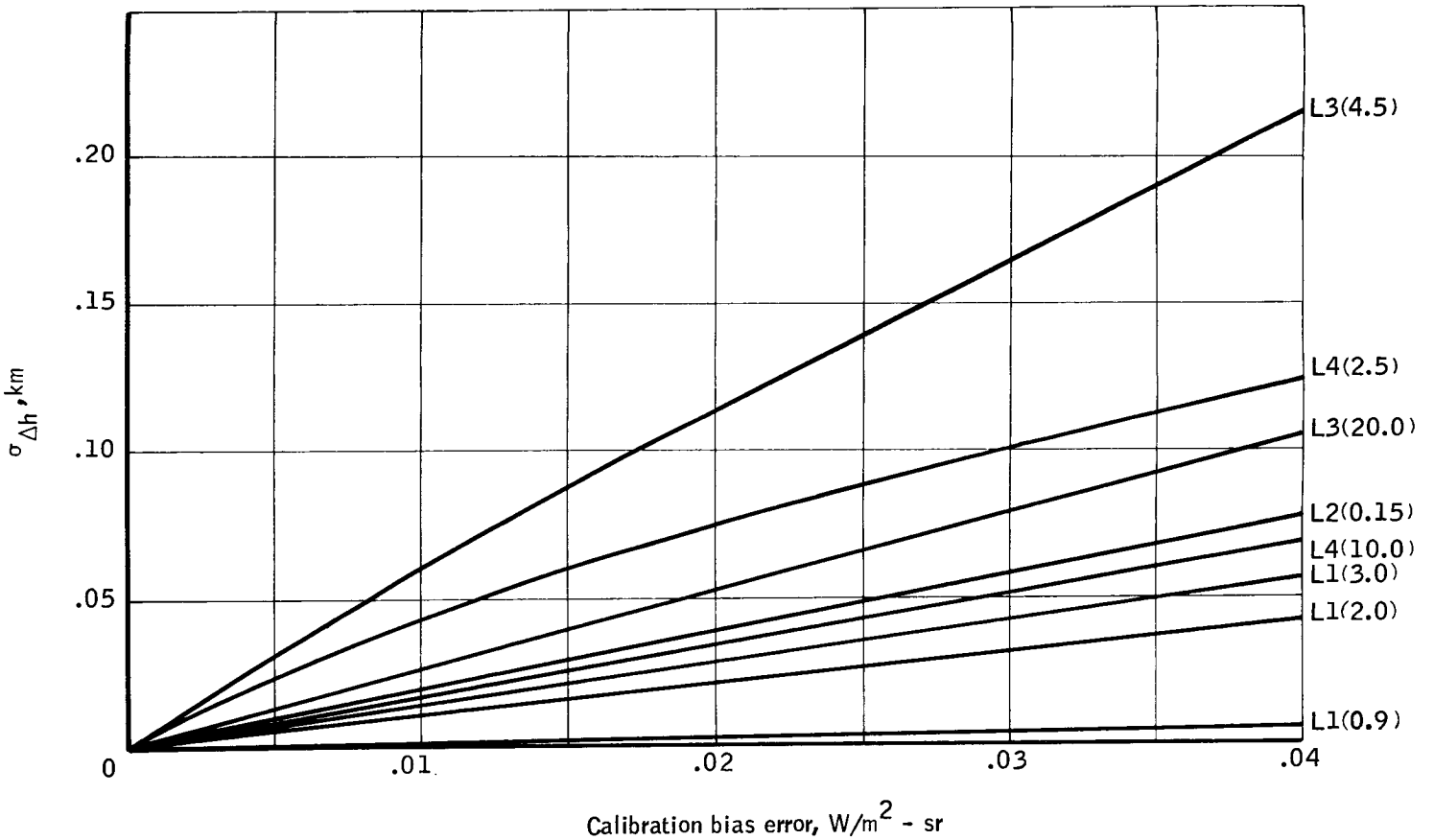

Figure 35. Located Horizon Error Standard Deviation Caused by Instrument Calibration Bias

- Optics diameter: 20, 40, and 60 cm
- Detector field of view: 0.005°, 0.01°, and 0.02°
- Electronics 3-dB bandwidth: 750, 1500, and 3000 Hz (where 750 corresponds to 1 cycle/km)

The above represents a variation in system bandwidth of from 1/3 to 1-1/3 cycles/km.

Other parameters used in the simulation were:

- Scan rate: 18°/sec
- Altitude: 500 km
- Radiometer focal length: 40 cm

Output of the electronics was obtained by assuming that the detector time output is linear from point to point as the horizon profile is scanned in finite time increments. The electronics transfer function was assumed to be given by a single-order, low-pass filter. Output of the low-pass filter to each input was calculated and summed to give the electronics output.

Maximum mean errors obtained from this simulation are in the range 0.2 to 0.3 km and appear to be relatively independent of variation in aperture size or detector field. More thorough examination of the results indicated this error to be almost totally due to the low-frequency phase shift of the assumed linear, first-order electronics filter. It is, therefore, correctable to within its standard deviation and does not exhibit a significant dependence upon electronic bandwidth.

Radiometer sensitivity. -- The foregoing discussions have implied that the one remaining parameter NER would naturally emerge from the error analysis. This parameter is, in fact, one of the contributors to noise bias errors and, as such, should be maintained at no greater than 1/3 the total error allotment, i.e., $0.003 W/m^2$ -sr. This is also consistent with the program measurement requirements of detecting a minimum absolute radiance of $0.01 W/m^2$ -sr as well as measuring fluctuations of the same amount regardless of absolute radiance level.

Radiometric sensitivity is

$$NER = \frac{4}{\pi} \quad \frac{f/no. \sqrt{\Delta f}}{D^* \; D_c \; \delta \sqrt{\Delta \Omega}} \tag{19}$$

where

f/no. = optics effective f number,

Δf = post-detection noise equivalent bandwidth,

D_c = aperture diameter,

D^* = detector detectivity normalized to unity area and bandwidth,

$\Delta \Omega$ = detector field of view,

= $\Delta \theta$ (oz) x $\Delta \phi$ (eℓ), and

δ = system efficiency,

Since

$$\Delta f = k (\Delta \phi)^{-1} \dot{\phi}$$

where

$\dot{\phi}$ = scan rate, and

k = constant of proportionality of electronics cutoff in terms of resolution elements/sec,

then an alternate form exists:

$$NER = \frac{4}{\pi} \quad \frac{f/no. \sqrt{k \dot{\phi}}}{D^* \; D_c \; \Delta \phi \; \delta \sqrt{\Delta \theta}} \qquad (19a)$$

Now $\delta = \delta_o \delta_e$ where δ_o and δ_e are the efficiencies of the optics and electronics, respectively,

and $\sqrt{\frac{k}{\delta_e}} \simeq$ constant ± 5 percent, $1/2 < k < 2$;

therefore, any k in that range and the corresponding δ_e can be used for the purpose of computing NER. (Note, there are other factors involving the choice of sampling rate, memory size, etc., that enter into the actual choice of k.) In particular, k can be taken as one, and δ_e computed for the specific electronic operations utilized.

The quantity f/no. can reasonably be taken to be one for the purpose of this analysis; ϕ, the scan rate, is 18°/sec.

The azimuthal resolution $\Delta\theta$ can be as great as 25 km ($\sim$ 10 mr). However, since the elevation resolution will lie between 0.25 and 1.0 km and since aspect ratios on the detector of greater than 5 to 10 will be difficult to achieve, $\Delta\theta$ will be taken as equivalent to 2 km, 0.8 mr. Owing to the required low frequency response, the system will undoubtedly employ a chopper implying a 50-percent energy load/resolution element. Further losses lie in the spectral filter ($\sim$40 percent) and the optics ($\sim$ 40 percent), which taken with δ_e ($\sim$ 0.80) yield a system efficiency in the range 10 to 15 percent. Using 0.15 yields the following relation

$$\text{NER} = \frac{1.7 \times 10^2}{D^* D_c \Delta\phi} \text{ W/cm}^2\text{-sr}$$

with D^* in cm - $\text{Hz}^{1/2}$/W, D_c in cm, and $\Delta\phi$ in radians.

This quantity is plotted Figure 36 for a range of D^* corresponding to the applicable technology in detectors and coolers. Note that to get a room-temperature system onto the same graph required giving it a 25-km azimuthal resolution, so that the difference between it and the other two temperature regimes is quite real. Such is not the case between the lower two bands which can be made to converge by means of increasing the aspect ratio somewhat.

Radiometer Design

Development of the actual design of the radiometer must include determination of the following elements: type of detector, operating temperatures, optical system, and the calibration techniques used to produce the accuracy required of the radiometer system.

Detector selection. -- Primary detector parameters are:

1. Detectivity - the capability of the detector acting as an irradiance-voltage transducer expressed in W^{-1}-cm -$\text{Hz}^{1/2}$.
2. Noise characteristics - the spectrum of the noise relative to the signal spectrum defines the information processing system characteristics.
3. Cooling requirements - since most long-wavelength infrared detectors require some form of cooling and this is a long-life mission, the cooling requirements clearly play a strong part in the design selection.

The detector field was surveyed and four detectors with response in the required wavelength region were found. These are:

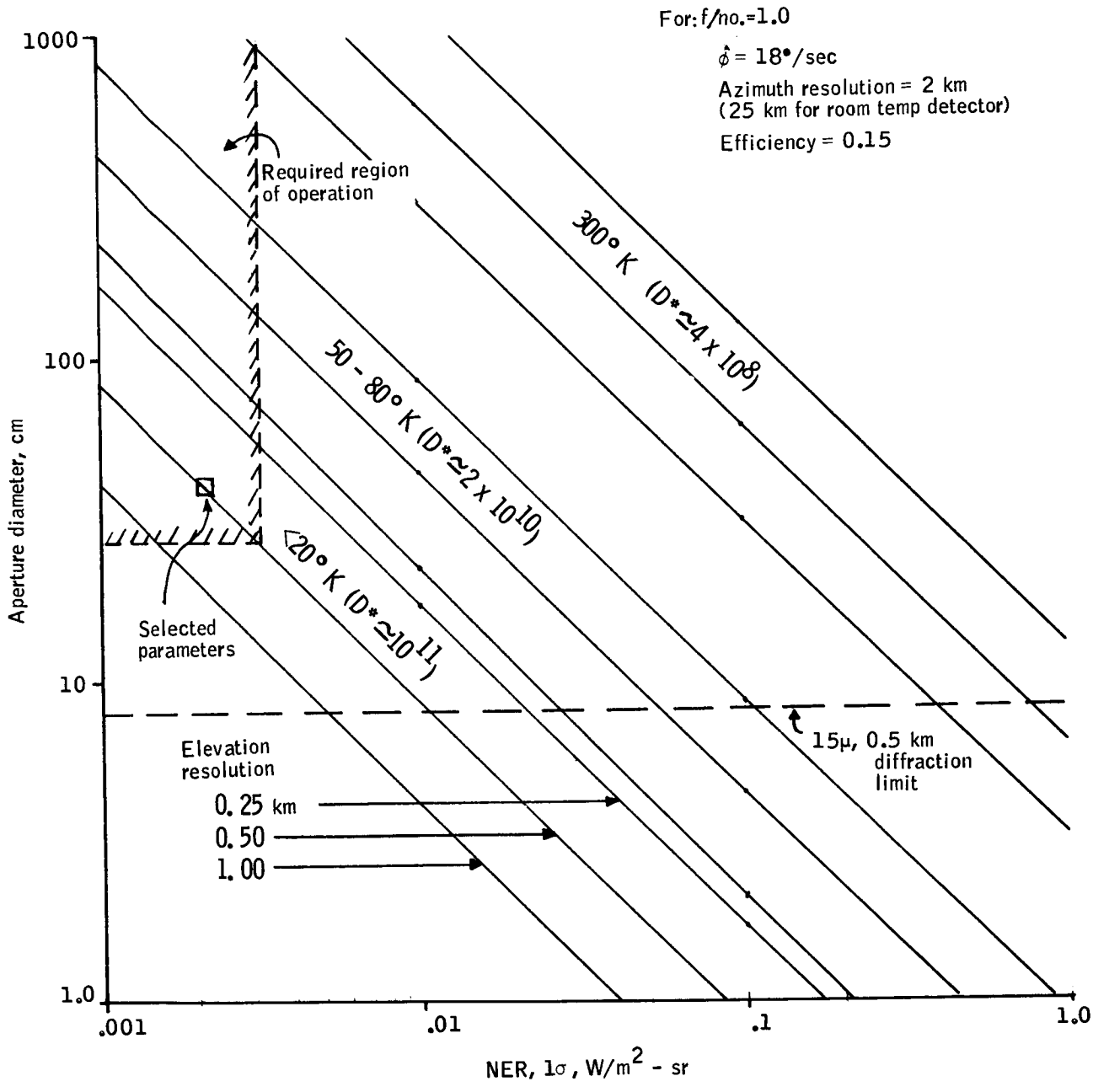

Figure 36. Minimum Detectable Radiance

1. Thermistor bolometers
2. Copper-doped germanium
3. Cadmium-doped germanium
4. Mercury cadmium telluride (theoretical only)

The detectivity requirements obtained from the radiance measurement requirements immediately eliminated the thermister bolometer from consideration. Copper-doped germanium, while extremely sensitive, requires cooling to liquid-helium temperatures for safe operation and was eliminated for this reason. Cadmium-doped germanium requires cooling to the region of 15 to 20°K and has reasonable detectivity. Mercury cadmium telluride is in the developmental stages but requires cooling only to 60 to 70°K. Because of the developmental nature of mercury cadmium telluride, the only other acceptable candidate, cadmium-doped germanium, was chosen to develop a conceptual design.

As soon as the type of detector is chosen, virtually all of the remaining characteristics can be determined (see Figure 36). With the choice of Ge:Cd, the following parameters may then be defined:

Detector type: Ge: Cd

Detector temperature: 15 to 20°K

$D^*_{15\mu,\ 1500,\ 1}$: $\geq 1 \times 10^{11}$ cm - $Hz^{1/2}/W$

Aperture diameter: 40 cm

f/no.: f/1.0

Detector field of view: $0.2 \times 0.8\ (mr)^2$

Electronic bandwidth: 1600 Hz
(0.1 to 1600 Hz post detection)
($f_c \pm 1600$ Hz predetection where f_c = chopping frequency)

Actually the requirement upon aperture size is sufficiently loose, considerin resolution, and since the radiometer NER is really proportional to $\frac{Do_o}{f/no.}$, the latter quantity should be specified as whole rather than in terms of its components. To meet the NER requirement of 0.003 W/m^2 -sr, with the D* and other parameters defined as above, $\frac{Do_o}{f/no.}$ must be $\geq$ 25 cm.

Operating temperature. -- In a long-wavelength radiometer such as this is, thermal emission within the instrument can produce signals greater than that due to the horizon itself. Figure 37 illustrates the various effects of this thermal emission upon the radiometer. These spurious signals are effectively constant in time and can be subtracted from the data and hence produce, theoretically, no error. However, gradients (either time or space) in the emission will produce unknown signal components and, therefore, errors. For the purpose of feasibility demonstration, the operating temperature of the radiometer will be set as low as is practical for the spacecraft.

Only active refrigeration and passive cooling with a subliming cryogen, of the cooling systems investigated, are applicable for the temperature ranges required and for the long-life requirement. Active refrigerators, however, have not yet demonstrated the lifetime requirements, are inefficient power consumers, and would require redundancy. Thus, passive cooling with a subliming cryogen was chosen. There are internal tradeoffs in the design of the passive cooler involving the temperature of the cooler surroundings, the use of a two-stage cooler, and the choice of cooling medium. The resultant conceptual design is a two-stage cooler, with surrounding environment held to approximately 200°K, using solid methane and solid neon as refrigerants.

Table 21 shows the elements used to design the detector cooler, and Figure 38 shows a schematic of the cooler.

The requirement for 200°K on the cooler environment is met by using the spacecraft baseplate as a radiator. The entire experiment package is thermally isolated from the spacecraft and connected directly to the baseplate.

Optical system. -- The general classes of optical systems investigated were:

a. Off-axis Herschelian

b. Classical Newtonian

c. Cassegrainian

Primary optical requirements are stated in terms of clear aperture, effective focal length, and resolution which yields f/no. and resolution as fixed parameters. In addition to these primary requirements the secondary requirements of balance and inertia requirements for the spacecraft, cooler placement, and requirements for baffling against the earth were imposed. Using these requirements a folded Newtonian optical system imaging on detectors on the spacecraft spin axis was developed as the conceptual design. Ray-trace studies were used to verify performance of this system.

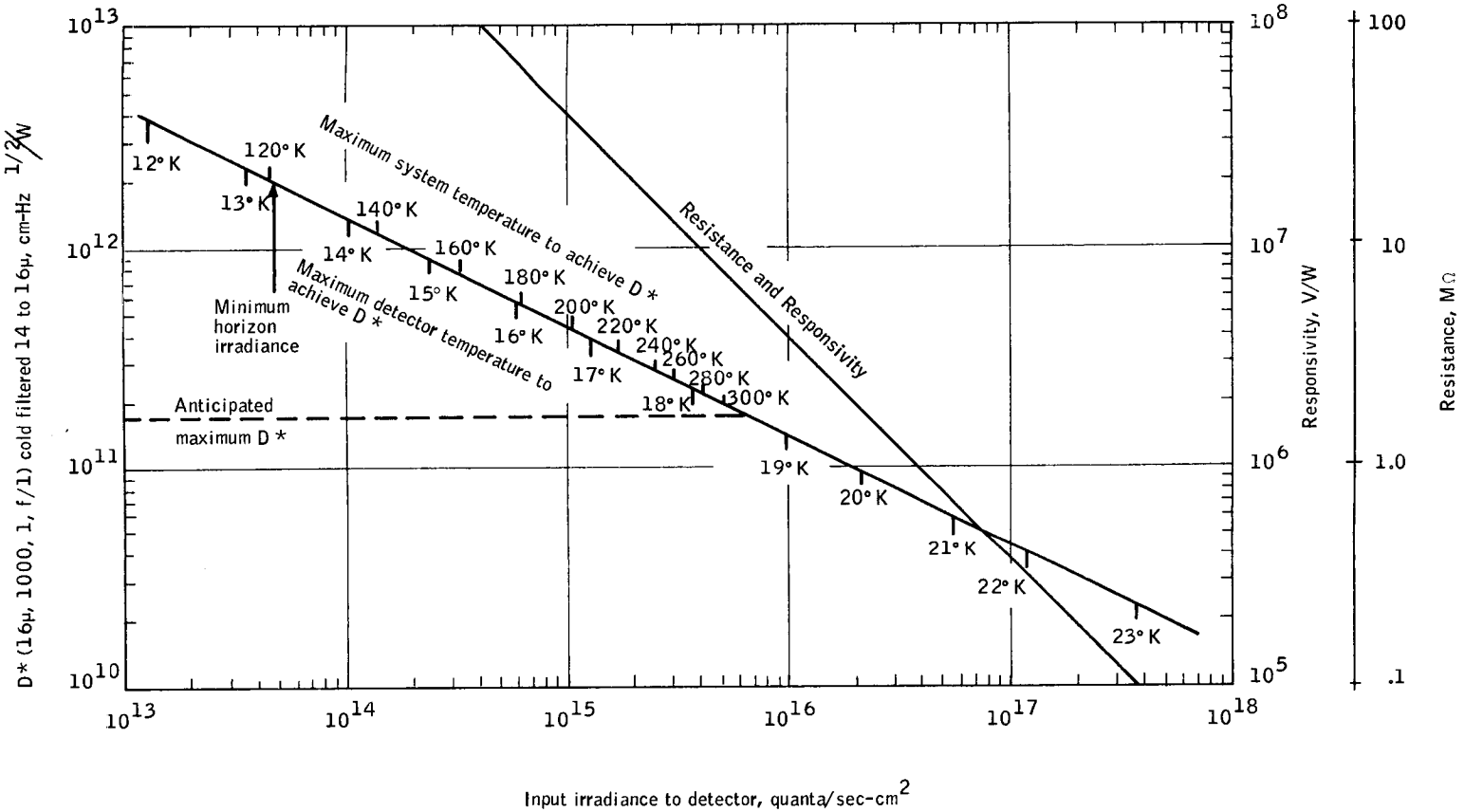

Figure 37. Variation of Responsive Properties of Ge:Cd with Input Irradiance

TABLE 21. - PRELIMINARY SIZING OF A 10 mW, 15°K REFRIGERATOR[a]

Sensor requirements

T, °K	15 to 20
Duration, years	1
Total heat load, mW	6.4

Refrigerator requirements

Refrigerants	Neon	Methane
density, g/cm^3	1.495	0.49
latent heat, joules/g	105.2	615
Containers		
volume, cm^3	2200	3600
dimensions, cm	11.2 o.d. x 22.4 high	14.9 i.d. x 20.1 o.d. x 25 high
mass, grams		
refrigerants	3000	1600

Heat rates, milliwatts

Heat exchanger lines	< 0.6	< 0.3
Insulation	< --	< 8.0
Radiation	< 1.0	< 2.8
Supports	< 2.0	< 14.0
Detector	< 6.4	< --
	< 10.0	< 25.1

Estimated weight

Neon and methane	11.1 lbs
Vacuum container	8.0
Insulation	2.0
Containers	2.5
Heat exchanger	0.5
Support	0.5
Miscellaneous	2.0
Total weight	26.6 lbs

[a]Total heat load is 10 mW on neon; actual total detector heat load is 6.4 mW including provision for 5 mW of detector bias current heating.

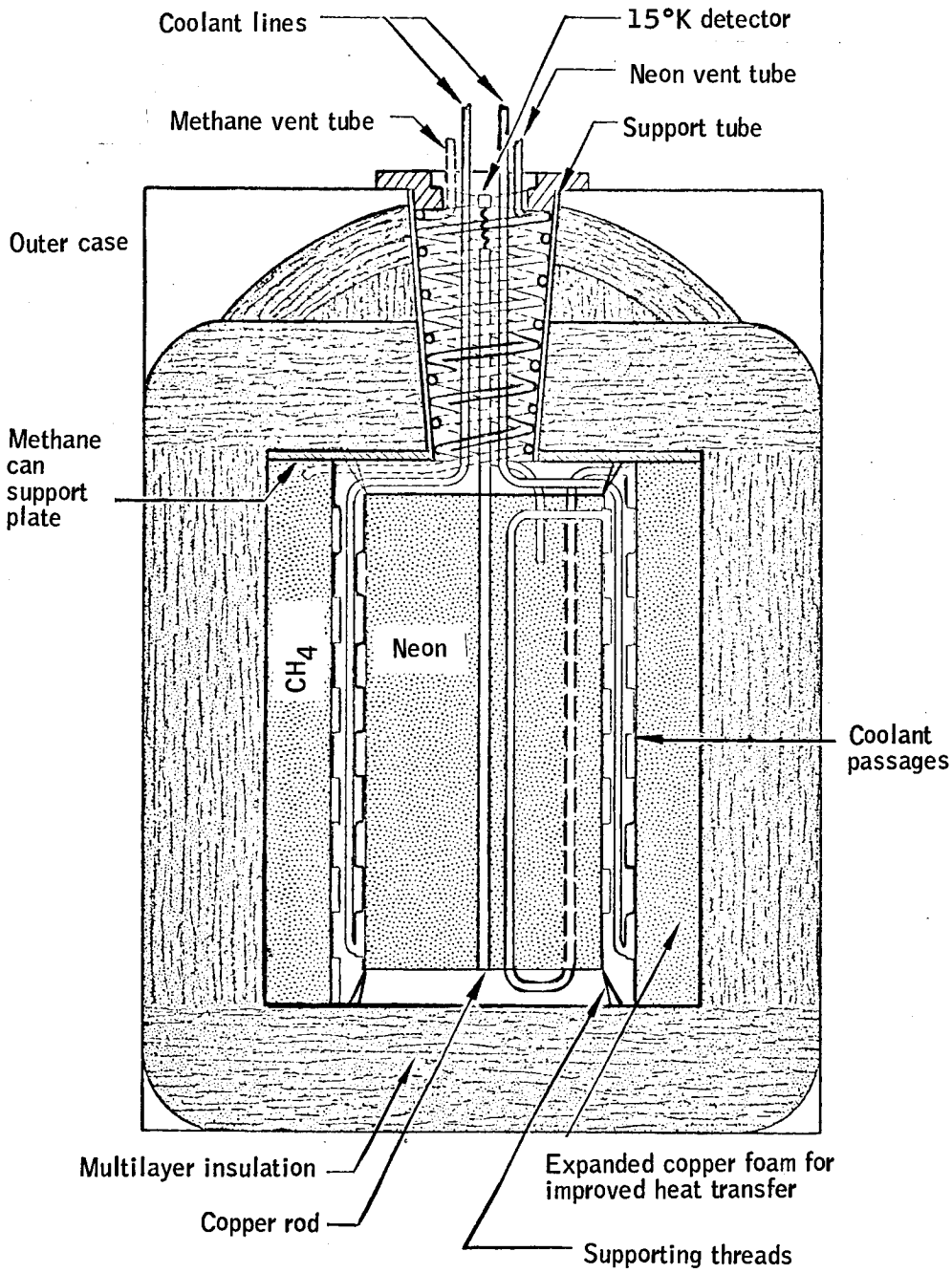

Figure 38. Schematic of Neon-Methane Refrigerator

Calibration techniques. -- Calibration of the radiometer against an absolute standard to the accuracy required is an advance in the state of the art.

Although there are significant problems in other areas, the major problem is the present lack of a source in the wavelength region of interest. Two avenues of investigation have been pursued: the development of a precision attenuator for use with already developed sources and the development of a new standard source. Results indicate that both systems are feasible, and development of both approaches has been recommended.

For the feasibility demonstration of the HDS radiometer, the approach to primary calibration is shown in the block diagram of Figure 39 and has the following features:

- Calibration sources: One fixed radiance, fixed temperature-Hg freezing point
  One adjustable temperature
  One fixed temperature (Sn freezing point), adjustable radiance
- Spectral calibration: Sn freezing point (NBS) source and monochromator

Thermal control is required to accurately position and vary the radiometer temperature and to maintain the source surroundings and optical elements near liquid-nitrogen temperatures to avoid errors due to their emission.

The expected absolute radiometric measurement accuracy is as tabulated in Table 22. Note that although the noise bias and drift scale errors slightly exceed specification, they are more than compensated by the degree to which the other types of errors are below their specified value. As was noted before, these errors may, to a degree, be traded against one another.

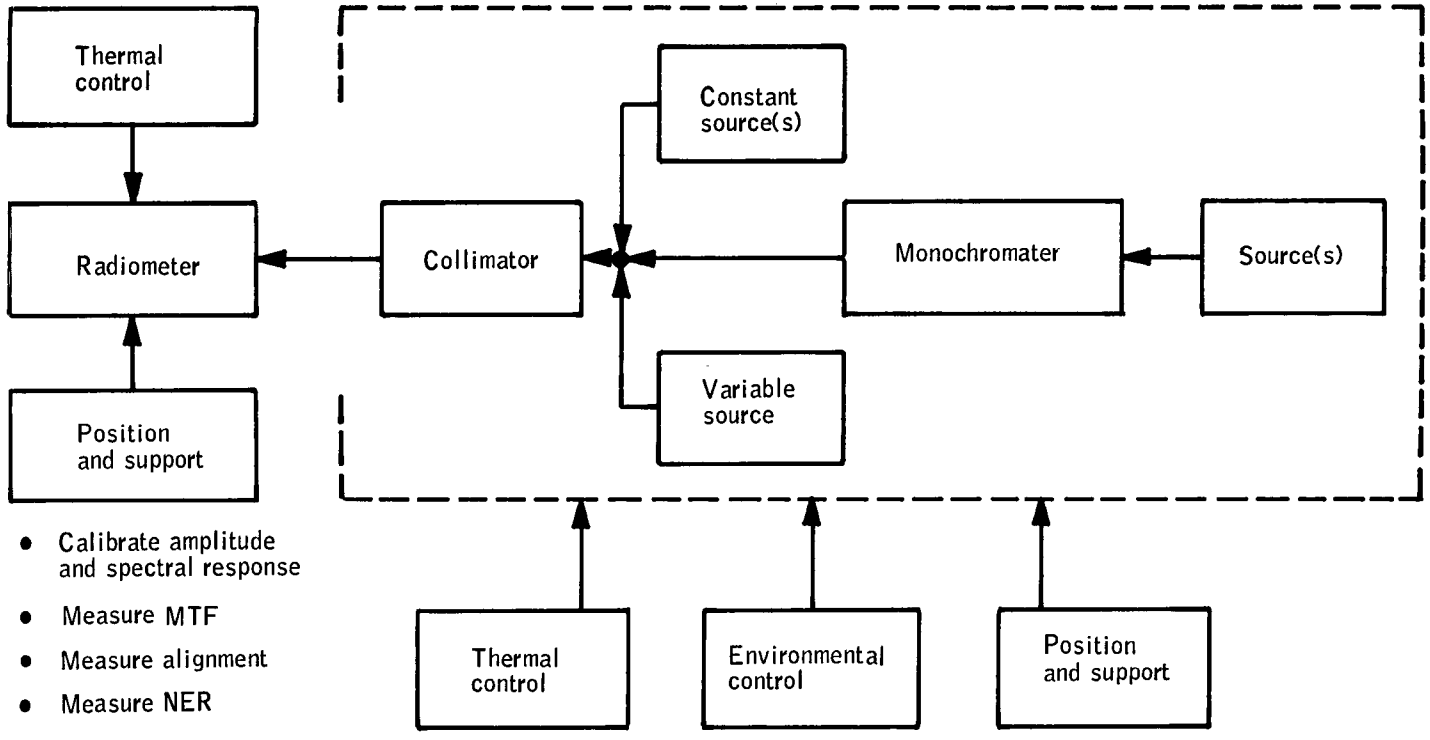

Figure 39. Primary Calibration Schematic Block Diagram

TABLE 22. - ABSOLUTE RADIOMETRIC MEASUREMENT ACCURACY

Error source	Magnitude		Error type: Noise N, Drift D, Cal C
	Scale, %	Bias, W/m^2 - sr	
1. Primary calibration	0.5	0.0006	C
2. In-flight calibration	0.4	<0.001	D D
3. Primary optics	0.2	0.0015	D N
4. Chopper	0.1	N.A.	D
5. Spectral filter	<<0.1	N.A.	D
6. Detector/cooler	0.1	0.0015	D D
7. Detector bias	≪0.1	0.0003	D N
8. Signal conditioning electronics	0.1	0.0015	N N
9. System transfer function	<0.1	0.003	D N
10. Sensitivity	N.A.	0.003	N

Some of the error sources should be further clarified:

- Primary optics: scale is primarily nonuniform; reflectivity variation bias is stray light
- Chopper: synchronization and amplitude variations
- Detector/cooler: temperature versus responsivity effects

Spectral calibration will be performed at the radiometer system level using the 500°K, NBS, tin-freezing-point blackbody and a monochromator. Between the 10-percent points of the system spectral band, the relative response will be measured with a spectral resolution of 0.02 μ (1/100 of the total band) and a relative accuracy of ≤ 5 percent per wavelength increment.

During spectral calibration the out-of-band resolution will be degraded proportionately to the filter attenuation to maintain a signal-to-noise level at which out-of-band suppression can be established.

Design analyses. -- Many other detail analyses were conducted to assure feasibility of the radiometer design. Major areas of design receiving special emphasis were:

- Thermal control
- Radiation chopping (how performed without spurious signal production)
- Detector bias power (minimized D* degradation)
- Stray radiation suppression (baffling required to suppress radiation from earth beyond instantaneous field)
- In-flight calibration (stability, non-interference with measurement)
- Redundancy (how achieved at no compromise in performance)
- Primary calibration (source/technique/facilities required)
- Detector cooling

All but the last two items were demonstrably feasible in terms of both analysis and comparison to similar hardware applications. In the areas of primary calibration and detector cooling the design approaches involved the use of standard techniques but in new application and combinations such that feasibility was established analytically.

Radiometer design summary. -- The feasibility design concept is illustrated in Figure 40 and incorporates the following design features:

- Type of optics system: classical Newtonian, f/1.0 (f/2.0 primary), 40-cm aperture diameter
- Detector: Ge:Cd at 16°K, 0.2 x 0.8 $(mr)^2$ field
- Cooling: solid-neon primary coolant, solid-methane secondary coolant
- Operating temperature: 200 ± 20°K

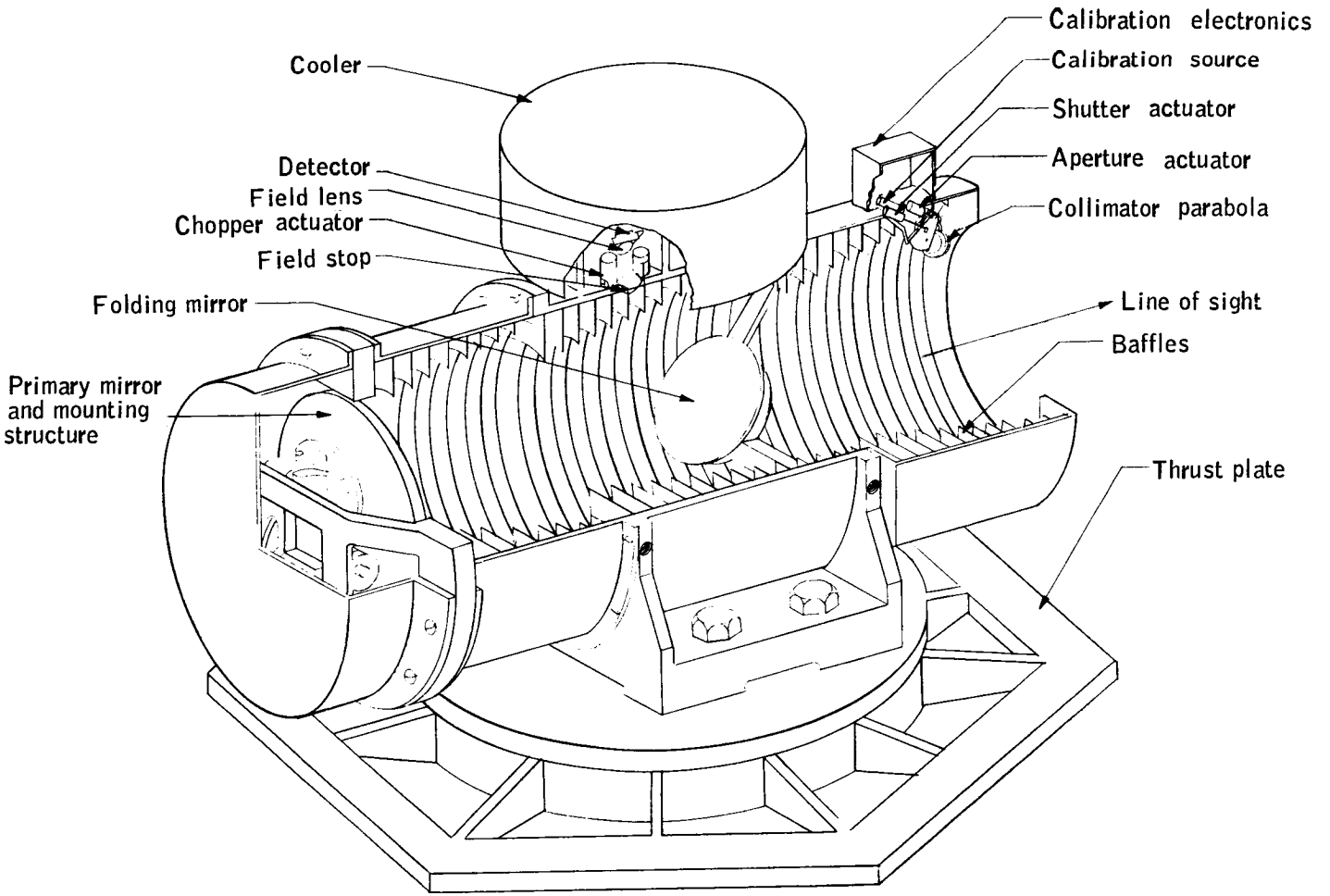

Figure 40. Radiometer Conceptual Detail Design

- Chopper: torsional pendulum at 2500 Hz (generates 5000 "chops"/second).
- In-flight calibration: three levels through entire system (including optics), a fourth directly in front of the field stop, coated self-measuring platinum sources.
- Redundancy: calibration subsystems and chopper, detector, electronics channels.

The radiometer subsystems and their interrelationships are as shown in the block diagram of Figure 41. Note that all the elements inside the dotted line denoted "thermal control shroud" are at the radiometer operating temperature of 200°K.

Attitude Determination Subsystem

Precise spacecraft attitude with respect to the earth's hard horizon must be known in order to fix accurately the abscissa of the earth's horizon profile, i.e., the tangent-height axis. Analyses of the synthesized radiance profiles and the errors expected from the radiometer led to a requirement for 0.25 km tangent-height accuracy for each radiometric measurement. This accuracy must be maintained continuously for a full year in orbit.

Translation of this error to an equivalent angular error in the determination of the inertial direction of the optical axis of the radiometer yields an angular error of 20 arc seconds. The allocation of this error among the constituent elements is shown in Table 23.

TABLE 23. - ATTITUDE DETERMINATION ERROR ALLOCATION

Item	Allocation, arc seconds
Attitude of attitude subsystem with respect to the celestial sphere	± 14
Orbit determination	± 10
Spacecraft data processing	± 3
Time correlation	± 3
Ground data reduction and star ephemeris	± 3
Alignment of radiometer with respect to the attitude subsystem	± 8.6

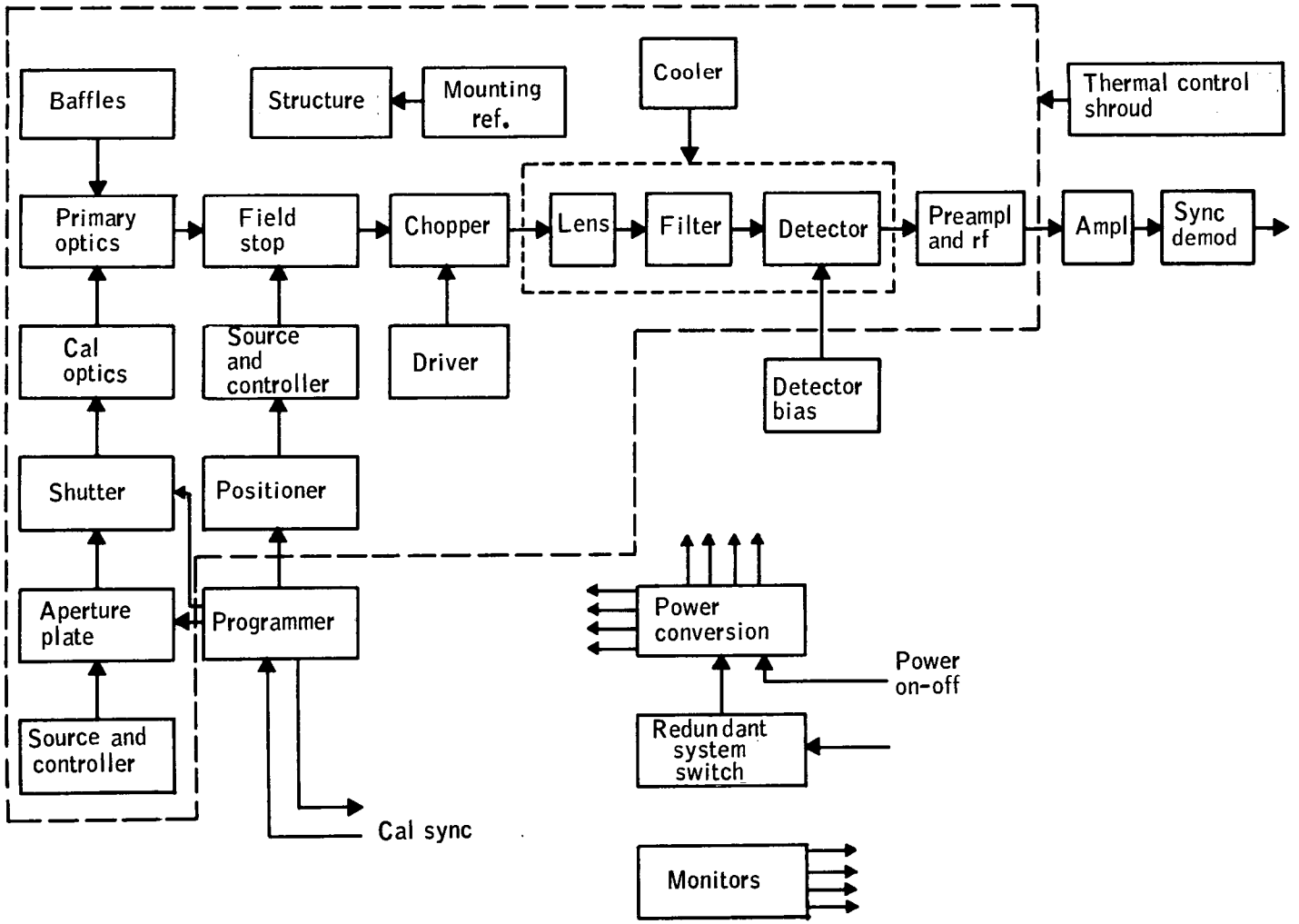

Figure 41. Radiometer Schematic Block Diagram

A rotating satellite with passive scanning implies sampling of the celestial sphere as opposed to continuous attitude information input. With a rotating satellite a continuous input device with passive scanning must provide an instantaneous field-of-view with symmetry about the spin axis. In the system being examined here, information is required regarding the radiometer axis, which is normal to the spin axis. Clearly, if the field of view is confined to the spin axis, no information is obtained regarding the radiometer axis. The field of view must then be sufficiently wide that the normal component can be measured within the accuracy requirements. In addition, to ensure continuous input, at least two stars must be in the field of view at all times. The attitude error is a secant function of the spherical angle separating these two stars, and separations less than 10 degrees lead to large errors. Previous studies of this type led to the conclusion that they are not feasible

1. Because of the background noise admitted into the system, and
2. Since data is required regarding the axis normal to the spin axis, an extremely wide field and high resolution is required to obtain data sufficiently separated to obtain a solution.

For passive attitude determination to the requirements listed above, only one conceptual system could be identified as applicable-the passive starmapper with discontinuous input.

The impact of this discontinuous input is a strong feedback into spacecraft dynamics, much stronger than would be implied by a tracking system. Either stringent requirements must be placed upon spacecraft angular rates and acceleration, or a precise model of the spacecraft motion must be available to allow interpolation across those intervals where attitude data is unavailable. The error allocated to the attitude of the subsystem with respect to the celestial sphere is then attributable to two sources: the measurement of line of sight itself, and the error in the model of spacecraft motion.

The data requirements dictate a sun-synchronous polar orbit which places the spacecraft in the sunlight for approximately 65 percent of the orbit. As originally configured, the attitude determination system concept consisted of two baffled starmappers operating continuously. Baffle requirements were established as approximately 12 orders of magnitude attenuation for daylight operation. Although feasible, attentuations of this order present an extremely difficult problem in design, fabrication, and testing and are difficult to fit into the volume envelope defined by the Thor-Delta. As a consequence, alternate techniques for obtaining attitude in daylight were investigated.

This attitude determination problem was solved by using the sun alone during the daylight portion of the orbit. The solution clearly was dependent upon the predictability of the spacecraft dynamics. An analytical study of the dynamics, a modeling of the spacecraft, and a modeling of a data reduction system indicated that the sun alone was adequate for solution of the attitude determination problem if sufficient information was gained from data on the dark side.

Accordingly, a mechanization using an unbaffled starmapper and sun sensor was selected. This mechanization satisfies the passive scanning requirement. The mechanization of the starmapper and sun-sensor instruments are discussed next followed by a discussion of the mathematical process of attitude determination from these instrument's data.

Starmapper design. -- The basic parameters in starmapper design are field of view, sensitivity, and resolution. Field of view and sensitivity are directly related in defining sample rate, resolution, and sensitivity in trade-offs with system complexity.

Sample rate: The critical parameter in starmapper design is the number of stars required per unit time, which is the sample rate on spacecraft position. For the general case of an untorqued spacecraft, three stellar observations are adequate for a solution. For a torqued spacecraft, where there is no general analytical solution, the required sample rate cannot be determined without a numerical solution. Since, for this study, the numerical investigation of the equations of motion was concurrent with sensor design, the required sample rate could not be precisely determined before proceeding with instrument design. Accordingly, a conservative position was taken, fixing the number of stars at four. Since each star observation yields two independent equations, this number allows an eight-variable fix on attitude for each spacecraft revolution. The number of variables required to fix a solution for the torqued model is presently estimated to be 15, with several of these variables having periods of the order of several spacecraft revolutions; hence, with four stars per revolution the solution is over-determined, and the excess data can be used in an error-reduction system. Simulation results indicated that four stars per scan was the correct choice for the accuracies desired.

Field of view and sensitivity: Having defined a requirement for four stars per spacecraft revolution, a strong tradeoff between instrument field of view and sensitivity exists. The basic mechanical parameters of an optical system are aperture and f/number; aperture controls sensitivity and f/number controls achievable resolution and, of course, length of the system. As field-of-view requirements increase, to obtain the required optical resolution which to first order can be considered a constant requirement, the f/number will increase. However, the aperture diameter required will decrease as sensitivity requirements decrease. The parameter being traded is total instrument size. The trade is strongly in favor of wide field of view since the number of stars seen increases approximately quadratically with field of view and linearly with sensitivity (aperture diameter). Visual magnitude data is used in Figure 42 and shows the effect of aperture upon total number of stars seen.

In general, resolution at wide field can be more simply obtained than an increased aperture diameter. An optimum design process then will select the widest field of view and the smallest f/number consistent with the required resolution. The aperture diameter requirement is then fixed by the required sample rate (number of stars) and will be a minimum for the design, yielding the smallest instrument. For the system described below, a 20° field of view was determined as a result of sky-scan studies to produce the required number of stars per revolution. This field-of-view selection yields a minimum detectable star at visual magnitude +3.2 for four stars per scan.

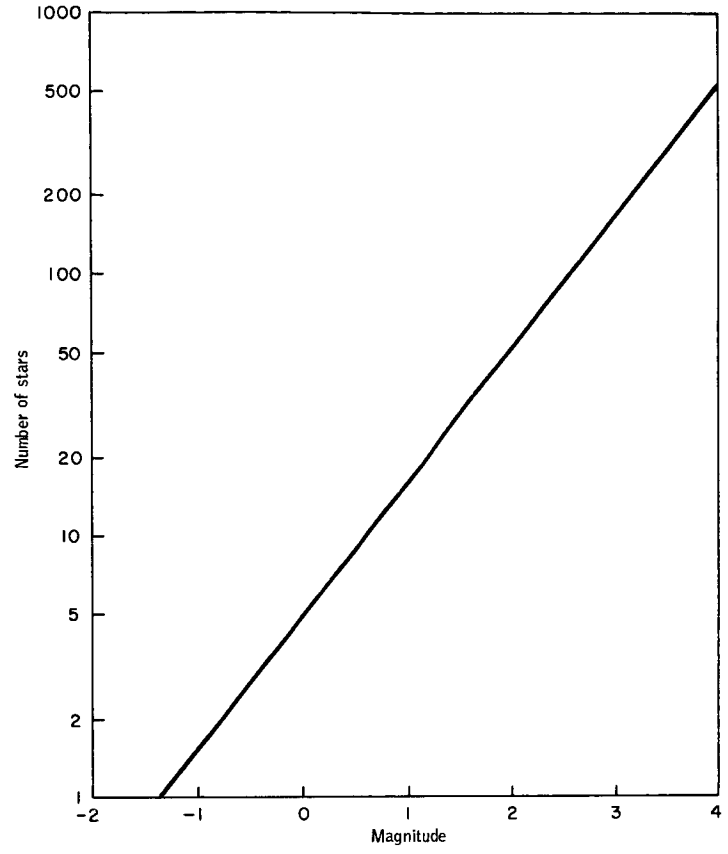

a. Star availability

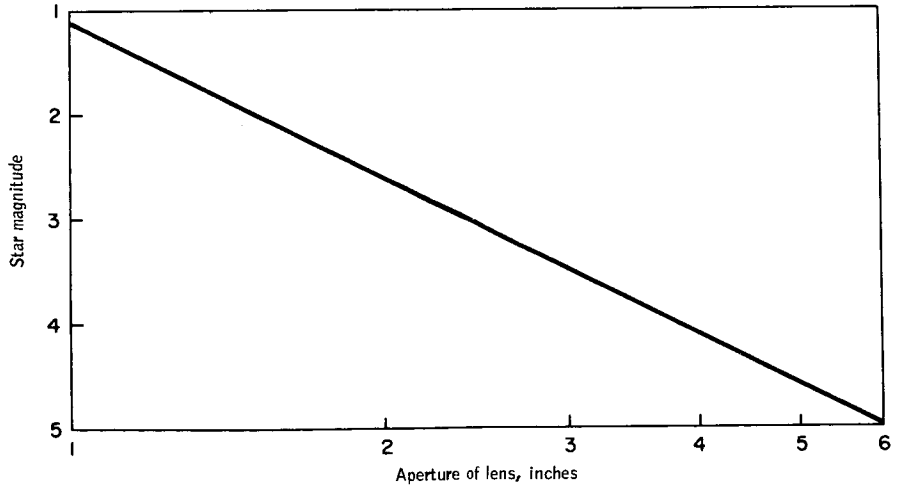

b. Required lens aperture

Figure 42. Star Sample Obtained as a Function of Aperture

For any aperture well beyond the diffraction limit (diffraction limit for one minute of arc resolution at 0.5 micron is less than 1 cm), the aperture diameter is fixed by the sensitivity requirement. Using nominal characteristics for the EMR 541N photomultiplier and a threshold-to-noise value of 10:1 for the interpolation system, a three-inch aperture is required for detection of stars at magnitude +3.2.

Since f/number affects directly the length of the system, use of the lowest possible value was desirable. A survey of similar systems indicated that a value in the region of f/4 was a resonable design goal.

Detector: The stringent requirements for sensitivity in a device which must possess the capability of detecting stars of magnitudes greater than +3 limits the possible detectors to photomultipliers and silicon photodiodes. Photodiodes possess marginal sensitivity and, because of the small sensitive surfaces, require complex optical and electrical designs, typically involving a matrix of detectors. A photomultiplier has a large surface with adequate sensitivity and yields simple optical and electrical designs. The photomultiplier was the only device investigated in detail for this application. The photomultiplier has one significant disadvantage - the deterioration of performance under high-intensity illumination. It was determined that removal of the high-voltage bias provides adequate protection against daylight earth inputs, the only significant input under the conditions of operation imposed by the sun-synchronous orbit. Short-time-constant operation is not required since starmapper data is not used in the daylight with this system design. Of the photomultipliers available, the EMR 541N was selected because of its adequate sensitivity and its ability to withstand high-intensity illumination. The phosphor is catalogued as S-11, visible response.

Resolution: Instrument resolution was defined as the variance of the distribution of output timing errors from a data processing system; these time errors are referenced to an attitude error through the vehicle spin rate. At a spin rate of three rpm, the time error equivalent to 10 arc seconds is 154 microseconds.

Resolution is directly related to sensitivity in a tradeoff involving optic blur circle, reticle slit width, and amplifier-detector bandwidth. The linear chain of optics, slit, and amplifier yields an output signal for point-source input which is the impulse response of the product of the transfer characteristics of each of the elements taken separately. To first order, the system has an optimum in signal/noise for matched transfer characteristics (i.e., slit width matched to blur circle, amplifier time constant matched to slit). Resolution is directly proportional to bandwidth.

The simplest system has a transfer characteristic such that the output pulse has a time duration less than 154 microseconds. This system would have the maximum bandwidth and is a limiting system from aperture diameter (requires largest possible aperture) and optical resolution (requires largest f/number).

It was of interest to determine whether a more complex system offers significant relief in these optical parameters. Examining the output pulse from

a starmapper system, it was evident that there is a significant amount of information in the pulse shape. In particular, if reasonable symmetry in the output pulse is preserved, a thresholding system operating well above noise level, with simple linear interpolation on the times of threshold crossing, yields an effective resolution considerably better than is indicated by the reciprocal system bandwidth, the usual criterion for resolution.

For an optics-limited system, a matched reticle and amplifier have produced, in simulation, effective resolution approximately one ninth of the blur circle. This gain in flexibility of system design is well worth the added complexity.

Reticle design: The basic starmapper reticle pattern is a V slit with azimuthal information being obtained from time of crossing of the V and elevation information from the difference between times of crossings of the two slits forming the V.

The major problems with use of a V slit are the ambiguities in stellar identification. Pairing the correct slit crossings from two stars which are in the V at the same time is extremely difficult. Since the optimum apex angle for the V is of the order of 45 degrees, stars fairly well separated can be ambiguously identified.

A solution to the ambiguity problem is obtained if a third slit, equidistant in angle from the two V slits, is inserted. The grouping of slit crossings for star identification then consists of a search for equally spaced triplets. The equal-space condition essentially eliminates ambiguities except for the uncertainty in time introduced by spacecraft motion.

One of the requirements of the interpolation system is symmetry in the output pulse. A reticle pattern in which the slits follow radial contours in the image surface was desirable in that the most significant optical aberrations are symmetric about a radial line. The major problem with a radially symmetric reticle pattern is the fact that its center is coincident with the optical axis, and means must be provided for separation of the upper set of slits from the lower set. There are two techniques for accomplishing this separation: use of separate optical systems and detectors, or coding of one of the sets.

The simplest coding consists of doubling the number of slits on one set. This leads to an increase in background noise and requires approximately a 20-percent increase in aperture. In addition, the processing of these data is considerably more complex. The solution of using a system with twice the field required and using the upper half only is discarded as causing too severe an optical design problem. A system using two separate detector systems behind the reticle was chosen as the best means of separating upper and lower reticles.

Mounting position: The sample rate is determined by the total, swept solid angle on the celestial sphere. With a rotating spacecraft the swept solid angle is a sine function of angle of the starmapper optical axis from the spin axis.

Clearly, with no other restrictions, mounting the system with the optical axis normal to the spin axis is an optimum solution, and this position has been selected.

Data-processing electronics: The data-processing electronics are required to output a time word which is an estimate of the time at which the star is in the center of the slit. The processes involved are dc amplification, threshold, and clock. A simplified block diagram of the processing system is shown in Figure 43. A dc amplifier with a long-time-constant feedback loop is used for signal amplication to working level. The signal is then passed through a linear phase, matched filter for noise filtering. The output of this amplifier is fed to a set of four level detectors (threshold). The output of each level detector is fed to a counter, whose function is to identify the proper threshold for the next revolution through an overflow detector, which, through gating logic, selects the operative level detector. An excession of the operative level detector triggers a counter on; the following excession cuts off the counter; and the time word from the counter is sent to memory as the transit time of the star.

Photomultiplier power supply: One of the major problems with photomultipliers is the susceptibility of the photocathode to damage under high-intensity light input. Under the orbital conditions of HDS during approximately 65 percent of an orbit, the starmapper is exposed to full daylight for a major portion of each spacecraft revolution. In addition, the moon is in the field of view for two days each month. As described earlier, the solution adopted for attitude determination relies upon a sun sensor during the daylight part of the orbit, and there are no requirements for starmapper operation during this period; hence, there are no requirements for protection systems with rapid recovery (i.e., of the order of seconds). Manufacturers' data indicates that the triple alkali photosurfaces (e.g., EMR 541N) are not degraded by exposure to daylight with power off. The recommended system compares peak anode power with a preset reference to develop a switching signal. An alternate design involving a shutter plate was rejected because of the moving part involved.

Mechanical: Since the system uses on-orbit alignment sensors, the requirements for structural rigidity allow up to 30 arc-second motion of the image relative to the alignment reference. Aluminum structure with standard design practice can meet these requirements. The structure of the instrument is a simple aluminum tube with a mounting flange tying the starmapper(s) to the radiometer. With the lengths and diameters obtained, the system remains unfolded to the reticle, and the fiber optics/photomultiplier substructure is folded.

Figure 44 presents a summary of the design parameters analyzed in the conceptual development of the starmapper. The starmapper conceptual design is shown in Figure 45.

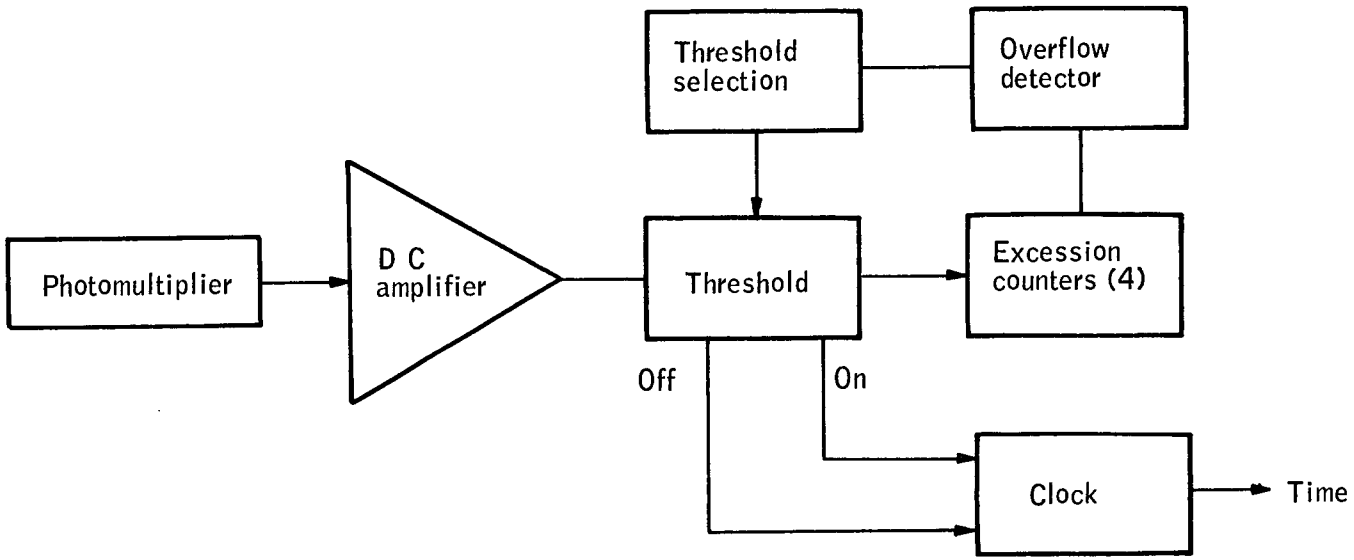

Figure 43. Block Diagram of Data-Processing Electronics

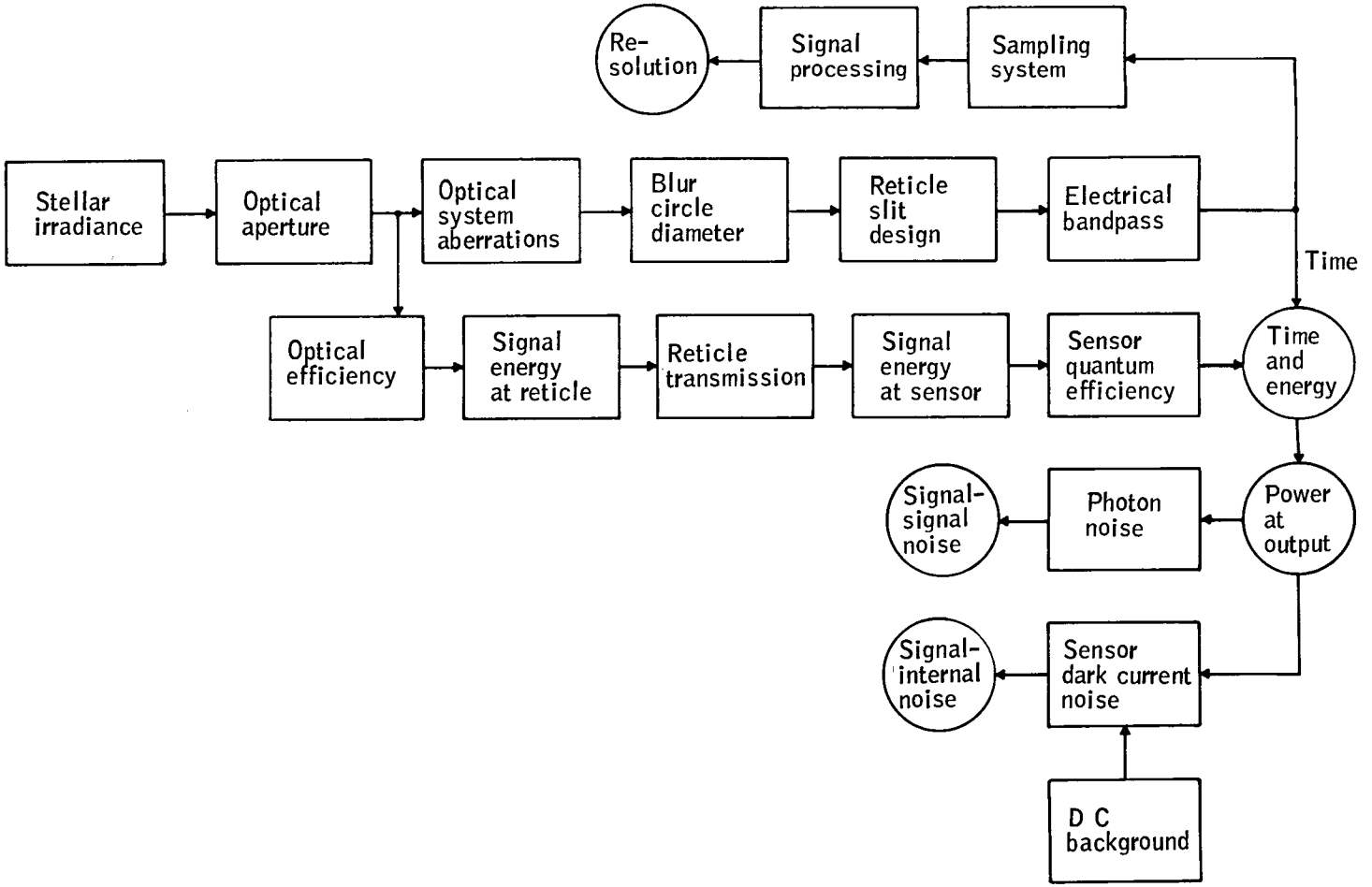

Figure 44. Summary of Starmapper Design Parameters

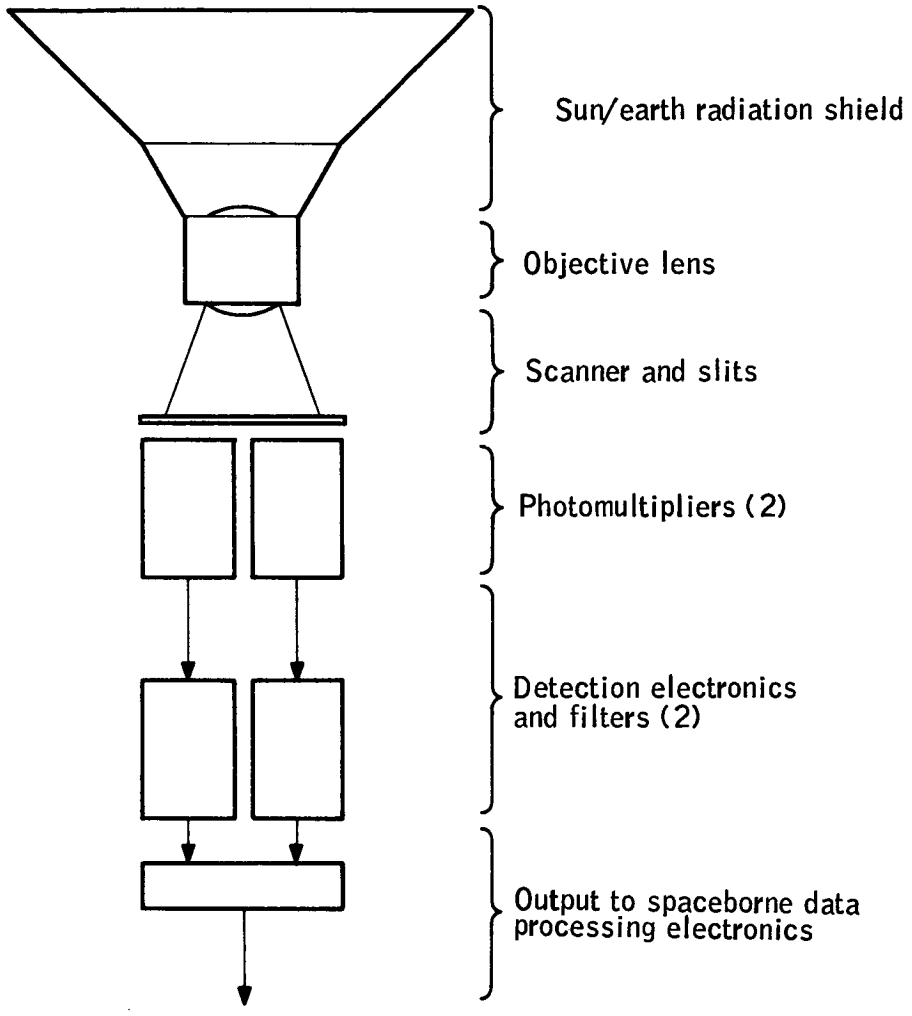

Figure 45. Starmapper Conceptual Design

Sun-sensor design. -- In the design of the sun sensor, sensitivity and resolution do not exhibit the same problems as were evident in the starmapper design. The requirement for sun crossing under all orbital conditions defines the basic field of view of the sun sensor when coupled with mounting of the instrument on the spacecraft.

Mounting position: The orbital parameters have defined an orbit with nominal 45° orientation between the orbit normal and a sun line, and an error analysis has shown as much as 17° deviation from this nominal due to injection errors. A continuously operating, passively scanned sun sensor then requires mounting at 45° with respect to the spacecraft spin axis and a field of view of 35° simply to be capable of viewing the sun each spacecraft rotation under all conditions.

Detector: Clearly, sensitivity is not a problem with sun-sensor design. There are a number of applicable detectors; selection is primarily based upon availability and required circuit complexity. The silicon photovoltaic sensor is an obvious candidate for this application; the primary disadvantage of this sensor is variation of surface responsivity.

Basic system: An obvious candidate for a sun-sensor design is the simple V-slit system used for starmappers. Emphasis was placed upon the design of a V-slit system since two-axis information is obtained from a single detector in this system, and the energy-balance systems require four detectors to develop this same information.

In the V-slit system, the central problem is definition of the solar limb. A search of the literature and analysis of the characteristics of a limb detector indicate that the limb is well defined to less than a few seconds of arc. Figure 46 is indicative of the information obtained. In most of these data, the solar limb is shown dropping two or three orders of magnitude in one to two arc seconds. System requirements are approximately 10 arc seconds, and, clearly, the system is not limited by the solar characteristics.

The effect of solar flares and sun spots upon the signal obtained from the limb was investigated and determined to be negligible.

Optics: Aperture diameter is defined solely by resolution requirements (diffractional effects). The system is not affected by chromatic aberration since narrow-band operation only is required. Also, because of the sharpness of the solar limb, high-resolution optics are not a requirement; the requirement is that the output signal have rise/decay times capable of being resolved to approximately 10 arc seconds. To avoid surface responsivity variations and allow use of a single sensor, an integrating sphere is used to project the reticle onto the sensor.

Reticle: Since ambiguous identification is not a problem with a sun sensor, the simplest two-axis reticle, the V-slit, was chosen. The apex angle of the V and the position of the apex has not been selected, since these quantities apparently enter strongly into the use of the device in a data-reduction algorithm and final optimization will require further study. The reticle is mounted directly on the integrating sphere.

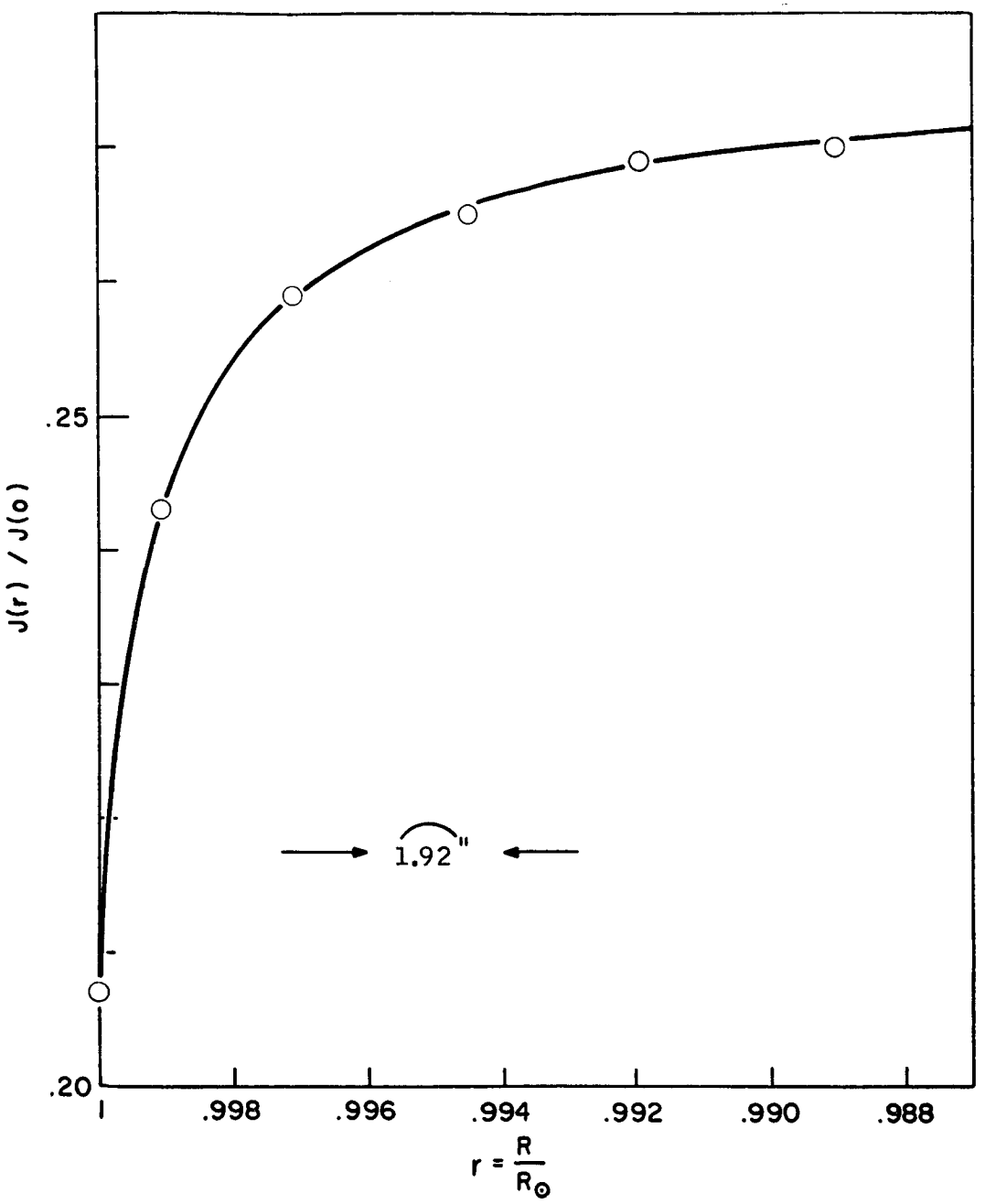

Figure 46. Solar Limb Darkening at Extreme Edge

Electronics: A simple amplifier and level detector are used for data-processing electronics. No cell bias is required for silicon photodiodes, one of the reasons for recommending this sensor.

Mechanical: With the mechanical parameters of the sun sensor, the alignment system used for the radiometer and starmapper is difficult to implement. The sun-sensor device is sufficiently small that internal structural rigidity to the order required can be obtained if the proper materials are used. The sun-sensor barrel will be a quartz tube with optical-quality surfaces to receive the reticle and lens system. A flat will be ground on the outer surface to receive a quartz, miniature autocollimator which will be optically tied to an optical flat referenced to the radiometer.

Final design parameters for the sun sensor are summarized in Table 24, and the conceptual design of the instrument is shown in Figure 47.

TABLE 24. - SUN-SENSOR DESIGN PARAMETERS

Aperture	1 inch
f/no.	2
Field of view	35 degrees
Detector	Silicon photodiode
Reticle slits	V Shape, 2 arc min width
Filter	Interference band pass 5400 - 5600 Å

Instrument Systems Integration

After examination of the interfaces between the three instrument systems, the major interface is that of mechanical alignment. The proposed system uses an integrating structure to tie the instruments together. Alignment testing of the package is against optical flats, to which each supplier has referenced his internal alignment. Thus, integrated measurements are against these flats and do not require operation of the radiometer against critically aligned infrared sources during integration. An on-board alignment measurement, using internal sources and sensors mounted on the instrument proper, is proposed.

The systems impact in terms of the data handling, particularly during in-flight calibration, is resolved by providing separate data-handling channels and sufficient input buffering to provide for simultaneous operation of the attitude determination and radiometer subsystems.

Power systems are independent. The only area where an interface can exist is in ground loops between instruments, a standard design problem.

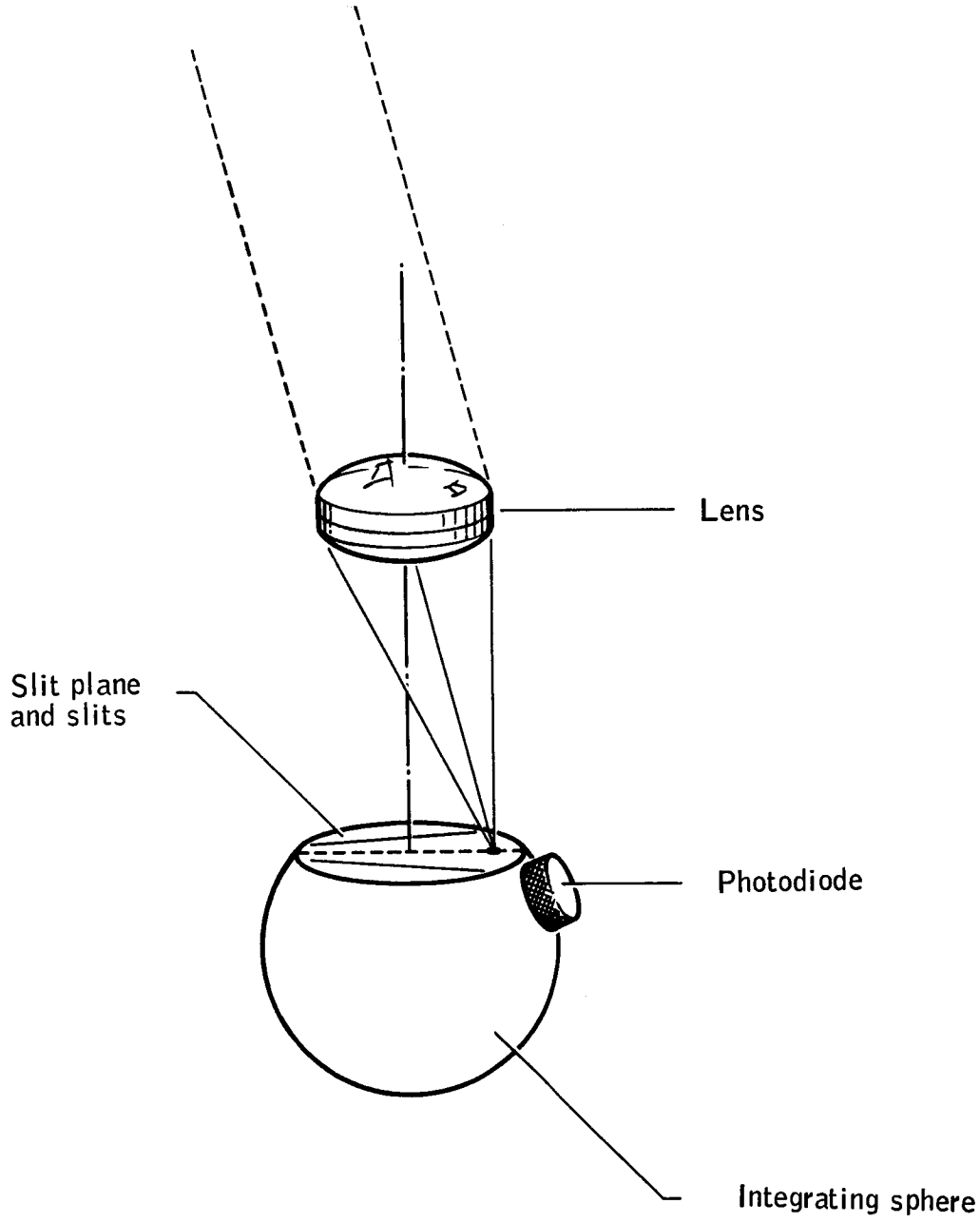

Figure 47. Conceptual Design of Sun Sensor

Attitude Determination Algorithm

Attitude determination is defined as the estimation of the attitude of the measurement system with respect to the celestial coordinate system. The conceptual design of the attitude measurement system consists of a set of measurement devices and ground data processing. To determine feasibility of the attitude measurement system, the instrument outputs were simulated, and an attitude determination data reduction algorithm was formulated that utilizes these data to estimate attitude.

The ideal measurement device provides an error-free measurement of the spacecraft's attitude. One set of data is sufficient for complete determination of the spacecraft state for all time. However, instrument noise and uncertainties in the spacecraft motion model require that attitude determination of the spacecraft be treated as a stochastic process.

Since the attitude determination measurement system involves a stochastic process, the determination of the spacecraft attitude becomes more complex than a simple determination of initial conditions. The complexity arises from measurement noise and uncertainty in the knowledge of the spacecraft's environment. Under these conditions the initial conditions must now be determined by data obtained from an imperfect measurement device and applied to equations of motion which do not describe the exact behavior of the spacecraft. Consequently, an uncertainty in the determination of the initial conditions of the spacecraft's state leads to errors in attitude. A periodic correction must then be applied in order to estimate the spacecraft's attitude, i.e., the initial conditions must be statistically determined, periodically corrected, and a new solution begun.

The conceptual spacecraft is a spin-stabilized disk, free of control torque during the data collection cycle. The orientation of the spacecraft's spin axis is nominally normal to the orbit plane. A starmapper and sun-sensor combination was recommended as the attitude measurement devices providing the necessary information to allow a fix of the state variables of the attitude. The state variables were defined as Euler angles, body rates, torque coefficient, inertia ratios, and experiment offset angles.

In the absence of actual celestial measurements, the study had to be conducted in two phases:

1. A data generation program to simulate the spacecraft motion and produce simulated star and sun crossings, and
2. The development of a data reduction algorithm to reduce these data to spacecraft position, the process by which real spacecraft attitude is determined.

Figure 48 shows the elements of this total study in a schematic form.

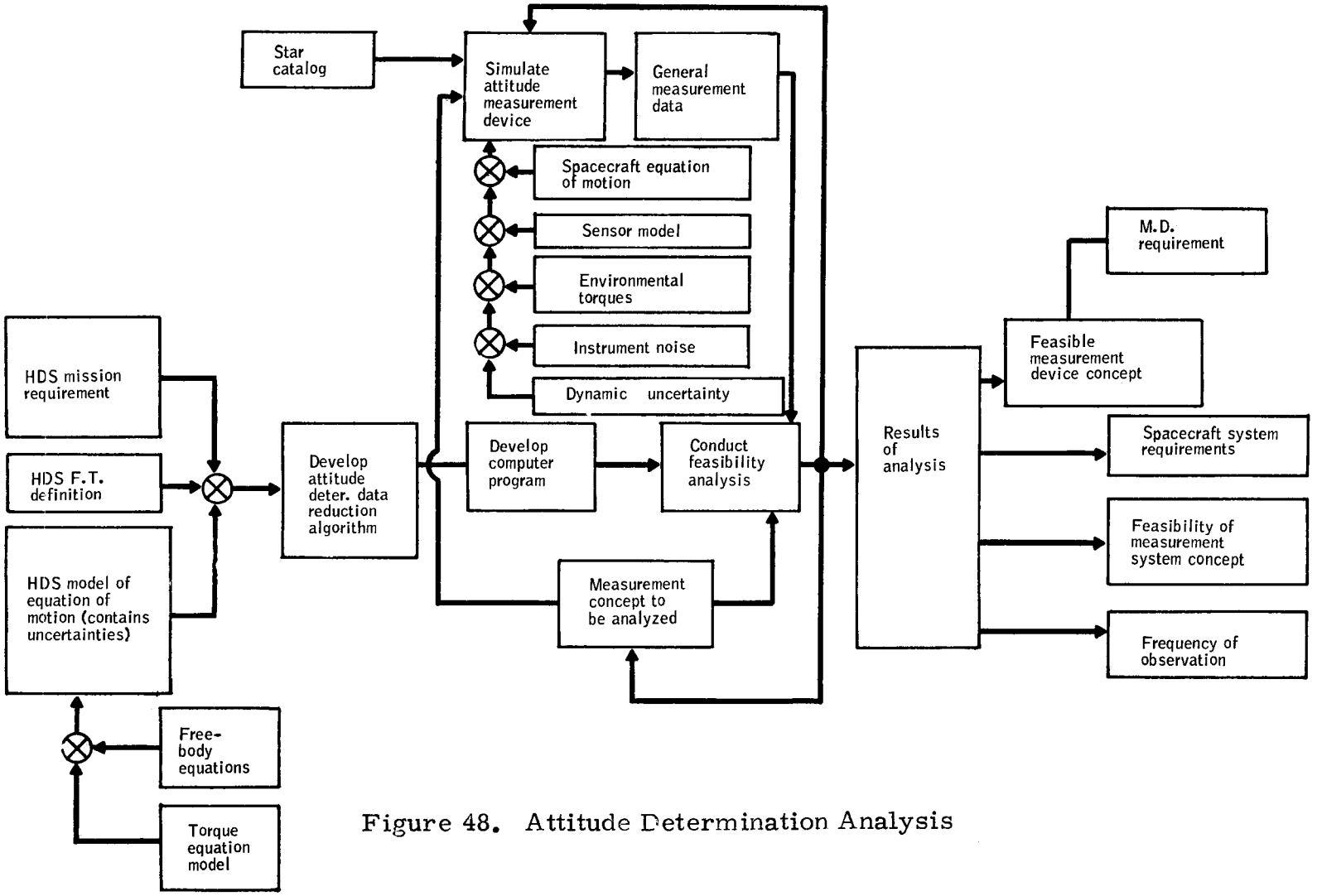

Figure 48. Attitude Determination Analysis

Data generation program. -- Input parameters to the orbital simulation are initial conditions on the orbit, on position of the spacecraft in the orbit, and on the attitude of the experiment axes. Input parameters to the spacecraft simulation are residual magnetic moment of the spacecraft, eddy-current coefficient, principal moments of inertia of the spacecraft, and initial rates of the spacecraft

Data output consists of the star and/or sun-sensor transit times, spacecraft rates, attitude at transit time, inertia ratios, magnetic-torque coefficients, and experiment mismatch angles (i.e., the angles between the experiment package and the spacecraft). This output constitutes the state of the spacecraft at the transit time. Data is generated for all stars whose magnitude is 3.4 or less. The data reduction program edits the data to select the number of stars per revolution of the spacecraft. The editing simulated the starmapper viewing threshold. Therefore, only the brightest stars were selected for a particular viewing threshold.

The spacecraft dynamics model consisted of the free-body equations and the torque equations. The spacecraft's environment imposes the following torques:

- Solar pressure
- Aerodynamic
- Residual magnetic moment
- Eddy current
- Gravity gradient
- Internal
- Outgassing (spacecraft)
- Meteoroid impact

Preliminary analysis showed that the most significant torques on the spacecraft are eddy current and the residual magnetic moment. The next most significant torques were shown to be aerodynamic and solar-pressure torques. Only the magnetic torques were modeled in the feasibility analysis.

Sensor model and instrument noise. -- The measurement device/devices were modeled, and capability for noise simulation was provided. The noise introduced into the data output was white with gaussian distribution with mean zero and variance of 10 arc seconds.

The model has the capability of simple modification of the starmapper configuration, the number and orientation of the viewing slits, and adding or incorporating the sun-sensor configuration.

Dynamics uncertainties. -- Sinusoidal variations in the earth's magnetic field were added to the data generation program to provide an uncertainty with respect to the data-reduction algorithm; otherwise, the two systems of equations would be identical, and no significant result would be obtained. The residual magnetic moment is changed at the earth's twilight point because of the changes in the spacecraft current loops.

Data reduction algorithm. -- The data reduction algorithm accepts data from the starmapper and/or sun sensor and estimates the state of the spacecraft. The state of the spacecraft is represented by 14 variables

$$W_{x_o}, W_{y_o}, W_{z_o}, \psi_o, \phi_o, \theta_o, A, C, M'_x, M'_y, M'_z, K', \Sigma_1, \Sigma_2,$$

The model of the spacecraft dynamics is the same as the data-generation model.

The data-reduction algorithm operates on the data to make a best fit for the spacecraft's state in a mean-squared error sense over a defined period of time, i.e., a least-square error data match. Mission analyses yield an accuracy requirement of 14 seconds of arc attitude error for the estimate of the spacecraft' s state.

The initial conditions of the spacecraft are chosen to be different from those used to generate the data, i. e., initial guesses of the spacecraft' s state. The tape containing the simulated star and/or sun transit time data is edited by selecting only those star/sun transit times which meet the amplitude criteria.

Two tape records are provided. The first provides initial conditions used to generate the star and sun-sensor data. The second tape contains the star transit time and the spacecraft state vector at the transit time. These data are used to establish differences between the estimated and the actual state of the spacecraft. The program then proceeds to set up the output for the first output point. Another tape is read to establish the first star observation time. The program then integrates to the first observation point. The least-squares output section is updated and differences in the state of the spacecraft are printed out. The next observation is read, and integration to that point is made, followed by update of the least-square section. This process continues until the last observation is sensed. The least-squares solution is then performed to compute the correction to the spacecraft initial-state vector. The initial state of the spacecraft is now corrected. The percent change in the state vector is computed and compared to a convergence criteria. If the criteria is met the solution has converged, giving the estimate of the initial state of the spacecraft. If the criteria is not met, the data tape is rewound, the corrected state vector replaces the old initial conditions, and the program prepares for another iteration. Figure 49 presents a flow diagram of the data-reduction program for attitude determination.

Results of analysis. -- The experiment performed to determine the feasibility of the sun-sensor/starmapper attitude measurement concept is a least-squares solution for the Euler angles (ψ, ϕ, θ) over 1/2 of the orbit. (See Figure 50 which shows the portion of the orbit over which star and sun data was used.) Only the bottom half of the orbit was used during simulation runs since the numerical integration caused computer running time to be excessive.

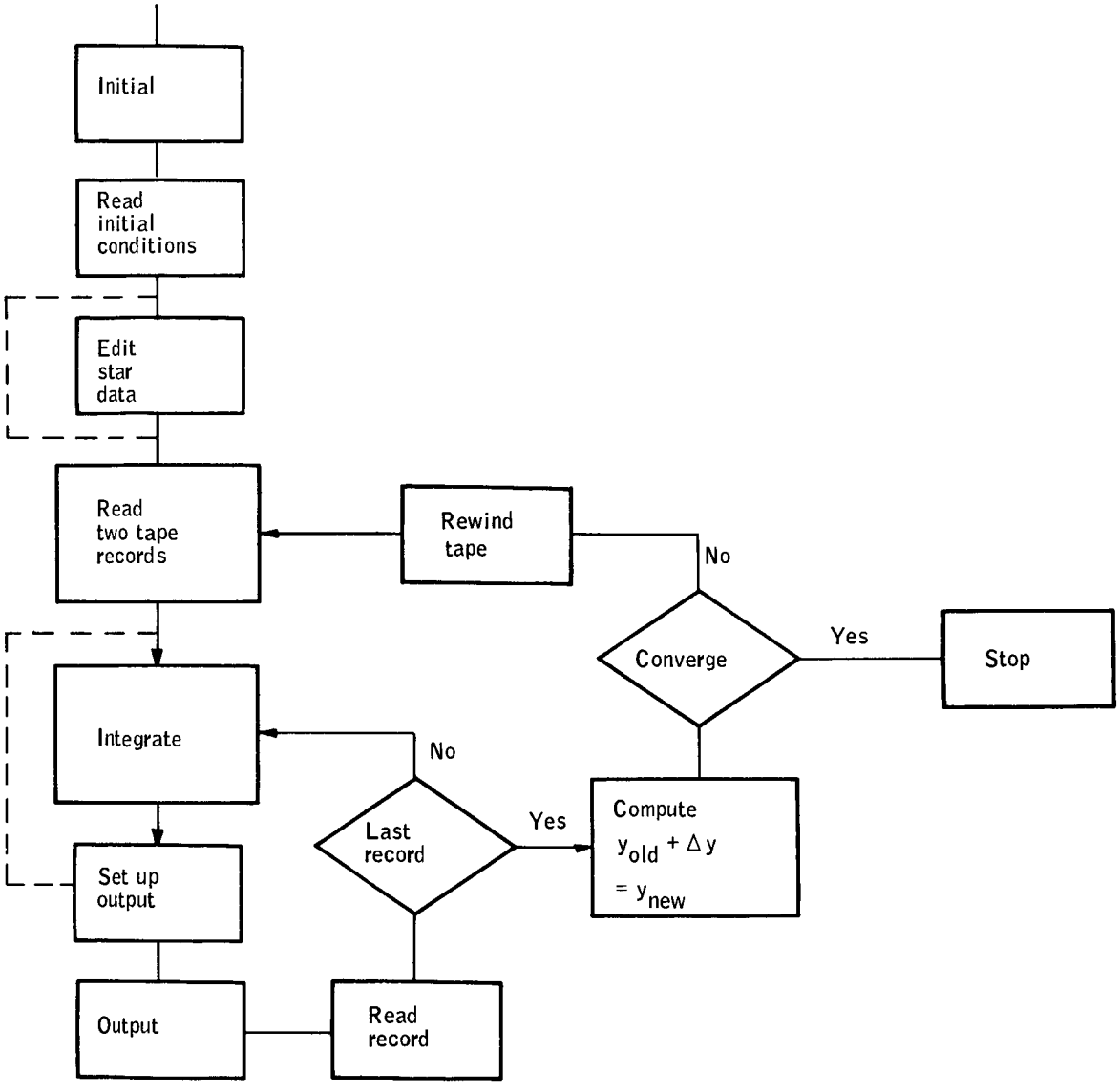

Figure 49. Attitude Determination Flow Diagram of the Data Reduction

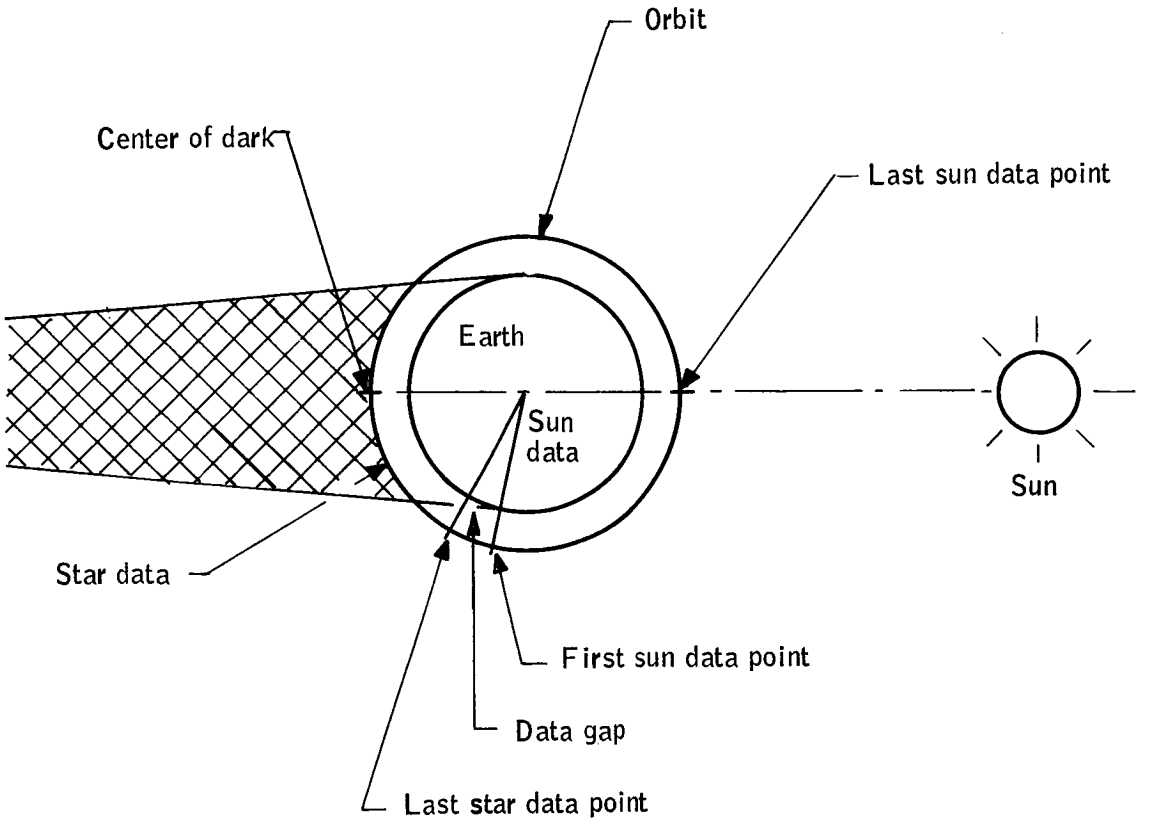

Figure 50. Relationship of Orbit and Sun

It is clear that the problem is symmetric and that results obtained hold for the remainder of the orbit.

Computer runs start at $t = 0$ in the center of the dark side of the orbit (Figure 50). The dividing point between daylight and dark is approximately one sixth of an orbit later at about $t = 940$ seconds. Star data is collected over the interval $0 \leq t \leq 880$ seconds. Thus, a data gap of about one minute is introduced in the star data to allow for earth atmospheric refraction of sun rays and earth glow effects on the starmapper optics.

An additional time gap of one minute is allowed from the twilight point to the first run sighting data point. This is sufficient time for the spacecraft to rise above the earth's atmosphere, so that refraction effects can be neglected. Sun data is collected for the remainder of the half orbit.

Runs of the least-squares data reduction program are split into two parts, one for the dark part and one for the sunlit part of the orbit. Thus, star data (suitably edited) is used to determine the attitude from the center of the dark to approximately one minute before the twilight point.

The converged condition for the star runs become the initial conditions for the sunlit portion of the orbit. Since a complete solution of the attitude determination problem cannot be obtained from sun sightings alone, reduced state variable dimensions were used for this part of the orbit.

Star-sighting results -- Three tests were run for two, four, and six star sightings per revolution of the spacecraft. The data began at the center of the dark and ended at the last star data point (Figure 50), $0 \leq t \leq 880$ seconds.

The parameters used to generate the star data are

$$M_x = M_y = M_z = 5.16 \times 10^{-6} \text{ ft-lb/gauss}$$

$$K = 1.42 \times 10^{-5} \text{ ft-lb-sec/gauss}^2$$

$$A = C = 0.83328$$

$$\Sigma_1 = 0$$

$$\Sigma_2 = 0$$

Output of the least-squares program showed that all three runs converged. Table 25 shows the extreme values of the difference in the estimated attitude and the actual attitude of the vehicle over ($0 \leq t \leq 880$ seconds) the dark side of the orbit for the six stars per revolution sightings.

TABLE 25. - EXTREME ERRORS IN EULER ANGLES RELATING PRINCIPAL AXES TO INERTIAL SPAN AT STAR SIGHTING INSTANTS

$\Delta\psi$, arc sec		$\Delta\phi$, arc sec		$\Delta\theta$, arc sec	
Max.	Min.	Max.	Min.	Max.	Min.
-3.04	-13.25	4.21	-5.90	0.31	-3.75

A very accurate fit is made at the data points. Figure 51 illustrates typical results from t = 300 seconds to t = 450 seconds of the error in the least-square fit for the six-star-per-revolution case. The errors are well within the accuracy requirements.

The four-star-per-revolution case gave an adequate solution for the star sightings; however, larger spread in the data was noticed.

The two-star-per-revolution case gave a convergent solution at the data points but appears to be inadequate because of the small number of sightings per revolution, although insufficient output was available to verify this conclusion.

The pitch angle θ in all cases was determined better than the ψ and ϕ angles. This is due primarily to the greater sensitivity of the starmapper about the spin axis. The four star configuration provides an adequate estimate. The six-star configuration provides a better estimate of the spacecraft state.

Sun-sensor results. -- Since the sun is equivalent to one star sighting per revolution in providing information, tests were conducted to define those variables which could be determined from the sun data.

The rank of the least-squares solution matrix was tested and it was determined that:

- A single, two-slit sun sensor produces a least-squares matrix with a maximum rank of 12. Thus, solutions for a 12 variable problem are available.
- Two, two-slit sun sensors (four slits total) produces a least-squares matrix with rank 13.
- One of the initial angles (ψ_o, ϕ_o, or θ_o) can always be deleted without reducing the rank of the matrix.

Having established the types of solutions expected for the various number of sun-sensor slits, several runs were made to determine the feasibility of the sun sensor for the two- and four-slit sun sensors.

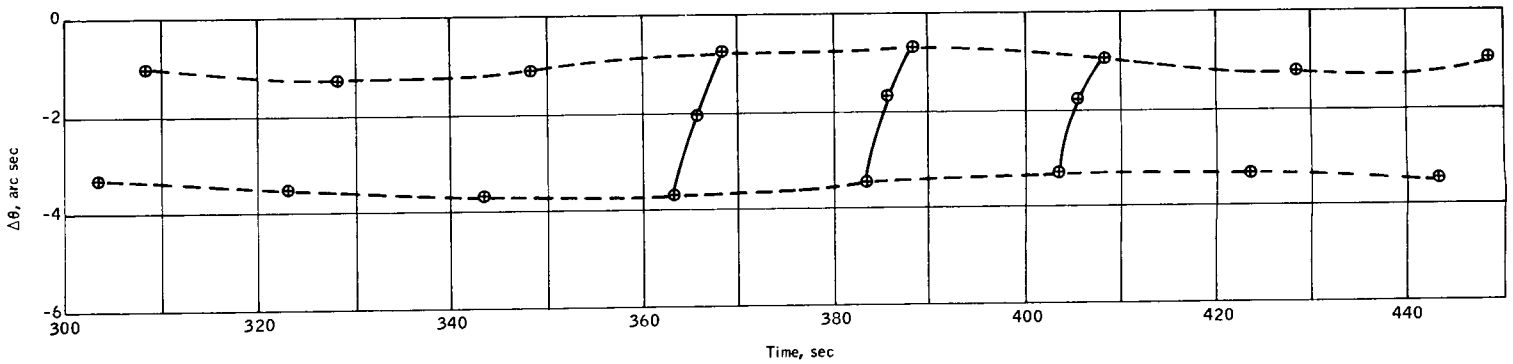

Figure 51. Experimental Axis Pitch Angle Error for Case I

The four-slit sun sensor was found to give a sufficiently accurate estimate of the spacecraft's attitude when θ_o is held fixed. It was found in the star sighting results that θ_o was determined most accurately. Consequently, the sun data is best used to estimate the remaining 13 variables and parameters holding θ_o fixed. Table 26 gives the extreme values of the differences in the estimated and the actual attitude of the spacecraft.

TABLE 26. - EXTREME ERRORS IN THE SPACECRAFT'S ATTITUDE DETERMINED AT THE SUN TRANSIT TIMES

Case	Variable fixed	$\Delta\psi$, arc sec		$\Delta\phi$, arc sec		$\Delta\theta$, arc sec	
		Max.	Min.	Max.	Min.	Max.	Min.
I	θ_o	15.06	-15.05	11.17	-9.19	9.53	-7.26
II	θ_o	5.38	- 7.46	-1.79	-9.84	0.40	-11.58

Case I extends halfway through the daylight part of the trajectory, whereas Case II extends all the way. Case II results are well within the required estimated accuracies. Also, Case I is adequate because θ is the angle to which the 14 seconds of arc applies.

Figure 52 shows the pitch angle error θ for the experimental frame over a selected time period. The dashed line bounds the error, and the solid line is the curve connecting the points. More computation is needed between data points to establish the upper limits; however, the limits are expected to increase only slightly. It is seen that a sinusoidal curve fits the errors quite well between sighting instants with little overshoot, and that errors appear to be within the 14 arc second error bound.

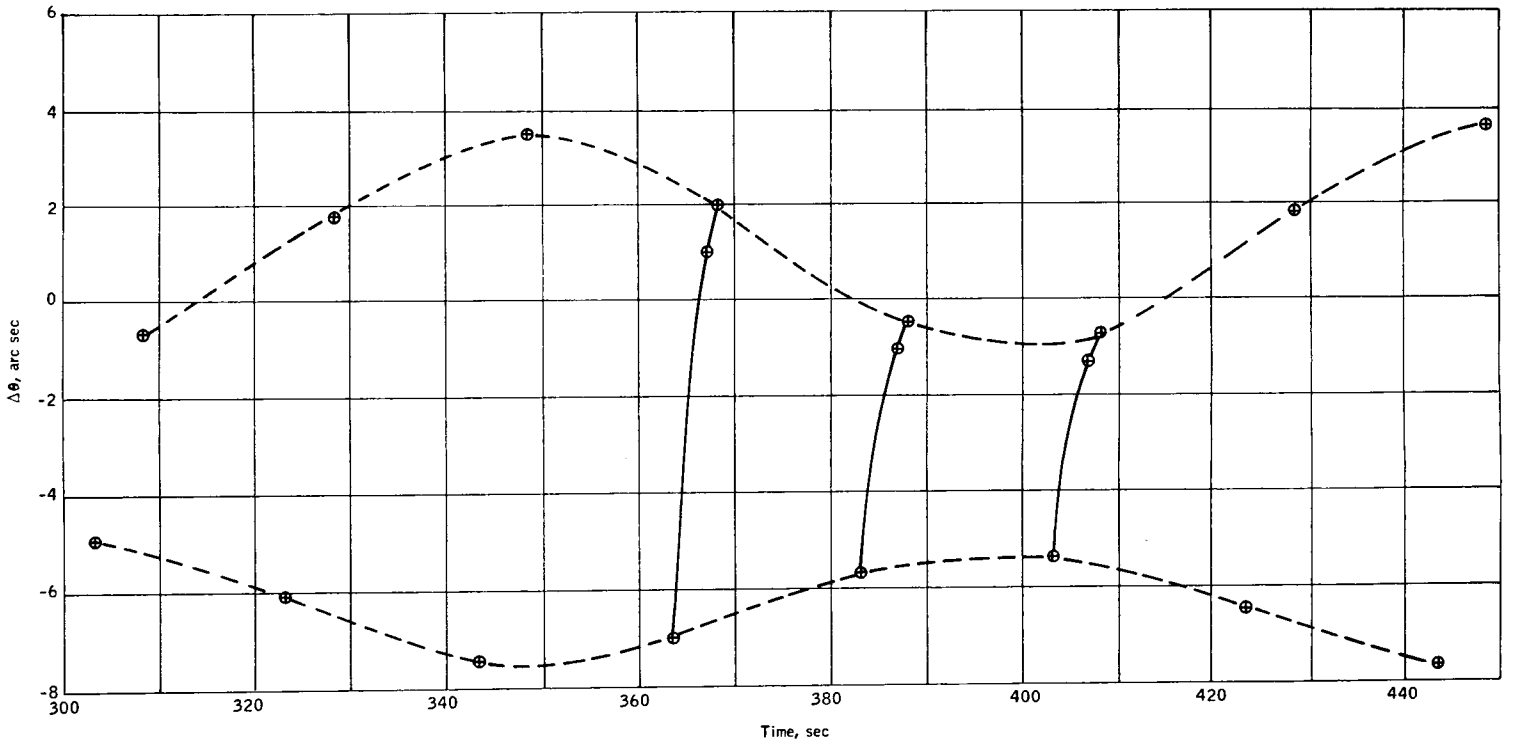

Figure 52. Experimental Axis Pitch Angle Error for Case II

Summary of Attitude Determination Subsystem Feasibility

A starmapper has been designed with the capability of viewing a minimum of four stars each spacecraft revolution. Data processing electronics provide a variable threshold to maintain the output data rate at a maximum of six stars per revolution. The optics are refractive, imaging on a three-slit reticle, with fiber optics line-to-circle scan conversion to a photomultiplier detector. Resolution from the system is 10 seconds of arc, obtained by first-order interpolation of the pulse.

A sun sensor has been designed with 10 seconds of arc resolution. The optics are refractive, imaging on a two-slit reticle, using an integrating sphere and silicon photo detector. Sun sensor and starmappers share a common data processing system.

An algorithm has been developed which uses least-squares fitting to a spacecraft model to develop a continuous attitude history of the spacecraft from the discontinuous starmapper and sun-sensor input. Simulation results indicate that radiometer attitude is defined within eight seconds of arc in the scan direction with four stars per revolution. The simulation further indicates that with two sun sensors operating simultaneously (four slits) a solution to the radiometer attitude is found with an error of 11.58 arc seconds maximum.

An alignment system has been designed which will measure the alignment of the starmapper and sun sensor with respect the radiometer to within four arc seconds throughout the life of the system.

The various errors discussed are summarized below.

Item	Allocated, arc sec	Designed to, arc sec
Attitude of attitude subsystem with respect to the celestial sphere	±14	±11.58
Orbit determination	±10	± 10
Spacecraft data processing	± 3	± 3
Time correlation	± 3	± 3
Ground data reduction and star ephemeris	± 3	± 3
Alignment of radiometer with respect to the attitude subsystem	±8.6	± 4

ATTITUDE CONTROL SUBSYSTEM

The conceptual design for feasibility of the attitude control system proceeded along the following steps:

1. Definition of functional requirements
2. Tradeoff studies of control concepts
3. Mechanization of a conceptual design
4. Analysis of feasibility

As in the total conceptual study, a functional analysis was utilized to ensure that all aspects of the mission and its interrelationship with spacecraft control were considered.

The precision to which the experiment requires an instantaneous knowledge of the field of view of the radiometer with respect to the earth's horizon and the long life of the experiment (one year) had a significant effect on the spacecraft/control concepts considered and the resulting requirements. Since most real-time attitude determination systems are inconsistent with the experimental requirements, the control concepts considered were quickly narrowed to those involving utilization of the properties of the orbital environment and spacecraft dynamics itself for the necessary control.

Functional Requirements

Considering the concepts of attitude control and attitude determination, joint performance of many of the studies was necessary to ensure that each is complimentary with the other. A brief review of the functions of each system follows.

The function of the attitude determination "system" is to determine the attitude of the spacecraft and, consequently, of the radiometer during the time when the field of view of the radiometer is traversing the earth's horizon. This function is accomplished by measuring the relationships between the spacecraft and the stars and sun, reversing these relationships, and later using these data to compute the attitude of the spacecraft with respect to time.

The attitude control function is described diagramatically in Figure 53; as may be noted, this function includes initial orientation of the spacecraft and its attitude throughout the useful life of the spacecraft in orbit. This latter function includes all control of the motions of the spacecraft with respect to the orbit plane including coning, spin rate, nutation, and precession.

The desired spacecraft motions (see Figure 54) are:

- Spin at constant rate about an axis perpendicular to the orbit plane.
- Translation of the spin axis along the orbit.

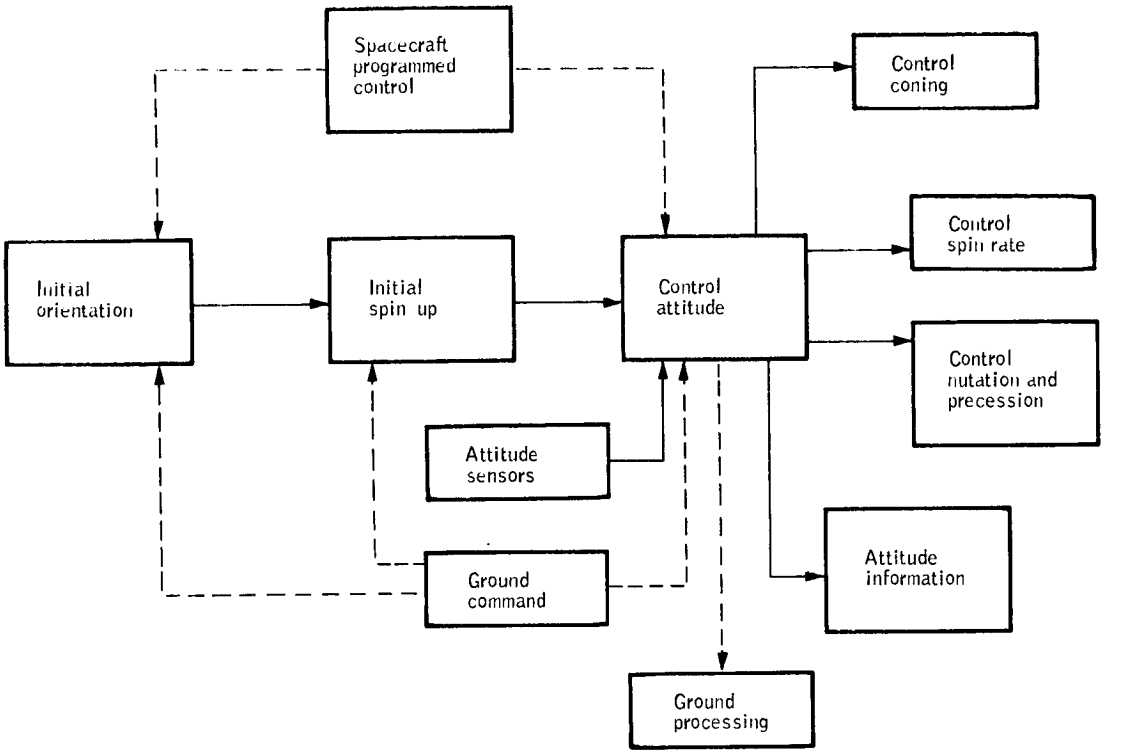

Figure 53. Attitude Control Functional Diagram

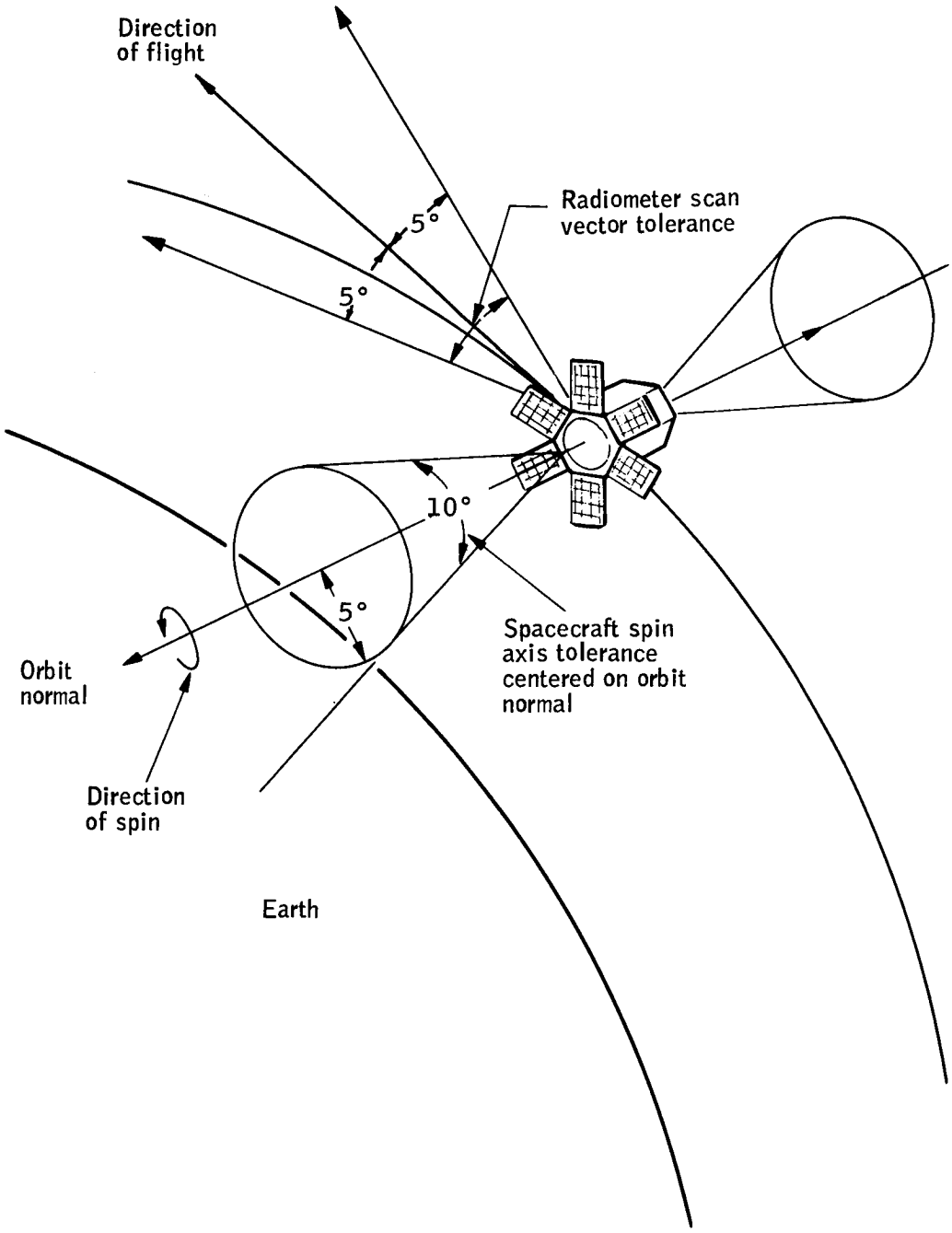

Figure 54. Control Limits

The actual motions, however, will consist of the following components:

- Spin about an axis stable in inertial space.
- Nutation and coning.
- Precession of the spin axis due to disturbing torques.
- Translation along the orbit.
- Slow-down (decay) of the spin rate.

The attitude control consequently is needed to provide the following functions:

- Damp or limit the nutation and coning.
- Overcome the torque-induced precessions.
- Add precession to make the spin axis perpendicular to the orbit plane.
- Overcome the spin-rate decay.

Tradeoff Studies

Trade studies were conducted for each of the control functions shown in Figure 53. In general, the attitude control and attitude determination tradeoffs were conducted as illustrated in Figure 55.

To provide a basis for determining the preferred approaches to attitude control and to attitude determination, the simulation study described by the four blocks on the left side of Figure 55 were performed. That is, the dynamic characteristics of candidate spacecraft configurations were first determined. The disturbing torques which would affect spacecraft motions were then estimated. Finally, a computer simulation was performed to determine the spacecraft motions under both "open loop" (no attitude control) and "closed loop" conditions. The "open loop" simulations showed that the spacecraft motions were highly predictable and that the most significant departures from ideal spacecraft motions were:

- Spin-axis precession due to coupling of the magnetic moments of the spacecraft with the earth's magnetic field
- Spin-rate decay as a result of eddy currents induced into the spacecraft by the earth's magnetic field
- Precession of the orbit

Under "closed loop" conditions the motions would be highly dependent upon the characteristics of the various attitude control loops and probably would not be as readily predictable as under "open loop" conditions. Using the information from these simulations, the attitude control and attitude determination concepts were traded off essentially simultaneously.

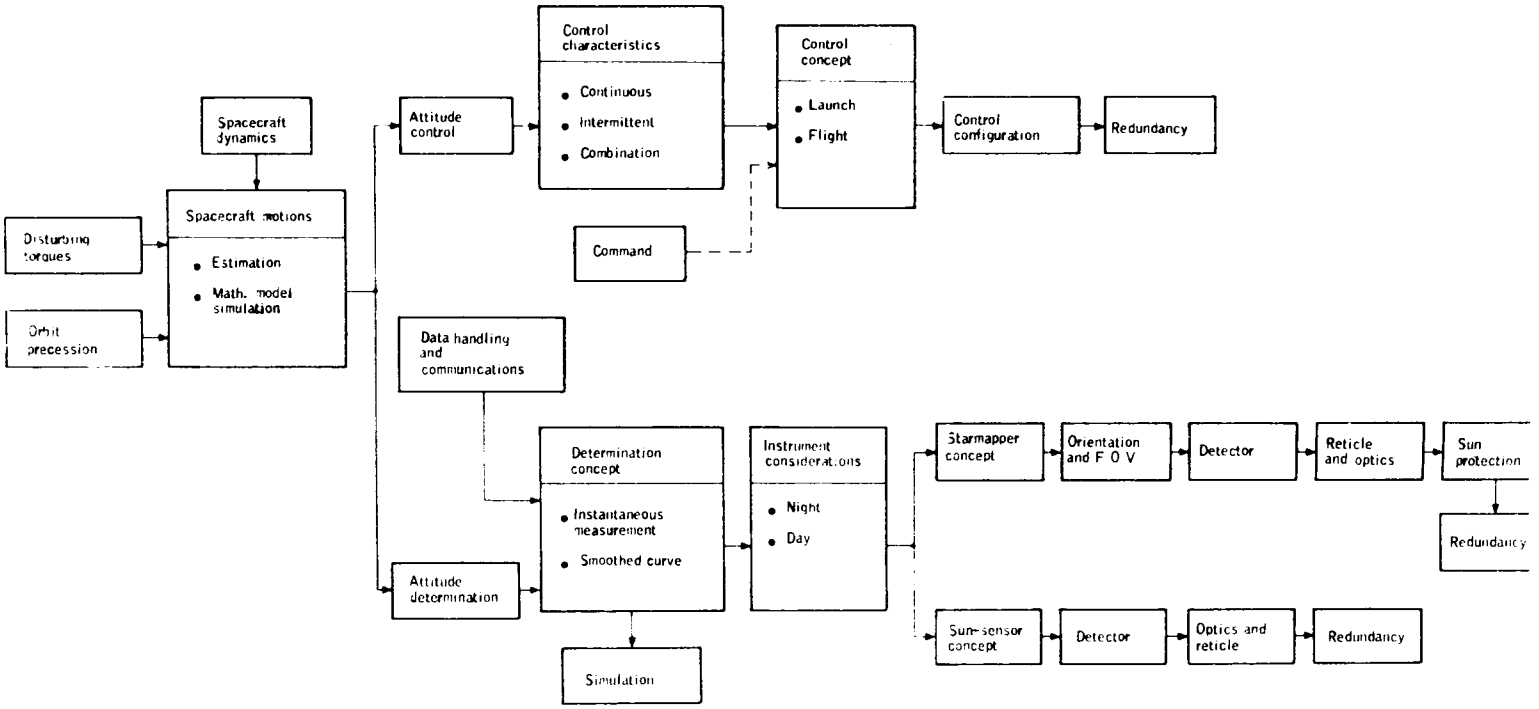

Figure 55. Attitude Determination and Control Study Flow Diagram

The most significant tradeoffs in the attitude control area were concerned with:

- Intermittent versus continuous control.
- Computation location.
- Respin and reorientation concept.

The decision having the most impact on related systems tradeoffs was the selection of a combination of continuous and intermittent control of spin rate, yaw, and roll. This decision is summarized in Table 27. The effect of this decision was that attitude could be predicted when the spacecraft is in the highly predictable "open loop" configuration.

The selection of magnetic torquing for respin and reorientation of the spacecraft with respect to the orbit caused this function to be accomplished in a highly reliable manner uncomplicated by moving parts or other "wearout" type problems. These are illustrated in Table 28.

Conceptual Design

The attitude control subsystem configured for the orbital horizon definition experiment resulting from the detailed trade studies is a simple, part-time, ground-commanded magnetically torqued control system which reacts with the earth's magnetic field.

The satellite derives its basic attitude stability from the gyroscopic properties of the spinning body. Because of this and the experiment requirements, an active control system is not required continuously, and the subsystem will only be used when necessary to correct attitude. The desired attitude for the satellite is with the spin axis normal to the orbit plane. Disturbance torques such as gravity gradient, solar pressure, and magnetic moment will cause the spin axis to drift from this desired orientation. Because of attitude determination observations and radiometer pointing, the spin axis should be held within ±5 degrees. Also, no torques are to be applied during attitude determination observations; therefore, the attitude control subsystem will be normally de-energized. The spin control portion of the attitude control subsystem will be operated in the same manner. The attitude and spin rate will be monitored by ground personnel who will decide when the attitude and spin rate are to be corrected.

The preferred attitude control subsystem resulting from the trade studies and analyzed for feasibility consists of four units as follows:

- V-head horizon sensor (14- to 16-micron CO_2 band)
- Logic control unit
- Three torquer coils
- Passive damper

TABLE 27. - ATTITUDE CONTROL TRADEOFFS, ROLL, YAW, AND SPIN CONTROL

Concepts	Disadvantages	Advantages
Continuous	• Spacecraft motions dependent upon characteristics of control system as well as past and present disturbances. Motions are difficult to predict. • Continuous control difficult within practical limitations of power, weight, and orbit precession over one-year period	• Desired attitude is maintained within errors of sensor and control loops
Intermittent	• Attitude departs from "nominal" attitude during open-loop periods	• Motions are highly predictable during period when control is not applied (open loop). • Compatible with use of magnetic torquing (coupling with earth's magnetic field)
Combination • Magnetic moment trim - continuous • Re-erection, realignment to orbit (precess), and respin - intermittent	• Continuous power drain for trim • Requires controls for both the continuous and the intermittent loops	• Permits "exact" correction of most significant disturbance torques - the residual magnetic moment • Minimizes "drifts" of the spin axis • Maximizes time required between re-erections

The decision was to utilize the combination of continuous magnetic moment trim and intermittent torquing to accomplish re-erection, realignment to orbit, and respin. Added complexity is offset by improved stability of spacecraft motions in "open loop" periods, which simplifies attitude determination.

TABLE 28. - ATTITUDE CONTROL TRADEOFFS, ROLL, YAW, TORQUING

Concepts	Disadvantages	Advantages
Momentum interchange • Inertia wheels • Control moment gyros	• Continuous power consumption (or wheel rundown) • Complicated spacecraft motions due to cross-couplings • Bearing wear-out • Requires (practically) additional torquing source to take care of long time effects (such as orbit precession)	• Continuous control possible • Can provide damping of undesired motions
Mass expulsion • Reaction jets	• Moving parts wear-out • Gas leakage generates unknown torques • Possible mass shifts upon depletion of gas supply	• Quick correction of attitude errors • Weight compatible with one-year life
Magnetic	• Continuous control impossible • Requires commutation to match earth's field • Limited practical torque capability	• No moving parts • Can compensate for residual magnetic moment • No rundown or similar limitation to life • Spacecraft motions highly predictable during no-torque period

Magnetic torquing was chosen because:

- Simplest - no moving parts
- Most reliable
- Highly predictable spacecraft motions
- Compensation for residual magnetic moments possible

The V-head sensor provides information to determine the angle between the spin axis and the normal to the orbit plane, the coning angle, and to commutate the spin control coil. The sensor will measure the angle between the spin axis and the local horizontal plane. This angle is determined by comparing the earth intercept periods of the two heads. The difference in the two periods is an indication of the roll angle.

The V-head sensor can also provide cone-angle information. This is found by noting the difference in on-times of the two heads. One head starts the count and the other head stops the count. This will be measured on every revolution of the spacecraft for a period of time. The roll angle will be essentially constant over this period; therefore, variations in this reading will be due to the cone angle. A curve fitting can then determine the magnitude of the angle.

Information necessary to commutate the current in the spin-control coil is also provided by the V-head sensor. The output of one head initiates a counter at the first "on-time" and stops it on the second "on-time". A right shift is performed on the counter, and the contents are transferred to the 1/2 spin counter which is counted down by the clock. The output of the head accomplishes one current change, and the output of the 1/2 spin counter accomplishes the second current change one-half spin cycle later. The spin-control coil is oriented in the spacecraft so that the current change occurs at the proper time relative to the magnetic field. Figure 56 illustrates the scan geometry relative to the spacecraft and the earth infrared horizon. (References 8 and 9 provide a more detailed discussion of the above topics.)

The logic control unit contains the counters indicated above plus the logic necessary to perform the required operations. It also contains the coil driver electronics. These consist of a bridge-type circuit for reversing the current through the coil and adjusting the current level.

The control coils have an air core and are wound on frames which are oriented in the spacecraft to generate a magnetic field as required for control torques. The attitude and residual correction coils can be wound on the same frame and are oriented so that the plane of the coils is perpendicular to the spin axis of the spacecraft. The residual coil also provides the required moment for orbit-regression compensation. The spin-control coil is oriented so that its plane is parallel to the spin axis and is 68 degrees from the optical axis of the V-head sensor. This provides the proper orientation so that the current will be switched when the plane of the coil coincides with local vertical.

The passive damper is used to reduce the coning angle which may be introduced by the separation of the spacecraft from the booster. As indicated, the damper is designed to remove this energy passively. Extrapolation of data from presently designed and tested dampers indicates that damping the spacecraft to 0.5 degree is quite feasible.

The total feasibility of the attitude control concept could not be completely analyzed until the operational characteristics of the mission was configured. These characteristics included initial orientation and orbital operations. A brief description of these topics follows.

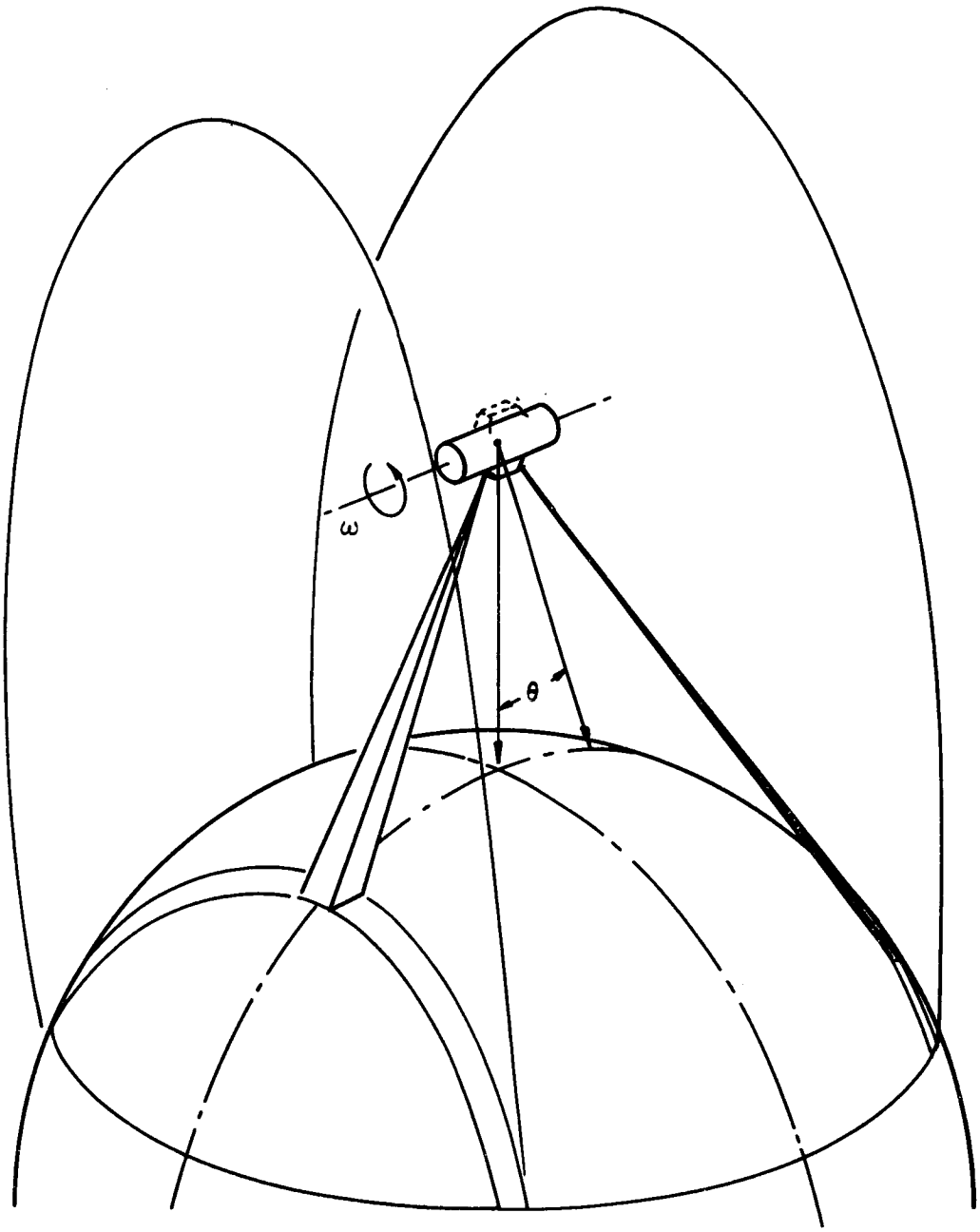

Figure 56. Horizon Sensor Scan Geometry

Initial orientation. -- The operational plan is based on having the booster orient the spacecraft spin axis normal to the orbit plane. The orientation is expected to be within two degrees of the normal. Before separating the spacecraft from the booster, the solar panels are extended and the spacecraft is spun up to three rpm ± five percent by the spin table on the Delta stage.

With a tip-off rate of three degrees per second and a spin rate of three rpm, the spacecraft will be precessing with a half-cone angle of eight degrees. The sequence of operation is shown in Figure 57. All commands for attitude control will be transmitted from the College station.

Upon separation of the spacecraft from the booster, the passive damper is activated. One full orbit has been allowed for damping of the coning motion. Attitude and spin-rate measurements are made approximately 2/3 of an orbit, so that the data can be read out at the second pass over the College station. The deviation of the spin axis from normal should not exceed five figures, so one correction period should be adequate to correct the attitude as well as the spin rate. The desired corrections are computed on the ground and transmitted to the spacecraft on the third pass over the College station.

After torquing has been completed, an attitude measurement by the V-head sensor of approximately 20 minutes can be transmitted to College on the fourth pass. The passive damper will be deactivated at this time. Spacecraft attitude will then be monitored for a period of 10 to 12 orbits to determine the magnetic moment of the spacecraft. The command to cancel the residual moment can then be made in the sixteenth orbit or the twelfth pass over College. If the drift during the 10 to 12 orbits has been large, it may be desirable to correct the attitude before starting to take data.

Orbital operations. -- The output of the V-head sensor will be monitored every two minutes during an orbit. In addition, every reading (three per minute) of the V-head sensor will be monitored for a 10-minute period prior to passing over the College station. The readings taken during the 10-minute period will provide knowledge of the coning angle. Spin rate will also be monitored.

When it is determined that an attitude and/or spin-rate correction is required, the command will be transmitted from the College station. The command will select the proper time delay required for the orbital conditions and the correction required. Figure 58 shows the ground control interface with the HDS spacecraft.

Analysis of Feasibility and Conclusions

The attitude control subsystem requirements derived from the mission and experimental requirements for the concept configured in this study are shown in Table 29. Analysis of these requirements and the operational plan reveals that all elements of the system are well within the current state of the art.

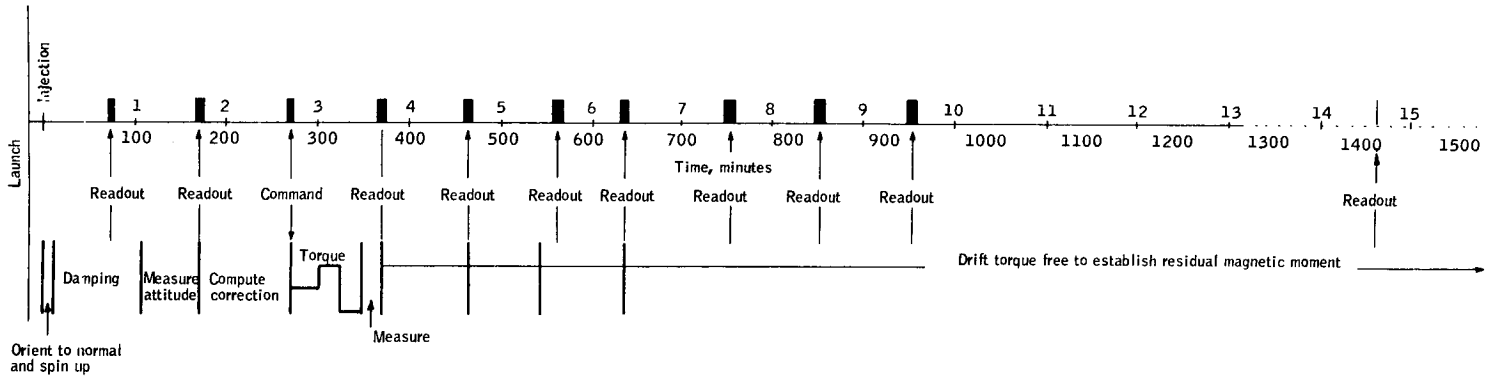

Figure 57. Operational Plan for Attitude Control

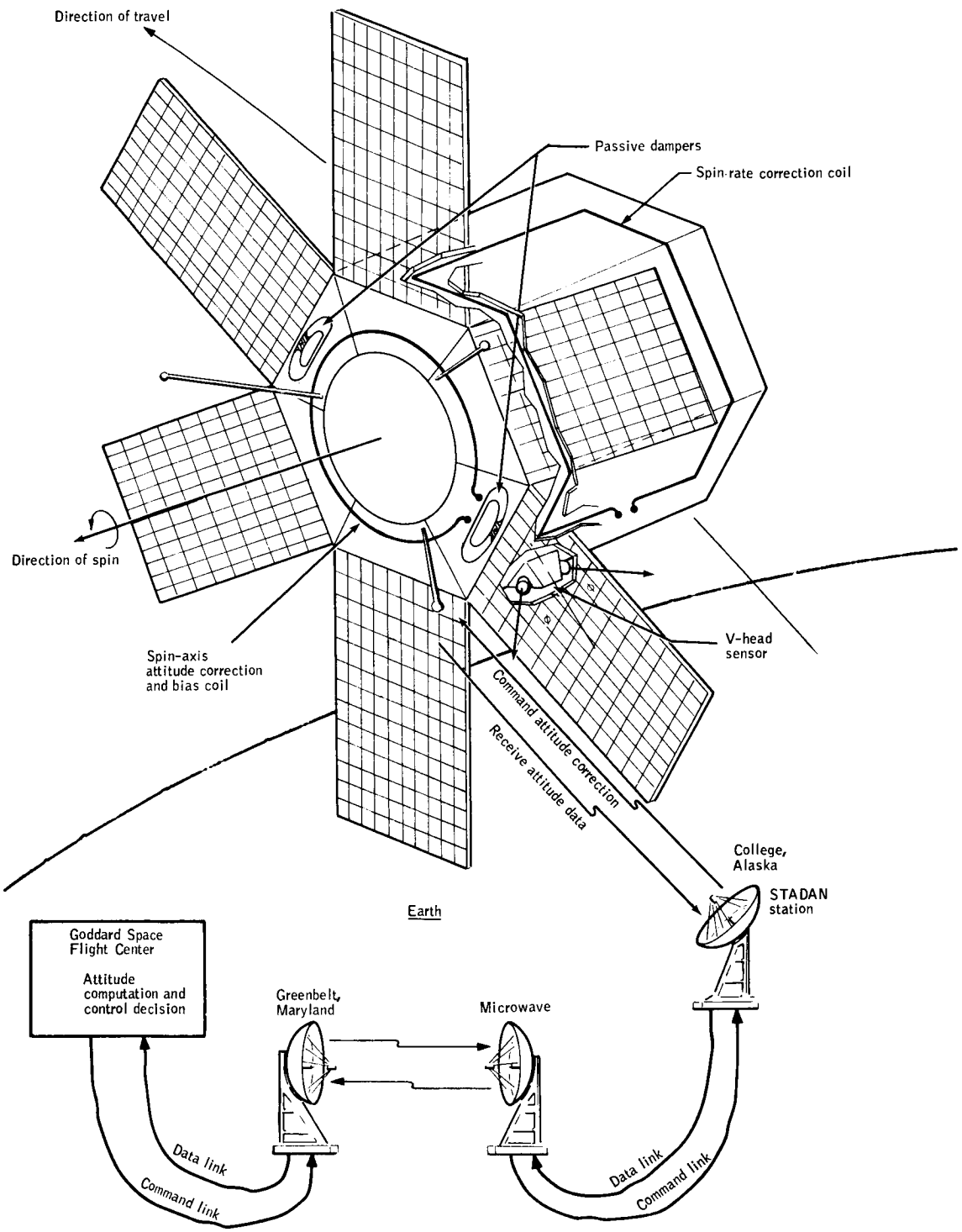

Figure 58. Ground-Commanded Attitude Control Subsystem

TABLE 29. - ATTITUDE CONTROL SUBSYSTEM REQUIREMENTS

Function	Requirements	Remarks
Control spin axis attitude	The attitude control subsystem (ACS) shall provide a magnetic bias torquer. It shall be used to reduce the residual magnetic moment along the spin axis and compensate for orbit regression.	The most significant torques acting on the spacecraft are due to interactions with the earth's field. It appears quite logical to take advantage of the existence of these fields and use interactions with them to re-erect periodically the attitude of the spacecraft, correct for orbital regression, and reduce the spacecraft residual magnetic moment.
	The ACS shall provide a magnetic quarter orbit torquer capable of correcting ± 5.0 degrees of spin-axis attitude in one half orbit.	Attitude correction should take place in as short a period as possible. Two quarter orbit periods are required to minimize cross coupling when trying to correct an attitude error.
	The ACS shall provide at least two levels of torquing in the quarter orbit torquer.	Two levels permit versatility in choice of torquing intervals. To maximize system effectiveness, spin axis attitude corrections are made at the same time that spin rate corrections are made.
	The ACS quarter orbit torquer shall not operate during the data cycle.	The attitude determination system can not operate with the induced spacecraft rates that will exist with the torquers operating.
Control spin rate	The ACS shall provide a torquer capable of correcting ± 5 percent of the nominal spin rate within one half orbit.	Spin rate must be corrected when it exceeds 5 percent of nominal to avoid complexities in data storage and attitude determination computation. The best earth's field conditions for correction of spin rate occur over the magnetic poles.
Provide attitude position information	The ACS shall provide a sensor to measure spin axis attitude and spin rate. The spin axis attitude shall be measured to ±0.5 degree, and spin rate shall be measured to ±0.5 percent of the nominal spin rate.	An accuracy of ±0.5 degree is required by attitude determination for initial estimation of attitude. Sensor output is also used for ground-base attitude computations to determine ACS sequences required.
Provide cone angle control	The ACS shall provide a damper to reduce body half-cone angle to 0.5 degree.	The cone angle must be kept small in order to maintain the radiometer scan vector within ±5 degrees of the orbit plane for longer periods of time. Present calculations give 180 days to grow one degree due to the residual magnetic moment and eddy-current torques.
	The ACS damper shall not operate during the data cycle.	
	The ACS damper shall have the capability to remove eight degrees of cone in no more than two orbits.	The spacecraft may have approximately eight degrees of half cone angle generated due to booster tipoff rates. The operational plan is such that two orbits are available for cone-angle damping. Ninety percent of the cone angle should be removed during the first orbit.
	The ACS shall be designed to operate for a spacecraft with inertia ratio I_s/I_t greater than or equal to 1.2 and a spin rate greater or equal to 3 rpm.	The inertia ratio was determined by the packaging constraints and the dynamics of a spinning body. It was shown in the analysis that a spinning body is stable about its maximum moment of inertia axis for a flexible spacecraft. Packaging constraints showed that an inertia ratio of approximately 1.4 could be obtained. Analytical results showed that the spacecraft was stable for an inertia ratio of 1.2 at 3, 4, and 5 rpm. Since the HDS spacecraft is adequately stable for r = 1.2 and packaging constraints allow up to a 1.4 inertia ratio, it is then recommended that r be greater than or equal to 1.2. The 1.2 ratio gives a margin of safety to the maximum moment of inertia axis.
	The ACS shall be designed to operate for a spacecraft whose asymmetry about the preferred spin axis is not greater than three percent.	The spacecraft will undergo more complex motion since an asymmetric body causes the cone angle to vary about a mean, and the extent of variation is directly related to the asymmetry of the body. The body is more unstable about a preferred axis as the asymmetry about that axis increases. For ACS control, three-percent asymmetry was found to be acceptable.

An analysis of free-body motion (see Figure 59) was conducted for a symmetric, spinning cylinder whose inertia ratio I_s/I_t was greater than one. The objective was to determine the characteristic motion of this specific body. Secondly, the analysis was extended to the asymmetric spinning body (transverse inertia very nearly equal).

The results of the symmetric-body analysis indicate that:

- Motion is stable about the maximum moment of inertia, assuming small perturbation to the spacecraft.
- The spacecraft must have an $I_s/I_t > 1$ to have a preferred spin axis and be stable about that axis. Due to launch vehicle payload constraints and the dynamics, I_s/I_t is recommended to be greater or equal to 1.2.
- Initial tip-off rate imparted to spacecraft at separation requires that a cone-angle damper be supplied to damp the initial spin vector to coincide nearly with the principal moment of inertia axis. The damper will be required to remove the approximately eight degrees of half-cone angle that was generated by the maximum booster tip-off rates. The operational plan provides for two orbits of damping prior to performing mission.

The results of the asymmetric-body motion indicate that:

- The greater the asymmetry, the more complex the motion of the spacecraft. In addition to the body having a cone angle, the cone angle varies with a period five times that of the spin period.
- Asymmetry causes the spacecraft to depart from the preferred spin axis, i.e., the spacecraft is somewhat less stable about the preferred spin axis.
- Attitude control is not affected by at least a three-percent asymmetric body. However, for attitude prediction accuracies the asymmetry should be minimized because asymmetry produces variations in the frequencies of motion of the spacecraft and results in degradation of the attitude determination. Balancing to within one percent is well within state of the art for dynamic balancing techniques. It is then recommended that the spacecraft be balanced as well as the state of the art allows to minimize complex motion. The design intent is to have a spacecraft spinning about a preferred body axis. Since an exact coincidence is not possible, the objective is to design the spacecraft to spin as near to the preferred spin axis as possible.
- The attitude control control math model can be adequately represented by a symmetric body, providing the asymmetry is less than three percent.

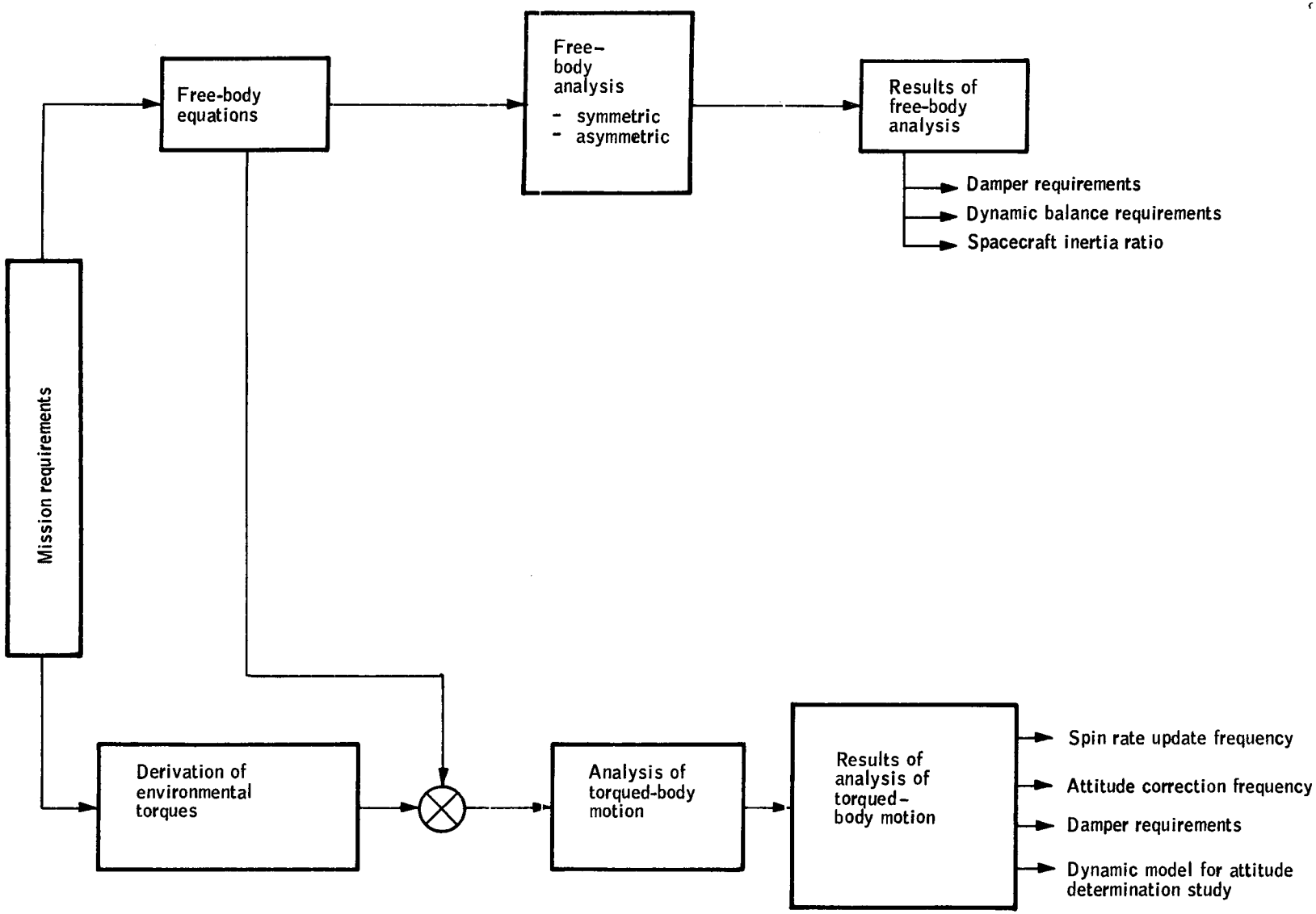

Figure 59. Spacecraft Dynamics Analysis Study Plan

- The attitude prediction model must include asymmetry effects regardless of the level of asymmetry.

Analysis of the disturbance torques indicates that solar pressure, gravity gradient, vehicle outgassing, and aerodynamic torques are small compared to magnetic interaction and eddy-current torques. Meteoroid impact torques are impulsive and unpredictable and must be handled in the attitude determination model as impulsive changes to body rates. In addition, the rotating elements in the radiometer calibration system could impose large coning motions if symmetric balancing was not employed.

In this analysis, the major continuous torques considered were the magnetic interaction torque and the eddy-current torque. A nominal residual magnetic moment of 1.0 amp-turns-m^2 and an eddy-current conductivity coefficient of 2.86×10^{-5} ft-lb-sec/$gauss^2$ were used. The disturbed motion of the spacecraft was determined parametrically for 3, 4, and 5 rpm. As the spin rate increases, the pitch attitude change due to eddy-current torques increases. The combined influence of magnetic interaction and eddy currents, however, causes the spin-axis precession to decrease as spin rate is increased. The spin-axis precession will accumulate to five degrees in 55 or 72 orbits for spin rates of three or four rpm, respectively. This assumes that no attempt is made to balance continuously the observed residual magnetic moment on orbit regression by applying a balancing current to the attitude update magnetic coils. Spin-rate decay will amount to a five-percent decrease in about 125 orbits due primarily to eddy-current torque effects. This then provides a basis for establishing requirements on the attitude control system and update interval. In addition, the form and magnitude of the motion provides a basis for the attitude determination model.

The results of the analysis were:

- A mathematical description of the significant disturbance torques for use in the attitude determination model was completed. The major torques are the magnetic interaction torque and the eddy-current torque.

- A spin rate of the three rpm was selected because of the minimum composite effect of residual and eddy-current torque on the pointing-vector prediction between three to four rpm. Further, the lower spin rate increases the energy received by the radiometer on each interception of the horizon.

- Spin rate need be updated only once every 125 orbits to keep spin rate within five percent of nominal.

- Attitude correction due to spin-axis precession needs updating once per 55 orbits if the residual moment is not compensated. With compensation for residual moment and orbit regression, the update period can possibly be extended to 300 orbits.

- Magnetic torques cause no significant increase in cone angle over a period of four orbits.

DATA HANDLING SUBSYSTEM

The constraints having a significant impact on the data handling subsystem conceptual studies include both the experimental requirements on data (global coverage and data rates) and the requirement to be compatible with the STADAN network during the 1972 to 1973 time period.

To begin development of the spacecraft data-handling system concept, a comparison of ground telemetry station availability with the basic data requirement is necessary to determine if data-storage capability is required on the spacecraft.

The basic data requirements specify complete global profile sampling of the earth's horizon with roughly uniform spatial and temporal sampling rates over a one-year time period. To meet the profile tangent height resolution requirements with a feasible radiometer, a relatively low altitude orbit (nominally 500 km) is necessary. Global coverage dictates an essentially continuous data sampling over the complete surface of the earth, and the low-altitude orbit reduces possible contact time with the existing STADAN stations.

A map displaying the maximum area of data collection for a spacecraft with only direct transmission capability in a 500-km circular orbit is shown in Figure 60. The stations shown are all of the STADAN stations with capability for command and reception in the 136 MHz vhf band. The area covered is based on the assumption that the satellite can be at maximum line-of-sight distance with the radiometer scanning the opposite horizon from the ground station. This assumption implies spacecraft capability to take profiles at all azimuths and may not be technically feasible. An estimate of the maximum possible area coverage to be made is allowed, however.

As can be seen from the map, profiles could be taken with maximum coverage of approximately one half of the earth's surface. The spacecraft could be in contact with a ground station approximately one fifth of the time in orbit, although station down times, priorities, and acquisition times would, in practice, significantly reduce this number. These data indicate data storage on the spacecraft is required in order to meet the basic data requirements since area coverage by direct transmission is inadequate.

Functional Requirements

Once the basic decision regarding direct transmission or storage had been analyzed, a functional analysis of the spacecraft/data handling concept indicated the following functions are required:

- Receive and process ground commands
- Provide system sequencing
- Provide mode switching

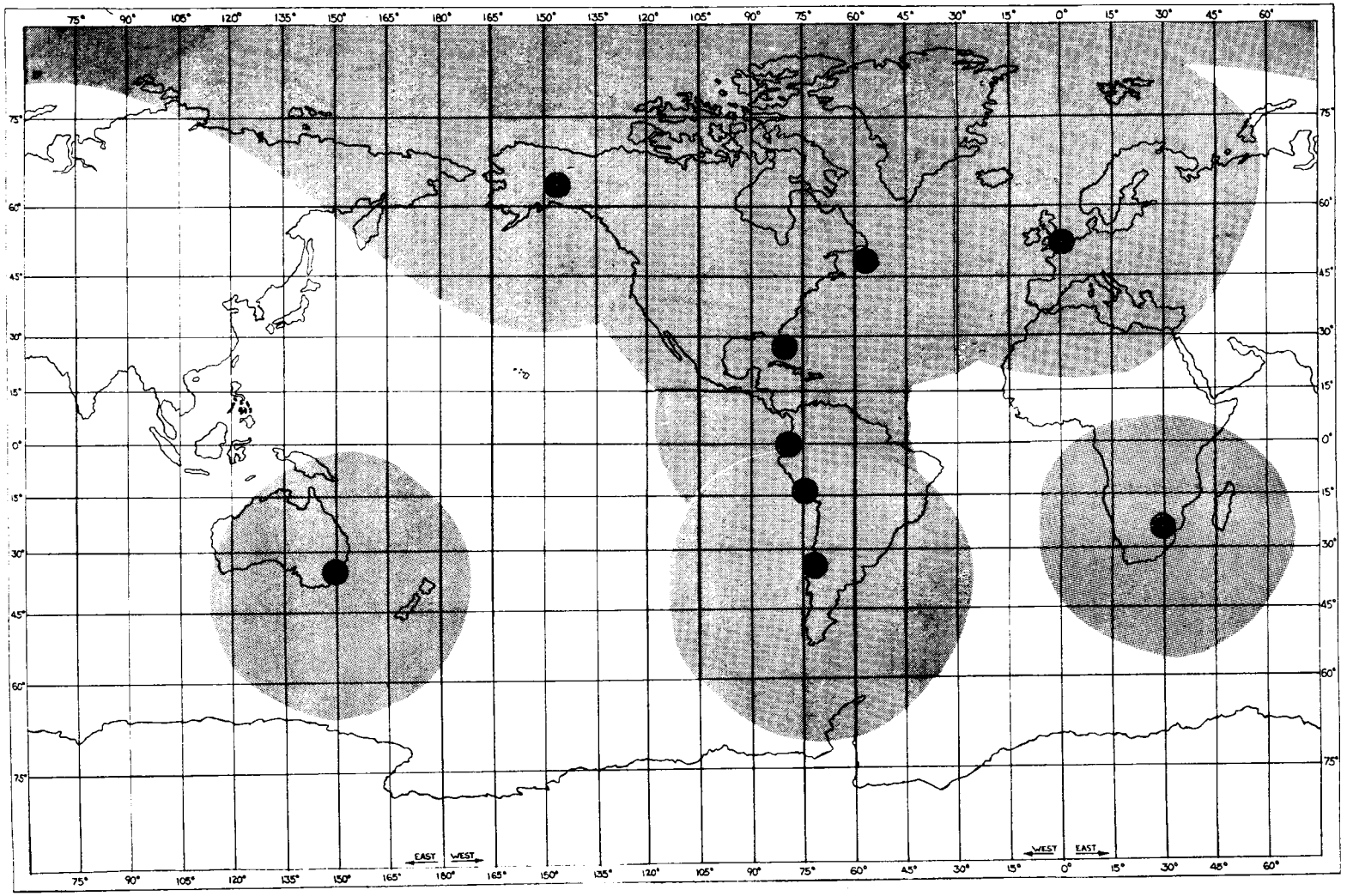

Figure 60. Potential Coverage with Direct Transmission (500 km Altitude)

- Provide spaceborne time reference
- Gather and process spacecraft data
- Store spacecraft data
- Organize and label telemetry outputs in standard data format

These functions are illustrated in Figure 61. Each of the functions were traded off to insure the basic mission and experimental objectives were met.

Tradeoff Studies

The tradeoff studies in the data handling subsystem followed the general pattern outlined in Figure 62. Many of the data handling tradeoffs were strongly influenced by other parts of the system, especially by the experiment package (radiometer, starmapper, and sun sensor). There were, however, several areas in which the bases for decision were largely within the data handling area alone. The most significant of these are listed in the order of their significance to the total system concept:

- Memory type
- Time reference correlation
- Sampling control

A brief discussion of the factors involved in these tradeoffs follows.

Analog versus digital storage. -- Two possibilities exist for storage of data on the spacecraft - analog and digital. In analog storage, the data is taken directly from the sensors and stored on magnetic tape along with time information. Magnetic tape speed is increased over the telemetry station, and the data is transmitted in analog with the conversion to digital data accomplished on the ground. In the digital system, the analog sensor outputs are digitized immediately, stored in solid-state or tape systems, and transmitted in digital form.

In this system, the measurement resolution requirements and the methods of data generation dictate a digital data-handling system.

The resolution requirements of radiance magnitude of 0.01 W/m^2 - sr and tangent height of 0.25 km transform to data-bandwidth requirements on the order of 5 kHz and 100 kHz from the radiometer and starmapper, respectively. If a spacecraft storage time of one orbit (94 minutes) and a telemetry contact time of two minutes are assumed, the transmission bandwidth is a factor of 47 times the required storage bandwidth, or 235 kHz and 4.7 kHz for the radiometer and starmapper, respectively. These bandwidths are not compatible with STADAN and, in addition, would require excessively high transmission power on the spacecraft. For the digital system, no errors are introduced in the storage and transmission loops, as in the case of analog systems. Analog systems normally have accuracies to within one to five percent.

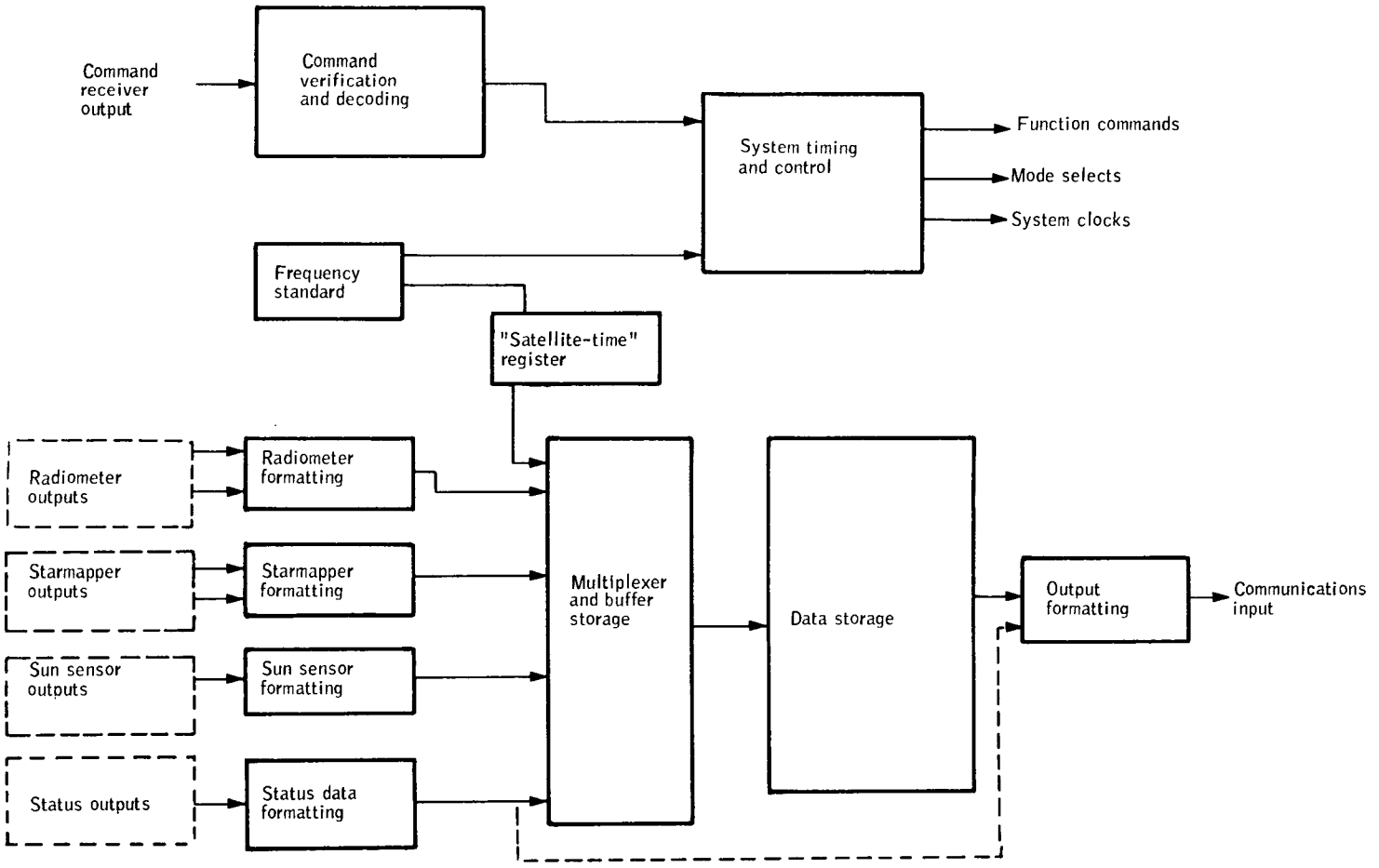

Figure 61. Data Handling Functional Diagram

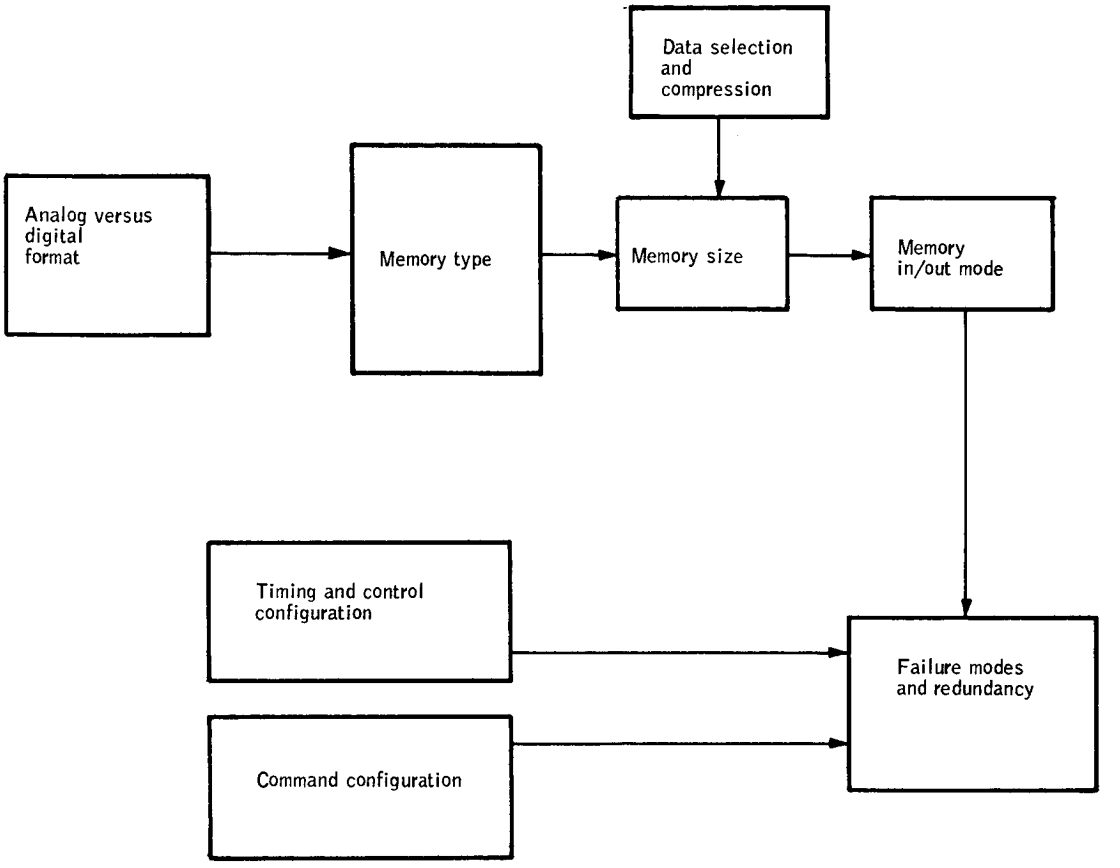

Figure 62. Data Handling Flow Diagram

Passive radiometers in the spinning-spacecraft configuration read the horizon profile of interest in less than three degrees of the spacecraft revolution of 360°. The starmapper output consists of a small number of pulses corresponding to star positions occurring at random times with the desired information being the times of occurrence of the pulses. To store and transmit data of this type efficiently, it is necessary to eliminate the data collection and recording during times when no outputs of interest are occurring. In analog recording with magnetic tape, this method of data compression cannot be easily achieved for this system because of the randomly occurring star data and the start-stop disturbance torques generated by an incremental tape recorder. This type of data compression is very easily achieved in a digital system with solid-state storage. Profile samples need only be taken over the fraction of the revolution of interest. The time of occurrence of each star pulse and a measure of its magnitude can be digitized into a single binary word and stored. If no data of interest is occurring, no data is recorded or transmitted. For this system, a transmission bandwidth on the order of 10 kHz is sufficient, providing there is a data-compression factor of approximately 500 for the digital system over the analog system.

In summary, careful investigation of the amount of data required to be stored between "dumps" to the telemetry system disclosed that the memory requirements were compatible with existing "solid-state" memory technology. Consequently, this memory type was chosen in preference to magnetic-tape or magnetic-drum storage techniques, thereby eliminating any memory "wearout" problems or torque reactions upon the spacecraft due to rotating components.

Time reference correlation. -- A frequency monitoring chosen (see Table 30) to provide the necessary time reference correlation between the spacecraft and ground stations. This relatively simple technique involves transmitting a "time pulse" to the ground periodically during data dump. Simultaneously with transmission, a "time count" is temporarily stored and then transmitted to the ground at a convenient interval during the data dump. Upon receipt of the "time pulse", the ground station similarly picks and stores a "time count" from the ground station's time register. The spaceborne-derived "time count" is then later compared with the ground-derived "time count" to determine an incremental time correction factor. This concept is considerably simpler than other concepts that potentially could be used for this purpose.

Sampling control. -- Analysis of the problem of providing on-board sampling of data to be stored from the experiment package instruments disclosed that addition of the necessary controls could permit the memory size to be kept within practical bounds. Moreover, by making the sampling control variable (i.e., having various modes which could be selected by ground command), many advantages in the data collection could be realized such as obtaining an optimum data distribution over all space/time cells and providing ability to accommodate special situations during the life of the mission when it would be desirable to alter the distribution of samples. A complete list of tradeoff considerations is illustrated in Table 31.

TABLE 30. - DATA HANDLING TRADEOFFS, TIME REFERENCE CORRELATION

Concepts	Disadvantages	Advantages
Precise frequency standard	• Size, weight, and power is large compared to other approaches • Most expensive	• All data obtained against true time; no correction routines or clock reset required if performance is maintained throughout flight
Synchronized oscillator	• Requires continuous comparison with a ground standard ► Coverage not presently available ► Disturbed by doppler and other propagation effects	• Can tolerate oscillator instability if synchronization is continuous
Frequency monitor	• Requires periodic transmission of spacecraft time for comparison with ground • Single readings affected by doppler and other propagation effects	• Can use conventional crystal-controlled oscillator • Simplest • Lowest cost

Frequency monitor approach chosen since it is simplest and has lowest cost approach and since the propagation effects are tolerable.

TABLE 31. - DATA HANDLING TRADEOFFS, SAMPLING CONTROL

Concepts	Disadvantages	Advantages
Store all samples	• Excessively large memory required; major development item • Excess data collected does not represent equal redundancy in all space/time cells	• All possible data collected
Store constant percentage of samples	• Data collected does not represent equal redundancy in all space/time cells	• Practical memory size
Constant latitude (store percentage of samples according to a constant function of latitude)	• Requires knowledge of orbit period and polar crossing times ► Ground processing and command to spacecraft • Lacks flexibility for seasonal effects, concentrated data taking, etc.	• Practical memory size • Optimum data redundancy distribution over space/time cells.
Variable (adjustable by ground command; normal mode of operation is above-listed constant latitude)	• Requires determining orbit period and polar crossing times on ground • Requires logic necessary to provide the variable timing	• Practical memory size • Optimum data redundancy over all time/space cells • Can accommodate special situations: ► Seasonal effects ► Lost transmissions ► Concentrated data taking (such as polar warming)

Variable approach was selected because maximum capability is provided for obtaining useful data with a practical memory size. Experiment flexibility gained offsets the added logic circuitry.

Conceptual Design and Analysis of Feasibility

A general functional block diagram of the data-handling subsystem configured to examine for feasibility is shown in Figure 63. The subsystem consists of a ground-command processing unit, system time reference, programming and control logic, data processing for the sensors, data-storage unit, and an output formatting unit.

The data-handling subsystem in its present concept is a completely solid-state system well within state of the art. All data on the spacecraft is digitized, stored in a solid-state memory, and transmitted to telemetry stations approximately once per orbit.

The basic mission data requirements and the STADAN compatibility requirement were the primary factors in determining the data-handling-system size and organization. The primary mission goal is to perform a one-year global mapping of the earth's CO_2 horizon by recording 378 508 horizon profiles at appropriate spatial and temporal points. Ten STADAN stations can be used for reception of telemetry data. These requirements reduce to data-handling requirements for data collection and storage of approximately 500 000 bits per orbit (see Table 32 for detailed data budget) and transmission once per orbit continuously for the year. Flexibility is included in the concept wherever it does not degrade the primary mission goal. For example, where more than one station can be contacted in an orbit to unload the memory, profiles can be taken at high rates over interesting locations.

The command processing unit is compatible with the STADAN Tone Digital Command System (available at all stations with capacity of 70 commands). Commands are verified to be legitimate on reception, and a reception or response indication is transmitted back to the ground. A total of 58 ground commands are required for system operation.

Precision time labeling on the spacecraft is required for correlation of the radiance sample and the attitude data. In addition, the on-board time will be transmitted to the ground telemetry stations where its drift can be measured, thus eliminating the need for resetting or correcting the spacecraft time reference.

Sequences will be generated in the programming unit to control spacecraft functions at locations remote from ground stations. Among the required sequences are magnetic torquing control for attitude-error correction and spin-rate correction and variable profile sampling rates as a function of latitude.

Data sources on the spacecraft are the radiometers, starmappers, sun sensors, and multiple status test points. All data is processed from the analog sensor outputs to binary digital form to achieve feasible data bandwidths and eliminate data accuracy degradation due to the transmission link.

A ferrite-core memory system of approximately 500 000 bits in size is recommended for the system. A solid-state memory is selected to eliminate the momentum and buffer storage problems of magnetic tapes and to provide a

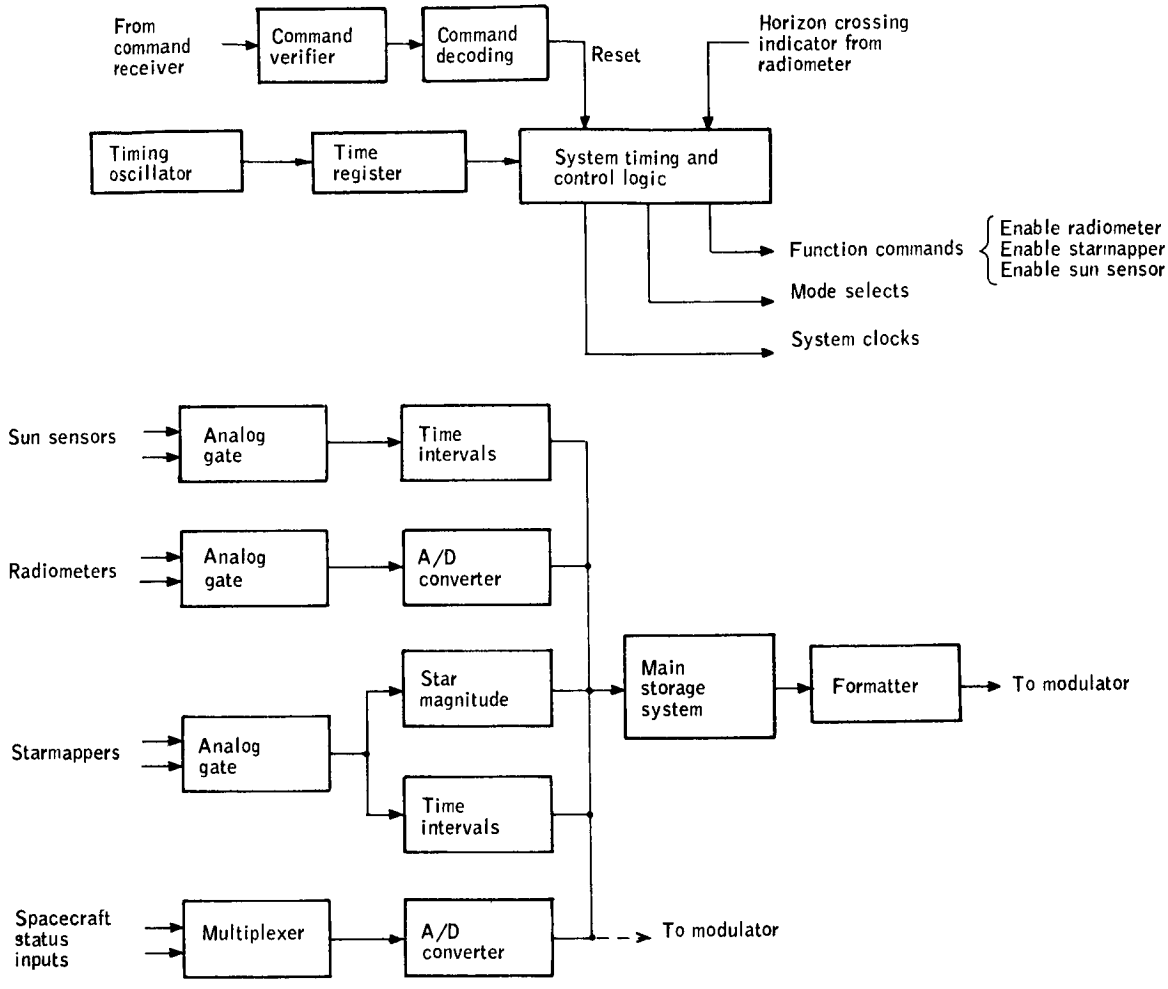

Figure 63. Data Handling Subsystem Block Diagram

TABLE 32. - DATA STORAGE ESTIMATES

(RECOMMENDED DATA BUDGET)

Radiometer	
550 10-bit samples/profile	5500 bits/profile
26 10-bit calibration samples/profile	230 bits/profile
3 time labels	50 bits/profile
	5810 bits/profile
68 profiles/orbit	395 080 bits/orbit
Starmapper	
18 20-bit times/rev	360 bits/rev
18 5-bit transit times/rev	90 bits/rev
1 threshold level/rev	5 bits/rev
1 time label	10 bits/rev
	465 bits/rev
282 rev/orbit - 1/3 orbit	43 710 bits/orbit
Sun sensor	
4 20-bit times/rev	80 bits/rev
1 time label	10 bits/rev
	90 bits/rev
282 rev/orbit - 2/3 orbit	16 920 bits/orbit
Status	
30 8-bit words	240 bits/profile
1 set/recorded profile	16 320 bits/orbit
Total on-board storage equipment	
Raw data	472 030 bits/orbit
Storage inefficiency, 5%	23 600 bits/orbit
Parity, sync words, 4%	19 825 bits/orbit
Total	515 455 bits/orbit

high reliability system with no wear-out factors. Ferrite core is recommended for the memory element over other solid-state systems under development because of its flight-proven feasibility and minimum development time.

Output formatting will be achieved directly in the memory system organization. Formatting, to be compatible with STADAN, requires addition of parity error checking, synchronization words, and standard framing of the output data. Including this in the memory organization provides error testing of the memory system as well as the transmission link.

COMMUNICATIONS SUBSYSTEM

A general review of the system requirements and their general impact on the spacecraft/communications concept revealed the most significant problems in the communications subsystem would be the requirement to maintain compatibility with the STADAN system, to maintain tracking accuracies, and to provide for a conceptual design consistent with the life requirements of maintaining spacecraft/ground communications for a period of up to one year in the orbital environment. The specific systems requirements having an effect on the functional requirements of the communications concept are data transmission, tracking, command, and acquisition aid.

The first function is that of transmission of scientific data from the moving spacecraft to the ground telemetry stations comprising the NASA STADAN. Data rates of the order of 4000 bits per second will be necessary to insure adequate quantity and accuracy of scientific data sampling points. The nature of the scientific data dictates a pulse-code-modulation system to insure the necessary accuracy of the scientific data samples.

The second function is that of enabling the ground STADAN to determine the spacecraft location at any time with a high degree of accuracy. The accuracy must be high since the requirements of the experiment dictate that measurements on the order of ±125 meters in tangent height of the horizon are desired. This requirements translates to an approximate ±200 meters error budget for the "in-track" location of the spacecraft.

The third required function is that of enabling a ground STADAN station to command certain functions to be performed on the spacecraft. The commanded functions required typically are - transmit data, adjust position, actuate radiometers, etc. - up to a total of approximately 58 different commands.

The fourth function needed is that of furnishing a beacon signal to permit ground stations to acquire the spacecraft with ease.

Functional Requirements

Primary elements of the HDS experiment are the radiance profiles taken by the experiment package and the position and attitude of the spacecraft. Data of these elements must be transmitted between the spacecraft and the STADAN. Command and control must also be exercised via the communication link. The essential functions, then, of the communications subsystem are (see Figure 64):

- Data transmission,
- Tracking and acquisition aid, and
- Command.

The subsystem must be capable of data transmission from the radio horizon to a ground station to insure maximum data delivery, particularly in those instances where the spacecraft's path will be at low angles above the horizon. Data rates of the order of 4000 bits per second will be necessary to insure adequate numbers and accuracy of scientific data sampling points. Furthermore, the nature of the scientific data dictates a pulse-code-modulation (PCM) system to insure the necessary accuracy of the scientific data samples.

The ground STADAN must be able to determine where the spacecraft is at any time with a high degree of accuracy. This objective may be accomplished over a period of time by successive refinements of the orbit in a computer program so that instantaneous determination is not necessary. The accuracy must be high since the requirements of the experiment dictate that measurements on the order of ±125 meters in tangent height of the horizon are desired. This requirement translates to an approximate ±200 meters error budget for the "in-track" locations of the spacecraft.

The ground STADAN must also be able to command certain functions to be performed on the spacecraft. These commands must be performed with a high degree of reliability in a relatively short time period because the time for which the spacecraft is over a ground station is relatively short. A total of up to 58 different command functions, such as transmit data, adjust position, actuate radiometers, etc., will be required.

A beacon signal must be provided to permit ground stations to acquire the spacecraft at long ranges with relatively wide-pattern antennas.

A complete summary of the specific requirements and constraints placed on the communications subsystem resulting from an analysis of systems requirements is shown in Figure 65. Notice the flow of these requirements into a conceptual design.

Tradeoff Studies

The functions previously mentioned and the STADAN interface requirement, projected to the mission time period, define the tradeoff subject areas. Within these constraints a number of decisions were necessary with respect

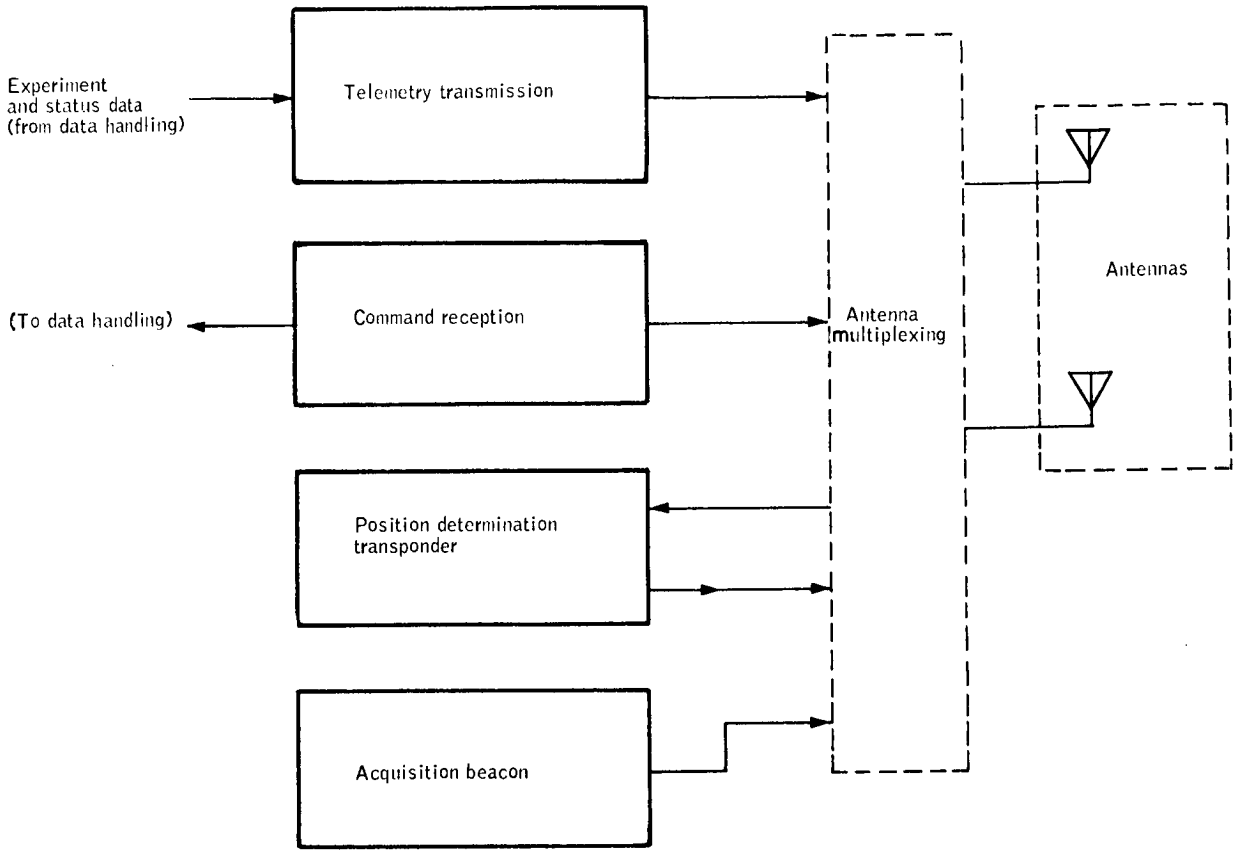

Figure 64. Communication Functional Diagram

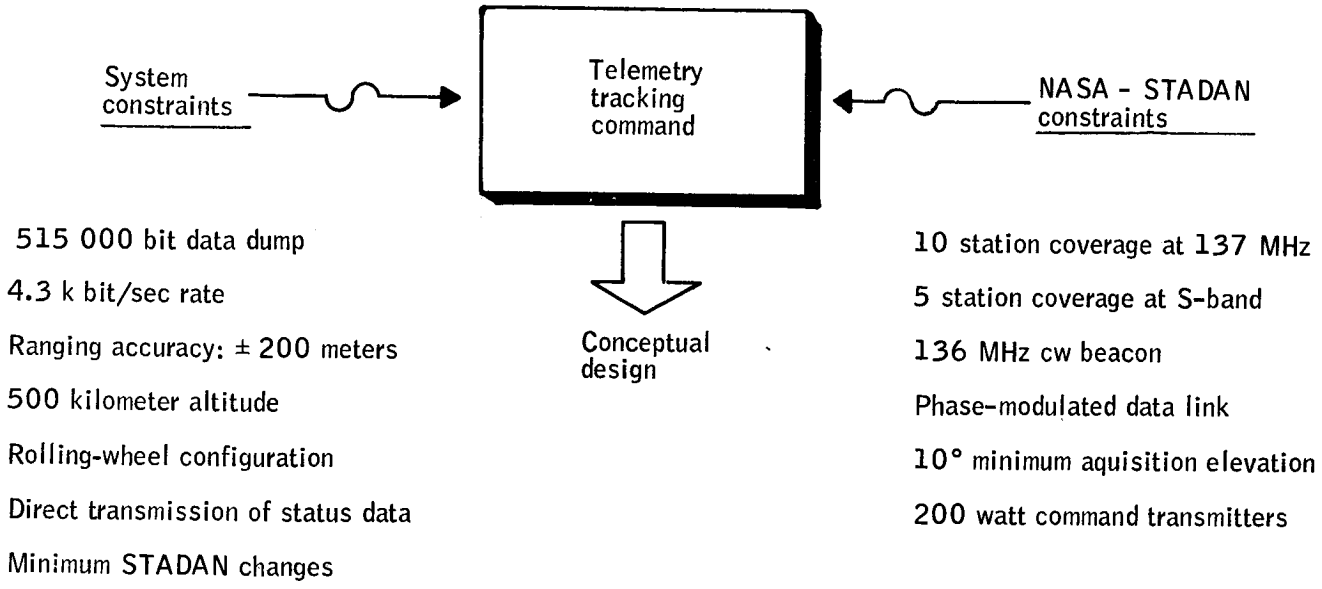

Figure 65 . Communications Subsystem Requirements and Constraints

to total system configuration. Figure 66 outlines the subject areas involved. The telemetry frequency selected was that of vhf. This frequency band was selected, rather than S band, primarily because of the larger vhf ground station capability. The vhf band was also selected as the command receiver frequency band since this is the standard STADAN configuration. Acquisition-beacon modulation was selected to be beacon code and status data. This configuration has more favorable redundancy features than modulation by beacon code alone. Other significant tradeoffs were those of:

- S-band tracking beacon
- Antenna locations
- Redundancy and alternate modes

Tracking beacon. -- A vhf system was considered for use as the range and range-rate transponder. Advantages of such a system are that, since the telemetry and command functions could be accomplished in the vhf spectrum, simplification of the spacecraft, reduction of number of antennas, and possibly redundant configurations may result. However, accuracy requirements in measuring range rate precluded the use of vhf. Consequently, S-band was chosen since it is compatible with the accuracy requirements.

Antenna locations. -- The location of antennas required reconciling the requirements for adequate antenna patterns, minimum coupling with the radiometers and starmappers, and a practical mechanical design.

Mounting of the S-band antennas on the spacecraft rim was considered. However, pattern distortion and excessive coupling of energy into the radiometers and starmappers more than offset the mechanical advantages of this location. Therefore, mounting of the S-band antennas (slots) on the tips of the solar panels was selected as the preferred configuration. At this location, the mechanical problems are more complex, but pattern distortion and optical instrument interference is reduced.

Although preliminary studies indicate the desirability of S-band antennas on the solar paddles, a preferred location should only be established after modeling verifies that the anticipated patterns are correct. This activity would properly be conducted during preliminary design.

Optimum mounting locations for the vhf antennas were the rear and front faces. This configuration provides good patterns. The simpler mounting configuration of rear face only was considered but was eliminated because of the resultant pattern distortions.

Redundancy and alternate modes. -- Considerable attention was given to securing adequate redundancy and providing for alternate modes of operation that could be utilized in the event of failure of one or more elements of the communications subsystem. These considerations were important because of the long lifetime requirements. A configuration (see Figure 67) was devised whereby at least two subsystem failures must occur before the communications function is impaired. The alternate modes of operation are summarized in Table 33.

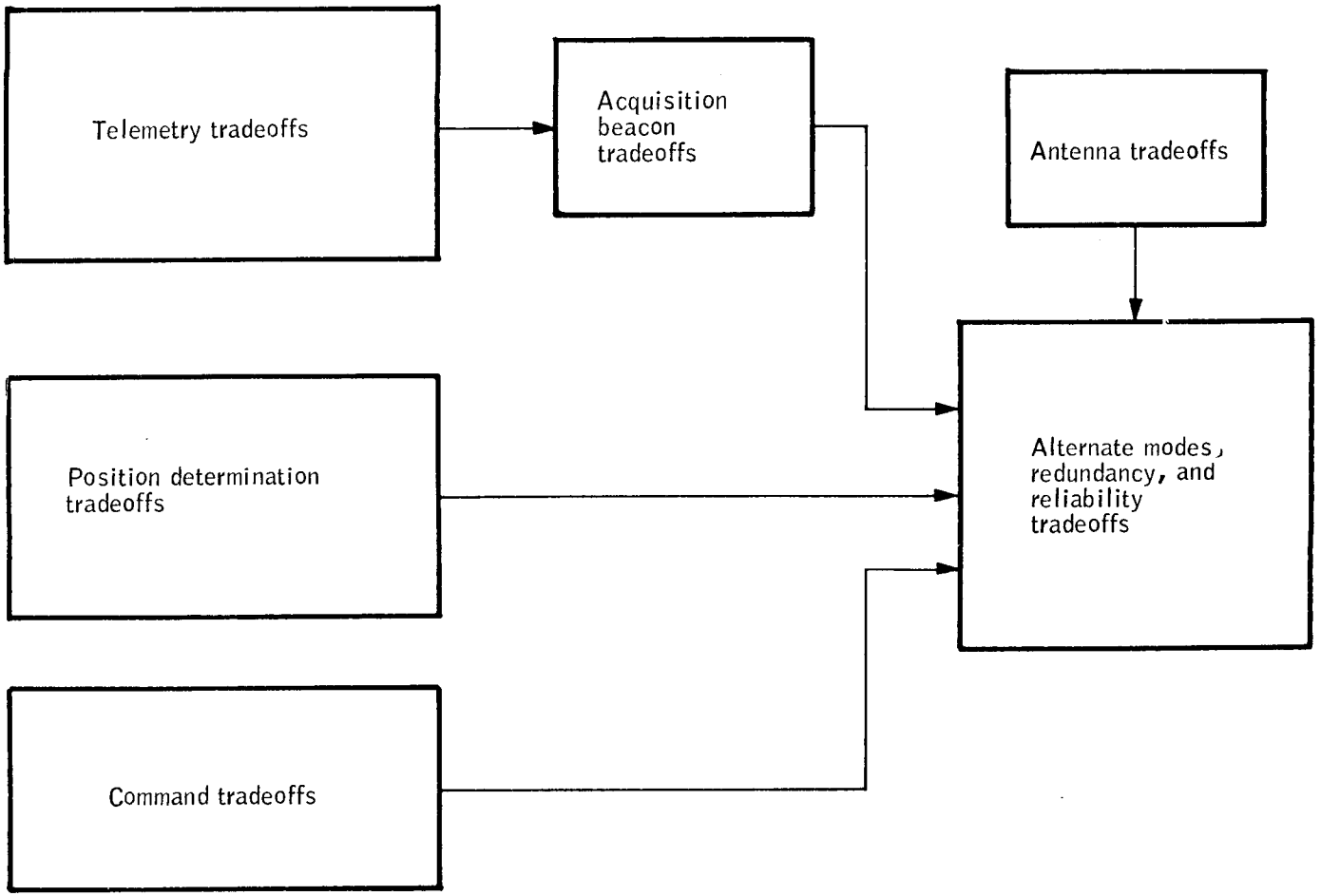

Figure 66. Communication Tradeoffs Flow Diagram

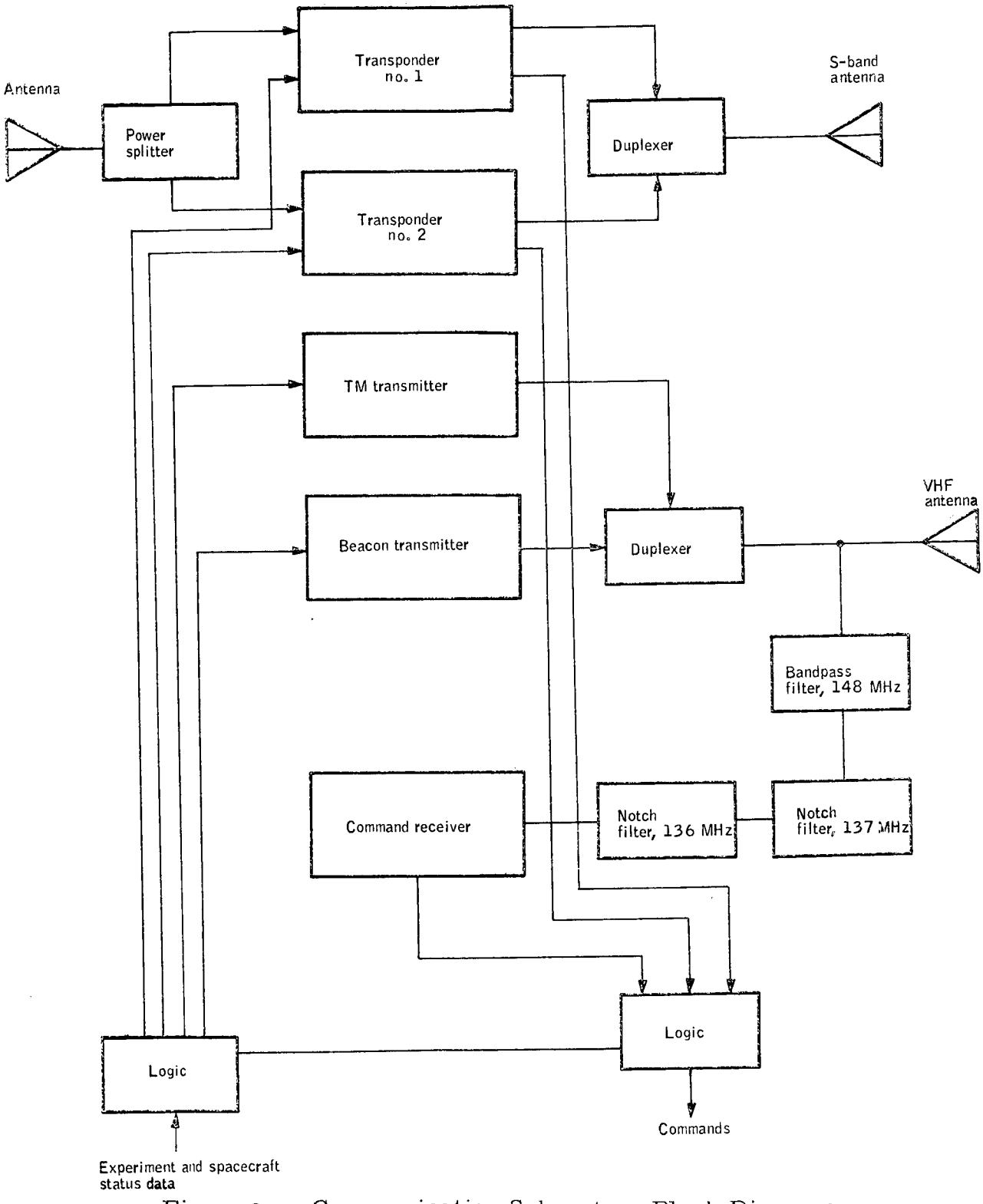

Figure 64. Communication Subsystem Block Diagram

TABLE 33. - COMMUNICATIONS SYSTEM ALTERNATE FUNCTION COMBINATIONS

Failure	Function	TM transmitter	Command receiver	Beacon transmitter	Transponder #1	Transponder #2
	Telemetry	X				
	Command		X			
	Beacon			X		
	Tracking				X	
*	Telemetry					
	Command		X			
	Beacon			XX		
	Tracking				X	
	Telemetry	X				
*	Command					
	Beacon			X		
	Tracking				XX	
	Telemetry	XX				
	Command		X			
*	Beacon					
	Tracking				X	
	Telemetry	X				
	Command		X			
	Beacon			X		
*	Tracking					X
*	Telemetry					
	Command		X			
	Beacon			X		
	Tracking				XX	
	Telemetry	X				
*	Command					
	Beacon			X		
	Tracking				XX	

Conceptual Design

A general, functional block diagram of the communications subsystem is shown in Figure 67. This subsystem possesses enough flexibility to permit continued functional operation over long time periods even after failure of individual components. General subsystem characteristics are listed in Table 34.

A single vhf antenna system may be used for the 136 MHz telemetry and the 148 MHz command functions of the spacecraft. Multiplexing is as shown basically in Figure 67. The antennas are two sets of either three or six broadly tuned stubs located on either end of the spacecraft.

The S-band antenna system consists of a set of six transmitting and receiving slots. One set of these slots is located on the end of each of the six solar panels.

In summary, the NASA STADAN network can satisfy the program requirements for data acquisition, command, and tracking with no STADAN modifications being required. Data acquisition and command will use vhf, while high-accuracy orbital position determination dictates the use of the S-band range and range-rate system of the STADAN. The communications subsystem requires essentially no new development.

ELECTRICAL POWER SUBSYSTEM

The electrical power subsystem for a spacecraft is contingent upon the project mission, experiment requirements, and system and subsystem requirements. Orbit, spacecraft, launch vehicle interface, and environmental constraints all have been described in previous sections of this report; these constraints (e.g., shadow fraction, sun angle, hexagonal spin-stabilized spacecraft, spacecraft envelope, and temperature) further serve to define the requirements and constraints imposed upon the electrical power subsystem. The power subsystem must be capable of supplying all the required electrical power during the one-year mission.

Functional Requirements

The essential functional requirements of the electrical power subsystem are shown in Figure 68.

The electrical power source must be compatible with the power requirements generated by other feasible subsystem concepts and the experiment package. Consideration of loading and growth were essential inputs into the trade studies. For concepts using solar energy, the power load per orbit must be deliverable under the worst sun conditions of the baseline orbit which exhibits a sun angle of 64° relative to the orbit normal and a shadow fraction of 0.364.

Storage capability is required to supply power during peak loads and to meet the requirements of one-year life. If a solar array is utilized, the storage must accommodate the eclipsed orbit.

TABLE 34. - COMMUNICATIONS SUBSYSTEM SUMMARY

	Telemetry transmitter	Beacon transmitter	Command receiver	Tracking transponder
Input frequency			148 MHz	1801 MHz
Output frequency	137.0 MHz	136.0 MHz		2253 MHz
Input signal	PCM digital	PCM digital		-110 dBm
Power output	0.25 W	0.25 W		0.286 W
Frequency stability	0.005%	0.005%		0.005%
Modulation	Phase	Phase	AM	Phase
Data rate	4.0 kilo-bits/sec	4.0 kilo-bits/sec	50 bits/sec	Range tones and 4.0 kilo-bits/sec

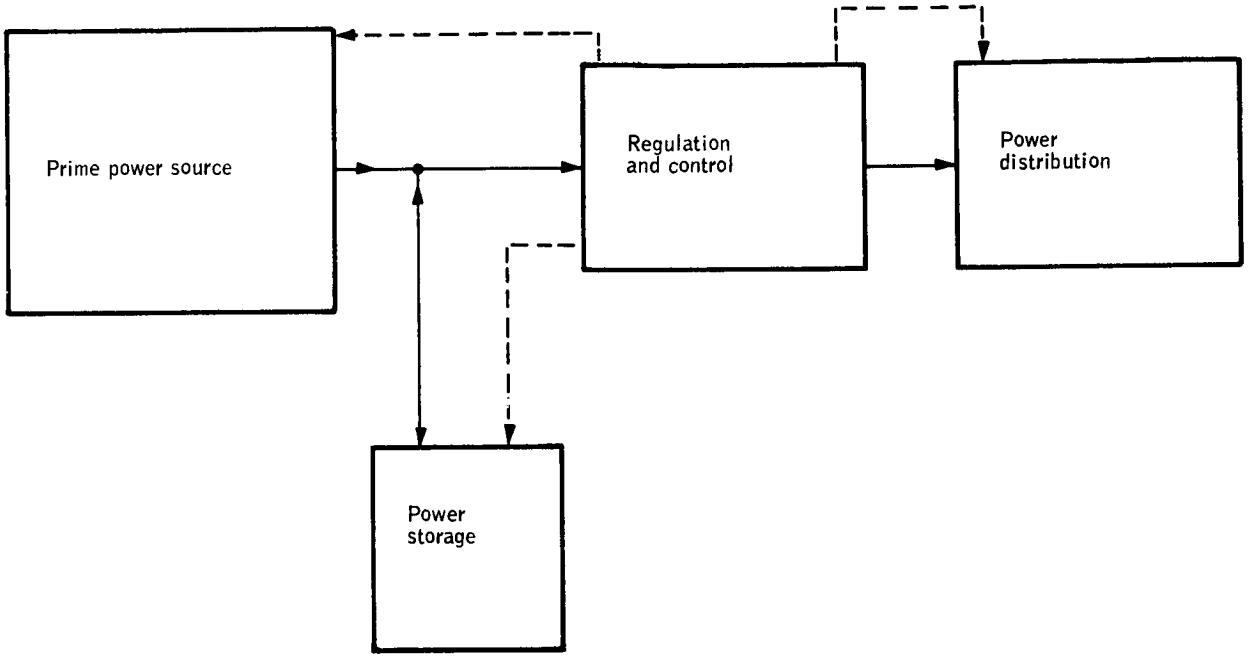

Figure 68. Power Subsystem Functional Diagram

Electrical power regulation and control is required to minimize system complexity and weight.

In the distribution system, the requirements having an impact on the design include fault protection and isolation. The magnetic moment of the spacecraft shall be controlled with limits required by the attitude control system. Radiated and conducted electromagnetic interference (EMI) shall be minimized.

Tradeoff Studies

Each of the functional areas shown in Figure 68 was examined to determine the most feasible electrical power subsystem for the HDS spacecraft. The tradeoff studies followed the general sequence shown in Figure 69. The most significant tradeoff decisions involved the:

- Prime power source
- Solar cell configuration
- Storage battery type

Prime power sources. -- Three prime power sources were considered to be potentially feasible for the HDS spacecraft:

1. Fuel cell
2. Radioisotope - thermoelectric
3. Solar cell-battery

The life expectancy of available fuel-cell batteries, however, does not approach the one-year operational requirement. Also, the weight of fuel and fuel tanks is prohibitive.

Cost, schedule, interference with the experiment package, and the inherent problems of handling radioisotopes precluded the use of the radioisotope-thermoelectric system.

The solar-cell battery system imposes restrictions on allowable orbit or requires active orientation of the solar panels. The above restrictions are not limiting considerations, however, in the 3 o'clock, sun-synchronous orbit selected for the HDS experiment. Of more importance, the solar array-battery system has the most extensive flight history, the lightest weight, and the lowest cost of the systems considered.

A more complete listing of the characteristics of the above energy sources is given in Table 35.

Solar-cell configuration. -- Careful study was made of the possible locations of the silicon solar cells. Body-mounted cells minimize the mechanical complexity of the spacecraft by eliminating the need for deploying solar panels. Unfortunately, the body-mounted configuration is inefficient. The most

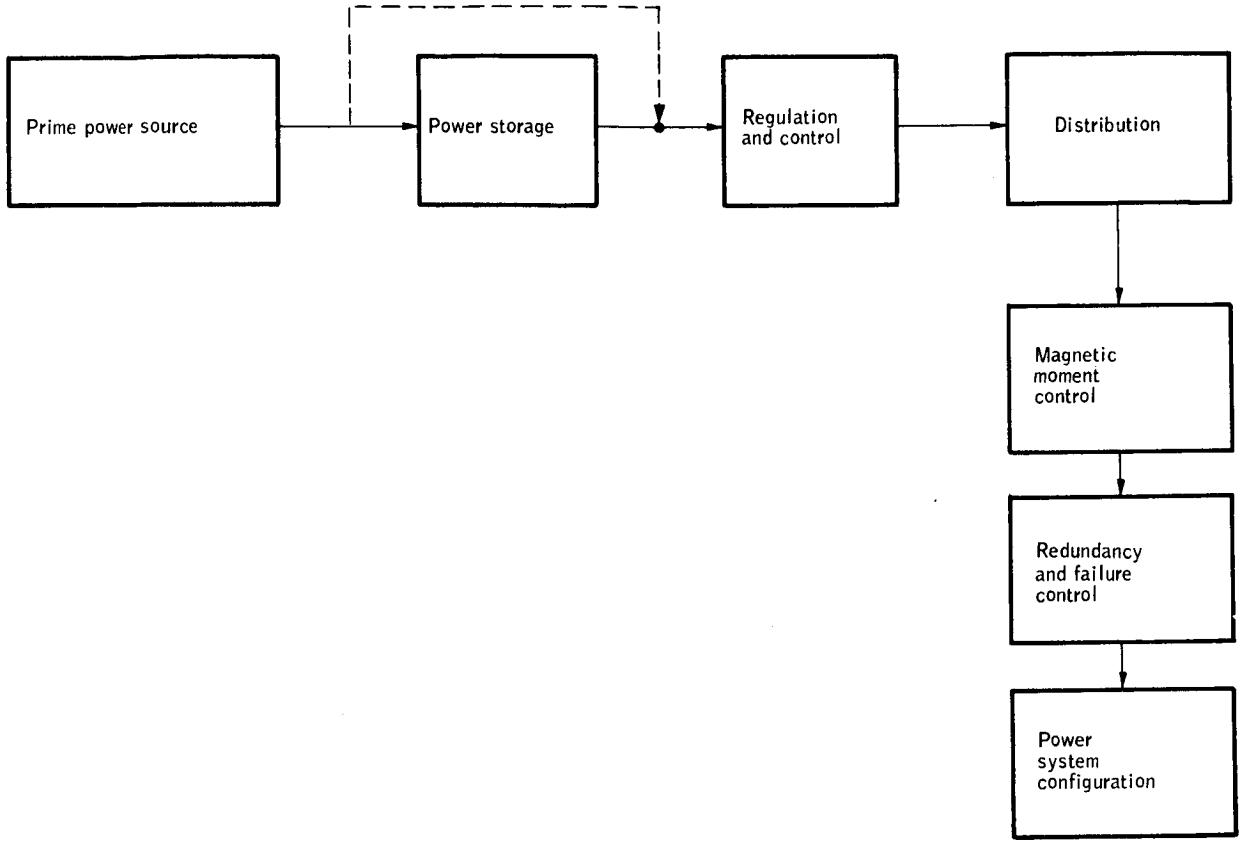

Figure 69. Power Subsystem Tradeoff Flow

TABLE 35. - POWER SUBSYSTEM TRADEOFFS, PRIME POWER SOURCE

Concept	Disadvantages	Advantages
Batteries	• Weight is prohibitive for one-year orbit	• Simple • Insensitive to orbit
Fuel cell	• Weight is prohibitive for one-year orbit, 840 pounds for estimated load • One-year life not available in existing systems (500 - 1000 hours now) • Exhaust of combustion products ► Can affect spacecraft motions ► Radiation and absorption affects radiometer	• Insensitive to orbit • Does not require power storage
Radioisotope-thermoelectric	• Launch path restricted due to safety requirements • Ground handling and launch restrictions because of radioactive material • Accountability and recovery restrictions on radioactive material • Internal high temperatures must be well insulated from radiometer cryogenic cooling • Considerable design effort required • High fuel cost ($2 to 3 million)	• Insensitive to orbit • Does not require power storage • Weight probably compatible with program
Silicon solar cells	• Sensitive to orbit • Requires storage of power for launch and during "night" • Requires careful design to minimize magnetic moments	• Lightest weight system (including storage batteries) of the concepts considered • Greatest space experience of any of the concepts considered

Silicon solar cells (with battery storage) were chosen because light weight and proven space experience offsets the need for storage (batteries).

Sensitivity to orbit orientation can be tolerated in comparison with the disadvantages of the only other usable concept, radioisotope - thermoelectric generator.

efficient concept considered was articulated (movable) solar panels. Movable panels, however, can be expected to generate undesirable reactions on the spacecraft motions. Consequently, fixed solar panels that are folded against the spacecraft until orbit injection and then permanently deployed were chosen as the most effective compromise.

Storage battery type. -- Battery power is utilized when solar-array power is not available. Three types of batteries were considered for the HDS application:

1. Nickel cadmium
2. Silver cadmium
3. Silver zinc

The charge-discharge requirement of 5600 cycles/orbit eliminated the silver-zinc system from consideration. Analyses of battery life, battery cycle, power storage requirements, available charge time, discharge rate, voltage limits, and battery environment were conducted. The nickel-cadmium battery was selected primarily due to mission-duration and cycle-life requirements.

Table 36 lists the pertinent characteristics of the batteries considered.

Charge control. -- The two-terminal battery was chosen because its proven capability offsets the small increase in size and power dissipation over the other candidate, the three-terminal adhydrode.

Regulation and control. -- Analysis of system requirements and available regulation circuits resulted in the selection of a series pulse-width-modulated system for bus and battery-charge regulators. This system of regulation had the highest efficiency of the methods considered; the radio frequency interference problems which could occur with this system can be controlled by proper design and shielding.

Conceptual Design

Conceptual design of the electrical power subsystem led to a feasible subsystem which is capable of supplying the system requirements. A block diagram of the subsystem is shown in Figure 70. This subsystem meets the needs of the explicit component load requirements given in Table 37.

DC buses of +28 and +5 volts are provided. Power output capability is 20 watts at 5 volts and 50 watts at 28 volts with an additional 26-watt periodic load on the 28-volt bus. Regulated outputs are supplied by switching regulators which operate from the unregulated bus.

The unregulated bus derives its power from six passively oriented solar panels during satellite day and from the battery during satellite night. The battery is diode coupled to the unregulated bus so that load power is automatically taken from the array when it is available and from the battery

TABLE 36. - POWER SUBSYSTEM TRADEOFFS, POWER STORAGE BATTERIES

Concepts	Disadvantages	Advantages
Nickel-cadmium	• Nickel being magnetic can have remanent magnetism causing a magnetic moment to be present even when current is not flowing	• Maximum usable storage of types considered. (4-watt-hr/pound utilizing 40 percent discharge - 7000 cycles or greater than one-year operating life.) • Longest shelf life of types considered
Silver-cadmium	• Usable storage is only 1.75 watt-hr/pound for 7000 cycles (only 10 percent discharge is practical for 7000 cycles) • More expensive than nickel-cadmium for equivalent usable capacity and life	• Uses no magnetic material
Silver-zinc	• Operational life limited to less than 1000 charge-discharge cycles	• Uses no magnetic material

Nickel-cadmium battery was selected because of weight, charge-discharge cycle capability, and cost advantages.

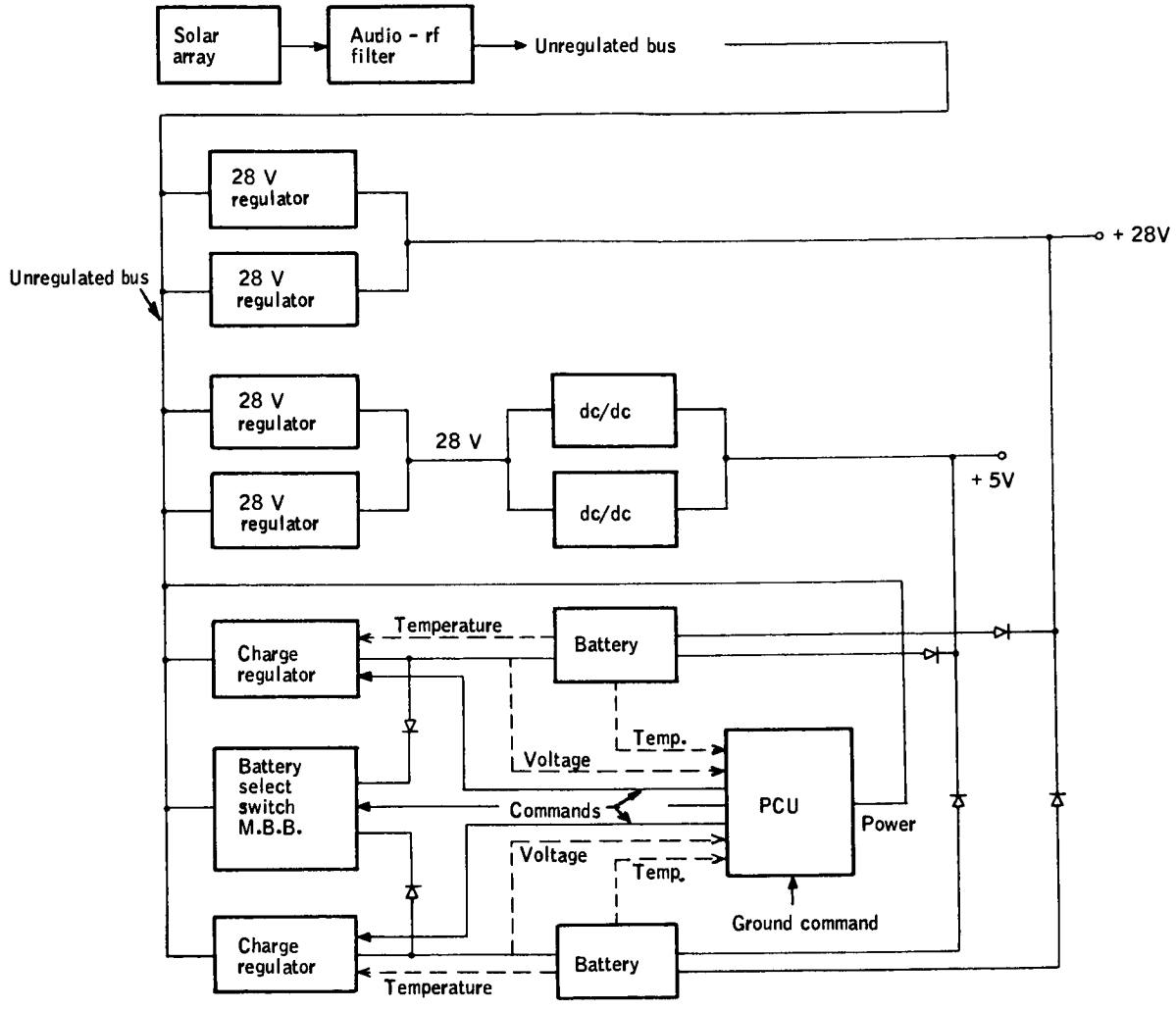

Figure 70. Electrical Power Subsystem Block Diagram

TABLE 37. - ELECTRICAL LOAD ANALYSIS

Item	Standby power, watts	Peak power, watts	Peaks per orbit	Time per peak, minutes	Average watts/ item	Power /orbit/ subsystem, watts
Radiometer	11.0	11.0	--	--	--	11.0
Starmapper	10.0	10.0	--	--	--	10.0
Sun sensor	1.0	1.0	--	--	--	1.0
System timing and control	3.9	5.7	1	2	--	3.94
Command verifier and decoder	0.2	2.0	1	2	0.24	--
Timing oscillator	0.7	0.7	--	--	0.7	--
Time register	1.0	1.0	--	--	1.0	--
Timing and control	2.0	2.0	--	--	2.0	--
Storage	2.72	2.72	--	--	--	2.72
Main storage	0.72	0.72	--	--	0.72	--
Multiplexer and buffer storage	2.0	2.0	--	--	2.0	--
Formatter	2.0	2.0	--	--	--	2.0
Data collection and control	12.7	12.7	--	--	--	12.7
10 bit A/D converter	3.0	3.0	--	--	3.0	--
Starmapper digitization	4.0	4.0	--	--	4.0	--
8-bit multiplexer	4.2	4.2	--	--	4.2	--
Status A/D converter	1.5	1.5	--	--	1.5	--
Communications	9.22	--	--	--	--	9.6
Command receiver	0.22	0.22	--	--	0.22	--
Telemetry transmitter	--	5.0	1	2	0.12	--
Tracking beacon	5.0	5.0	--	--	5.0	--
Range and range-rate transponder	4.0	15.8	1	2	4.26	--
Attitude control	5.5	10.0	1	47.3	--	7.75
Miscellaneous control circuits	3.0	3.0	--	--	--	3.0
Total						63.7

when array power is not available. The standby battery and charger are available for use if the working set fails.

A switching-type regulator is used to provide constant-current battery charging. If either of the regulated bus voltages is pulled significantly below their regulated value, a large fault current is supplied by means of a rectifier which couples the lower cells of the battery directly to the line. Thus, large currents are available for actuating protection devices or clearing faults.

STRUCTURAL SUBSYSTEM

Some of the preceding basic system requirements directly affect and constrain the conceptual configuring of an integrated spacecraft subsystem while others have very little input to configuration variations. The critical requirements and constraints, as applied to the spacecraft conceptual design and integration study effort, are:

- Utilize a near-polar orbit at about 500-km altitude.
- Utilize proven state-of-the-art subsystems whenever possible.
- Keep spacecraft maximum weight under 800 pounds.
- Utilize passive systems wherever possible.
- Provide a "stabilized platform" from which to make scientific measurements.
- Utilize spin-stabilized spacecraft with spin axis normal to the orbit plane.

These requirements were then translated into the functions that must be accomplished by the spacecraft structural subsystem. They are depicted in the functional flow diagram shown in Figure 71. There are certain requirements associated with these functional blocks that must be fulfilled by the structural subsystem or must be interfaced through it with the other spacecraft subsystems. A discussion of these functional blocks describing these requirements and interfaces is contained in the following paragraphs.

Support and Enclose Subsystem

The spacecraft structural subsystems must define the enclosed spacecraft volume within the booster interface constraints and must within this volume support and maintain the subsystems components and equipment. Inherent in this support and maintenance requirement is the positioning and arranging of these components to insure compatibility with spacecraft dynamics requirements and inter- and intra-system interfaces.

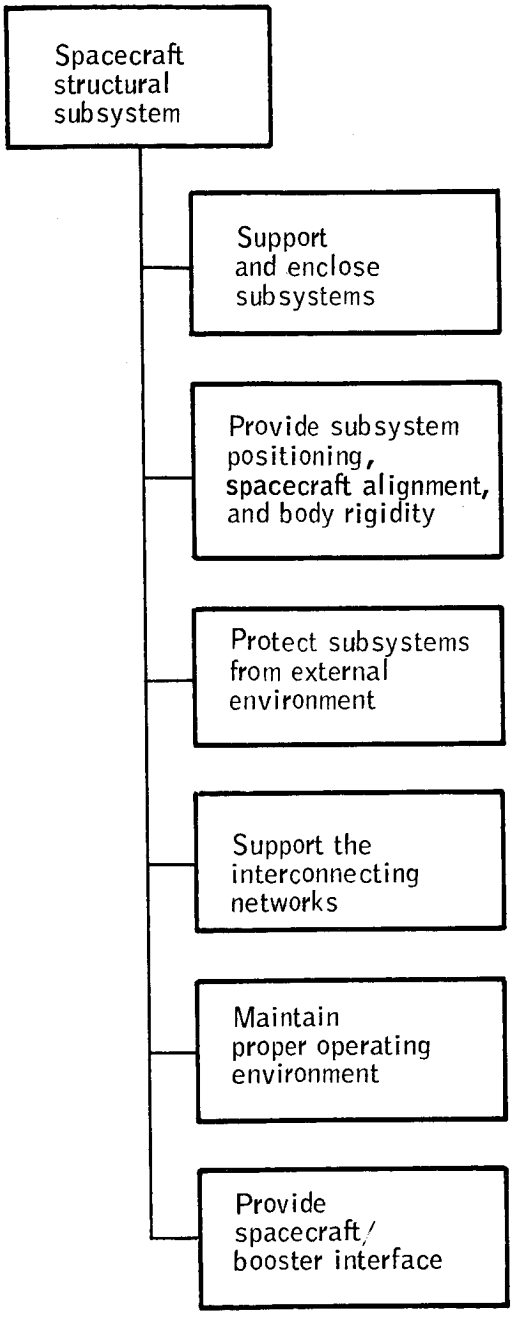

Figure 71. Spacecraft Structural Subsystem Functional Flow Diagram

Provide Subsystem Positioning, Spacecraft Alignment, and Body Rigidity

The structural subsystem must provide the initial component alignment and must, in the critical experiment areas, maintain that alignment throughout the mission life within the prescribed tolerances. The mechanism contained in the structural subsystem must fulfill the deployment, erection, or unfolding requirements of any of the subsystems and must position and maintain position of these items (solar panels, sun shields, antennas, etc.) within the system performance and spacecraft dynamic tolerance constraints.

Protect Subsystems from External Environments

The spacecraft structural skin must protect the internal components from the launch and orbital environments. The component requirements will determine the degree of protection necessary.

Support the Interconnecting Networks

The spacecraft structure must support and maintain the system interconnecting networks (electrical, pneumatic, etc.).

Maintain Proper Thermal Environment

The spacecraft structural subsystem must incorporate a passive thermal control system which will, through conduction and radiation, maintain the desired thermal paths and balance within the spacecraft system.

Provide Spacecraft/Booster Interface

The spacecraft structural subsystem must provide a mechanical interface with the booster, must provide a configuration compatible with the booster fairing envelope, and must be structurally compatible with the launch vehicle environments.

Tradeoff Studies

Although trade studies were conducted in the structural subsystem to examine such things as a preferred configuration (see Table 38), the more important studies involved the critical elements of the spacecraft/experiment concept. These critical items were the spacecraft balance problem associated with a spinning spacecraft, thermal control of the experiment package, and the requirement for structural rigidity as a result of the precision alignment problems associated with the spacecraft experiment package interface.

Conceptual Design

The first structural subsystem concept was, very simply, a cylindrical skeleton with skin and bulkheads as needed to provide rigidity and component mounting frames. After early concepts of the subsystems were described, a

TABLE 38. - COMPARISON OF VARIOUS CROSS-SECTIONAL CONFIGURATIONS TO THE HEXAGONAL BASELINE CONCEPT

Configuration	Advantages	Disadvantages
Triangular	Fewer fold-outs	Non-symmetrical Uneven power output from body-mounted cells Lower structural strength Lower balance flexibility Inefficient fairing volume usage
Square	Fewer fold-outs	Uneven power output from body-mounted cells Lower structural strength Lower balance flexibility Inefficient fairing volume usage
Pentagonal	Fewer fold-outs	Unsymmetrical Uneven power output from body-mounted cells Lower balance flexibility
Octagonal	Smoother power output from body-mounted cells	More fold-out panels needed
Multi-sided	Smoother power output from body-mounted cells Higher booster fairing volume usage	Fold-outs complicated Internal accessibility restricted
Circular	Total symmetry High booster fairing volume usage	Fold-outs difficult Internal accessibility restricted Curved internal mounting surfaces
Elongated hexagonal	Could possibly have sufficient area for body-mounted cells	Experimental package interference Excess volume, drag area, solar energy intercept area, etc. Thermal control interference Balance interference
Spherical	Constant projected area to sun Total symmetry	Fold-outs difficult Thermal control interference Balance restricted

hexagonal cylinder with enclosing bulkheads at each end and another in the center for component mounting was considered. It was envisioned that thermal control of the components would be through the sidewalls. Booster thrust loads would be carried from the end bulkhead to the center component-mounting bulkhead through supporting struts.

The requirements that the entire experiment package be radiatively cooled changed the concept to that roughly depicted in Figure 72. Superinsulation encloses the cooler, radiometer, sun sensors, and starmappers except for the megaphone baffles. The heavy, cast baseplate serves as a thermal radiator for the experiment package and as a thrust-carrying member. Sidewalls and longerons, which are thermally insulated from the baseplate, carry some of the thrust during boost and serve as a thermal radiator for internal thermal control of the units mounted on the bulkhead. The upper cover and fold-out solar panels are thermally insulated from the rest of the spacecraft. Considerably more detail of the spacecraft subsystem concept will be presented in a subsequent section covering spacecraft conceptual design.

Thermal Design

The thermal analyses were undertaken to help provide a rational basis for choosing among alternative spacecraft configurations and to lend assurance that the thermal design of the spacecraft was within the state of the art. In order to realize this objective, the assumptions that were required in the analyses were as realistic as possible, yet conservative.

Major problem study areas were:

- Solar cell temperatures
- Experiment package cooling
- Electronic package thermal control

Each area was studied in its quasi-steady-state conditions, i.e., operating conditions in and out of the earth's shadow. No extensive analyses covering the launch and initial erection period were required since the booster was determined to have the capability to orient the spacecraft properly and quickly. Furthermore, no damage should occur to the spacecraft under any random orientation with the sun while the proper orbital orientation is being achieved, even if several days are needed. An estimated seven days after orbit injection will elapse before the experiment package will begin to accumulate data.

The study approach undertaken was to show the feasibility of proper thermal design and not to conduct detailed analyses. For example, the feasibility of controlling each internal electronic package temperature within its allowable range is demonstrated. The actual temperature of each package can be kept within this range by using proper, detailed thermal design and known and proven techniques. The most critical problem, of course, was to examine the control on the experiment package baseplate while the spacecraft endures the extremes in environment it will see during the eclipsed orbit and over the

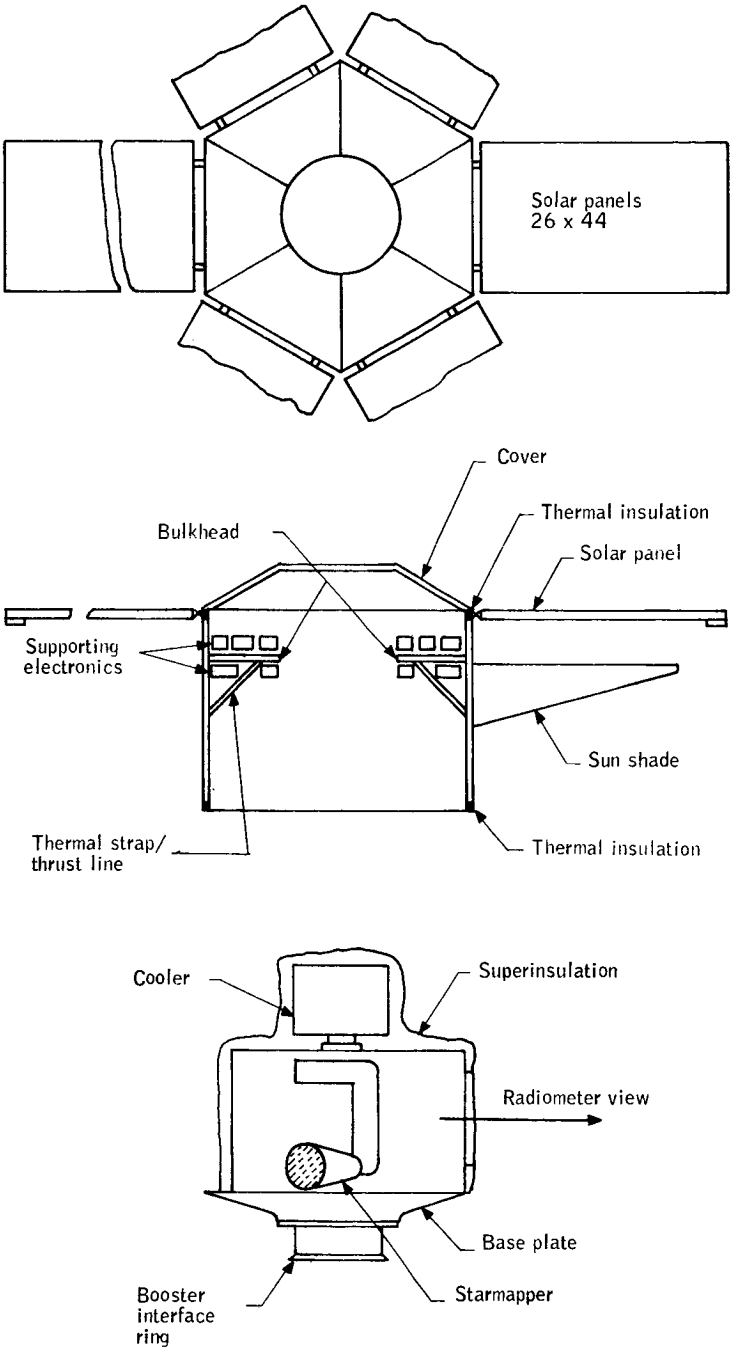

Figure 72. Conceptual Spacecraft Thermal Control Compartments and Structural Assemblies

lifetime of the spacecraft. The thermal environment of the spacecraft while in earth orbit was simulated. The environment consists of heat input from three sources outside the spacecraft: direct solar heating, indirect earth-reflected solar heating or albedo, and infrared radiation emitted by the earth. The amount of heat from each source is a function of spacecraft attitude and orbital position and is different for each surface of the spacecraft. A computer program was used to compute the incident heating simultaneously for each surface.

Figure 73 illustrates one computer run of heating incident to the rear face of the vehicle for different albedo conditions. In all cases, the total incident heating is greatest on the front (sunlit) face of the spacecraft, less on the sidewalls (spinning averages the direct solar heating), and least on the rear face and back of the solar panels. Shadowing of the sidewalls by extended solar panels reduces the incident heating shown in Figure 74 but also results in radiant interchange between the back of the panels and sidewalls.

These effects, along with the effect of the skin thermal inertia, internal equipment dissipation, different thermal control coatings, and conduction through the spacecraft external structure, were studied as a function of time.

The degree of control on the baseplate for the conceptual design configured is illustrated in Figure 75, and the results are well within requirements to demonstrate the feasibility of the experiment package.

The thermal study resulted in the following findings:

1. Low solar absorptance/infrared emittance coatings on all external surfaces (except the solar-cell surfaces).
2. Thermal isolation of the cover and solar panels from the rest of the spacecraft (except by radiation).
3. Thermal connections as needed from the electronic support equipment to the sidewalls only by way of mounting bulkhead, thermal straps, and radiation.
4. A local sun shield around the radiometer view port to eliminate solar energy incident to the experiment package.
5. Very careful thermal isolation of the experiment package - radiometer, starmappers, sun sensors, cryogenic cooler - from all parts of the spacecraft except the highly radiative baseplate.

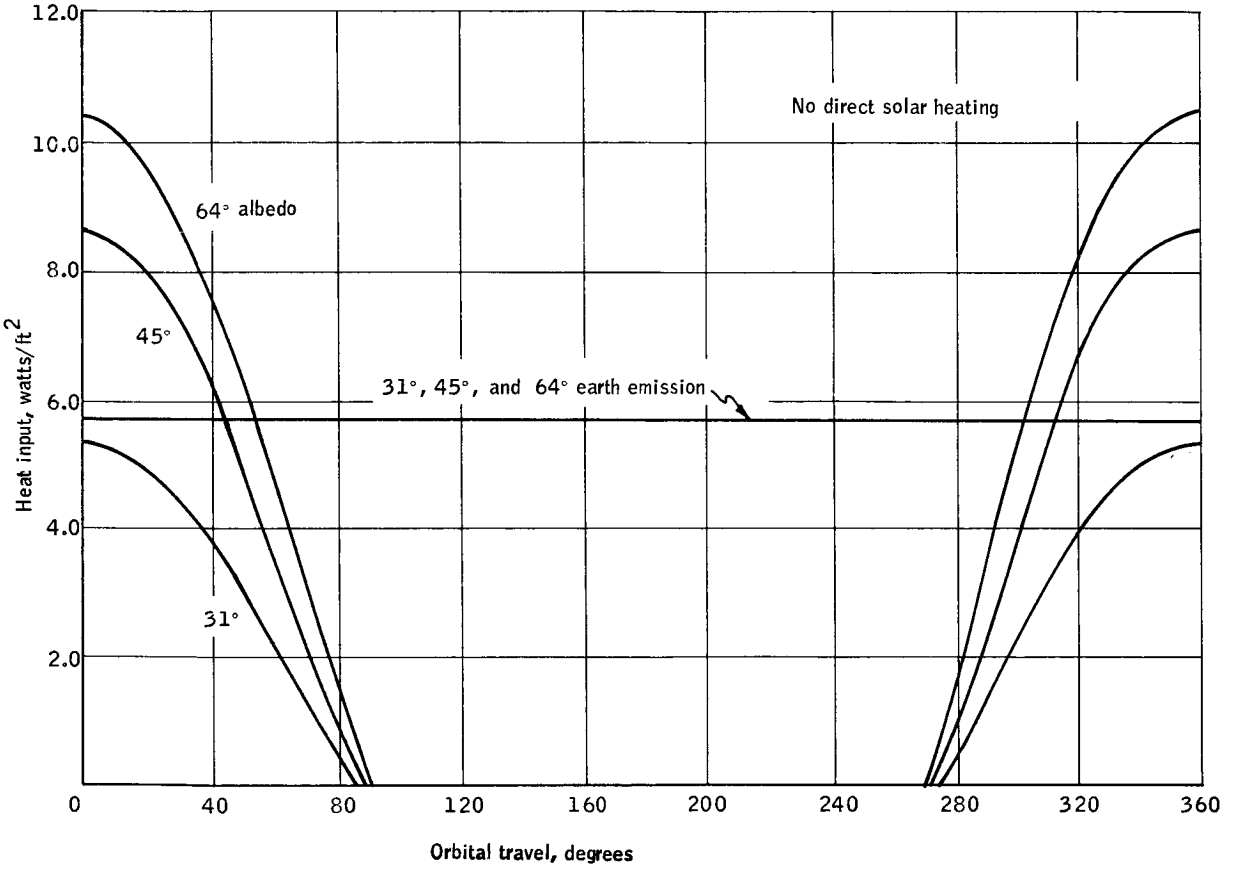

Figure 73. Space Heating Incident to Rear Face of HDS Spacecraft

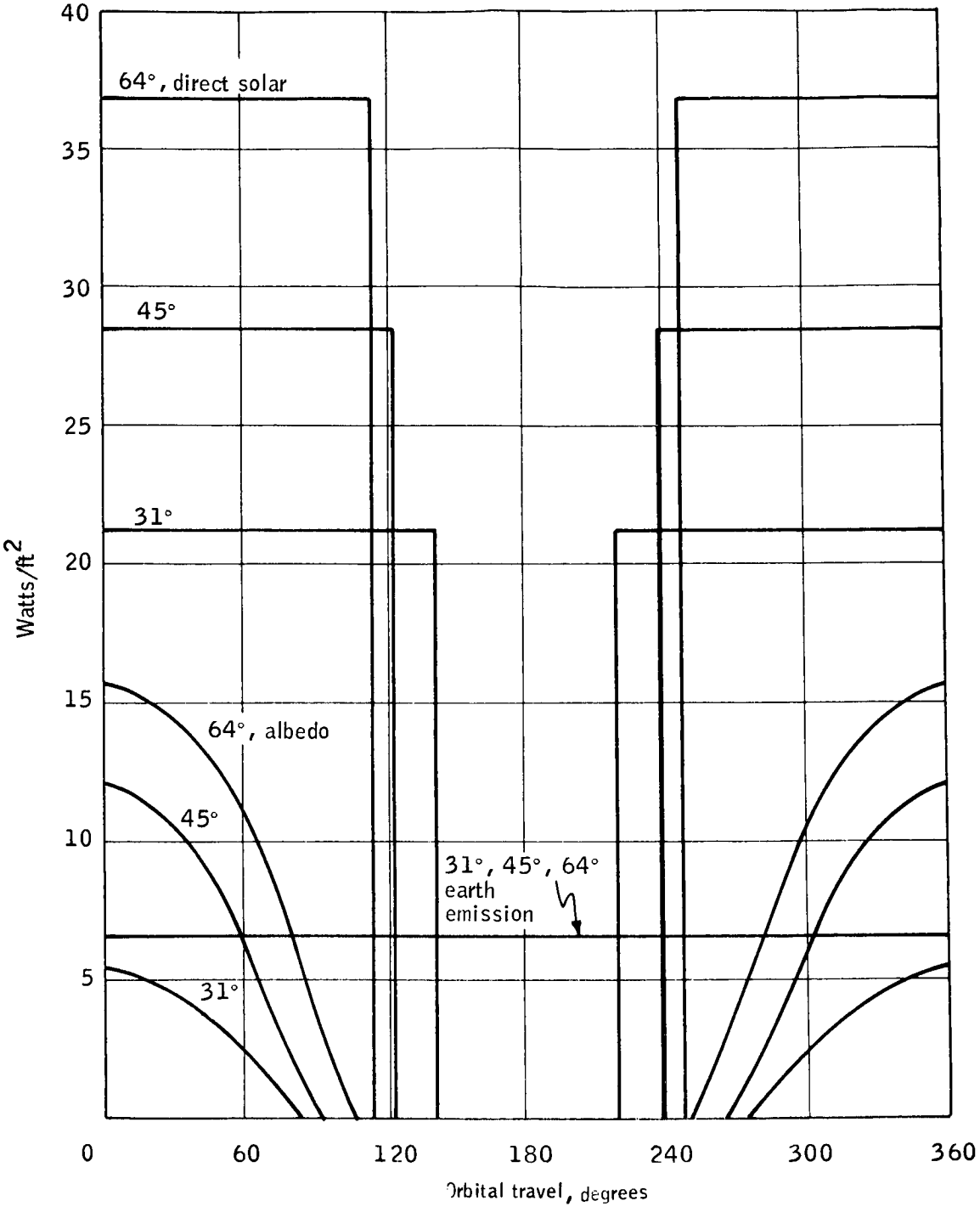

Figure 74. Space Heating Incident to Sidewalls, No Shadowing by Panels or Other Objects

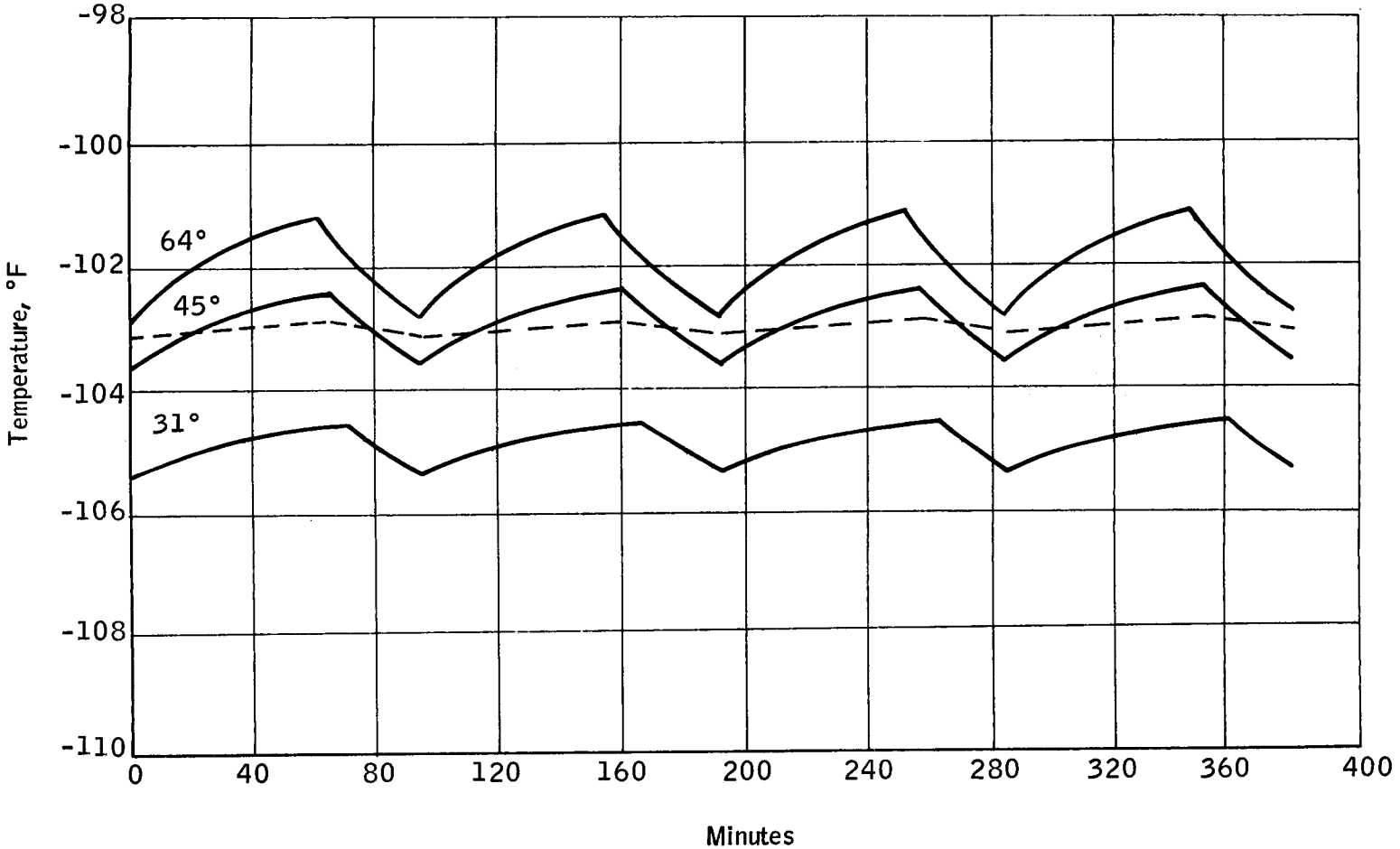

Figure 75. Orbital Temperature Variation of Baseplate

FINAL SPACECRAFT CONCEPT DESCRIPTION

The conceptual spacecraft, shown pictorially in Figure 76, was configured to meet the requirements of the six subsystems. Several important features of this final concept are:

- A dual temperature environment is maintained within the spacecraft; the experiment package is kept at approximately -100°F and the supporting equipment at about 75°F.
- The domed ends allow room for the long experiment package without upsetting the spacecraft balance.
- The solar panels and sun shade are folded along the body of the spacecraft in the launch configuration. Upon orbital orientation by the booster, the solar panels fold out to their final position. The spacecraft is then ready for spin-up.
- A very clean and simple external surface is available for complete use in spacecraft thermal control.

SPACECRAFT STRUCTURE

The final configuration of the structural subsystem is shown in Figure 77. This configuration demonstrates compatibility with both the system requirements and the selected launch vehicle. The heavy, cast aluminum baseplate carries thrust from the booster out to the periphery of the spacecraft where the load from the upper portion of the spacecraft will be supported. Even more important, it serves as the mounting platform and cooling radiator for the experiment package. The casting assures good thermal conduction (minimum thermal gradients) and a minimum of internal stresses. The flat, external surfaces offer no cavities for higher heat absorption and can be covered with special coatings if needed. Mating surfaces, such as the booster interface bolt circle, the internal mounting platform, the periphery, and the spacecraft sidewall mounting surfaces will be machined surfaces. The baseplate and experiment package are thermally isolated from the rest of the spacecraft.

The superinsulation will enclose all parts of the experiment package except the megaphone baffles on the starmappers. It will require special attachment and support design to minimize heat transfer and will tie directly into the plastic supports between the baseplate and sidewall.

The plastic supports between the baseplate and the sidewall serve to reduce the heat transfer from the sidewall into the baseplate. They must also carry the thrust load, but these plastics are typically in the 20 000 psi compressive-yield strength class, so several square inches of plastic would yield a very high safety factor and reduce the heat conduction to an acceptable level. The plastic insulating ring at the top of the sidewall is of similar design; however, the thrust level is greatly reduced.

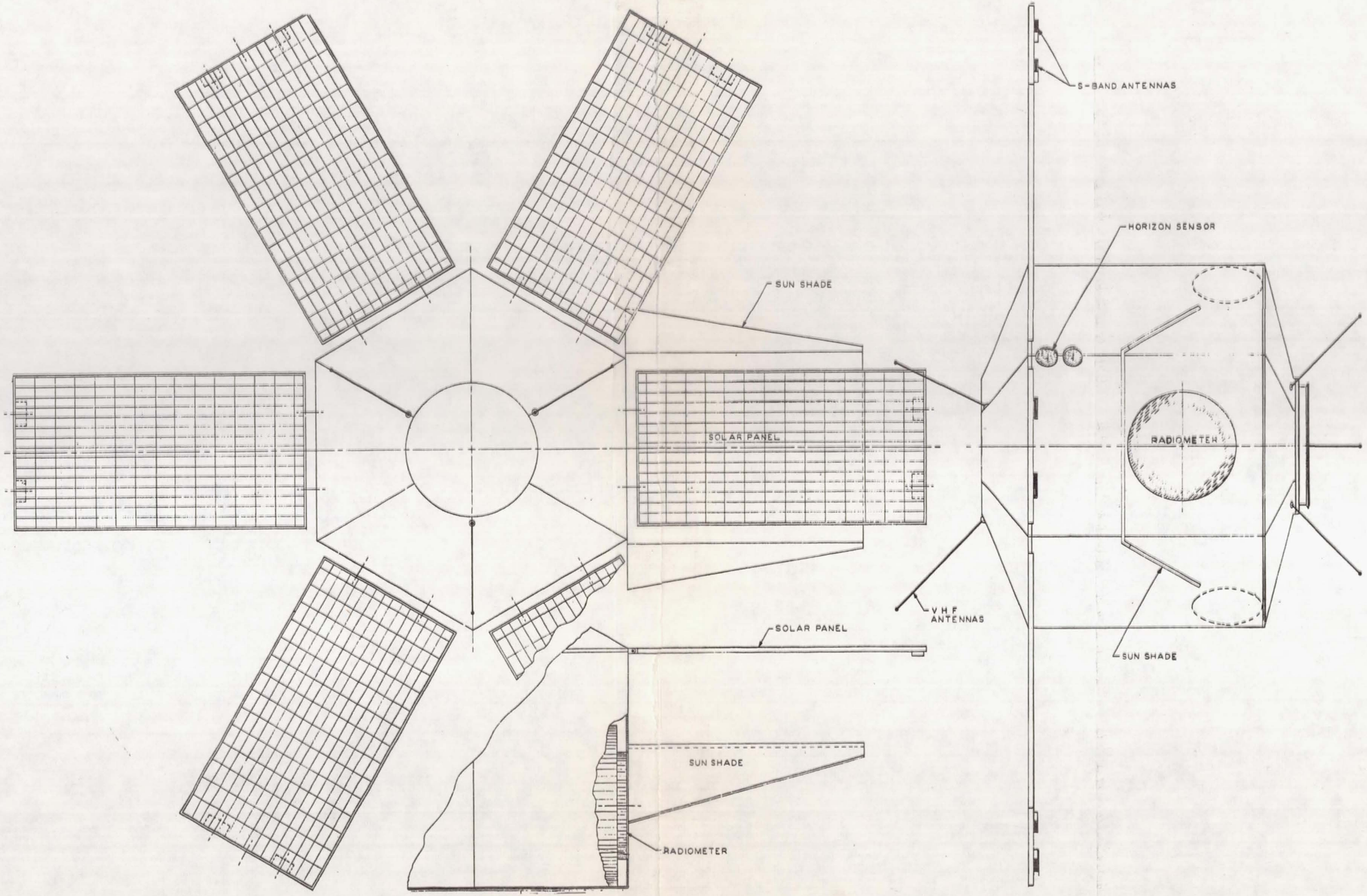

Figure 76. Conceptual Spacecraft - External Layout

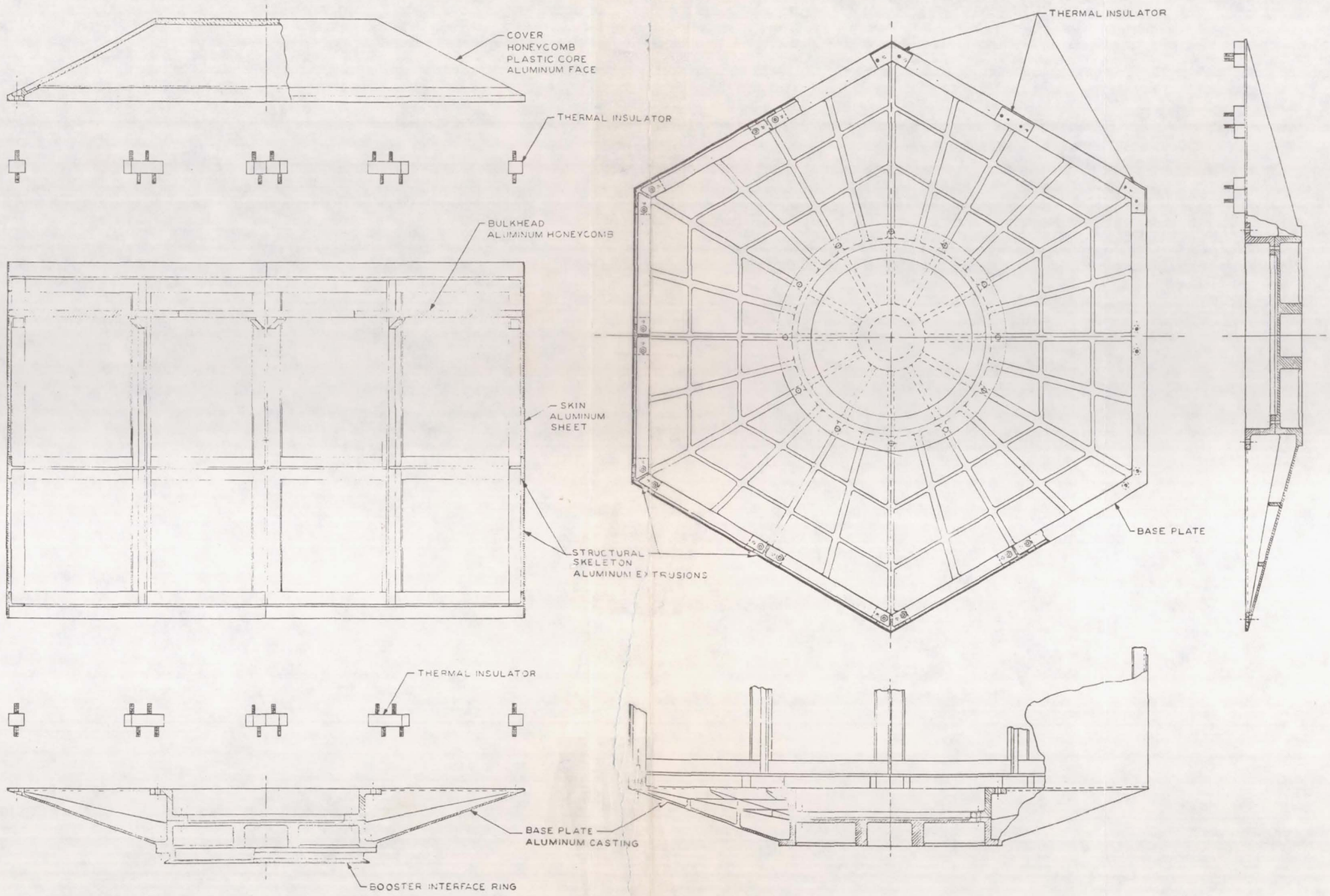

Figure 77. Spacecraft Structural Subsystem

The white, painted aluminum sidewalls and the structural skeleton are fully described in Figure 77. Screw attachments between the wall panels and skeleton stringers will allow removal of each panel as needed for access to internal components.

The spacecraft cover serves to enclose the structure and reflect solar energy. The cover will be fabricated of a plastic honeycomb core between two highly reflective sandwich faces; high strength and good insulating properties should result.

The solar-panel substrates will be an aluminum-honeycomb material with very high strength-to-weight properties, high resonant frequencies, and satisfactory thermal conduction, an approach proven a number of times in space applications. The substrates will be thermally insulated from the body of the spacecraft.

The radiometer view port sun shade, which folds around the hexagonal corners of the spacecraft, will be constructed of a highly insulated sandwich material with a very radiative surface on the shaded side. The shape, shown in Figure 78, is such that the sun can never shine on any part of the radiometer port.

A restraining scheme, deploying mechanism, and hinges will be required for the solar panels and sun shade. These areas were only studied in a cursory manner since they are well within the state of the art and will not have an effect on the feasibility of the concept. Their reliability would be commensurate with the level of design effort expended.

The internal component mounting bulkhead, made of aluminum-honeycomb material, also serves as a heat conductor. Combined with the thermal control/thrust lines that were designed into the thermal control scheme, a heat path to the sidewalls is provided. Heat then may be dissipated into space by radiation.

SYSTEM FEATURES

The total orbital system selected by tradeoff studies and examined by feasibility, illustrated in functional form as presented earlier, is shown in Figure 79. The salient features of this system are summarized below.

Structural

The structural concept is a spin-stabilized hexagonal cylinder configured for launch on a two-stage Improved Delta. This configuration, 49 in. deep and 54 in. across the corners of the hexagon, has a launch weight of 723 lb. It maintains the required balance ratios for the proposed spin-stablized concept. Separate thermal environments are provided, i. e., a -100°F (200°K) compartment for the experiment package and a near-room temperature section for the supporting subsystem components.

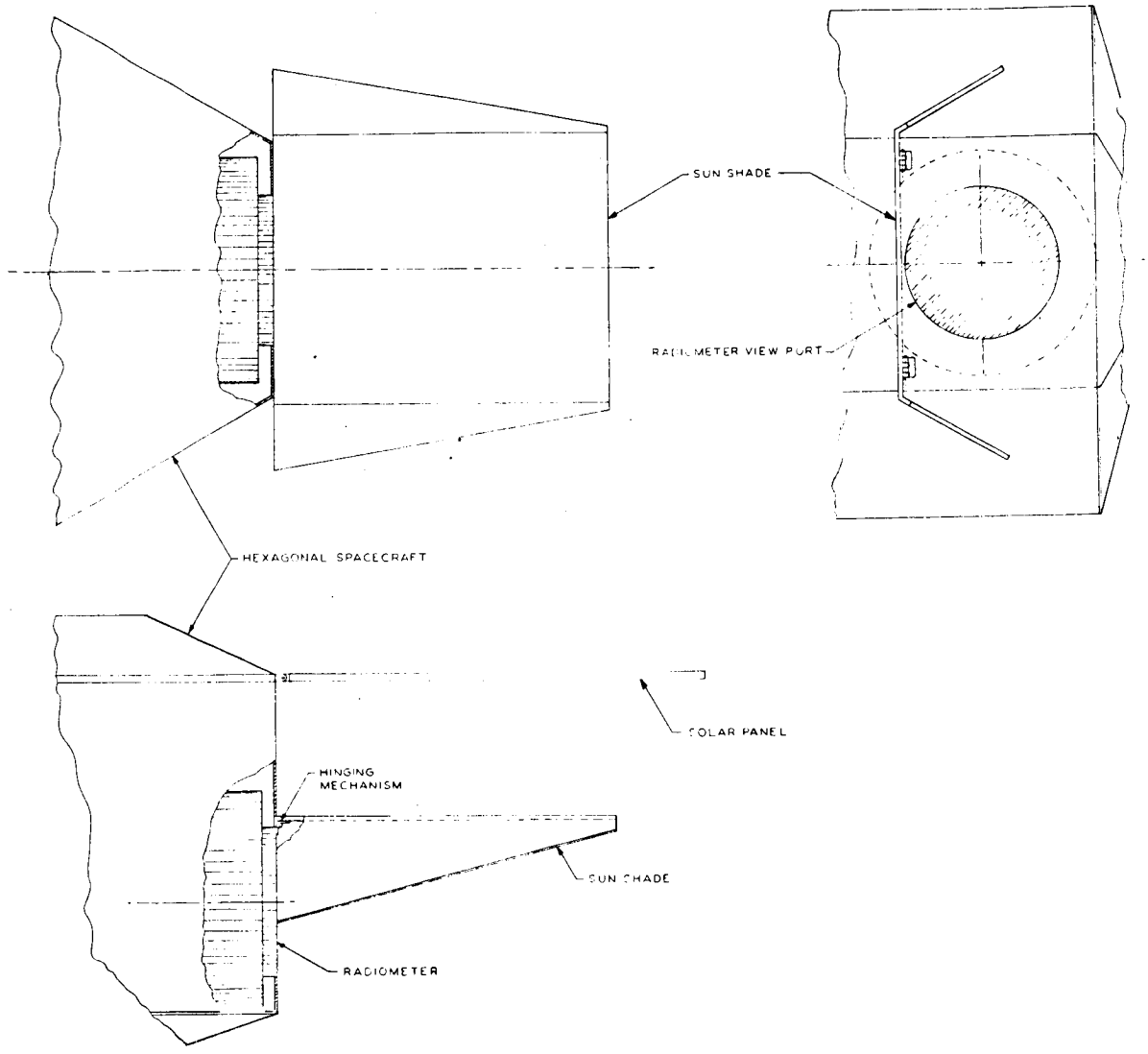

Figure 78. Radiometer View Port Sun Shade

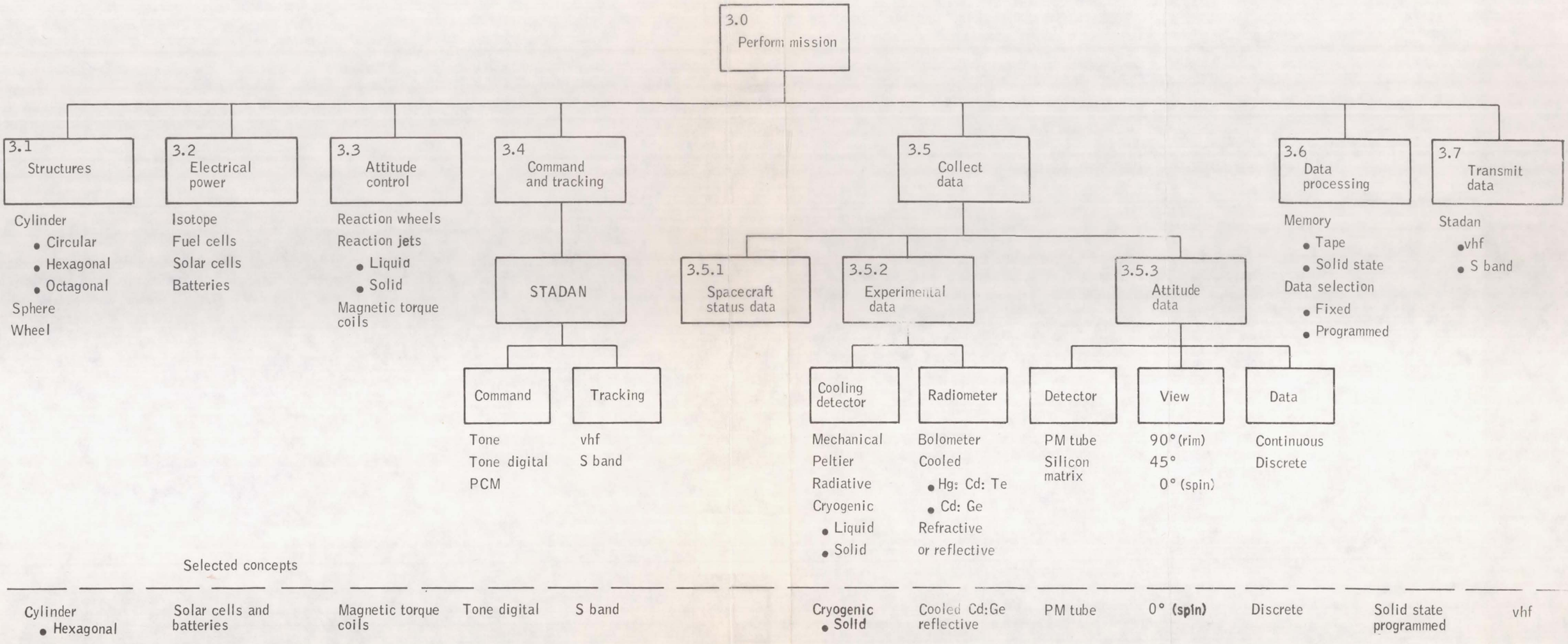

Figure 79. Orbital Operations Concept

Radiometer

The radiometer utilizes a photon detector of cadmium-doped germanium. The operating temperature of the detector will be produced using a solid cryogenic cooling system containing a prime refrigerant of neon and a buffer refrigerant of methane. Reflective optics utilizing a classical Newtonian configuration will be employed. Optical modulation of the radiant energy will be performed utilizing a mirror driven by a torsional pendulum. Redundancy of detectors, electronics, calibration, and modulation elements will be provided.

Attitude Control

Magnetic torquing will be utilized for spin and attitude corrections, compensation for the residual magnetic moment of the spacecraft, and precessions of the spin axis at the sun-synchronous orbit plane rate. Torquing periods will be intermittent for the spin and attitude corrections and continuous for the compensation functions. Damping of coning motions will be provided and activated upon ground command. Computation of torquing levels and sequences will be ground computed and implemented on the spacecraft through stored programs.

A V-head horizon sensor will be utilized as a roll-yaw sensor to produce the necessary information for ground computation of commands.

Attitude Determination

The on-board attitude determination instruments consist of a starmapper and a sun sensor. The starmapper will view in the orbit plane, restricting its use to the shadow periods. Star signals will be obtained using a photomultiplier detector under a "triple-x" slot-reticle configuration. The sun sensor will be a V-slit configuration measuring the solar disk using an integrating sphere detector. An intermittent data process will be implemented which utilizes a number of sets of data, but not all sets. A smooth curve is produced which yields the required attitude information for individual radiance profiles.

Data Handling

The data handling subsystem is a completely solid-state system and is well within the state of the art. All data on the spacecraft is digitized, stored in a 500 000 bit solid-state memory, and transmitted to telemetry stations approximately once per orbit. The concept provides the capability of meeting the recommended data requirements of 378 508 horizon profiles in one year and has the flexibility to take additional data in "interesting" locations.

Communications and Tracking

The communications subsystem requires telemetry transmission in the 136 MHz vhf band to achieve maximum station contact and S-band transponder operation for spacecraft tracking to achieve the required tracking accuracy. Including the capability of connecting these units into redundant and/or back-up

modes of operation provides a highly reliable communications subsystem. The subsystem is feasible, within the state of the art, and requires no alterations to the NASA STADAN.

Power

Silicon solar cells mounted on fixed (fold-out) panels and conventional two-terminal nickel-cadmium batteries will provide continuous power. Regulation will be with a nondissipative voltage regulator. Two voltage levels will be provided.

RELIABILITY

To examine the feasibility of this spacecraft/mission concept meeting the requirement to collect data continuously over a one-year period, a reliability analysis was conducted in two steps:

1. The failure rate of the spacecraft and its subsystems was calculated;
2. This failure rate was utilized in establishing an optimum multiple-launch configuration.

Considerations utilized in the selection of failure rates and a discussion of the predicted failure rates of each subsystem are included below.

Reliability Failure Rate Sources

Table 39 presents the failure rates used in determining the reliability assessment of equipment based on an estimated component parts list. These failure rates are based on high-reliability procurement employing 100-percent screening for known weaknesses, approved derating policies, and improved fabrication techniques. For parts that probably would not be procured and handled in this way, MIL Handbook 217A failure rates were used.

In specific areas where field operating experience data was available, such data has been used where a significant similarity between equipment exists and where the equipment complexity is considered to be approximately equivalent. In the case of integrated circuits, it is reasonable that a somewhat lower failure rate could be used for digital circuit applications than for analog applications since a failure due to parameter drift in an analog circuit may not be a failure in a digital circuit (also the duty cycle is somewhat less in a digital application).

TABLE 39. - FAILURE RATES FOR HIGH RELIABILITY PROCUREMENT

Item	Failure rate (a)
Solder joint	$.0001 \times 10^{-6}$
Integrated circuit	.10
Transistor (silicon planar)	.02
Diode (spring type)	.04
Diode (solid-glass type)	.01
Resistor (carbon)	.001
Resistor (metal film)	.001
Capacitor (mica)	.002
Capacitor (ceramic)	.002
Capacitor (tantalum)	.02

[a]Failure rates correspond to:
65°C (50°C max. ambient and 15°C temperature for part)
50-percent rated stress (conservative stress estimate for high reliability design)

Although historically reliability improvements continue to appear in successive generations of equipment, no attempt has been made to adjust the observed experience data or the predicted failure rates to allow for any predicted improvements in reliability. However, it is reasonable to expect that some reliability improvements may appear during succeeding phases of the HDS program. Certainly, during the design phases, the reliability effort will include consideration of worst-case analysis, significant piece-part derating, and an extensive part-application review program. A parts-reliability improvement program will consider burn-in of piece parts and reliability testing as required to insure high equipment reliability.

Reliability Prediction

A reliability analysis has been made of the individual subsystems of the system and then combined. A summary of the estimated individual subsystem reliabilities, including their internal redundancies, is presented in Table 40. The estimated reliability of the total system for one year of operation is shown to be 0.71.

TABLE 40. - RELIABILITY PREDICTION, ONE-YEAR MISSION

Subsystem	Reliability
Experiment package	.948
Communications	.977
Data handling	.909
Attitude control	.994
Electrical power	.944
Launch, boost, and injection	.900
System total	.71

Redundancy and Critical Failure Modes

Only a minimum effort was spent in attempting to obtain a precise reliability prediction. Instead, emphasis was towards insuring that the major subsystem failure modes were considered, that alternate modes of operation were provided for in case of a subsystem failure, and that the design concepts were chosen that conceptually have a high probability of resulting in reliable designs. The key redundancy features incorporated as a result of these analyses are given below.

Experiment package. -- Critical failure modes were minimized in the radiometer by using redundant choppers, calibration sources, IR detectors, detector power supplies, and electronics. Completely redundant starmappers and sun sensors were included as a practical redundancy approach in these areas. The remaining elements of these subsystems are not critical reliability elements.

Communications. -- In the event of a failure of one of the major items in the communications subsystem, there are several alternate modes of operation. As long as the S-band range and range-rate system is operating and either the TM transmitter or the 136 MHz beacon is operating, the communications subsystem could still perform its functions. To increase the subsystem probability of success, a redundant S-band range and range-rate system has been added.

Data handling. -- An analysis of the data handling subsystem resulted in recommending redundancy in the command verifier and decoder, the timing oscillator and register, the programmer, the radiometer data collection unit, the attitude determination data collection unit, and in critical circuit areas of the memory.

Attitude control. -- The attitude control subsystem includes redundant V-head sensors and redundant control logic.

Power supply. -- The power supply subsystem includes two battery sets, two charge regulators, and internal redundancy within the regulators. The concept of standby redundancy has been used for the battery and charger combination.

Multiple Flight Techniques

An analysis was conducted to determine the potential improvements in achieving the HDS mission goals that might be obtained by using more than one spacecraft. This was accomplished by assuming conservative values for "random" failures and "wearout" failures for the spacecraft and then calculating the probability of survival of the system for a number of flight techniques.

It was assumed that the "random" system failures could be approximated by a Poisson distribution such that an individual spacecraft has a probability of operating for a year equal to 0.55. (This number is much smaller than the number presented in Table 40, to be conservative.) However, since "wearout" effects do not obey the Poisson distribution, they must be handled in a different manner. The dominant wearout effect will be the depletion of the cryogen in the radiometer detector's cooler. This effect was approximated by assuming that the usage rate had a standard deviation about a mean rate and the quantity of cryogen was sized for 14-months life at the mean usage rate.

Examination of Figures 80 and 81 shows that if a second spacecraft is launched at the end of the first or second month the probability that the first one is still operating (and hence causing no interruption of data) will be greater than 90 percent. Moreover, after both are launched, the probability that a spacecraft will function for the specified mission period does not fall below 90 percent for several months. Following the second launch then, a good strategy might be to withhold launching a third satellite until one of the two orbiting satellites has failed. Then, if launch preparations are immediately begun and the third satellite is launched within one month, there is at most a five-percent probability that an interruption will occur (since there is a 95-percent probability that the surviving satellite will continue to function for a month).

This strategy can be utilized in many ways to:

- Minimize program cost.
- Achieve added program benefits.

For instance, if both satellites continue to perform well and the data appears to be satisfactory as the 12-month point is approached, a decision could be made not to launch any additional satellites. In this way the cost of the booster and the cost of storing and processing the additional data can be eliminated.

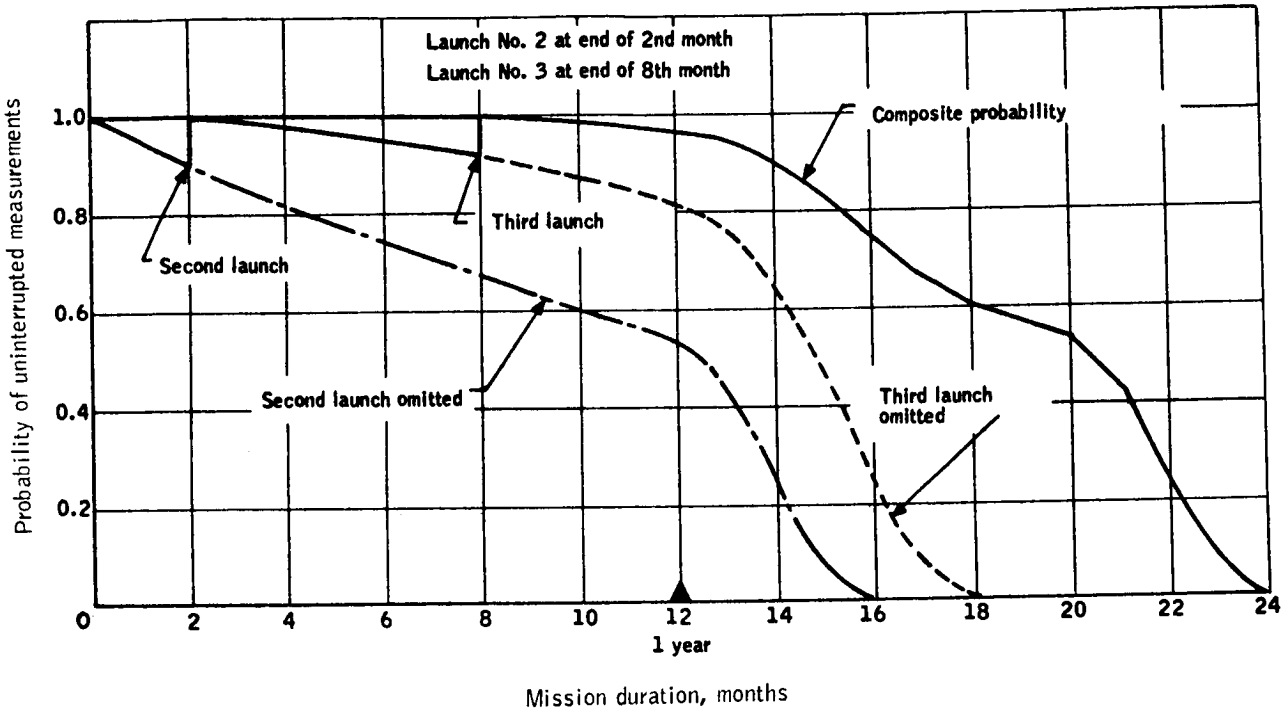

Figure 80. Multiple Launches, 2 - 8

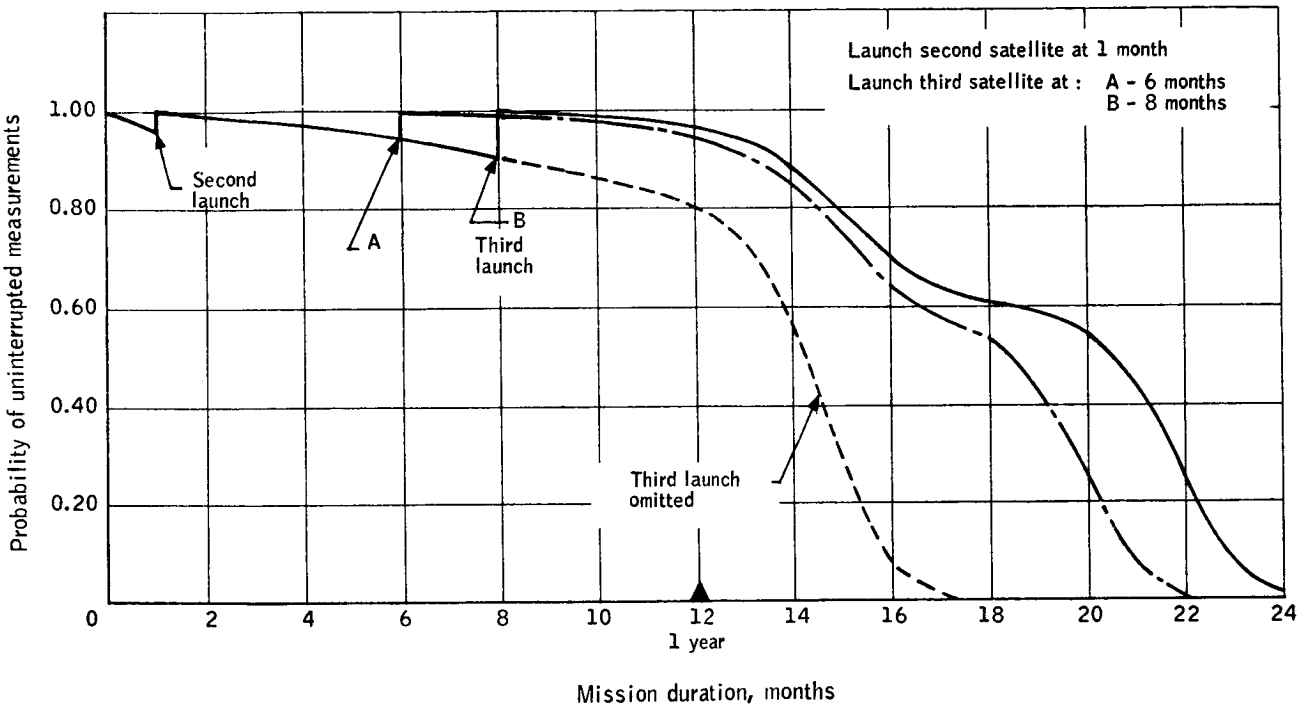

Figure 81. Multiple Launches, 1 - 6, 1 - 8

The option exists to launch a third satellite to obtain data for a period longer than a year. Among the useful results of such a lengthened data-taking period would be acquisition of data useful for determining year-to-year effects. Figures 80 and 81 show that the data-taking period could be extended to 20 or more months while preserving great flexibility in the launch dates of each satellite. If it was decided to maximize the data-collection time, a full two-year program could be accomplished by suitable adjustment of launch times.

Alternatively, one or more of the satellites could be launched in an orbit (s) other than the preferred 3:00 p.m. - 3:00 a.m. orbit. In this way added points could be obtained for extracting diurnal information. For instance (as shown in Figure 82), if the flight plan of Curve A, Figure 81 was used with each orbit at a separate hour, there would be over 50-per(.t probability that a 4-point fit to a diurnal model could be made for 12 months. However, the probability that a 6-point fit could be made is only greater than 50 percent for one month.

If the wearout time of the cooler is considerably greater than estimated at this time, then the above periods could be extended further. Greater probability of time overlap could, of course, be obtained by launching the third satellite earlier with a corresponding reduction in the probability of obtaining data beyond the first year.

Based on the present estimate of the probability of operation of a single satellite, it is recommended that a second satellite be launched within one to three months after the successful orbiting of the first satellite in a sun-synchronous orbit one to two hours later than the initial satellite. If a failure of one of the first two satellites occurs within the first four to five months, a third satellite should be launched into the same orbit as the failed satellite. This approach maximizes the probability of obtaining a continuous one-year set of data, provides a 4-point diurnal data fit, and provides a high probability of collecting a significant amount of data in the second year.

OPERATIONAL PLAN

To insure that the mission/spacecraft concept was feasible, it was necessary to examine all operations involved in the experiment and assess their impact on feasibility. A plan was created which included prelaunch, launch, and orbital operations. Examination of the total, required operations resulted in the identification of the critical areas which include

- Cryogenic ground handling
- Initial real-time data requirements
- Attitude and spin-correction cycles
- Potential STADAN priority conflicts
- Radiometer data programming
- Star occultations

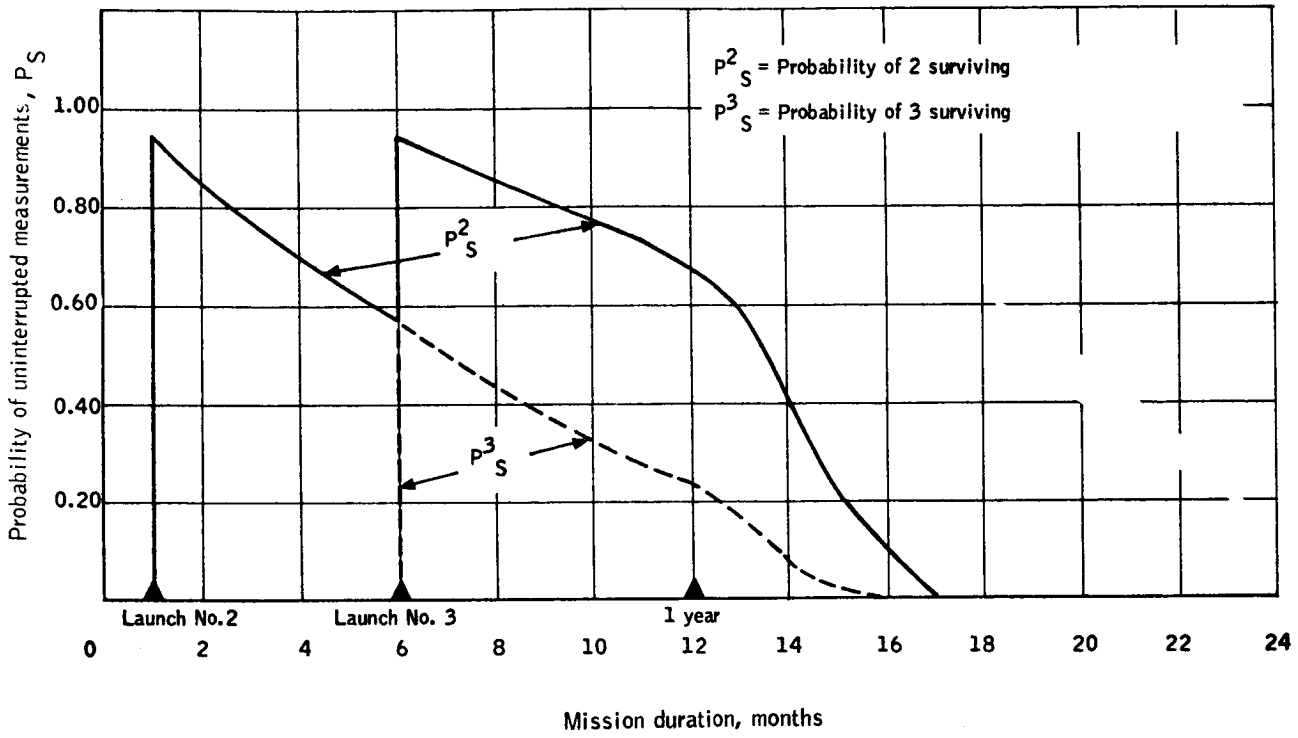

Figure 82. Probability of More Than One Satellite Being in Operation, Sequence of Figure 81

The ground handling of the cryogenic cooling system is not a major problem area except to establish the requirement for assuring, at time of launch, the system is provided with its full supply of solid cryogen. This results in the necessity for "top-off" and/or supercooling capability to cover all contingencies, e.g., launch delays.

The inital real-time data requirements appear during the first two weeks following launch. Spacecraft data is utilized by ground computation facilities to calculate the spacecraft's residual magnetic moment from the attitude control subsystem sensors and the initial solution of the spacecraft attitude from the attitude determination subsystem data. To implement this requirement, the spacecraft data must be transmitted only to STADAN facilities possessing direct communication links with the program control center located at Goddard. The Alaska and Rosman stations can accomodate this requirement for any sun-synchronous orbit.

The attitude and spin-correction cycles are implemented by ground command. To minimize spacecraft complexity, a single ground station has been designated as the command station. The Alaska station has been selected as it produces the greatest coverage in the sun-synchronous orbit. Commands are designated by the program control center, transmitted to the Alaska station, and implemented by the spacecraft. Simultaneous torquing for both spin and attitude is possible and desirable to minimize the loss of data. Radiometer data is not valid during the torquing periods due to attitude error growth; however, immediately following these torquing cycles the data is again considered valid through interpolation. The current estimate for the interval between these torquing periods is five days, resulting in a potential data loss of approximately 0.6 percent.

The conceptual spacecraft has data storage for one orbit. STADAN provides maximum coverage with a set of four stations; however, data will be lost for approximately three hours between contacts which occur statistically every third day. This represents a data loss of approximately 2.0 percent. However, to prevent greater losses due to priority problems or failures to one of these four stations, alternate contacts must be established. A set of secondary stations has been established which, together with the primary stations, should allow scheduling of the telemetry data without an increase in the predictable losses due to basic station locations.

Radiometer data programming to accommodate the instrument's directional sensitivities must be fully developed. The switching details are directly a function of the orbit. For the current sun-synchronous orbit with no nodal crossing at 3:00 a.m. and 3:00 p.m., switching at ±45 degrees about the minimum sun angle for each orbit has been suggested. Other switching requirements include latitude rejection ratio changes, profile occultation due to moon ratio changes, and shifts to accomodate the STADAN coverage data loss previously discussed.

The star occultation problem results when the moon is in view during nightside operation of the starmapper. The current angle estimate of 35 degrees relative to the starmapper line of sight results in approximately six days of

conflict during the 29+ days in the lunar cycle when switching must occur. Solution possibilities include turning the instrument off for six days or switching at the sensitivity point, 35°. The first solution represents a severe penalty in lost data and is not recommended. The latter results in star data losses and, therefore, potential attitude-error growth.

An operational plan has been formulated which accomodates all of the above either directly or by the establishment of typical functions, e.g., radiometer switching which establishes the necessary feasibility of similar functions.

The full operational cycle is summarized by an identification of the phases, followed by a task/time sequence to establish a repetitive cycle.

The operational phases are:

- Prelaunch
- Boost, injection, orientation, and spin-up
- Attitude trim and magnetic moment compensation
- Initial attitude determination and thermal stabilization
- Profile collection
- Attitude and spin correction
- Data reduction, analysis, and applications

The prelaunch phase is defined as beginning with hardware delivery to the launch site and ending with lift-off. The launch vehicle operational functions of boost and injection, followed by an orientation producing the desired spacecraft attitude and spin-up, make up the second phase. The first 24 hours of orbital operation constitutes the third phase wherein the spacecraft attitude readouts are utilized to perform ground computation to determine the necessary commands to trim spacecraft attitude and magnetic moment compensation current level. The second orbital phase is devoted to the initial attitude solution from attitude determination data collected at greater than operational rates to maximize convergence to the attitude solution. Simultaneous with this operation, thermal gradients are diminished throughout the spacecraft to allow operational accuracies to be achieved between radiometer calibration cycles. This phase has been allocated from the second through seventh day.

The profile collection phase is the prime operational phase wherein radiometer data is collected every orbit. The duration will be established by the necessity for either spin or attitude corrections.

The attitude- and spin-correction phase is performed as required by status measurements. The Alaska STADAN station originates all commands which are provided from the command center located at Goddard.

The final phase involves the ground operation of data reduction, analysis, and applications required to produce the body of horizon profiles.

RESULTS AND CONCLUSIONS

The scope of this study has yielded a significant number of findings which have impact on the state of the art in horizon definition. The objective, at the outset of this study, was to examine rigorously the present knowledge and theories of the earth' s radiance characteristics and to delineate an effective measurement program which would produce data suitable for use in the design and application of instruments which employ the earth' s infrared horizon. Upon conclusion, these objectives have been met successfully; the results have, in addition, led to many conclusions which are important in themselves.

PART I - MEASUREMENT REQUIREMENTS

Specifically, the first part of the study resulted in the following:

- A comprehensive state-of-the-art compilation of present knowledge and theories on the earth' s infrared 15μ horizon and computational techniques associated therewith.
- A computer programmed bibliography of over 400 pertinent publications in fields related to horizon definition.
- Definition of 88 locator techniques and input constants defining present and future horizon sensor operating principles.
- A complete definition of temporal, spatial, and statistical sampling requirements for defining a global infrared horizon for scientific applications.
- Definition of a flight technique which is capable of meeting the data sampling requirement with a reasonable mission success value.

The major conclusions which can be drawn for this data are:

Profile Analysis

- The infrared horizon (615 to 715 cm^{-1}) is an extremely stable source offering potential of 0. 01-degree accuracy in the vertical.
- Deterministic errors exist in the CO_2 horizon. Variations with season are most significant, and latitudinal variations are second.
- The infrared CO_2 horizon is not significantly affected by weather (clouds). Additionally, concentrations of CO_2, ozone, and water vapor do not significantly add to horizon profile variability for the 615 to 715 cm^{-1} spectral region.

Locators

- Use of locator L4, Integral of Normalized Radiance, offers the greatest potential for local vertical determination.
- Stability of any locator technique is enhanced if input constants corresponding to regions above the troposphere are used.
- Locators based on derivatives of the radiance profiles are much less stable than locators which use either radiance or integrated radiance.

Data Requirements

- To define the earth's infrared horizon (615 to 715 cm^{-1}) over the range of -30 to +80 km:
  a. 378 508 samples are required;
  b. Samples must be collected over a one-year period (13 28-day time cells);
  c. Global coverage is required (588 space cells);
  d. Sampling rate is limited to two samples per day per space cell; and
  e. Diurnal content is important.

Flight Techniques Evaluation

- A rolling-wheel spacecraft (passive optical systems) in a polar orbit is the most cost effective.
- Three vehicles launched at scheduled intervals will result in a high probability of success over a one-year data collection mission.
- Suborbital probes cannot collect the required data.
- A heavy, long-life vehicle is not cost effective.
- AAP is not cost effective and cannot collect the required data.

Many additional results and conclusions have been reached as a result of this Horizon Definition Study, the most important of which are:

- The compilation of the most comprehensive set of infrared horizon radiance profiles ever prepared.
- Development of a COmprehensive Radiance Profile Synthesizer (CORPS) computer program which provides a versatile state-of-the-art scientific tool for analysis of horizon radiance profile phenomena.

- Development of a theoretical approach for potentially inferring atmospheric temperature structure from radiance profiles.
- Establishing a potential capability for synthesizing horizon radiance profiles for any location to an accuracy of several percent without the aid of meteorological input data.
- A significant improvement in existing atmospheric transmissivity data.
- Significant developments in statistical analysis which will prove to be a useful tool in data processing techniques for a later experimental horizon measurement program.
- Further theoretical verification that cloud effects on horizon radiance profiles are minimal near the earth's limb in this spectral region.
- Development of radiance weighting functions for incremental spectral intervals which represent a valuable scientific tool for infrared horizon analyses of many types.

The results of this study lead to the conclusion that an experimental horizon definition measurement program should be conducted using an orbiting vehicle of one-year duration. The basic configuration recommended, based on the selected analysis of this study program, is the "rolling wheel" type operating in a near-polar orbit and using multiple-vehicle-launch redundancy.

PART II - CONCEPTUAL DESIGN AND FEASIBILITY ANALYSIS OF A MEASUREMENT PROGRAM

The objective of this part of the study was to configure a mission/spacecraft concept to meet the experiment requirements and to evaluate the mechanized concept to determine its feasibility.

The primary conclusion reached in the Part II study was that the experiment is feasible and within the current state of the art. Certain critical elements of the experiment should be studied further to verify these conclusions where verification is beyond the intent of a conceptual study. These areas include:

- Primary calibration
- In-orbit tracking
- Attitude determination

The basic requirements as derived in this study are listed on the next page.

Radiance Profile Measurements

- Spectral interval: 615 to 715 cm^{-1} (14.0 to 16.28 μ)
- Profile accuracy
  - ► Tangent height range: +80 km to -30 km
  - ► Instantaneous value of radiance measured must be assignable to a tangent-height value to within ±0.25 km.
  - ► Radiance characteristics and resolution:

    Maximum peak radiance = 7.0 W/m^2 - sr.

    Minimum peak radiance = 3.0 W/m^2 - sr.

    Maximum slope = 0.6 W/m^2 - sr - km.

    Minimum slope = 0.02 W/m^2 - sr - km.

    Maximum slope change = 0.15 W/m^2 - sr - km^2.

    Radiance magnitude resolution = 0.01 W/m^2 - sr.
  - ► Horizontal resolution: 25 km.

Mission Profile

Nominal, circular, polar orbit of approximately 500-km altitude.

Tracking and Data Acquisition

Limited to the existing Satellite Tracking and Data Acquisition Network (STADAN) with minimum modification.

Experiment Package

- Passive radiometric and attitude measurements with redundancy (more than one unit) in the experiment package for the radiometer and attitude determination device.
- Minimum scan rate > 0.5 scan/min average.
- Maximum scan angle with respect to orbit plane ≤ 5°.

Spacecraft

- Rolling-wheel configuration (spin axis normal to the orbit plane).
- Weight in less than 800-pound class mandatory.

The experiment concept configured to meet these requirements included:

- Orbit
  a. Sun synchronous (3 p.m. - 28 October)
  b. 500-km altitude
  c. Inclination: 97.38°
- Spacecraft
  a. Three vehicles
  b. 700 pounds
  c. Hexagonal shape - spin stabilized
  d. Passively scanning optics
- Launch concept - scheduled at intervals defined by spacecraft predicted failure rate.
- Launch site - Western Test Range
- Booster - Thor-Delta

The final, conceptual configuration of the spacecraft (Figure 83) recommended in this study is a spin-stabilized, hexagonal-cylinder configuration, 49 inches deep and 54 inches across the corner of the hexagon. The spacecraft has an estimated launch weight of 723 pounds which allows an approximate 10-percent margin for growth within the capability of the Improved Delta (two-stage direct injection) vehicle. The concept is compatible with subsystem requirements and constraints and maintains the required balance ratios for the proposed spin-stabilized concept. Separate thermal environments are provided: a -100°F (200°K) compartment for the experiment package and an approximately 75°F (279°K) section for the supporting subsystem components. This recommended concept demonstrates that a very simple, highly reliable, state-of-the-art spacecraft can fulfill the mission performance requirements as defined in this study.

The experiment package (Figure 84) consists of a radiometer, redundant starmappers, redundant sun sensors, a cryogenic cooler, and associated electronics. The radiometer is a passive measuring instrument that incorporates a single optical system using a primary parabolic mirror with redundant choppers, detectors, in-flight calibration sources, electronic signal processing circuits, and a cryogenic cooler. The attitude determination function is accomplished by the use of a starmapper system while the spacecraft is on the dark side of the orbit and by the use of a sun-sensor system, which continuously updates the attitude information and preserves its accuracy, while on the sunlit side. The associated electronics includes the power supplies, amplifiers, filters, level detectors, counters, and switching circuits.

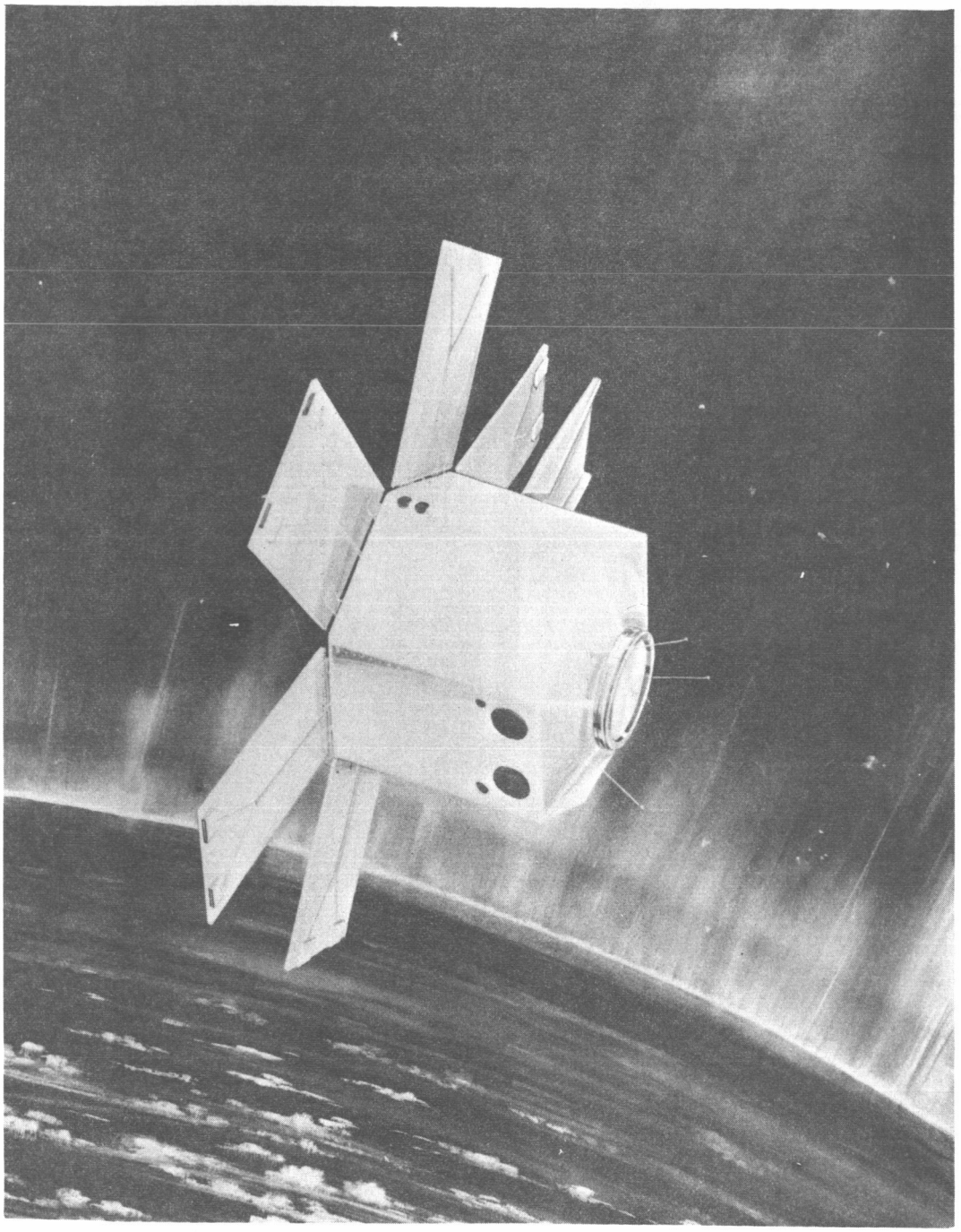

Figure 83. Spacecraft Conceptual Configuration

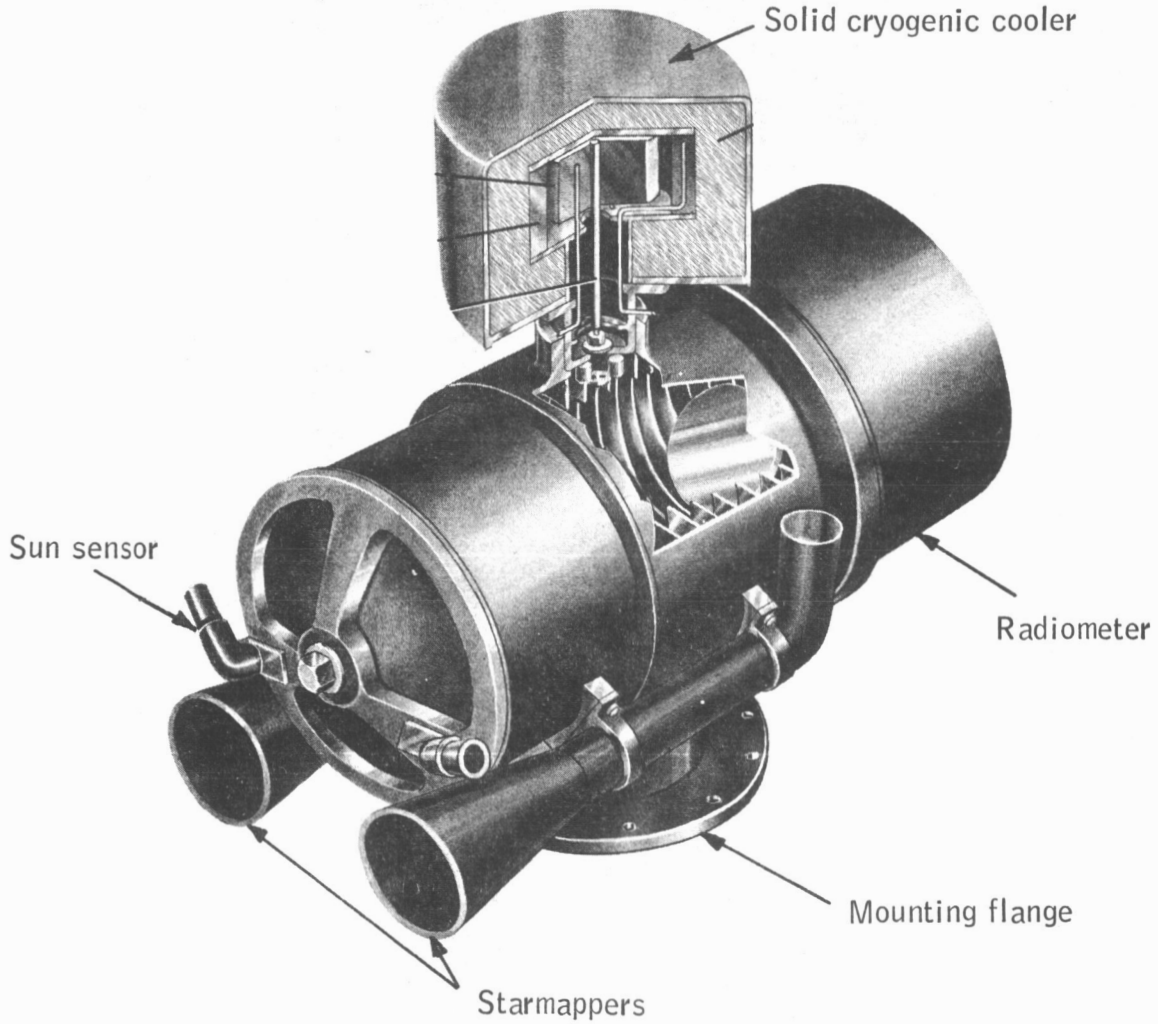

Figure 84. Experiment Package

The system described is capable of resolving the radiometric measurements to the sensitivity required, and starmapper and attitude determination techniques are capable of determining the pointing direction of the spacecraft radiometer to an accuracy of 0.25 km in tangent height of the earth's horizon.

In addition to the above,

- A solar cell-battery electrical power subsystem conceptual design was defined which is completely compatible with the orbital and experimental constraints. This system is capable of delivering 70 watts of continuous electrical power for one year in the sun-synchronous, 3 o'clock nodal crossing, 500-km orbit.
- A data handling subsystem conceptual design was defined which is capable of processing in digital form all the scientific and status data from the spacecraft. The subsystem is completely solid state and is designed to store the 515 455 bits of digital information obtained in one orbit of the earth. This subsystem also includes command verification and execute logic.
- A communications subsystem conceptual design was developed to interface between the data handling system of the spacecraft and the STADAN network. The 136 MHz band is used for primary data transmission, and S band is used for the range and range-rate transponder.
- A spacecraft structural concept was evolved to contain, align, and control the thermal environment for the spaceborne subsystems. The spacecraft is compatible with the Thor-Delta launch vehicle.
- An open-loop, ground-commanded attitude control subsystem conceptual design was defined utilizing primarily magnetic torquing which interacts with the earth's field as the force for correcting attitude and spin rates.
- A selection of the Thor-Delta as booster was made from the 1972 NASA "stable" which provides low cost and adequate capability.
- Western Test Range was selected as the launch site due to polar-orbit requirements. This site has adequate facilities except for minor modifications to handle the program and is compatible with the polar orbital requirements.

REFERENCES

1. Hanel, R.A.; Bandeen, W.R.; and Conrath, B.J.: The Infrared Horizon of the Planet Earth. J. of the Atmospheric Sciences, vol. 20, no. 2, March 1963, pp. 73-86.

2. McKee, Thomas B.; Whitman, Ruth I.; and Davis, Richard E.: Preliminary Infrared Horizon Profiles from Project Scanner. NASA TM X-1483, December 1967.

3. Curtis, A.R.; and Goody, R.M.: Thermal Radiation in the Upper Atmosphere. Proc. of the Royal Meteorological Society, vol. 236A, no. 193, 1956.

4. Stull, V.R.; Wyatt, P.J.; and Plass, G.N.: Infrared Transmission Studies, vol. III, The Infrared Absorption of Carbon Dioxide. Aeronutronic Div., Ford Motor Company, Final Report no. SSD-TDR-62-127, 1962.

5. Duncan, J.: Horizon Detector Techniques Providing 0.05° Accuracy at Low Satellite Altitudes. Proceedings of the IRIS, volume 9, no. 1, January 1964, pp. 155 - 159.

6. Thomas, John R.; Jones, Ennis E.; Carpenter, Robert O'B.; and Ohring, George: The Analysis of 15μ Infrared Horizon Radiance Profile Variations over a Range of Meteorological, Geographical and Seasonal Conditions. NASA CR-725, October 1966.

7. Vogelzang, W.F.; and Ohring, G.: The 15μ Infrared Horizon Radiance Profile Temporal, Spatial, and Statistical Sampling Requirements for a Global Measurement Program. NASA CR-66190, October 1966.

8. Eckstrom, William E.; and Berry, Henry W.: System Analysis and Integration Studies for a 15-Micron Horizon Radiance Measurement Experiment. NASA CR-66377, May 1967.

9. Tidwell, Norris W.; Senechal, Calvin G.; and Hartman, David J.: Conceptual Mechanization Studies for a Horizon Definition Spacecraft Attitude Control Subsystem. NASA CR-66382, May 1967.